

Effective quantum theories with short- and long-range forces

Dissertation

zur

Erlangung des Doktorgrades (Dr. rer. nat.)

der

Mathematisch-Naturwissenschaftlichen Fakultät

der

Rheinischen Friedrich-Wilhelms-Universität Bonn

vorgelegt von

Sebastian König

aus

Northeim

Bonn, August 2013

Angefertigt mit Genehmigung der
Mathematisch-Naturwissenschaftlichen Fakultät der
Rheinischen Friedrich-Wilhelms-Universität Bonn

1. Gutachter: Prof. Dr. Hans-Werner Hammer
 2. Gutachter: Prof. Dr. Ulf-G. Meißner
- Tag der Promotion: 23. Oktober 2013
Erscheinungsjahr: 2013

Abstract

At low energies, nonrelativistic quantum systems are essentially governed by their wave functions at large distances. For this reason, it is possible to describe a wide range of phenomena with short- or even finite-range interactions. In this thesis, we discuss several topics in connection with such an effective description and consider, in particular, modifications introduced by the presence of additional long-range potentials.

In the first part we derive general results for the mass (binding energy) shift of bound states with angular momentum $\ell \geq 1$ in a periodic cubic box in two and three spatial dimensions. Our results have applications to lattice simulations of hadronic molecules, halo nuclei, and Feshbach molecules. The sign of the mass shift can be related to the symmetry properties of the state under consideration. We verify our analytical results with explicit numerical calculations. Moreover, we discuss the case of twisted boundary conditions that arise when one considers moving bound states in finite boxes. The corresponding finite-volume shifts in the binding energies play an important role in the study of composite-particle scattering on the lattice, where they give rise to topological correction factors.

While the above results are derived under the assumption of a pure finite-range interaction—and are still true up to exponentially small correction in the short-range case—in the second part we consider primarily systems of charged particles, where the Coulomb force determines the long-range part of the potential.

In quantum systems with short-range interactions, causality imposes nontrivial constraints on low-energy scattering parameters. We investigate these causality constraints for systems where a long-range Coulomb potential is present in addition to a short-range interaction. The main result is an upper bound for the Coulomb-modified effective range parameter. We discuss the implications of this bound to the effective field theory (EFT) for nuclear halo systems. In particular, we consider several examples of proton–nucleus and nucleus–nucleus scattering. For the bound-state regime, we find relations for the asymptotic normalization coefficients (ANCs) of nuclear halo states. Moreover, we also consider the case of other singular inverse-power-law potentials and in particular discuss the case of an asymptotic van der Waals tail, which plays an important role in atomic physics.

Finally, we consider the low-energy proton–deuteron system in pionless effective field theory. Amending our previous work, we focus on the doublet-channel spin configuration and the ${}^3\text{He}$ bound state. In particular, we study the situation at next-to-leading order in the EFT power counting and provide numerical evidence that a charge-dependent counterterm is necessary for correct renormalization of the theory at this order. We furthermore argue

that the previously employed power counting for the inclusion of Coulomb contributions should be given up in favor of a scheme that is consistent throughout the bound-state and the scattering regime. In order to probe the importance of Coulomb effects directly at the zero-energy threshold, we also present a first calculation of proton–deuteron scattering lengths in pionless effective field theory.

Parts of this thesis have been published in the following articles:

- S. KÖNIG and H.-W. HAMMER, Low-energy p-d scattering and He-3 in pionless EFT, *Phys. Rev. C* **83**, 064001 (2011)
- S. KÖNIG, D. LEE, and H.-W. HAMMER, Volume Dependence of Bound States with Angular Momentum, *Phys. Rev. Lett.* **107**, 112001 (2011)
- S. BOUR, S. KÖNIG, D. LEE, H.-W. HAMMER, and U.-G. MEISSNER, Topological phases for bound states moving in a finite volume, *Phys. Rev. D* **84**, 091503(R) (2011)
- S. KÖNIG, D. LEE, and H.-W. HAMMER, Non-relativistic bound states in a finite volume, *Annals Phys.* **327**, 1450–1471 (2012)
- S. KÖNIG, D. LEE, and H.-W. HAMMER, Causality constraints for charged particles, *J. Phys. G: Nucl. Part. Phys.* **40**, 045106 (2013)
- S. KÖNIG and H.-W. HAMMER, The Low-Energy p–d System in Pionless EFT, *Few-Body Syst.* **54**, 231–234 (2013)
- S. ELHATISARI, S. KÖNIG, D. LEE, and H.-W. HAMMER, Causality, universality, and effective field theory for van der Waals interactions, *Phys. Rev. A* **87**, 052705 (2013)

für meinen Opa

Contents

1	Introduction	1
2	General concepts	3
2.1	Finite-range interactions	3
2.1.1	Non-local interactions	4
2.1.2	Solutions of the free equation	5
2.1.3	Asymptotic form of the wave function	6
2.1.4	The effective range expansion	6
2.1.5	Bound states and asymptotic normalization constants	7
2.2	Some formal scattering theory	9
2.2.1	The Lippmann–Schwinger equation	9
2.2.2	The T-matrix	10
2.3	Universality	13
2.3.1	Hierarchy of partial waves	13
2.3.2	Universality for large scattering length	14
2.3.3	The theorist’s point of view	15
2.3.4	From potential models to a modern perspective	16
2.4	Effective field theory	16
2.4.1	Historical overview	17
2.4.2	Pionless effective field theory	18
2.4.3	Effective field theory for nuclear halo states	19
2.5	Lattice calculations	20
2.5.1	Lattice QCD	21
2.5.2	Nuclear lattice simulations	22
2.5.3	Numerical aspects	23

3	Finite-volume calculations	25
3.1	Introduction	25
3.2	Bound states in a finite volume	27
3.2.1	Infinite volume	27
3.2.2	Finite volume	28
3.3	S-wave result	31
3.4	Extension to higher partial waves	32
3.4.1	Results	33
3.4.2	Sign of the mass shift	35
3.4.3	Trace formula	37
3.5	Numerical tests	38
3.5.1	Lattice discretization	38
3.5.2	Methods	39
3.5.3	Results	39
3.6	Two-dimensional systems	42
3.7	Twisted boundary conditions	45
3.7.1	Generalized derivation	46
3.7.2	Topological volume factors	48
3.8	Summary and outlook	51
4	The Coulomb force	53
4.1	Coulomb wave functions	53
4.1.1	The Gamow factor	55
4.1.2	Analytic wave functions	56
4.2	Modified effective range expansion	56
4.3	Bound-state regime	58
4.3.1	Asymptotic wave function	58
4.3.2	Bound-state condition and ANC	59
4.4	The Coulomb T-matrix	60
4.4.1	Yukawa screening	61
4.4.2	Expression in terms of hypergeometric functions	64
5	Causality bounds for charged particles	67
5.1	Introduction	67

5.2	Setup and preliminaries	69
5.3	Derivation of the causality bound	70
5.3.1	Wronskian identities	70
5.3.2	Rewriting the wave functions	71
5.3.3	The causality-bound function	72
5.3.4	Calculating the Wronskians	73
5.3.5	Constant terms in the causality-bound function	76
5.4	The causal range	78
5.4.1	Practical considerations	78
5.5	Examples and results	79
5.5.1	Proton–proton scattering	80
5.5.2	Proton–deuteron scattering	81
5.5.3	Proton–helion scattering	82
5.5.4	Alpha–alpha scattering	82
5.6	Numerical calculations	83
5.7	Relation for asymptotic normalization constants	86
5.7.1	Derivation for the neutral system	86
5.7.2	Derivation for charged particles	88
5.7.3	Application to the oxygen-16 system	91
5.8	Other long-range forces	94
5.8.1	Singular potentials	94
5.8.2	Causality bounds for van der Waals interactions	95
5.9	Summary and outlook	100
6	The proton–deuteron system revisited	103
6.1	Introduction	103
6.2	Formalism and building blocks	104
6.2.1	Full dibaryon propagators	106
6.2.2	Coulomb contributions in the proton–proton system	108
6.2.3	Power counting	109
6.2.4	Integral equations	112
6.2.5	Numerical implementation	118
6.3	Scattering phase shifts	118

6.3.1	Quartet channel	119
6.3.2	Doublet channel	119
6.4	Trinucleon wave functions	121
6.4.1	Homogeneous equation	122
6.4.2	Normalization condition	122
6.5	Helium-3 properties	124
6.5.1	Energy shift in perturbation theory	126
6.5.2	Nonperturbative calculation	127
6.5.3	Leading-order results	129
6.6	The Coulomb problem at next-to-leading order	132
6.6.1	Scaling of the dibaryon propagators	133
6.6.2	Ultraviolet behavior of the amplitude	133
6.6.3	Consequences	135
6.6.4	Nonperturbative calculation	136
6.6.5	Back to the scattering regime	137
6.7	Proton–deuteron scattering lengths	142
6.7.1	Numerical calculation of the Gamow factor	143
6.7.2	Bubble diagram with full off-shell Coulomb T-matrix	145
6.7.3	Results	147
6.8	Summary and outlook	152
7	Concluding remarks	153
A	The Coulomb wave functions of Bollé and Gesztesy	157
B	Explicit expressions for the causality bound function	159
B.1	Repulsive case, $\gamma > 0$	159
B.2	Attractive case, $\gamma < 0$	160
C	Equivalence of ANC relations	161
D	Bound states in nonrelativistic effective field theory	163
D.1	Simplified nucleon–deuteron system	163
D.2	Bethe–Salpeter equation	164
D.2.1	Momentum space	165

D.2.2	Bound state contribution	167
D.2.3	Homogeneous equation	168
D.2.4	Three-dimensional reduction	168
D.3	Operator formalism	169
D.3.1	Lippmann–Schwinger equation	169
D.4	Normalization condition	170
D.4.1	General derivation	170
D.4.2	Explicit form in three dimensions	171
D.4.3	Factorization of the T-matrix	173
D.5	Some remarks	175

Chapter 1

Introduction

A lot of interesting physics can be done with short or even finite-range interactions. In many situations physicists encounter “universality” in the sense that observables are independent, or at least approximately so, of the short-range details of a given system. The simple—yet very powerful—concept behind this observation is that low-energy phenomena do not probe physics at short distances. This separation of scales is also the foundation of effective field theory.

However, such universal aspects are usually just the starting point for a deeper understanding. In general, universal behavior is not exactly realized in nature and as soon as one wants to go beyond a certain basic level of precision, it is necessary to take into account corrections. One such correction that plays indeed a very prominent role at low energies is the Coulomb interaction. It is particularly important in nuclear physics because most processes in that field involve charged particles.

The above two paragraphs already mention the most important aspects of the topics to be discussed in this thesis. It summarizes the work done in a little more than three years of doctoral studies, divided into several projects that will be presented in separate chapters. Starting with a quick tour through quantum mechanics with short- and finite-range interactions, we will discuss low-energy universality and its connection to effective field theory (EFT) in Chapter 2. With a focus on applications in nuclear physics, we will present there the general concepts that will be important throughout this work, both as theoretical foundations and to put the results to be derived in a broader context.

In Chapter 3 we consider how calculations in finite volumes with periodic boundary conditions, as they appear frequently in numerical lattice calculations, affect the properties of nonrelativistic bound states. When the latter arise from a finite-range interaction, it is possible to derive an analytic formula for their leading-order volume dependence. Generalizing a result for S-waves that has been obtained by Lüscher in the 1980s [8], we derive the finite-volume mass shift for states with arbitrary orbital angular momentum.

For the rest of this work we will then mainly be concerned with systems of charged particles, where the Coulomb force plays an important role, and particularly so at low energies. Chapter 4 is dedicated to collecting and reviewing several results concerning this topic.

Subsequently, in Chapter 5, we derive a generalization of the so-called Wigner causality bound to interactions with Coulomb tails. Results of this kind are both interesting theoretically and as a guide to improve the convergence of effective-field-theory calculations. We also consider other long-range forces and in particular the van der Waals interaction, which plays an important role in low-energy atomic physics.

While in the derivation of the causality bounds the Coulomb force enters mainly as a theoretical challenge in a configuration-space treatment, we will look at the difficulties it creates from a more practical point of view in Chapter 6, where we consider the low-energy proton–deuteron system in pionless effective field theory. Performing calculations in both the scattering and the bound-state regime, we obtain results for phase shifts, scattering lengths, and the Helium-3 binding energy. In all cases, Coulomb effects raise the interesting question of how to treat them consistently in an EFT power counting scheme. At the same time, they also constitute a challenge for numerical calculations in momentum space.

Finally, we close with some concluding remarks in Chapter 7.

Chapter 2

General concepts

Overview

In the first part of this chapter, we review several well-known results from nonrelativistic quantum mechanics. Focussing first on solutions of the radial Schrödinger equation and the effective range expansion in Section 2.1, we subsequently give an overview of scattering theory from a more formal point of view in Section 2.2. Moving on, we then discuss low-energy universality and its connection to effective field theories Sections 2.3 and 2.4. Finally, in Section 2.5, we briefly discuss lattice calculations as a prelude to the following Chapter 3.

2.1 Finite-range interactions

Consider a two-particle system with reduced mass μ interacting via a spherically-symmetric potential $V(r)$, where $r = |\mathbf{r}_1 - \mathbf{r}_2|$ is the relative distance of the two particles in their center-of-mass frame. It is a well-known fact in quantum mechanics that a solution $\psi(\mathbf{r})$ of the time-independent Schrödinger equation^{1,2}

$$\left[-\frac{\Delta_r}{2\mu} + V(r) - E \right] \psi(\mathbf{r}) = 0, \quad (2.1)$$

describing a state with energy E and angular momentum quantum numbers (ℓ, m) , can be separated as

$$\psi(\mathbf{r}) = \psi_{\ell m}(\mathbf{r}) = R_\ell(r) Y_\ell^m(\theta, \phi) = \frac{u_\ell(r)}{r} Y_\ell^m(\theta, \phi) \quad (2.2)$$

into a known angular part, given by the spherical harmonics $Y_\ell^m(\theta, \phi)$, and a (reduced) radial wave function $u_\ell(r)$, which is a solution of

$$\left[-\frac{d^2}{dr^2} + \frac{\ell(\ell+1)}{r^2} + 2\mu[V(r) - E] \right] u_\ell(r) = 0. \quad (2.3)$$

¹ Δ_r denotes the Laplacian. Throughout this work, we always indicate the coordinate that a differential operator acts on with an explicit subscript.

²Here and in the following we work in natural units where $\hbar = c = 1$.

This is known as the *radial Schrödinger equation*.

In the following, we are primarily interested in interactions with a finite range R . For the potential $V(r)$ this means that it fulfills the condition

$$V(r) = 0 \quad \text{for } r > R. \quad (2.4)$$

Moreover, throughout this work we employ the following canonical classification scheme for potentials:

- if for $r \rightarrow \infty$ the potential falls off faster than any power law, *e.g.*, like an exponential, we call it *short-ranged*.
- if, on the other hand, the potential has a power-law form $r^{-\alpha}$ with $\alpha \geq 1$ at large r , we call it a *long-range* potential. A very prominent member of this class is the Coulomb potential $V_C(r) \sim 1/r$, which will be discussed in more detail in Chapter 4.

We do not consider potentials that do not fall off at large distances.

2.1.1 Non-local interactions

The interaction of a quantum system can be described in more general terms by a real symmetric operator

$$V(\mathbf{r}, \mathbf{r}') = \langle \mathbf{r} | \hat{V} | \mathbf{r}' \rangle. \quad (2.5)$$

Assuming, as we will do throughout this work whenever we consider such *non-local* interactions, that $V(\mathbf{r}, \mathbf{r}')$ allows an expansion in Legendre polynomials (partial-wave decomposition),

$$V(\mathbf{r}, \mathbf{r}') = \sum_{\ell=0}^{\infty} (2\ell + 1) V_{\ell}(r, r') P_{\ell}(\cos \theta) \quad , \quad \cos \theta = \frac{\mathbf{r} \cdot \mathbf{r}'}{rr'}, \quad (2.6)$$

a generalized form of the radial Schrödinger equation (2.3) can be written as

$$p^2 u_{\ell}(r) = -\frac{d^2}{dr^2} u_{\ell}(r) + \frac{\ell(\ell + 1)}{r^2} u_{\ell}(r) + 2\mu \int_0^{\infty} dr' 4\pi r' V_{\ell}(r, r') u_{\ell}(r'), \quad (2.7)$$

where we have furthermore introduced the momentum scale $p^2 = 2\mu E$. From this one directly sees that the interaction no longer depends on the wave function at just a single point but over some extended range and is thus “smeared out” or “non-local” in that sense. For the special case where

$$V(\mathbf{r}, \mathbf{r}') = V(\mathbf{r}) \times \delta^{(3)}(\mathbf{r} - \mathbf{r}'), \quad (2.8)$$

we simply get back Eq. (2.3).

Note that the partial-wave decomposition (2.6) is in particular possible for non-local potentials which are a function of the relative distance only,

$$V(\mathbf{r}, \mathbf{r}') = V(|\mathbf{r} - \mathbf{r}'|), \quad (2.9)$$

which is the straightforward generalization of spherical symmetry to the case of non-local interactions. This condition, however, is only a sufficient and not a necessary one, and we do not make such explicit assumptions on the interaction in the following.

Due to the symmetry of $V(\mathbf{r}, \mathbf{r}')$, which ensures that the full Hamiltonian is a symmetric operator, the generalized condition for the interaction to have a finite range now reads

$$V(\mathbf{r}, \mathbf{r}') = 0 \quad \text{if } r = |\mathbf{r}| > R \quad \text{or} \quad r' = |\mathbf{r}'| > R, \quad (2.10)$$

which implies the same for all partial-wave components $V_\ell(r, r')$. The integral in Eq. (2.7) does then not extend all the way to infinity but is cut off at $r' = R$. Since in this work we are not concerned with the exact form of the interaction, we will from now on absorb the prefactor $4\pi r'$ in Eq. (2.7) into the potential and also omit the subscript ℓ in writing down the radial Schrödinger equation.

2.1.2 Solutions of the free equation

In the absence of any interaction (in particular, outside the range of a finite-range potential), one is left with the free radial Schrödinger equation,

$$p^2 u_\ell(r) = \left[-\frac{d^2}{dr^2} + \frac{\ell(\ell+1)}{r^2} \right] u_\ell(r), \quad (2.11)$$

the solutions of which are well known. Commonly (see, *e.g.*, Ref. [9]) the Riccati–Bessel and Riccati–Neumann functions $S_\ell(pr)$ and $C_\ell(pr)$ are chosen as a base pair of linearly-independent solutions.³ They are defined as

$$S_\ell(z) = \sqrt{\frac{\pi z}{2}} J_{\ell+1/2}(z), \quad (2.12a)$$

$$C_\ell(z) = (-1)^\ell \sqrt{\frac{\pi z}{2}} J_{-\ell-1/2}(z), \quad (2.12b)$$

where $J_n(z)$ denotes the ordinary Bessel function. Any solution of Eq. (2.11) can be written as a linear combination of $S_\ell(pr)$ and $C_\ell(pr)$. Their asymptotic behavior for large arguments is determined by

$$S_\ell(z) \stackrel{|z| \rightarrow \infty}{\sim} \sin(z - \ell\pi/2) \quad , \quad C_\ell(z) \stackrel{|z| \rightarrow \infty}{\sim} \cos(z - \ell\pi/2) \quad , \quad (2.13)$$

whereas close to the origin (in the limit $z \rightarrow 0$) S_ℓ and C_ℓ scale like $z^{\ell+1}$ and $z^{-\ell}$, respectively. Due to this behavior $S_\ell(pr)$ and $C_\ell(pr)$ are also called the regular and irregular solutions of (2.11). In some situations it is more convenient to work instead with the Riccati–Hankel functions

$$\hat{H}_\ell^\pm(z) = C_\ell(z) \pm iS_\ell(z), \quad (2.14)$$

which have the asymptotic form $e^{\pm iz}$ as $|z| \rightarrow \infty$ and thus, for $z = pr$, correspond to outgoing and incoming waves for $z = pr$, respectively.

³Ref. [9] actually uses the notation $S_\ell(z) = \hat{j}_\ell(z)$ and $C_\ell(z) = \hat{n}_\ell(z)$. The convention we employ here is the same as in Ref. [10] with $L = \ell$ and $d = 3$.

2.1.3 Asymptotic form of the wave function

Going back to Eq. (2.7), we now consider an arbitrary interaction that fulfills the finite-range condition (2.10), and which we assume to be sufficiently well-behaved at the origin to allow for a solution that is regular there (*i.e.*, $u_\ell(r) \rightarrow 0$ as $r \rightarrow 0$ with finite derivative). We denote such a solution for a given—possibly complex, to also cover the bound-state regime—momentum parameter p with an explicit superscript “ (p) .” Outside the range of the interaction, it can be written in the form

$$u_\ell^{(p)}(r) = p^\ell [\cot \delta_\ell(p) S_\ell(pr) + C_\ell(pr)] \quad (r > R), \quad (2.15)$$

where he have adopted the momentum-dependent normalization convention from Ref. [10]. In the following, whenever we write $u_\ell^{(p)}(r)$, it is also implied that the wave function is normalized exactly as in Eq. (2.15).

The scattering phase shift $\delta_\ell(p)$ can be interpreted as the additional phase (compared to the regular solution $S_\ell(pr)$ of the free equation) that the wave function picks up due to the interaction. It is related to the partial-wave S-matrix $s_\ell(p)$ via

$$s_\ell(p) = e^{2i\delta_\ell(p)}, \quad (2.16)$$

such that up to an overall change in the normalization, the asymptotic form of $u_\ell^{(p)}(r)$ can also be written as

$$u_\ell^{(p)}(r) \propto H_\ell^-(pr) - s_\ell(p)H_\ell^+(pr) \quad (r > R) \quad (2.17)$$

in terms of Riccati–Hankel functions. Alternatively, by factoring out an overall $e^{i\delta_\ell(p)}/\sin \delta_\ell(p)$, one finds that

$$u_\ell^{(p)}(r) \propto [\cot \delta_\ell(p) - i]H_\ell^-(pr) - [\cot \delta_\ell(p) + i]H_\ell^+(pr) \quad (r > R). \quad (2.18)$$

The latter form can also be derived directly by inverting Eq. (2.14) and inserting the result into Eq. (2.15). For interactions with a short but not strictly finite range, *e.g.*, a potential with an exponential or Gaussian tail, the relations above do not hold exactly, but are fulfilled asymptotically as $r \rightarrow \infty$.

2.1.4 The effective range expansion

For systems with short- or finite-range interactions, the scattering phase shift $\delta_\ell(p)$ can be expressed in terms of the well-known effective range expansion

$$p^{2\ell+1} \cot \delta_\ell(p) = -\frac{1}{a_\ell} + \frac{1}{2}r_\ell p^2 + \dots, \quad (2.19)$$

where a_ℓ and r_ℓ are the scattering and effective range parameters, respectively, and the ellipses stand for higher-order shape parameters ($\propto p^4, p^6, \dots$) that we have not written out here. Eq. (2.19) states that the cotangent of the scattering phase shift, multiplied by appropriate powers of the momentum, is an analytic function of p^2 and thus of the energy.

Historically, this expansion was first used to describe and interpret nucleon–nucleon scattering at low-energies. This is discussed, for example, in the review by Jackson and

Blatt [11]. As noted there (and already in an earlier publication by the same authors [12]), the S-wave ($\ell = 0$) version of Eq. (2.19) was first derived by Schwinger, but only published in lecture notes. A derivation based on a direct analysis of the radial wave functions was later given by Bethe in Ref. [13]. An extension of Bethe's formalism to also treat higher partial waves can be found in the textbook of Goldberger and Watson [14]. For a modern derivation of Eq. (2.19) for arbitrary ℓ , based directly on the analytic properties of the partial-wave S-matrix and scattering amplitude (both of which will be discussed in more detail in the following sections), see, for example, Ref. [9].

In general, an expansion as in Eq. (2.19), which is essentially a Taylor series of the left-hand side around $p^2 = 0$, only has a finite radius of convergence. For example, if the interaction is given by a short-range potential of the Yukawa form $\exp(-\mu r)/r$ (as it arises from the exchange of a particle with mass μ), $p^{2\ell+1} \cot \delta_\ell(p)$ has a cut starting at $-\mu^2/4$ in the complex p^2 plane (see, for example, Ref. [15]), which naturally limits the radius of convergence of the expansion. Within its region of analyticity, however, $p^{2\ell+1} \cot \delta_\ell(p)$ can also be expanded around points other than $p = 0$. For example, in the 3S_1 channel of neutron-proton scattering it is customary to work with an effective range expansion around the deuteron pole [16].

In the presence of long-range potentials $p^{2\ell+1} \cot \delta_\ell(p)$ is in general no longer analytic in p^2 and the ordinary effective range expansion as given above thus not valid for systems where the interaction has a power-law tail. It is, however, often possible to modify the left-hand side of Eq. (2.19) in such a way that analyticity is restored. Essentially, this means that known non-analytic terms due to the long-range component of the potential can be taken into account explicitly. Most notably, for the scattering of charged particles one has the so-called *Coulomb-modified effective range expansion* that will be discussed in Chapter 4. Note furthermore that a general modified effective range function for the case where the interaction can be written as the sum of a short-range and a long-range potential has been derived by van Haeringen and Kok in Ref. [17].

The methods just mentioned no longer work if the long-range part of the potential has a power-law form that is more singular than $1/r^2$ at the origin. For such cases, an extension of a formalism called *quantum defect theory* [18–20] has been developed by Gao [21]. This is particularly interesting for applications in atomic physics, where a long-range van der Waals tail ($\sim 1/r^6$) arises due to the mutual polarization of the atoms, a case we will come back to in Chapter 5.

2.1.5 Bound states and asymptotic normalization constants

Going back to the case of pure finite-range interactions, we now consider bound states. Their wave functions correspond to solutions of Eq. (5.2) for negative energies,

$$p^2 = 2\mu E < 0. \quad (2.20)$$

More precisely, in the complex p -plane, the bound states are located on the positive imaginary axis, whereas the negative imaginary axis is the location of virtual states [9]. We write $p = i\kappa$ in the bound-state regime and call $\kappa > 0$ the *binding momentum*.

A bound state with angular momentum ℓ corresponds to a (simple) pole in the partial-wave S-matrix $s_\ell(p)$ at $p = i\kappa$. From Eq. (2.17) it can be seen that this means that there is no incoming component because $s_\ell(p)$, the ratio of the outgoing wave compared to the incoming one, becomes infinite. Alternatively one can choose a normalization with an overall coefficient $s_\ell(p)$ factored out in Eq. (2.17), leaving $s_\ell(p)^{-1}$ in front of the incoming component $H_\ell^-(pr)$ that has to vanish for $p = i\kappa$. From Eq. (2.18) one furthermore sees that

$$\cot \delta_\ell(p = i\kappa) = i \quad (2.21)$$

is the bound-state condition for the scattering phase shift. The same result can be found more directly by writing the S-matrix as

$$s_\ell(p) = 1 + 2ikf_\ell(p) \quad (2.22)$$

with the partial-wave scattering amplitude

$$f_\ell(p) = \frac{p^{2\ell}}{p^{2\ell+1} [\cot \delta_\ell(p) - i]}. \quad (2.23)$$

Since the pole in $s_\ell(p)$ has to come from the second term in (2.22) we again obtain the condition stated in Eq. (2.21).

On the bound-state wave function we impose the usual normalization condition

$$\int_0^\infty dr |u_\ell(r)|^2 = 1. \quad (2.24)$$

From the above discussion it follows immediately that

$$u_\ell^{(i\kappa)}(r) \propto H_\ell^+(i\kappa r) \sim e^{-\kappa r} \quad (2.25)$$

as $r \rightarrow \infty$, which together with our regularity assumption on the interaction ensures that the wave function is indeed normalizable.

Note, however, that the bound-state normalization condition (2.24) is not directly compatible with the asymptotically fixed form as given in Eq. (2.15). In order to discuss the precise asymptotic form of the bound-state wave functions we closely follow Ref. [9] and define solutions $\chi_{\ell,p}^\pm(r)$ of (2.7) normalized such that they exactly fulfill the condition

$$\chi_{\ell,p}^\pm(r) \stackrel{r \rightarrow \infty}{\sim} H_\ell^\pm(pr). \quad (2.26)$$

The bound-state solution normalized according to (2.24), which in the following we denote as $u_{A,\ell}^{(i\kappa)}(r)$, can then be written as

$$u_{A,\ell}^{(i\kappa)}(r) = i^\ell A_\kappa \chi_{\ell,i\kappa}^+(r), \quad (2.27)$$

where

$$A_\kappa = \left(\int_0^\infty dr |\chi_{\ell,i\kappa}^+(r)|^2 \right)^{-1/2} \quad (2.28)$$

is the so-called *asymptotic normalization constant/coefficient (ANC)*. The factor i^ℓ conveniently adjusts the phase of $u_\ell^{(i\kappa)}(r)$ such that it is a real function. Outside the range of the interaction one then has the exact identity

$$u_{A,\ell}^{(i\kappa)}(r) = i^\ell A_\kappa H_\ell^+(i\kappa r) \quad \text{for } r > R. \quad (2.29)$$

The wave functions $u_\ell^{(i\kappa)}(r)$ with the asymptotic behavior determined by Eq. (5.3), on the other hand, have the form

$$u_\ell^{(i\kappa)}(r) = i^\ell \kappa^\ell H_\ell^+(i\kappa r) \quad \text{for } r > R. \quad (2.30)$$

We use the different notations given in Eqs. (2.29) and (2.30) to indicate which convention is used.

Asymptotic normalization constants are interesting quantities because for shallow bound states (*i.e.*, states with small binding energy/momentum) they are closely related to scattering processes. For example, they are directly connected to zero-energy capture reactions [22], which play an important role in nuclear astrophysics. In Chapter 5 (Section 5.7) we will discuss how the ANC can be expressed directly in terms of the parameters that appear in the effective range expansion (2.19).

2.2 Some formal scattering theory

In the preceding sections, we have established that for finite-range interactions the asymptotic radial wave functions of two-particle systems have an explicitly-known analytic form. Since low-energy physics is governed by large-distance scales, this fact will be very useful in the following chapters to derive relations based on just the properties of the wave-function tails.

Since the focus so far was on consequences of the finite-range assumption, we have worked directly with radial Schrödinger equations and wave functions in configuration space, and only introduced scattering concepts like the phase shift and the S-matrix as they appear in that context. In the following, we discuss quantum-mechanical scattering theory from a more formal point of view, establishing the connection with the relations given in Section 2.1 along the way and focussing on results that will be relevant later in this work. Unless otherwise indicated with an explicit citation, what follows is mostly taken from Sakurai's textbook [23], but uses slightly different conventions in some places. Until further notice, we also lift the finite-range assumption on the interaction.

2.2.1 The Lippmann–Schwinger equation

In its abstract operator form, the time-independent Schrödinger equation (2.1) reads

$$\hat{H}|\psi\rangle = E|\psi\rangle \quad (2.31)$$

with the Hamilton operator $\hat{H} = \hat{H}_0 + \hat{V}$ given by

$$\langle \mathbf{r} | \hat{H} | \psi \rangle = -\frac{\Delta_r}{2\mu} \psi(\mathbf{r}) + \int d^3\mathbf{r}' V(\mathbf{r}, \mathbf{r}') \psi(\mathbf{r}') \quad (2.32)$$

in configuration space, where we have allowed the interaction to be non-local. What we have ignored so far is that the Schrödinger equation alone does not specify the boundary condition for the solutions. In the time-independent scattering formalism we are considering here, one is primarily interested in solutions that reduce to a plane-wave state $|\mathbf{p}\rangle$ when the interaction is “switched off,” $\hat{V} \equiv 0$. This behavior can be enforced by making the ansatz

$$|\psi_{\mathbf{p}}^{(+)}\rangle = |\mathbf{p}\rangle + (E_{\mathbf{p}} - \hat{H}_0 + i\varepsilon)^{-1} \hat{V} |\psi_{\mathbf{p}}^{(+)}\rangle, \quad E_{\mathbf{p}} = \frac{p^2}{2\mu}, \quad (2.33)$$

where the small imaginary part $i\varepsilon$ has been introduced to make the otherwise singular operator $E - \hat{H}_0$ invertible. More precisely, the zero modes of $E - \hat{H}_0$ are given by the plane-wave states $|\mathbf{p}\rangle$,

$$(E_{\mathbf{p}} - \hat{H}_0)|\mathbf{p}\rangle = 0 \quad \text{for all } |\mathbf{p}\rangle. \quad (2.34)$$

Acting on both sides of Eq. (2.33) with $E - \hat{H}_0 + i\varepsilon$ and sending $\varepsilon \rightarrow 0$ (which in the following is always implicitly understood to be done at the end of all manipulations) gives back the Schrödinger equation in the form (3.3).

Equation (2.33) is called the *Lippmann-Schwinger equation* for the scattering states. It can be interpreted as an integral formulation of the Schrödinger equation with the boundary conditions determined by the inhomogeneous term $|\mathbf{p}\rangle$ and the $i\varepsilon$ -prescription. We have chosen a positive sign for the imaginary part and indicated this by writing $|\psi_{\mathbf{p}}^{(+)}\rangle$ for the scattering state. This gives the physically most relevant solution that corresponds to an incoming plane wave and an outgoing scattered wave when one goes over to a time-dependent framework.

By choosing a configuration-space basis $\{|\mathbf{r}\rangle : \mathbf{r} \in \mathbb{R}^3\}$ we get the ordinary wave functions

$$\psi_{\mathbf{p}}^{(+)}(\mathbf{r}) = \langle \mathbf{r} | \psi_{\mathbf{p}}^{(+)} \rangle, \quad (2.35)$$

and the plane-wave states are just $\langle \mathbf{r} | \mathbf{p} \rangle = \exp(i\mathbf{p} \cdot \mathbf{r})$. In general, the wave function $\psi_{\mathbf{p}}^{(+)}(\mathbf{r})$ is not characterized by a single pair of angular-momentum quantum numbers (ℓ, m) but rather has an expansion in spherical harmonics or Legendre polynomials [24],

$$\psi_{\mathbf{p}}^{(+)}(\mathbf{r}) = \left(\frac{2\mu}{\pi p}\right)^{1/2} \sum_{\ell=0}^{\infty} \sum_{m=-\ell}^{\ell} Y_{\ell}^m(\hat{\mathbf{r}}) Y_{\ell}^{m*}(\hat{\mathbf{p}}) \frac{u_{\ell}(r)}{r} \quad (2.36)$$

$$= \left(\frac{2\mu}{\pi p}\right)^{1/2} \frac{1}{4\pi} \sum_{\ell=0}^{\infty} (2\ell + 1) i^{\ell} P_{\ell}(\cos \theta) \frac{u_{\ell}(r)}{r}, \quad \cos \theta = \hat{\mathbf{p}} \cdot \hat{\mathbf{r}}, \quad (2.37)$$

with the unit vectors $\hat{\mathbf{p}} = \mathbf{p}/p$ and $\hat{\mathbf{r}} = \mathbf{r}/r$. The wave functions $u_{\ell}(r)$ are then solutions of the radial Schrödinger equation (5.2), and the normalization in Eq. (2.37) is chosen such that the latter can be rewritten as an integral equation with the inhomogeneous term given by the Riccati–Bessel function $S_{\ell}(pr)$.

2.2.2 The T-matrix

Defining the Green’s function operator (the free resolvent)

$$\hat{G}_0^{(+)}(E) = (E - \hat{H}_0 + i\varepsilon)^{-1}, \quad (2.38)$$

we can write the Lippmann-Schwinger equation (2.33) as

$$|\psi_{\mathbf{p}}^{(+)}\rangle = |\mathbf{p}\rangle + \hat{G}_0^{(+)}(E_{\mathbf{p}}) \hat{V} |\psi_{\mathbf{p}}^{(+)}\rangle. \quad (2.39)$$

For the free Hamiltonian defined implicitly in Eq. (2.32), the Green's function in configuration space is given by the expression

$$G_0^{(+)}(E; \mathbf{r}, \mathbf{r}') = \langle \mathbf{r} | \hat{G}_0^{(+)}(E) | \mathbf{r}' \rangle = -\frac{\mu}{2\pi} \frac{e^{ik|\mathbf{r}-\mathbf{r}'|}}{|\mathbf{r}-\mathbf{r}'|}, \quad (2.40)$$

where k is a momentum scale defined as $k = \sqrt{2\mu(E + i\varepsilon)}$. It satisfies the equation

$$\frac{1}{2\mu} (\Delta_r + k^2) G_0^{(+)}(E; \mathbf{r}, \mathbf{r}') = \delta^{(3)}(\mathbf{r} - \mathbf{r}'). \quad (2.41)$$

Note that other conventions exist in the literature where the factor $1/(2\mu)$ is absorbed into the definition of $G_0^{(+)}$. Our choice here has the advantage of staying close to the operator notation, such that from Eq. (2.38) one can directly read off the momentum-space expression

$$G_0^{(+)}(E; \mathbf{q}, \mathbf{q}') = \langle \mathbf{q} | \hat{G}_0^{(+)}(E) | \mathbf{q}' \rangle = \frac{(2\pi)^3 \delta^{(3)}(\mathbf{q} - \mathbf{q}')}{E - q^2/(2\mu) + i\varepsilon}. \quad (2.42)$$

Introducing now the operator \hat{T} , which in the following we simply refer to as the *T-matrix*, via the implicit definition

$$\hat{V} |\psi_{\mathbf{p}}^{(+)}\rangle = \hat{T} |\mathbf{p}\rangle, \quad (2.43)$$

we obtain the formal solution

$$|\psi_{\mathbf{p}}^{(+)}\rangle = \left(\mathbf{1} + \hat{G}_0^{(+)}(E_{\mathbf{p}}) \hat{T} \right) |\mathbf{p}\rangle \quad (2.44)$$

for the scattering state. The original problem of finding the solution for the scattering wave function is thus modified to the question of determining the T-matrix. In order to proceed in this direction, one can act with the potential operator \hat{V} on both sides of Eq. (2.44) from the left and then use Eq. (2.43) once again to find

$$\hat{T} |\mathbf{p}\rangle = \left(\hat{V} + \hat{V} \hat{G}_0^{(+)}(E_{\mathbf{p}}) \hat{T} \right) |\mathbf{p}\rangle. \quad (2.45)$$

Demanding further that this holds for *all* states $\{|\mathbf{p}\rangle : \mathbf{p} \in \mathbb{R}^3\}$ yields an operator equation for \hat{T} . In fact, at this point one can furthermore lift the restriction that the Green's function operator is evaluated at the on-shell energy $E = E_{\mathbf{p}}$ but rather allow this value to be an arbitrary complex parameter. The resulting equation reads

$$\hat{T}(E) = \hat{V} + \hat{V} \hat{G}_0^{(+)}(E) \hat{T}(E) \quad (2.46)$$

and is called the Lippmann-Schwinger equation for the T-matrix. The momentum-space representation

$$T(E; \mathbf{q}, \mathbf{p}) = \langle \mathbf{q} | \hat{T}(E) | \mathbf{p} \rangle \quad (2.47)$$

with no imposed connection between the variables E , \mathbf{p} , and \mathbf{q} is commonly referred to as the *full off-shell* T-matrix, whereas the quantity

$$T(\mathbf{q}, \mathbf{p}) = \langle \mathbf{q} | \hat{T}(E = E_{\mathbf{p}}) | \mathbf{p} \rangle \quad (2.48)$$

is called the *half off-shell* (or simply *half-shell*) T-matrix. It has the useful property of being directly related to the scattering wave function in momentum space via

$$\psi_{\mathbf{p}}^{(+)}(\mathbf{q}) = \langle \mathbf{q} | \psi_{\mathbf{p}}^{(+)} \rangle = (2\pi)^3 \delta^{(3)}(\mathbf{q} - \mathbf{p}) + \frac{2\mu T(\mathbf{q}, \mathbf{p})}{p^2 - q^2 + i\epsilon}, \quad (2.49)$$

according to Eq. (2.44).

The scattering amplitude

From the Green's function in configuration space, Eq. (2.40), one can deduce that at asymptotically large distances the scattering wave function $\psi_{\mathbf{p}}^{(+)}(\mathbf{r})$ can be written as the sum a plane wave (given by the state $|\mathbf{p}\rangle$ and interpreted as the originally incoming particle flux) and an outgoing spherical wave describing the effect of the scattering process,

$$\psi_{\mathbf{p}}^{(+)}(\mathbf{r}) \stackrel{r \rightarrow \infty}{\sim} e^{i\mathbf{p}\cdot\mathbf{r}} + \frac{e^{ipr}}{r} f(\mathbf{p}', \mathbf{p}), \quad (2.50)$$

where $\mathbf{p}' = p\hat{\mathbf{r}}$ and

$$f(\mathbf{p}', \mathbf{p}) = -\frac{\mu}{2\pi} \langle \mathbf{p}' | \hat{V} | \psi_{\mathbf{p}}^{(+)} \rangle = -\frac{\mu}{2\pi} \langle \mathbf{p}' | \hat{T} | \mathbf{p} \rangle \quad (2.51)$$

is the scattering amplitude. From the definitions above it is clear that $f(\mathbf{p}', \mathbf{p})$ only depends on the magnitude p of \mathbf{p} and the angle θ between \mathbf{p} and \mathbf{r} . It thus has an expansion in partial waves,

$$f(\mathbf{p}', \mathbf{p}) = \sum_{\ell=0}^{\infty} (2\ell + 1) f_{\ell}(p) P_{\ell}(\cos \theta), \quad (2.52)$$

and it is precisely the partial-wave amplitudes $f_{\ell}(p)$ appearing in Eq. (2.52) that were already mentioned in Section 2.1.5. Assuming that the potential can be expanded in Legendre polynomials (*cf.* Section 2.1.1), an analogous expansion also exists for the T-matrix,

$$T(E; \mathbf{q}, \mathbf{p}) = \sum_{\ell=0}^{\infty} (2\ell + 1) T_{\ell}(E; q, p) P_{\ell}(\cos \theta), \quad (2.53)$$

where θ is now the angle between the momentum vectors \mathbf{q} and \mathbf{p} . It then follows that the partial-wave scattering amplitude—and thus also the scattering phase shift $\delta_{\ell}(p)$ —is determined by the partial-wave T-matrix at the on-shell point:

$$f_{\ell}(p) = \frac{e^{2i\delta_{\ell}(p)} - 1}{2ip} = -\frac{\mu}{2\pi} T_{\ell}(E_{\mathbf{p}}; p, p). \quad (2.54)$$

2.3 Universality

We now turn back our attention to short- and finite-range interactions. As shown in Section 2.1, the asymptotic form of the radial wave function for a given two-particle scattering system is known analytically and can be parametrized in terms of the scattering phase shift $\delta_\ell(p)$. The relations for the wave functions in Eqs. (2.15) and (2.29) hold rigorously for pure finite-range potentials and still up to exponentially small (as $r \rightarrow \infty$) corrections if the interaction is short-ranged. In the latter situation, the interaction range is limited by the typical fall-off scale of the potential.

In either case, the effective-range expansion (2.19) furthermore provides a method to express the phase shifts in terms of just a few low-energy parameters. In many situations, already the scattering length and effective range parameter a_ℓ and r_ℓ are sufficient for a reasonably accurate description of the experimental data. The physics behind all this is that at sufficiently low energies (and thus small scattering momenta p) the details of the interaction cannot be resolved because the de Broglie wavelength $\lambda_p \propto 1/p$ corresponding to the incoming particle flux is too large compared to the spatial extent of the scattering center. More quantitatively, the criterion for not resolving the details of an interaction with range R is

$$p \ll R^{-1} \iff pR \ll 1. \quad (2.55)$$

This simple principle is very powerful because it means that—provided the underlying interaction has a finite (or short) range—low-energy quantum scattering can be described in a *universal* way by the parameters appearing in the effective range expansion.

2.3.1 Hierarchy of partial waves

In the formal discussion so far we have mostly considered some fixed but arbitrary angular momentum ℓ . The really important quantity, however, is the scattering amplitude $f(\mathbf{p}', \mathbf{p})$ defined in Section 2.2.2 since it is directly related to the differential cross section that is determined in experiments,

$$\frac{d\sigma}{d\Omega} = |f(\mathbf{p}', \mathbf{p})|^2. \quad (2.56)$$

This means that all physically significant information about the process is contained in the scattering amplitude.

Combining Eqs. (2.52) and (2.54), we can express the scattering amplitude in terms of the phase shifts $\delta_\ell(p)$ as

$$f(\mathbf{p}', \mathbf{p}) = \sum_{\ell=0}^{\infty} (2\ell + 1) \frac{e^{2i\delta_\ell(p)} - 1}{2ip} P_\ell(\cos \theta). \quad (2.57)$$

If all terms in this sum were equally important, the universal parametrization mentioned above would not be very useful because describing the physical system would still require an infinite number of parameters. Fortunately, the phase shifts themselves have the low-

energy behavior⁴

$$\delta_\ell(p) \propto p^{2\ell+1}, \quad (2.58)$$

which means that at low energies only a few partial waves are important. Usually, the dominant term is the S-wave ($\ell = 0$), but this is not necessarily always the case.⁵ The physical origin behind the behavior (2.58) is of course the centrifugal barrier $\sim \ell(\ell+1)/r^2$ that the scattering particles cannot penetrate appreciably at low energies.

2.3.2 Universality for large scattering length

A particularly interesting situation occurs if the S-wave scattering length of a system is unnaturally large. By “unnaturally large” we mean in this context that it is much larger than the range R of the potential, $a_0 \gg R$, because naïvely one would expect that all length scales in the system are of the “natural” order of magnitude.

Usually, one does of course not know the exact range R of the underlying interaction, nor is the notion of a strict finite-range interaction a very realistic picture. In general, if the interaction is assumed to be mediated by some kind of particle, the corresponding potential has an exponential (Yukawa) tail, and the inverse mass of the exchange particle provides a good estimate for the interaction range. In low-energy nuclear physics, for example, the typical length scale is set by the inverse pion mass, $m_\pi^{-1} \approx 1.4$ fm. Typically, the S-wave effective range is found to be of the order of magnitude estimated for the underlying interaction, such that, in the absence of more direct information, $a_0 \gg r_0$ can be used as a criterion for asserting that the scattering length is unnaturally large.

Since the total cross section for two-particle scattering at zero energy is given by⁶

$$\sigma_{\text{tot}}(0) = 4\pi a_0^2, \quad (2.59)$$

a large S-wave scattering length means that the particles interact strongly. In fact, one can say that the low-energy physics of such a system is completely governed by the large S-wave scattering length. For example, if the interaction supports a two-particle bound state (simply called a *dimer* in the following) at $p = i\kappa$, the combination of Eqs. (2.21) and (2.19) tells us that

$$\kappa \approx \frac{1}{a_0} + \frac{r_0}{2a_0^2} = \frac{1}{a_0} (1 + \mathcal{O}(a_0/r_0)), \quad (2.60)$$

where the correction is negligible if $r_0 \ll a_0$. This means that at leading order the dimer binding energy is just

$$E_d = \frac{1}{2\mu a_0^2}. \quad (2.61)$$

⁴This can be seen, for example, from the effective range expansion (2.19). Since $\cot(x) = 1 + \mathcal{O}(x)$, one has $p^{2\ell+1}/\delta_\ell(p) \approx \text{const.}$ as $p \rightarrow 0$.

⁵For example, in the scattering of two identical fermions the Pauli principle only allows odd ℓ , such that the leading low-energy contribution is given by the P-wave ($\ell = 1$).

⁶This follows from the discussion in the preceding sections by noting that $\lim_{p \rightarrow 0} f_0(p) = -a_0$.

Whether or not a bound state actually exists can furthermore be related to the sign of the scattering length. In the conventions that we are using here, a large positive scattering length implies the existence of a shallow dimer state.⁷

The Efimov effect

A very intriguing phenomenon occurs in the three-body sector of a system of particles that have a large two-body scattering length and in that sense a strong pairwise interaction. It can be shown that the bound-state spectrum of such a system exhibits a tower of (approximately) geometrically-spaced three-body “trimer” states, *i.e.*, a series of bound-state energies fulfilling

$$E_{\text{trimer}}^{(n+1)} / E_{\text{trimer}}^{(n)} \approx \text{const.} \quad . \quad (2.62)$$

In the limit where the magnitude of a_0 goes to infinity,⁸ so does the number of trimer states, and the geometrical spacing becomes exact with a *universal* scaling factor determined only by the mass ratio of the particles. This effect was first proposed by (and named after) V. Efimov [25] and later proven by Amado and Nobel [26, 27]. For a detailed discussion of quantum systems with a large scattering length and the Efimov effect, we refer here to the review by Braaten and Hammer [28].

To conclude this subsection, we summarize that we speak of *low-energy universality* in the general sense whenever a description with finite-range interaction is a good approximation to describe the physics of a given (two-particle) system. In a manner of speaking, physics at low energies is governed by the tails of the (radial) wave functions, which have a universal analytic form, and the essential features of the system can be well described by just a few parameters, namely the scattering lengths and effective ranges for a small number of partial waves. Since the effective range expansion is valid in the complex p -plane, this includes the description of bound states with small binding energies. Moreover, if the (S-wave) scattering length is unnaturally large, this parameter governs the whole system and one finds relations that are “even more universal,” like the binding energies of shallow dimer states or the Efimov effect in the three-body sector. Finally, it is important to point out again that the above statements still hold (up to corrections that are often negligible) in the more realistic setup where the interaction has no strictly finite range but is short-ranged and falls off rapidly.

2.3.3 The theorist’s point of view

Having read the preceding sections, the caption above this sentence might seem confusing at first. By no means do we want to say that we now switch gears to look at physics from the theoretical side, but rather that this is what we have been doing all along so far.

Here, we want to emphasize that finite-range potentials are *not* an experimental concept but, since potentials are even not observable quantities, really just a convenient theoretical

⁷For a derivation of this statement see, for example, Ref. [23].

⁸More precisely, the relevant limit is $|a_0/R| \rightarrow \infty$, which means that the effect can also be found for zero-range interactions.

tool. The same should be said in fact, at least to a good extent, about partial-wave scattering phase shifts. What is directly accessible in scattering experiments (via count rates and their angular distribution) are (differential) cross sections and thus, according to Eq. (2.56), the absolute value squared of the scattering amplitude. Phase shifts are then only obtained from an inversion of Eq. (2.52), necessarily *truncated* at some ℓ and based on data in only a limited energy (and usually angular) regime. This procedure can be very delicate in practice and that the result, due to the limited amount of data, is not truly unique.

Potentials are still a very useful tool for the theoretical description of physical processes, and scattering phase shifts provide a convenient “interface” to compare the results of calculations with experiments, but it is important to keep in mind the limitations described above.

2.3.4 From potential models to a modern perspective

Although low-energy universality arises naturally in the theory of finite- or short-range interactions, it was first found as an experimental phenomenon. It was observed⁹ that low-energy S-wave scattering phase shifts in the two-nucleon system could be well described with just two parameters since the data points could be fitted by a straight line in a suitable representation – the left-hand side of the effective range expansion (2.19) or its Coulomb-modified analog that will be discussed in Chapter 4. Different forms of potentials could thus be used equally well to model the system as long as they had two parameters that could be adjusted to reproduce that line.

At the time, it was concluded that measurements at higher energies were needed to really determine the shape of the nuclear potentials. This led, subsequently to the construction of very sophisticated potential models, many of which, like Nijmegen I,II [29], AV18 [30], and CD-Bonn [31], are still well known and often used today (a comparison of the different models and an historical overview of their development can be found, for example, in Ref. [32]).

All of these potentials describe the nucleon–nucleon phase shifts (and deuteron properties) very well, but differ quite substantially in their details. Of course, this ambiguity simply illustrates explicitly the fact that potentials are not observable. This, together with the difficulty of these approaches to consistently describe and/or implement the physics of more than two particles (see, for example, Ref. [33]), as well as the essentially unsystematic way they are constructed, has led to the development of a more modern perspective. Rather than continuing the ultimately futile endeavor of trying to find *the* nuclear potential, one simply constructs so-called *effective potentials* as a systematic expansion, where new operators are added to describe physics at subsequently higher energy scales (and/or of an increasing number of nucleons). This approach explicitly incorporates the observed low-energy universality, or can, in fact, be characterized as being based on it. More generally, the underlying concept is that of *effective field theory (EFT)*, which we now turn to discuss in some more detail.

⁹See, for example the review of proton–proton scattering by Jackson and Blatt [11] and original references therein.

2.4 Effective field theory

The main concepts of effective field theories can be summarized as follows:

- First, choose degrees of freedom that are appropriate for the energy scale under consideration (nucleons instead of quarks, for example).
- Then, construct a Lagrangian out of fields corresponding to these degrees of freedom, including all terms allowed by general principles like unitarity, analyticity and whatever other symmetries relevant for the system at hand (like isospin, in the example above).
- Finally, since such a Lagrangian contains in principle infinitely many terms, a further key ingredient is an ordering scheme (“power counting”) that serves to estimate the relative importance of the individual terms.

The connection to low-energy universality is that the ordering in the final step is often (but not necessarily always or exclusively) based on the relative momenta in the system one wishes to describe. We will illustrate this in the following by looking at a few explicit examples.

First, it is important to point out that the coefficients of operators in a Lagrangian constructed in the way laid out above are not normally dictated by general concepts. Instead, these so-called *low-energy constants* have to be determined by *matching* the results of calculations to known observables.¹⁰ The predictive power of the theory then lies in the fact that usually the same coefficients (or combinations thereof) appear in different observables. Having measured some of them, it is possible to make predictions for others.

2.4.1 Historical overview

The approach laid out above was pioneered by Weinberg in Ref. [34], where (in the context of pion physics) he formulated the idea that a quantum field theory has, ultimately, no other content than analyticity, unitarity, cluster decomposition, and symmetry. Such “phenomenological Lagrangians” had been used before, but were usually based on current-algebra concepts (see, *e.g.*, Ref. [35]). The big step that Weinberg took was to promote them to the starting point of calculations, thereby abandoning their unsystematic heritage.

A key role in Weinberg’s original application to hadron physics at low energies is played by the approximate chiral $SU(2)_L \times SU(2)_R$ symmetry of the strong interaction, the spontaneous breaking of which is responsible for the pion mass being so small.¹¹ This mass and the momenta of low-energy pions are used as small scales in the power counting.

¹⁰Alternatively, if an underlying more fundamental theory is known, they can sometimes also be calculated from that.

¹¹If there was no explicit chiral-symmetry breaking, they would be massless Goldstone bosons.

Weinberg’s approach, which became famous as *chiral perturbation theory*, was worked out further by Gasser and Leutwyler [36, 37] and has a vast number of applications and extensions today. In particular, the formalism has been extended to include also nucleons and other baryons (see, for example, Refs. [38–40]). This important step made it possible to construct the effective nuclear potentials mentioned at the end of Section 2.3.4. In an idea that again goes back to Weinberg [41, 42], a low-energy expansion of the effective interaction between nucleons is built out of diagrams derived from the chiral Lagrangian. This means that rather than doing plain perturbation theory by summing Feynman diagrams up to a given order, the power counting is applied to derive an *effective potential*, which can subsequently be used in calculations based on Schrödinger (or Lippmann–Schwinger) equations.

Of course, with the above summary we have only scratched the surface of a very complex field. Much more detailed discussions of the points mentioned here (and many more) can be found in the reviews by Epelbaum *et al.* [43], or Machleidt and Entem [44], which we just refer to here for simplicity.

Furthermore, it is important to point out that although the origins of effective field theory lie in hadron and nuclear physics, it is by no means limited to those applications. In fact, it is used in many areas of modern theoretical physics. Since the key ingredient is merely a *separation* of scales and not that the total energy of the system one wishes to describe is a small scale, there are even applications in high-energy physics, like the soft-collinear effective theory started in Refs. [45, 46]. We do not make here the futile attempt to give a comprehensive list of current EFT applications. Rather, we focus on two examples that will play a role later in this work.

2.4.2 Pionless effective field theory

At very low energies in nuclear physics, even the pions can be “integrated out,” which then leaves only nucleons as effective degrees of freedom. The interactions between them are simple contact terms, corresponding to delta-peak potentials and derivatives thereof in configuration space, and since in the low-energy regime all relative momenta are small, a nonrelativistic description is appropriate. The latter means that all particles only propagate forward in time and that there is no pair creation. In fact, this kind of EFT can be thought of as a convenient reformulation of quantum mechanics.

Naturally, this *pionless effective field theory* is limited to energy (momentum) scales below the pion mass, but nevertheless it is very interesting and exhibits a rich set of features. The reason for this is that the S-wave nucleon–nucleon system is an important example for the case of unnaturally large scattering lengths. Both $a_d \approx 5.42$ fm in the 3S_1 (isospin 0) and $a_t \approx -23.71$ fm in the 1S_0 (isospin 1) channel are significantly larger than the typical scale of about 1.4 fm set by the inverse pion mass (*cf.* Section 2.3.2). The corresponding effective ranges, on the other hand, have the values 1.75 and 2.73 fm, respectively, and are thus indeed of the expected natural order of magnitude.¹²

¹²The numbers quoted here for the scattering lengths and effective ranges are quoted from Refs. [16] and [47].

The deuteron appears in this picture as a nearly universal shallow dimer state corresponding to the large positive scattering length a_d . From Eq. (2.61) one obtains $E_d \approx 1.4$ MeV as leading-order result for its binding energy, which is not far from the experimental value $E_d^{\text{exp}} = 2.225$ MeV [48]. The agreement here is rather coarse because the effective range in this channel is only about a factor of three smaller than the scattering length, which makes the range corrections to the leading-order expression quite significant. Indeed, if Eq. (2.60) is used to calculate the binding momentum including the effective-range term, the result is $\kappa \approx 45.6$ MeV, corresponding to a binding energy of about 2.21 MeV, much closer to the experimental value.

The presence of the shallow deuteron state has a significant impact on the construction of pionless effective field theory. Since perturbation theory cannot produce bound states, the applicability of the approach would naïvely be limited to momentum scales Q below the deuteron pole, $Q < \kappa_d \sim 1/a_d$. If one also takes into account the pole corresponding to the virtual bound state in the 1S_0 channel, where the scattering length is larger yet, the range of applicability is even narrowed down to $Q < 1/a_t$. In either case, this is much smaller than the natural breakdown scale set by the pion mass. The solution, introduced in Refs. [49–52], is to include certain contributions up to all orders in the perturbative expansion and thus generate the shallow states corresponding to the large scattering lengths in a nonperturbative manner. The theory with this scheme applied and its low-energy constants fixed by matching two-body amplitudes to the effective range expansion is then valid for low-energy scales of the order $Q \sim 1/a_{d,t}$ and with the natural breakdown scale $\Lambda \sim m_\pi^{-1}$, corresponding to an EFT expansion parameter $Q/\Lambda \sim 1/3$.¹³ In Refs. [53–55], the formalism has been extended to the three-nucleon sector. The situation there is particularly interesting because the triton can be interpreted as an approximate Efimov state.

Since the physics it describes are to a significant extent governed by the large S-wave scattering lengths, pionless effective field theory has a lot in common with a simpler EFT that describes identical bosons with a large two-body scattering length. The key features mentioned above (nonperturbative resummation to reproduce shallow dimer bound states and the Efimov effect in the three-body sector) can be studied there without complications due to different spin and isospin channels. A comprehensive review of this EFT and a broader discussion of universality in systems with large scattering length can be found in the review by Braaten and Hammer [28]. For applications to cold-atomic systems with large scattering lengths, see also K. Helfrich’s doctoral thesis [56] and further references therein. In Chapter 6, we will discuss pionless effective theory in more detail and use it to analyze the proton–deuteron system.

2.4.3 Effective field theory for nuclear halo states

Almost the same formalism as for the pionless EFT discussed above can also be used to construct an effective field theory that is useful to calculate properties of nuclear halo systems. Such states, also called *halo nuclei*, can be thought of as a tightly bound core

¹³Note that if the size of corrections is estimated directly in terms of the effective range parameters, one gets the same result: $1.75/5.42 \approx 0.32$.

nucleus with one or more weakly-bound valence nucleons (for reviews of such states see, for example, Refs. [57, 58]). The separation of scales, which is the crucial ingredient for the construction of an EFT, is given for such systems by the small separation energy of the valence nucleons compared to the binding energy of the core.¹⁴

In an effective two-body picture that neglects the internal structure of the core (which cannot be resolved at low energies), a one-nucleon halo nucleus can be thought of as a shallow dimer state that occurs due to a large scattering length in the corresponding nucleon–nucleus scattering system. This is exactly the same situation as with the deuteron in the few-nucleon sector, and it is thus natural to adopt the concepts of the pionless effective field theory described in the previous section. The resulting effective Lagrangian contains, in addition to the nucleon terms, an additional field to describe the core as a whole, interacting with the nucleons via contact terms and/or derivatives thereof. This so-called *halo EFT* was first introduced in Refs. [60, 61] to study neutron–alpha and has since then been extended to describe a number of other phenomena like alpha–alpha scattering [62], bound single-neutron halo states such as ^{11}Be [59] and ^8Li [63, 64], and various two-neutron halo systems [65–67]. Recently, it has also been used to calculate charge form factors of two-neutron halo nuclei [68].

2.5 Lattice calculations

In the preceding sections we have repeatedly touched the subject of nuclear physics, but almost exclusively discussed it directly from an effective point of view. It is thus due time to mention quantum chromodynamics (QCD) as the widely accepted underlying¹⁵ theory of the strong interaction which, up to electromagnetic and weak effects, ultimately governs the properties of nucleons and nuclei.¹⁶ It is defined by the Lagrangian

$$\begin{aligned} \mathcal{L}_{\text{QCD}} &= \sum_f \bar{\psi}_f (iD_\mu \gamma^\mu - m_f) \psi_f - \frac{1}{4} \sum_a F_{\mu\nu}^a F^{\mu\nu,a}, \\ D_\mu &= \partial_\mu + igA_\mu^a t^a, \quad F_{\mu\nu}^a = \partial_\mu A_\nu^a - \partial_\nu A_\mu^a + igf^{abc} A_\mu^b A_\nu^c, \end{aligned} \quad (2.63)$$

which is an essential component of the Standard Model of particle physics. In Eq. (2.63), the sum runs over all quark flavors f represented by the Dirac fermion field ψ_f and $A_\mu^a(x)$ are the gluon gauge fields. Furthermore, t^a and f^{abc} are the $SU(3)$ group generators and structure constants, and $a, b, c = 1, \dots, 8$ are the corresponding color indices.

In the limit of vanishing quark masses, $m_f = 0$ for all f , \mathcal{L}_{QCD} exhibits an exact chiral symmetry, which means that right and left-handed quark fields $\psi_{f,R/L} = (1 \pm \gamma_5)/2 \psi_f$ decouple. If one only considers two light quark flavors $f = u, d$, which is usually sufficient

¹⁴Alternatively, as it is done for example in Ref. [59], one can compare the large matter radius of the halo nucleus as a whole to the small radius of the core alone.

¹⁵We write “underlying” here to avoid the question of whether QCD can also be regarded as a *fundamental* theory. It is of course possible, if not likely, that QCD and the standard model in general are also just effective theories of some sort, and the author takes the stance that it is not even logically possible to assert any given theory as truly “fundamental.”

¹⁶Note that in nuclear physics electromagnetic effects are not a small correction, but play an important role for the description of all nuclei heavier than the deuteron.

for nuclear-physics applications, this is broken down spontaneously to the approximate isospin symmetry (exact in the limit $m_u = m_d$) that is still visible in the hadronic spectrum.

We assume all this to be well-known and will not go into further detail here. The only aspect really important for the present discussion is that the running of the strong coupling constant $\alpha_s = g^2/(4\pi)$ that makes QCD perturbative at high energy scales and leads to the famous “asymptotic freedom” at the same time renders the theory strongly-interacting and thus non-perturbative at low energies. This is directly reflected by the fact that quarks and gluons are not physically observable degrees of freedom, but only exist *confined* into hadrons.

One way to circumvent the breakdown of perturbation theory are the effective field theories introduced in Section 2.4. Yet, as powerful as they are, it is nevertheless desirable to also deduce the properties of hadrons, their interactions, and ultimately those of nuclei, directly from \mathcal{L}_{QCD} . A way to achieve this is to “solve” the theory numerically by putting it on a discretized space-time lattice.

2.5.1 Lattice QCD

The idea just mentioned was initially conceived by Wilson [69] in 1974 as an attempt to explain confinement. Although the latter is still an unsolved problem, with the rapid advance of computer power during the last two decades, the lattice formulation of QCD has evolved into a very successful tool. In the following few paragraphs, we will briefly review its main concepts. Much more thorough discussions of the topic can be found in introductory lattice QCD texts such as Refs. [70, 71].

As Davies puts it in Ref. [70], “*Lattice QCD is just QCD, no more and no less.*” Although in practice there are a number of technical issues—in particular with the implementation of fermions and chiral symmetry—this statement provides a good summary of the approach. Its starting point is the Feynman path-integral formulation of field theory, which encodes all physical information in the partition function

$$Z = \int \mathcal{D}\psi \mathcal{D}\bar{\psi} \mathcal{D}A_\mu^a e^{iS_{\text{QCD}}[\psi, \bar{\psi}, A_\mu^a]} . \quad (2.64)$$

Here,

$$S_{\text{QCD}} = \int d^4x \mathcal{L}_{\text{QCD}} \quad (2.65)$$

denotes the QCD action and we have omitted all flavor indices f for simplicity. Physical observables can be calculated by considering vacuum expectation values of suitable operators \mathcal{O} given by

$$\langle \mathcal{O} \rangle = \frac{1}{Z} \int \mathcal{D}\psi \mathcal{D}\bar{\psi} \mathcal{D}A_\mu^a \mathcal{O}[\psi, \bar{\psi}, A_\mu^a] e^{iS_{\text{QCD}}[\psi, \bar{\psi}, A_\mu^a]} . \quad (2.66)$$

Under a Wick rotation that yields a description in Euclidean spacetime, the exponential term in the above expression becomes

$$e^{iS_{\text{QCD}}[\psi, \bar{\psi}, A_\mu^a]} \longrightarrow e^{-S_{\text{QCD}}^E[\psi, \bar{\psi}, A_\mu^a]} , \quad (2.67)$$

where the superscript E indicates the Euclidean action. With this, complex phase oscillations in Eqs. (2.64) and (2.66) go over into exponential suppression factors of terms away from the classical (*i.e.*, minimal) action. The resulting expressions are then numerically well-behaved and one can calculate the functional integrals over the symbolic measure $\mathcal{D}\psi\mathcal{D}\bar{\psi}\mathcal{D}A_\mu^a$ by sampling all fields on a discrete space-time mesh, giving an ordinary four-dimensional integral at each point.¹⁷ This integral is, of course, a tremendously high-dimensional one and cannot be performed with straightforward numerical quadrature rules. Instead, one has to resort to Monte Carlo methods to make the calculation feasible at all. Even with that, the procedure in general still requires supercomputing power, and in practice one furthermore has to cope with a number of problems related to the numerical treatment, some of which we will come back to shortly in Section 2.5.3.

Still, over the last few years lattice QCD has been very successful in calculating hadronic properties “from first principles.” With steady improvements in both algorithms and computational facilities, hadron spectroscopy, as one of lattice QCD’s prime disciplines, is moving towards precision calculations [72, 73]. Beyond that, it is also possible to extract resonance properties [74] and pion scattering parameters [75–77], to name just a few examples. There are furthermore promising efforts to calculate nuclear physics processes directly with lattice QCD (see, for example, Ref. [78] and further references therein).

Despite the successes just mentioned, lattice QCD is still far from replacing effective field theory in low-energy hadron and nuclear physics. Instead, the two methods are to a good extent complementary. For example, due to computational limitations lattice calculations are usually performed at unphysically large quark masses, and results from chiral perturbation theory are then needed to perform extrapolations of the results back to the point of physical quark masses. On the other hand, lattice QCD can be used to calculate low-energy constants of chiral perturbation theory that would otherwise have to be fixed from experiments [79]. In that sense, it is possible to “close the gap” between the EFT and the underlying theory.

2.5.2 Nuclear lattice simulations

One can go even further and adopt the lattice approach directly to perform EFT calculations. This rather new idea opens the door for efficient calculations of few- and many-body systems, ranging from nuclear physics to condensed matter and atomic physics (overviews of computational methods and applications can be found in Refs. [80, 81]).

For nuclear physics, the EFT approach is interesting because in lattice QCD it is still very challenging to extract the properties of systems with more than two nucleons. The reason for this is that in such calculations most of the computational effort has to be spent for generating the correct degrees of freedom rather than the interactions between them. An overview of nuclear lattice simulations based on chiral effective theory and applied to selected nuclei with mass number up to $A = 12$ can be found in Refs. [82, 83]. Unlike

¹⁷In practice, the integral over the fermion fields is typically performed analytically with the help of Grassmann variables, yielding a modified action for the gluon fields that involves the determinant of a large matrix.

other nuclear many-body approaches like Green's Function Monte Carlo (GFMC) [84] or the No-Core Shell Model (NCSM) [85], the nuclear lattice approach is particularly suited to study nuclei with a pronounced cluster substructure, such as the famous Hoyle state in carbon-12 [86, 87].

2.5.3 Numerical aspects

All methods mentioned in the preceding sections have in common that by putting the physical system on a discrete space-time mesh one necessarily introduces numerical approximations.

Inherent to the approach is that the degrees of freedom no longer reside in a continuous space and time, but only on fixed sites¹⁸ which are separated by a lattice spacing a (we focus on the spatial separation here and for simplicity ignore that one can choose a different lattice spacing in the time direction). Most prominently, this quantity enters in the definition of derivatives as finite differences on the lattice, which only gives the continuum result up to higher orders in a . In practice, a has thus to be kept small to avoid large discretization artifacts, and ideally calculations have to be performed at a number of different lattice spacings in order to extrapolate the results to their continuum values.

Furthermore, since computing power is a finite resource, so is the space and time that can be simulated in a lattice calculation. Typically, one chooses a cube of box length L with periodic boundary conditions for the spatial simulation volume, which is used to sample the path integral for a number of time steps L_t . Naturally, the volume must not be too small compared to the typical length scale of the system one wants to simulate.

Both, the need to increase the simulation volume and decrease the lattice spacing drive up the computer time (and memory) required for a given calculation. However, while the continuum extrapolation is something that simply has to be done, the volume dependence of physical observables can actually be used as a tool. This idea, pioneered by Lüscher in the 1980s [8, 88], will play an important role in the following chapter.

¹⁸Strictly speaking, gauge fields like the gluons in lattice QCD are actually defined not on the lattice sites but on the links between them.

Chapter 3

Finite-volume calculations

Overview

In this chapter we derive general results for the mass (binding energy) shift of bound states with angular momentum $\ell \geq 1$ in a periodic finite volume. Most of the following content is the same as published in Ref. [4], some results of which were first summarized in a letter [2]. Section 3.7 summarizes results from Ref. [3] after giving a detailed derivation of the present author's main contribution to that publication.

3.1 Introduction

As already mentioned at the end of the previous chapter, lattice simulations are used in many areas of quantum physics, ranging from nuclear and particle physics to atomic and condensed matter physics [78, 80, 81, 89]. In such calculations, the system is solved numerically using a discrete space-time lattice over a finite volume. In practice, this finite volume is usually taken to be a cubic box with periodic boundary conditions. When simulating composite objects such as bound states, these boundaries of the box modify quantum wave functions, leading to finite-volume shifts in the binding energies of the states. A detailed knowledge of such effects is necessary in order to improve high-precision lattice calculations.

In Ref. [8], Lüscher derived a formula for the finite-volume mass shift of S-wave bound states of two particles with reduced mass μ interacting via a potential with finite range R . When such a state with energy $E = -E_B$ is put in a periodic cubic box of length L , its mass (energy) in the rest frame¹ is shifted by an amount

$$\Delta m_B = -3|A_\kappa|^2 \frac{e^{-\kappa L}}{\mu L} + \mathcal{O}(e^{-\sqrt{2}\kappa L}), \quad (3.1)$$

where $\kappa = \sqrt{2\mu E_B}$ is the binding momentum and A_κ is the asymptotic wave function normalization defined by $\psi_B(r) = A_\kappa e^{-\kappa r}/(\sqrt{4\pi r})$ for $r > R$; *cf.* Section 2.1.5. For

¹Lüscher uses the term “mass shift” because he was more interested in a relativistic setup. We adopt this convention here, but sometimes also use the term “binding energy shift” synonymously.

potentials with exponential fall-off, $V(r) \sim \exp(-r/R)$ for large r , the formula is modified by exponentially small corrections provided that the binding momentum κ is smaller than $1/R$.

The generalization of Lüscher’s formula (3.1) for the finite-volume mass shift to bound states in higher partial waves was briefly discussed in Ref. [2]. In this chapter we present the full derivation of these results as it appeared in Ref. [4]. We give explicit results for the mass shift of states with angular momentum up to $\ell = 3$ and discuss how, in general, the mass shift for a given state depends on its transformation properties with respect to the symmetry group of the cubic box. In addition to reducing finite-volume effects in precision lattice calculations, our results can also be used as a diagnostic tool to probe the angular momentum and radial structure of the bound-state wave function. Furthermore, we discuss how the mass-shift formula can be generalized to two-dimensional systems and different (“twisted”) boundary conditions (in three dimensions).

The latter result is a key ingredient for studying bound states that are *moving* in a finite periodic volume, which have a topological phase correction to the energy [3, 90]. This factor contains information about the number and mass of the constituents of the bound states, and it must be included when determining scattering phase shifts for composite objects in a finite volume. For a discussion of how scattering phase shifts in S- and higher partial waves can be extracted from finite-volume energy levels, see Refs. [88, 91].

Our results are universal and can be applied to a wide range of systems. In particle physics, for example, there is some interest in hadronic molecules with angular momentum [92–94]. In the case of S-waves, the deuteron and some exotic weakly-bound states such as the H-dibaryon were recently studied in lattice QCD [95]. Similar investigations for exotic bound states with angular momentum appear feasible in the future. In atomic physics, several experiments have investigated strongly-interacting P-wave Feshbach resonances in ${}^6\text{Li}$ and ${}^{40}\text{K}$ [96–98], which can be tuned to produce bound P-wave dimers. If such systems are simulated in a finite volume, our results can be used to describe the volume dependence of the dimer binding energies.

Other systems that are relevant in this context are the halo nuclei introduced in Section 2.4.3. Among these weakly-bound nuclei with molecular character there are some systems with nonzero orbital angular momentum. A well-known example of a P-wave halo state is the $J^P = 1/2^-$ excited state in ${}^{11}\text{Be}$. The electromagnetic properties of the low-lying states in this nucleus can be well described in a two-body halo picture of a ${}^{10}\text{Be}$ core and a neutron [59, 99]. In order to study such a system in, for example, a nuclear lattice simulation as discussed in Section 2.5.2, it is crucial to understand the volume dependence. A related class of systems is given by nuclei with an α -cluster structure such as ${}^8\text{Be}$ and excited states of ${}^{12}\text{C}$ [86, 100, 101].

Finally, we point out that the asymptotic normalization coefficient (ANC) of the bound-state wave function appears in the mass-shift formula. Our results can hence be used to extract this quantity from lattice calculations at finite volumes.

The chapter is organized as follows. Based largely on the prerequisites given in Chapter 2, we start with a general discussion of the finite-volume mass shift in Section 3.2. Lüscher’s result for S-waves is recovered in Section 3.3, while our extension to higher partial waves is given in Section 3.4. In particular, we discuss the mass shift for the irreducible repre-

representations of the cubic group, relate the sign of the shift to the leading parity, and derive a trace formula for the multiplet-averaged mass shift of states with arbitrary angular momentum ℓ . In Section 3.5, we verify our results numerically for two model systems. The case of two spatial dimensions is treated in Section 3.6, while in Section 3.7 we discuss the mass shift for twisted boundary conditions and how it leads to topological phase factors in the finite-volume calculations of composite-particle scattering. Finally, a brief summary and outlook is given in Section 3.8.

3.2 Bound states in a finite volume

As a starting point, we first review several results from Ref. [8]. We closely follow Lüscher's derivation, but consider a more general system with arbitrary angular momentum and non-local interactions.

3.2.1 Infinite volume

Before we discuss the finite volume, we briefly review the infinite-volume case. Our basic setup is the one discussed in Section 2.1, *i.e.*, we consider a system of two spinless particles with reduced mass μ and zero total momentum with a rotationally-symmetric finite-range interaction described by the symmetric operator $V(\mathbf{r}, \mathbf{r}')$ in configuration space. We furthermore assume that the interaction is such that it supports a bound state $|\psi_B\rangle$ with energy $E = -E_B = -\kappa^2/(2\mu)$ and angular-momentum quantum numbers (ℓ, m) . We consider the full three-dimensional wave function in this chapter to capture the angular dependence of the state. Recall that the finite-range assumption on the potential implies that

$$V(\mathbf{r}, \mathbf{r}') = 0 \quad \text{if } |\mathbf{r}| > R \quad \text{or} \quad |\mathbf{r}'| > R. \quad (3.2)$$

The Schrödinger equation

$$\hat{H}|\psi_B\rangle = -E_B|\psi_B\rangle, \quad (3.3)$$

can be written as

$$-\frac{1}{2\mu}\Delta_r \psi_B(\mathbf{r}) + \int d^3r' V(\mathbf{r}, \mathbf{r}') \psi_B(\mathbf{r}') = -E_B \psi_B(\mathbf{r}) \quad (3.4)$$

in configuration space and for a local potential,

$$V(\mathbf{r}, \mathbf{r}') = V(\mathbf{r}) \delta^{(3)}(\mathbf{r} - \mathbf{r}'), \quad (3.5)$$

it reduces to the familiar form

$$\left[-\frac{1}{2\mu}\Delta_r + V(\mathbf{r}) \right] \psi_B(\mathbf{r}) = -E_B \psi_B(\mathbf{r}). \quad (3.6)$$

According to Eqs. (2.2) and (2.29), the asymptotic form of the wave function $\psi_B(\mathbf{r})$ is determined by the Riccati–Hankel function H_ℓ^+ ,

$$\psi_B(\mathbf{r}) = i^\ell A_\kappa Y_\ell^m(\mathbf{r}/r) \frac{H_\ell^+(i\kappa r)}{r} \quad (r > R), \quad (3.7)$$

regardless of the locality of the interaction, and where we have written the spherical harmonics as a function of the unit vector \mathbf{r}/r instead of the angles θ and ϕ . For future reference, we give here the explicit expressions for $H_\ell^+(z)$ for $\ell = 0, 1, 2$:

$$H_0^+(z) = e^{iz}, \quad (3.8a)$$

$$H_1^+(z) = \left(1 + \frac{i}{z}\right) e^{i(z-\pi/2)}, \quad (3.8b)$$

$$H_2^+(z) = \left(1 + \frac{3i}{z} - \frac{3}{z^2}\right) e^{i(z-\pi)}. \quad (3.8c)$$

3.2.2 Finite volume

We now consider what happens when the two-body system is put into a periodic cubic box with edge length $L \gg R$. For this problem it is convenient to define a periodic extension of the potential

$$V_L(\mathbf{r}, \mathbf{r}') = \sum_{\mathbf{n} \in \mathbb{Z}^3} V(\mathbf{r} + \mathbf{n}L, \mathbf{r}' + \mathbf{n}L). \quad (3.9)$$

We take $|\psi\rangle$ to be an exact periodic solution of the finite-volume Schrödinger equation,

$$\hat{H}_L |\psi\rangle = -E_B(L) |\psi\rangle, \quad (3.10)$$

with the finite-volume Hamiltonian $\hat{H}_L = \hat{H}_0 + \hat{V}_L$ and the volume-dependent binding energy $E_B(L)$. The periodic boundary conditions that we impose require that

$$\psi(\mathbf{r} + \mathbf{n}L) = \psi(\mathbf{r}) \quad (3.11)$$

for all integer vectors $\mathbf{n} \in \mathbb{Z}^3$. It is clear that $E_B(L)$ approaches the infinite-volume eigenvalue E_B and that $|\psi\rangle \rightarrow |\psi_B\rangle$ as $L \rightarrow \infty$.

We now derive a formula for the finite-volume mass (energy) shift,

$$\Delta m_B \equiv E_B(\infty) - E_B(L). \quad (3.12)$$

To proceed, we define a state $|\psi_0\rangle$ by adding together periodic copies of the infinite-volume wave function in (3.4),

$$\langle \mathbf{r} | \psi_0 \rangle = \psi_0(\mathbf{r}) = \sum_{\mathbf{n}} \psi_B(\mathbf{r} + \mathbf{n}L). \quad (3.13)$$

This clearly satisfies the periodicity condition (3.11). Acting upon this state with the

finite-volume Hamiltonian, we get

$$\begin{aligned}
H_L \psi_0(\mathbf{r}) &= H_0 \sum_{\mathbf{n}'} \psi_B(\mathbf{r} + \mathbf{n}'L) + \sum_{\mathbf{n}'} \sum_{\mathbf{n}} \int d^3 r' V(\mathbf{r} + \mathbf{n}L, \mathbf{r}' + \mathbf{n}L) \psi_B(\mathbf{r}' + \mathbf{n}'L) \\
&= \sum_{\mathbf{n}'} \left\{ H_0 \psi_B(\mathbf{r} + \mathbf{n}'L) + \int d^3 r' V(\mathbf{r} + \mathbf{n}'L, \mathbf{r}' + \mathbf{n}'L) \psi_B(\mathbf{r}' + \mathbf{n}'L) \right. \\
&\quad \left. + \sum_{\mathbf{n} \neq \mathbf{n}'} \int d^3 r' V(\mathbf{r} + \mathbf{n}L, \mathbf{r}' + \mathbf{n}L) \psi_B(\mathbf{r}' + \mathbf{n}'L) \right\} \\
&= -E_B(\infty) \sum_{\mathbf{n}'} \psi_B(\mathbf{r} + \mathbf{n}'L) + \sum_{\mathbf{n}'} \sum_{\mathbf{n} \neq \mathbf{n}'} \int d^3 r' V(\mathbf{r} + \mathbf{n}L, \mathbf{r}' + \mathbf{n}L) \psi_B(\mathbf{r}' + \mathbf{n}'L).
\end{aligned} \tag{3.14}$$

The final result can be written as

$$\hat{H}_L |\psi_0\rangle = -E_B(\infty) |\psi_0\rangle + |\eta\rangle, \tag{3.15}$$

where we have defined $|\eta\rangle$ as

$$\eta(\mathbf{r}) = \sum_{\mathbf{n}'} \sum_{\mathbf{n} \neq \mathbf{n}'} \int d^3 r' V(\mathbf{r} + \mathbf{n}L, \mathbf{r}' + \mathbf{n}L) \psi_B(\mathbf{r}' + \mathbf{n}'L). \tag{3.16}$$

With the substitution $\mathbf{r}' \rightarrow \mathbf{r}' - \mathbf{n}L$ for each term in the sum, this can be rewritten as

$$\eta(\mathbf{r}) = \sum_{\mathbf{n}'} \sum_{\mathbf{n} \neq \mathbf{n}'} \int d^3 r' V(\mathbf{r} + \mathbf{n}L, \mathbf{r}') \psi_B(\mathbf{r}' + (\mathbf{n}' - \mathbf{n})L). \tag{3.17}$$

Due to the finite range of the potential we only get contributions from the domain $|\mathbf{r}'| < R$. We note that $|\mathbf{r}' + (\mathbf{n}' - \mathbf{n})L| > R$ when $\mathbf{n} \neq \mathbf{n}'$ and $R \ll L$. Therefore, we can use the asymptotic form of the wave function and find that $|\eta\rangle = \mathcal{O}(e^{-\kappa L})$. This means that $|\psi_0\rangle$ is an approximate solution of the finite-volume Schrödinger equation (3.10) for large L . Motivated by this, we write the exact finite-volume solution $|\psi\rangle$ explicitly as

$$|\psi\rangle = \alpha |\psi_0\rangle + |\psi'\rangle \quad \text{with} \quad |\psi'\rangle = \mathcal{O}(e^{-\kappa L}). \tag{3.18}$$

We take $|\psi\rangle$ to be unit-normalized per volume L^3 . The same is true of $|\psi_0\rangle$ up to corrections of order $e^{-\kappa L}$. We will choose α in Eq. (3.18) such that

$$\langle \psi_0 | \psi' \rangle = 0. \tag{3.19}$$

Consider now the matrix element $\langle \psi | \hat{H}_L | \psi_0 \rangle$. Acting with \hat{H}_L on $|\psi_0\rangle$, we get

$$\langle \psi | \hat{H}_L | \psi_0 \rangle = -E_B(\infty) \langle \psi | \psi_0 \rangle + \langle \psi | \eta \rangle = -E_B(\infty) \langle \psi_0 | \psi_0 \rangle \cdot \alpha + \langle \psi | \eta \rangle \tag{3.20}$$

according to (3.15) and (3.18). On the other hand, acting with \hat{H}_L on $\langle \psi |$ yields

$$\langle \psi | \hat{H}_L | \psi_0 \rangle = -E_B(L) \langle \psi | \psi_0 \rangle = -E_B(L) \langle \psi_0 | \psi_0 \rangle \cdot \alpha. \tag{3.21}$$

Combining these two results we find

$$E_B(\infty) - E_B(L) = \Delta m_B = \frac{\langle \psi | \eta \rangle}{\alpha \langle \psi_0 | \psi_0 \rangle}. \quad (3.22)$$

We first consider the numerator in this expression. Obviously,

$$\langle \psi | \eta \rangle = \alpha \langle \psi_0 | \eta \rangle + \langle \psi' | \eta \rangle = \alpha \langle \psi_0 | \eta \rangle + \mathcal{O}(e^{-2\kappa L}). \quad (3.23)$$

Note that the factor of α here will cancel the α in the denominator of Eq. (3.22). We can now simplify further, starting with

$$\langle \psi_0 | \eta \rangle = \sum_{\mathbf{n}''} \sum_{\mathbf{n}'} \sum_{\mathbf{n} \neq \mathbf{n}'} \int d^3 r \int d^3 r' \psi_B^*(\mathbf{r} + \mathbf{n}''L) V(\mathbf{r} + \mathbf{n}L, \mathbf{r}' + \mathbf{n}L) \psi_B(\mathbf{r}' + \mathbf{n}'L). \quad (3.24)$$

For each \mathbf{n} we can make the substitutions $\mathbf{r} \rightarrow \mathbf{r} - \mathbf{n}L$ and $\mathbf{r}' \rightarrow \mathbf{r}' - \mathbf{n}L$. These leave the integrals invariant, and we get

$$\langle \psi_0 | \eta \rangle = \sum_{\mathbf{n}''} \sum_{\mathbf{n}'} \sum_{\mathbf{n} \neq \mathbf{n}'} \int d^3 r \int d^3 r' \psi_B^*(\mathbf{r} + (\mathbf{n}'' - \mathbf{n})L) V(\mathbf{r}, \mathbf{r}') \psi_B(\mathbf{r}' + (\mathbf{n}' - \mathbf{n})L). \quad (3.25)$$

Setting $\mathbf{m} = \mathbf{n}' - \mathbf{n}$ and $\mathbf{m}' = \mathbf{n}'' - \mathbf{n}$ yields

$$\langle \psi_0 | \eta \rangle = C \cdot \sum_{\mathbf{m}'} \sum_{\mathbf{m} \neq \mathbf{0}} \int d^3 r \int d^3 r' \psi_B^*(\mathbf{r} + \mathbf{m}'L) V(\mathbf{r}, \mathbf{r}') \psi_B(\mathbf{r}' + \mathbf{m}L), \quad (3.26)$$

where C counts the number of repeated periodic copies. The fact that C diverges simply reflects the fact that we are working with periodic wave functions with normalization measured per volume L^3 , and C will cancel in the final result. For the integral to be non-zero, both \mathbf{r} and \mathbf{r}' have to be close to $\mathbf{0}$ due to the finite range of the potential. From the assumption $L \gg R$ it then follows that all terms with $\mathbf{m}' \neq \mathbf{0}$ are suppressed by at least a factor of $e^{-2\kappa L}$, and we have

$$\langle \psi_0 | \eta \rangle = C \cdot \sum_{\mathbf{m} \neq \mathbf{0}} \int d^3 r \int d^3 r' \psi_B^*(\mathbf{r}) V(\mathbf{r}, \mathbf{r}') \psi_B(\mathbf{r}' + \mathbf{m}L) + \mathcal{O}(e^{-2\kappa L}). \quad (3.27)$$

The possible nonvanishing values of $|\mathbf{m}|$ are $1, \sqrt{2}, \sqrt{3}, \dots$. We therefore arrive at

$$\langle \psi_0 | \eta \rangle = C \cdot \sum_{|\mathbf{m}|=1} \int d^3 r \int d^3 r' \psi_B^*(\mathbf{r}) V(\mathbf{r}, \mathbf{r}') \psi_B(\mathbf{r}' + \mathbf{m}L) + \mathcal{O}(e^{-\sqrt{2}\kappa L}). \quad (3.28)$$

For the denominator in (3.22), an analogous procedure yields

$$\langle \psi_0 | \psi_0 \rangle = C \cdot \sum_{\mathbf{m}} \int d^3 r \psi_B^*(\mathbf{r}) \psi_B(\mathbf{r} + \mathbf{m}L) = C \cdot [1 + \mathcal{O}(e^{-\kappa L})] \quad (3.29)$$

with the same constant C as above. Combining (3.28) and (3.29), the constant cancels and we get

$$\Delta m_B = \sum_{|\mathbf{n}|=1} \int d^3 r \int d^3 r' \psi_B^*(\mathbf{r}) V(\mathbf{r}, \mathbf{r}') \psi_B(\mathbf{r}' + \mathbf{n}L) + \mathcal{O}(e^{-\sqrt{2}\kappa L}), \quad (3.30)$$

where we have renamed \mathbf{m} back to \mathbf{n} .

Eq. (3.30) is a general result valid for any angular momentum. The dependence of the mass shift on quantum numbers (ℓ, m) will emerge from the wave function ψ_B and the resulting overlap integrals in (3.30). In the following, we explore this dependence in detail and denote the mass shift as $\Delta m_B^{(\ell, m)}$.

3.3 S-wave result

For $\ell = 0$ the asymptotic wave function (3.7) is simply given as

$$\psi_B(\mathbf{r}) = \psi_B(|\mathbf{r}|) = \sqrt{\frac{1}{4\pi}} \frac{u_0(r)}{r} \quad (3.31a)$$

with

$$u_0(r) = A_\kappa H_0^+(i\kappa r) = A_\kappa e^{-\kappa r} \quad \text{for } r > R. \quad (3.31b)$$

Due to the finite range $R \ll L$ of the potential we only have contributions with $|\mathbf{r}' + \mathbf{n}L| > R$ in Eq. (3.30). Hence we can insert the asymptotic form for $\psi_B(\mathbf{r}' + \mathbf{n}L)$ and get

$$\Delta m_B^{(0,0)} = \frac{A_\kappa}{\sqrt{4\pi}} \sum_{|\mathbf{n}|=1} \int d^3r \int d^3r' \psi_B^*(|\mathbf{r}|) V(\mathbf{r}, \mathbf{r}') \frac{e^{-\kappa|\mathbf{r}'+\mathbf{n}L|}}{|\mathbf{r}'+\mathbf{n}L|} + \mathcal{O}(e^{-\sqrt{2}\kappa L}). \quad (3.32)$$

We can furthermore use the Schrödinger equation (3.4) to eliminate the potential. Doing this and then renaming $\mathbf{r}' \rightarrow \mathbf{r}$, we get

$$\begin{aligned} \Delta m_B^{(0,0)} &= \frac{A_\kappa}{\sqrt{4\pi}} \sum_{|\mathbf{n}|=1} \int d^3r \left\{ \left[\frac{\Delta_r}{2\mu} - E_B \right] \psi_B^*(|\mathbf{r}|) \right\} \frac{e^{-\kappa|\mathbf{r}+\mathbf{n}L|}}{|\mathbf{r}+\mathbf{n}L|} + \mathcal{O}(e^{-\sqrt{2}\kappa L}) \\ &= \frac{A_\kappa}{\sqrt{4\pi}} \sum_{|\mathbf{n}|=1} \int d^3r \psi_B^*(|\mathbf{r}-\mathbf{n}L|) \frac{1}{2\mu} [\Delta_r - \kappa^2] \frac{e^{-\kappa r}}{r} + \mathcal{O}(e^{-\sqrt{2}\kappa L}). \end{aligned} \quad (3.33)$$

In the second line we have shifted the integration variable and used partial integration to let the Laplacian act on $\exp(-\kappa r)/r$. Finally, we use the fact that $\exp(-\kappa r)/(4\pi r)$ is a Green's function for the operator $\Delta_r - \kappa^2$,

$$[\Delta_r - \kappa^2] \frac{e^{-\kappa r}}{4\pi r} = -\delta^{(3)}(\mathbf{r}), \quad (3.34)$$

cf. Eq.(2.41). This allows us to trivially solve the integral and arrive at

$$\begin{aligned} \Delta m_B^{(0,0)} &= -\frac{\sqrt{\pi} A_\kappa}{\mu} \sum_{|\mathbf{n}|=1} \psi_B^*(|\mathbf{n}L|) + \mathcal{O}(e^{-\sqrt{2}\kappa L}) \\ &= -3|A_\kappa|^2 \frac{e^{-\kappa L}}{\mu L} + \mathcal{O}(e^{-\sqrt{2}\kappa L}). \end{aligned} \quad (3.35)$$

In the last step we have inserted the asymptotic form of the wave function for $\psi_B^*(|\mathbf{n}L|) = \psi_B^*(L)$, and the sum yields a factor of six. This is just Lüscher's result (3.1) as given in the introduction.

3.4 Extension to higher partial waves

We now discuss the generalization of the mass-shift formula to arbitrary angular momentum. The general form for the asymptotic wave function is

$$\psi_{B,(\ell,m)}(\mathbf{r}) = Y_\ell^m(\theta, \phi) \frac{i^\ell A_\kappa H_\ell^+(i\kappa r)}{r}. \quad (3.36)$$

Inserting this into Eq. (3.30) and performing steps analogous to those for the S-wave case, we find

$$\Delta m_B = \sum_{|\mathbf{n}|=1} \int d^3r \left\{ \frac{1}{2\mu} [\Delta_r - \kappa^2] \psi_B^*(\mathbf{r} - \mathbf{n}L) \right\} Y_\ell^m(\theta, \phi) \frac{i^\ell A_\kappa H_\ell^+(i\kappa r)}{r} + \mathcal{O}(e^{-\sqrt{2}\kappa L}). \quad (3.37)$$

The crucial ingredient is now the relation

$$Y_\ell^m(\theta, \phi) \frac{H_\ell^+(i\kappa r)}{r} = (-i)^\ell R_\ell^m \left(-\frac{1}{\kappa} \nabla_r \right) \left[\frac{e^{-\kappa r}}{r} \right], \quad (3.38)$$

where R_ℓ^m are the solid harmonics defined via $R_\ell^m(x, y, z) = R_\ell^m(\mathbf{r}) = r^\ell Y_\ell^m(\theta, \phi)$. The result (3.38) follows from Lemma B.1 in Ref. [102], which proves that

$$R_\ell^m(\nabla_r) f(r) = R_\ell^m(\mathbf{r}) \left(\frac{1}{r} \frac{d}{dr} \right)^\ell f(r) \quad (3.39)$$

for any smooth function $f(r)$. From this we obtain Eq. (3.38) by using the relation²,

$$\left(\frac{1}{z} \frac{d}{dz} \right)^\ell h_0^{(1)}(z) = (-1)^\ell z^{-\ell} h_\ell^{(1)}(z) \quad (3.40)$$

and noting that $e^{-\kappa r} = H_0^+(i\kappa r)$ and $H_\ell^+(z) = iz h_\ell^{(1)}(z)$, where $h_\ell^{(1)}(z)$ is a spherical Hankel function of the first kind.

We can illustrate Eq. (3.38) with an example. For the case $\ell = 1$ and $m = 0$ we have

$$H_1^+(i\kappa r) \sim \left(1 + \frac{1}{\kappa r} \right) \frac{e^{-\kappa r}}{r} \quad (3.41)$$

and $Y_1^0(\theta, \phi) \propto \cos \theta$. A straightforward calculation using $\cos \theta = z/r$ shows that indeed

$$\cos \theta \left(1 + \frac{1}{\kappa r} \right) \frac{e^{-\kappa r}}{r} = -\frac{1}{\kappa} \frac{\partial}{\partial z} \left[\frac{e^{-\kappa r}}{r} \right]. \quad (3.42)$$

Rewriting Eq. (3.37) with the help of Eq. (3.38), we get

$$\Delta m_B = \frac{A_\kappa}{2\mu} \sum_{|\mathbf{n}|=1} \int d^3r \left\{ [\Delta_r - \kappa^2] \psi_B^*(\mathbf{r} - \mathbf{n}L) \right\} \left\{ R_\ell^m \left(-\frac{1}{\kappa} \nabla_r \right) \left[\frac{e^{-\kappa r}}{r} \right] \right\} + \mathcal{O}(e^{-\sqrt{2}\kappa L}). \quad (3.43)$$

²The relation (3.40) is just a special case of Eq. (10.1.24) in [103], which also holds for other spherical Bessel functions.

We now integrate by parts and pass the Laplacian through the differential operator $R_\ell^m(-\nabla_r/\kappa)$. Since the operators both consist of partial derivatives, this is not a problem when the wave function is smooth. We assume that this is the case, with the possible exception of a measure-zero region that can be omitted from the integral.

The partial integrations give a factor $(-1)^\ell$. We can now proceed in exactly the same way as for S-waves. Performing one more integration by parts so that the Laplacian acts on $\exp(-\kappa r)/r$ yields a delta function times a factor of -4π . The final result is then

$$\Delta m_B^{(\ell,m)} = (-1)^{\ell+1} \cdot \frac{2\pi A_\kappa}{\mu} \sum_{|\mathbf{n}|=1} R_\ell^m \left(-\frac{1}{\kappa} \nabla_r \right) \psi_{B,(\ell,m)}^*(\mathbf{r} - \mathbf{n}L) \Big|_{\mathbf{r}=\mathbf{0}} + \mathcal{O}(e^{-\sqrt{2}\kappa L}). \quad (3.44)$$

For $\psi_{B,(\ell,m)}^*$ we can insert the asymptotic form (3.36) since it is evaluated in the asymptotic region.

3.4.1 Results

For $\ell = 1$, we find the same result for all three P-wave states:

$$\Delta m_B^{(1,0)} = \Delta m_B^{(1,\pm 1)} = 3|A_\kappa|^2 \frac{e^{-\kappa L}}{\mu L} + \mathcal{O}(e^{-\sqrt{2}\kappa L}). \quad (3.45)$$

Compared to the S-wave case, the sign of the P-wave mass shift is reversed while the magnitude is exactly the same. Qualitatively, this means that S-wave bound states are more deeply bound when put in a finite volume while P-wave bound states are less bound (compared to the infinite-volume result). This behavior will be analyzed in more detail later.

We next discuss the results for $\ell = 2$. From Eq. (3.44) we find

$$\Delta m_B^{(2,0)} = -15|A_\kappa|^2 \frac{e^{-\kappa L}}{\mu L} \cdot F_2^0\left(\frac{1}{\kappa L}\right) + \mathcal{O}(e^{-\sqrt{2}\kappa L}), \quad (3.46)$$

$$\Delta m_B^{(2,\pm 1)} = +15|A_\kappa|^2 \frac{e^{-\kappa L}}{\mu L} \cdot F_2^1\left(\frac{1}{\kappa L}\right) + \mathcal{O}(e^{-\sqrt{2}\kappa L}), \quad (3.47)$$

$$\Delta m_B^{(2,\pm 2)} = -15|A_\kappa|^2 \frac{e^{-\kappa L}}{\mu L} \cdot F_2^2\left(\frac{1}{\kappa L}\right) + \mathcal{O}(e^{-\sqrt{2}\kappa L}), \quad (3.48)$$

where

$$F_2^0(x) = \frac{1}{2} + 3x + \frac{27}{2}x^2 + \frac{63}{2}x^3 + \frac{63}{2}x^4, \quad (3.49)$$

$$F_2^1(x) = 2x + 9x^2 + 21x^3 + 21x^4, \quad (3.50)$$

$$F_2^2(x) = \frac{1}{4} + \frac{1}{2}x + \frac{9}{4}x^2 + \frac{21}{4}x^3 + \frac{21}{4}x^4. \quad (3.51)$$

We note that here the size and even the sign of the mass shift both depend on the quantum number m . To understand this effects we need to take into account that our cubic finite volume breaks the rotational symmetry group down to a cubic subgroup.

Representations of the cubic group

The cubic symmetry group \mathcal{O} is a finite subgroup of $SO(3)$ with 24 elements. There are five irreducible representations of \mathcal{O} , conventionally called A_1 , A_2 , E , T_1 , and T_2 . Their dimensionalities are 1, 1, 2, 3, and 3, respectively. Irreducible representations D^ℓ of the rotation group $SO(3)$ are reducible with respect to \mathcal{O} for $\ell > 1$. For further details about the decomposition see, for example, Ref. [104].

In our discussion we assume that the infinite-volume system has no partial wave mixing, such that orbital angular momentum ℓ is a good quantum number. We also assume that there are no accidental degeneracies in the bound state spectrum, so we can use ℓ as a label for the family of cubic representations split apart at finite volume. Parity invariance remains unbroken by the cubic volume, and we have $P = (-1)^\ell$ just as in the infinite-volume case. For clarity, however, we will indicate parity explicitly with \pm superscripts in the following.

With our assumptions, an S-wave state in infinite volume will map onto an A_1^+ state at finite volume. Also a P-wave triplet will simply map onto the three elements of the T_1^- representation at finite volume. For $\ell = 2$, however, the five D-wave states are split into a T_2^+ triplet and an E^+ doublet,

$$D^2 = T_2^+ \oplus E^+. \quad (3.52)$$

In the following we use the notation $|\Gamma, \ell; \alpha\rangle$, $\alpha = 1, \dots, \dim(\Gamma)$ for the basis vectors of the irreducible cubic representations. We can rewrite the finite volume mass shift in Eq. (3.30) as

$$\Delta m_B^{(\Gamma, \ell, \alpha)} \equiv \langle \Gamma, \ell; \alpha | \hat{V} \sum_{|\mathbf{n}|=1} \hat{T}(\mathbf{n}L) | \Gamma, \ell; \alpha \rangle, \quad (3.53)$$

where $\hat{T}(\mathbf{x})$ is the translation operator for displacement by a vector \mathbf{x} . We can also calculate the matrix elements of Δm_B in the (ℓ, m) basis. In this case there will be off-diagonal matrix elements connecting (ℓ, m) and (ℓ, m') when m and m' are equivalent modulo 4.

According to Ref. [104], the unitary transformation between the two basis sets for the five D-wave states is

$$|T_2^+, 2; 1\rangle = -\frac{1}{\sqrt{2}} (|2, -1\rangle + |2, 1\rangle), \quad (3.54a)$$

$$|T_2^+, 2; 2\rangle = \frac{i}{\sqrt{2}} (|2, -1\rangle - |2, 1\rangle), \quad (3.54b)$$

$$|T_2^+, 2; 3\rangle = -\frac{1}{\sqrt{2}} (|2, -2\rangle - |2, 2\rangle) \quad (3.54c)$$

and

$$|E^+, 2; 1\rangle = |2, 0\rangle, \quad (3.55a)$$

$$|E^+, 2; 2\rangle = \frac{1}{\sqrt{2}} (|2, -2\rangle + |2, 2\rangle). \quad (3.55b)$$

So, for example, we have

$$\begin{aligned} \Delta m_B^{(T_2^+, 2; 1)} &= \frac{1}{2} \left(\Delta m_B^{(2, -1, -1)} + 2\Delta m_B^{(2, -1, 1)} + \Delta m_B^{(2, 1, 1)} \right) \\ &= -15|A_\kappa|^2 \frac{e^{-\kappa L}}{\mu L} \cdot \left(\frac{2}{\kappa L} + \frac{9}{\kappa^2 L^2} + \frac{21}{\kappa^3 L^3} + \frac{21}{\kappa^4 L^4} \right) + \mathcal{O}(e^{-\sqrt{2}\kappa L}), \end{aligned} \quad (3.56)$$

where we have defined

$$\Delta m_B^{(\ell, m_1, m_2)} = (-1)^{\ell+1} \cdot \frac{2\pi A_\kappa}{\mu} \sum_{|\mathbf{n}|=1} R_\ell^{m_1} \left(-\frac{1}{\kappa} \nabla_{\mathbf{r}} \right) \psi_{B,(\ell, m_2)}^*(\mathbf{r} - \mathbf{n}L) \Big|_{\mathbf{r}=0} + \mathcal{O}(e^{-\sqrt{2}\kappa L}) \quad (3.57)$$

as a straightforward generalization of Eq. (3.44).

As expected from cubic symmetry, the mass shift is the same for all three T_2^+ states and also within the E^+ doublet. To summarize our results, we write the mass shift for a state belonging to irreducible representation Γ with angular momentum ℓ as

$$\Delta m_B^{(\ell, \Gamma)} = \alpha \left(\frac{1}{\kappa L} \right) \cdot |A_\kappa|^2 \frac{e^{-\kappa L}}{\mu L} + \mathcal{O}(e^{-\sqrt{2}\kappa L}) \quad (3.58)$$

We list the coefficients $\alpha \left(\frac{1}{\kappa L} \right)$ for $\ell = 0, \dots, 3$ in Table 3.1.

ℓ	Γ	$\alpha(x)$
0	A_1^+	-3
1	T_1^-	+3
2	T_2^+	$30x + 135x^2 + 315x^3 + 315x^4$
2	E^+	$-1/2 (15 + 90x + 405x^2 + 945x^3 + 945x^4)$
3	A_2^-	$315x^2 + 2835x^3 + 12285x^4 + 28350x^5 + 28350x^6$
3	T_2^-	$-1/2 (105x + 945x^2 + 5355x^3 + 19530x^4 + 42525x^5 + 42525x^6)$
3	T_1^-	$1/2 (14 + 105x + 735x^2 + 3465x^3 + 11340x^4 + 23625x^5 + 23625x^6)$

Table 3.1: Coefficient $\alpha(x)$ in the expression for the finite-volume mass shifts for $\ell = 0, \dots, 3$. Γ indicates the corresponding representation of the cubic group.

3.4.2 Sign of the mass shift

The sign of the finite-volume mass shift can be understood in terms of the parity of the wave function. In infinite volume the tail of each bound state wave function must vanish at infinity. In the finite volume, however, the bound state wave functions with even parity along a given axis can remain nonzero everywhere. Only the derivative needs to vanish, and the kinetic energy is lowered by broadening the wave function profile. On the other hand, a wave function with odd parity along a given axis must change sign across the boundary. In this case the wave function profile is compressed and the kinetic energy thus increased. We have illustrated both cases for a one-dimensional square-well potential in Fig. 3.1.

In three dimensions, the situation is slightly more complicated, which can be seen from the fact that for $\ell = 2$ the sign of the mass shift depend on the representation of the cubic group even though the parity is just $(-1)^2 = +1$ for all states. In order to understand this we consider the basis polynomials for the cubic representations. These basis polynomials are obtained by decomposing the cubic basis vectors in terms of solid harmonics which

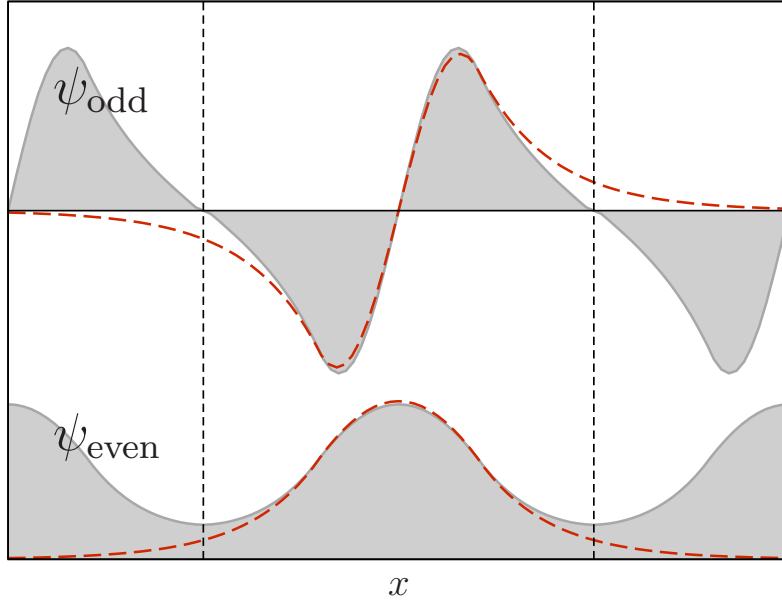


Figure 3.1: Wave functions with even (bottom) and odd parity (top) for a one-dimensional square well potential in a box with periodic boundary conditions. The dashed lines give the infinite volume solutions for comparison.

are homogeneous polynomials in x , y and z . For $\ell = 0, \dots, 4$ the basis polynomials are given explicitly in [102].

For a given polynomial $P(x, y, z)$, we define its *leading parity* as

$$\text{lp } P = (-1)^{d_{\max}}, \quad (3.59)$$

where

$$d_{\max} = \max\{\deg_x P, \deg_y P, \deg_z P\} \quad (3.60)$$

is the maximum degree of P with respect to any one of the three variables. It is this leading parity that determines the asymptotic behavior of the mass shift as $\kappa L \rightarrow \infty$. More precisely, we have

$$\alpha\left(\frac{1}{\kappa L}\right) \sim (-1)^{d_{\max}+1} \left(\frac{1}{\kappa L}\right)^{\ell-d_{\max}} \quad \text{as } \kappa L \rightarrow \infty \quad (3.61)$$

for the $\alpha\left(\frac{1}{\kappa L}\right)$ in Eq. (3.58).

It can easily be checked that this relation holds for all results presented in Table 3.1. For $\ell = 2$, for example, we have the basis polynomials

$$P_{2,T_2^+} \sim xy, yz, zx, \quad (3.62a)$$

$$P_{2,E^+} \sim x^2 - y^2, y^2 - z^2, \quad (3.62b)$$

and hence $d_{\max} = 1$ for the T_2^+ representation and $d_{\max} = 2$ for the E^+ representation.

3.4.3 Trace formula

The expressions for the finite-volume mass shift become simpler when we sum over all m for a given ℓ . We can rewrite Eq. (3.44) as

$$\Delta m_B^{(\ell,m)} = (-1)^{\ell+1} \cdot \frac{2\pi A_\kappa}{\mu} \sum_{|\mathbf{n}|=1} R_\ell^m \left(-\frac{1}{\kappa} \nabla_r \right) \psi_{B,(\ell,m)}^*(\mathbf{r}) \Big|_{\mathbf{r}=\mathbf{n}L} + \mathcal{O}(e^{-\sqrt{2}\kappa L}). \quad (3.63)$$

Inserting the asymptotic form of the wave function,

$$\psi_{B,(\ell,m)}^*(\mathbf{r}) \Big|_{\mathbf{r}=\mathbf{n}L} = \left[Y_\ell^m(\theta, \phi) \frac{i^\ell A_\kappa H_\ell^+(i\kappa r)}{r} \right]^* \Big|_{\mathbf{r}=\mathbf{n}L}, \quad (3.64)$$

and using Eq. (3.38) a second time yields

$$\Delta m_B^{(\ell,m)} = (-1)^{\ell+1} \cdot \frac{2\pi |A_\kappa|^2}{\mu} \sum_{|\mathbf{n}|=1} R_\ell^m \left(-\frac{1}{\kappa} \nabla_r \right) R_\ell^{*m} \left(-\frac{1}{\kappa} \nabla_r \right) \left[\frac{e^{-\kappa r}}{r} \right] \Big|_{\mathbf{r}=\mathbf{n}L} + \mathcal{O}(e^{-\sqrt{2}\kappa L}). \quad (3.65)$$

Now, from the well-known relation

$$\sum_{m=-\ell}^{\ell} Y_\ell^m(\theta, \phi) Y_\ell^{*m}(\theta, \phi) = \frac{2\ell + 1}{4\pi} \quad (3.66)$$

and $R_\ell^m(\mathbf{r}) = r^\ell Y_\ell^m(\theta, \phi)$ we get an analogous expression for the solid harmonics, which then carries over to

$$\sum_{m=-\ell}^{\ell} R_\ell^m \left(-\frac{1}{\kappa} \nabla_r \right) R_\ell^{*m} \left(-\frac{1}{\kappa} \nabla_r \right) f(r) = \frac{1}{\kappa^{2\ell}} \cdot \frac{2\ell + 1}{4\pi} (\Delta_r)^\ell f(r) \quad (3.67)$$

for any sufficiently smooth function $f(r)$. Finally, we have

$$(\Delta_r)^\ell \frac{e^{-\kappa r}}{r} = \kappa^{2\ell} \frac{e^{-\kappa r}}{r} \quad (r \neq 0), \quad (3.68)$$

which follows from Eq. (3.34). Putting everything together, we arrive at

$$\begin{aligned} \sum_{m=-\ell}^{\ell} \Delta m_B^{(\ell,m)} &= (-1)^{\ell+1} \cdot \frac{2\pi |A_\kappa|^2}{\mu} \cdot \frac{2\ell + 1}{4\pi} \sum_{|\mathbf{n}|=1} \frac{1}{\kappa^{2\ell}} (\Delta_r)^\ell \left[\frac{e^{-\kappa r}}{r} \right] \Big|_{\mathbf{r}=\mathbf{n}L} + \mathcal{O}(e^{-\sqrt{2}\kappa L}) \\ &= (-1)^{\ell+1} (2\ell + 1) \cdot 3 |A_\kappa|^2 \frac{e^{-\kappa L}}{\mu L} + \mathcal{O}(e^{-\sqrt{2}\kappa L}), \end{aligned} \quad (3.69)$$

where the sum just yields a factor of six. Dividing by $2\ell + 1$, we obtain the average mass shift for states with angular momentum ℓ ,

$$\Delta m_B^{(\ell)} = (-1)^{\ell+1} \cdot 3 |A_\kappa|^2 \frac{e^{-\kappa L}}{\mu L} + \mathcal{O}(e^{-\sqrt{2}\kappa L}). \quad (3.70)$$

Apart from the alternating sign, this average shift is independent of ℓ .

Eq. (3.70) can be verified explicitly for the results presented in Section 3.4.1 (*cf.* Table 3.1). For $\ell = 2$, for example, one has to average over the three-dimensional representation T_2^+ and the two-dimensional representation E^+ .³

3.5 Numerical tests

In order to verify our predictions numerically, we put the Schrödinger equation (3.10) on a discrete spatial lattice such that the Hamiltonian becomes an ordinary matrix. We then calculate the corresponding energy eigenvalues and eigenvectors.

3.5.1 Lattice discretization

We use a hat symbol to denote dimensionless lattice units. For example, we have

$$\hat{L} = L/a \quad \text{and} \quad \hat{E}_B = E_B \cdot a, \quad (3.71)$$

where a denotes the lattice spacing. The free lattice Hamiltonian is given by

$$\hat{H}_0 = \sum_{\hat{\mathbf{n}}} \left[\frac{3}{\hat{\mu}} a^\dagger(\hat{\mathbf{n}})a(\hat{\mathbf{n}}) - \frac{1}{2\hat{\mu}} \sum_{l=1,2,3} (a^\dagger(\hat{\mathbf{n}})a(\hat{\mathbf{n}} + \hat{\mathbf{e}}_l) + a^\dagger(\hat{\mathbf{n}})a(\hat{\mathbf{n}} - \hat{\mathbf{e}}_l)) \right] \quad (3.72)$$

where $a^\dagger(\hat{\mathbf{n}})$ and $a(\hat{\mathbf{n}})$ are creation and annihilation operators for a lattice site $\hat{\mathbf{n}}$ and $\hat{\mathbf{e}}_l$ is a unit vector in the l -direction. The corresponding lattice dispersion relation is

$$\hat{E}(\hat{\mathbf{q}}) = \frac{Q^2(\hat{\mathbf{q}})}{2\hat{\mu}} \quad (3.73)$$

with the lattice function

$$Q^2(\hat{\mathbf{q}}) = 2 \times \sum_{l=1,2,3} (1 - \cos \hat{q}_l) = \sum_{l=1,2,3} \hat{q}_l^2 [1 + \mathcal{O}(\hat{q}_l^2)] \quad (3.74)$$

and the lattice momenta

$$\hat{\mathbf{q}} = 2\pi\hat{\mathbf{n}}/\hat{L}. \quad (3.75)$$

The binding momentum for a bound state with energy $-\hat{E}_B$ is determined by

$$-\hat{\mu}\hat{E}_B = 1 - \cos(-i\hat{\kappa}) = 1 - \cosh(\hat{\kappa}). \quad (3.76)$$

The lattice Green's function for the Hamiltonian (3.72) is

$$\hat{G}(\hat{\mathbf{n}}, \hat{E}) = \frac{1}{L^3} \sum_{\hat{\mathbf{q}}} \frac{e^{-i\hat{\mathbf{q}} \cdot \hat{\mathbf{n}}}}{Q^2(\hat{\mathbf{q}}) + 2\hat{\mu}\hat{E}}. \quad (3.77)$$

³Note that the mapping from the angular momentum eigenstates to the cubic group states is a unitary transformation.

We impose periodic boundary conditions by defining the distance \hat{r} to the origin as

$$\hat{r}(\hat{\mathbf{n}}) = \sqrt{\sum_{l=1,2,3} \min \left\{ \hat{n}_l^2, (\hat{L} - \hat{n}_l)^2 \right\}}. \quad (3.78)$$

3.5.2 Methods

We calculate the mass shift using three different methods:

1. As a direct difference in energies, Eq. (3.12), where we use a very large volume (L_∞) to approximate the infinite-volume result.
2. From the overlap formula (3.30).
3. Using discretized versions of Eqs. (3.35) and (3.45), which we obtain by replacing $\exp(-\kappa r)/r$ with the lattice Green's function. More precisely, we write the asymptotic bound-state wave function (3.7) as

$$\psi_B(\mathbf{r}) = i^\ell A_\kappa Y_\ell^m(\mathbf{r}/r) H_\ell^+(i\kappa r) e^{\kappa r} \cdot 4\pi G_\kappa(r) \quad \text{for } r > R \quad (3.79)$$

and replace the continuum Green's function

$$G_\kappa(\mathbf{r}) = \frac{e^{-\kappa r}}{4\pi r} \quad (3.80)$$

with the lattice version

$$\hat{G}_{\hat{\kappa}}(\hat{\mathbf{n}}) \equiv \hat{G}\left(\hat{\mathbf{n}}, \frac{-\hat{\kappa}^2}{2\hat{\mu}}\right). \quad (3.81)$$

Effectively, this amounts to the replacement

$$e^{-\hat{\kappa}\hat{L}}/\hat{L} \longrightarrow 4\pi\hat{G}_{\hat{\kappa}}(\hat{L}, 0, 0) \quad (3.82)$$

in the mass-shift formula.

The lattice Green's function is also used to calculate the asymptotic normalization A_κ from the lattice data. This procedure has the advantage of avoiding large discretization errors.

3.5.3 Results

In the following we report physical quantities in units where the reduced mass μ is set to one.

Gaussian potential

We first use a Gaussian potential,

$$V_{\text{Gauss}}(r) = -V_0 \exp(-r^2/(2R^2)) , \quad (3.83)$$

with $R = 1$ and $V_0 = 6$. This potential does not have a finite range in a strict mathematical sense, but the range corrections can be entirely neglected in comparison with other errors in our numerical calculation. The smoothness of the Gaussian potential helps to minimize lattice discretization artifacts. In Fig. 3.2 we show the S- and P-wave mass shifts obtained with the three methods described in Section 3.5.2. The results from the three different methods described above agree well for both S- and P-waves. In order to compare the dependence on the box size L with the predicted behavior we have plotted $\log(L \cdot |\Delta m_B|)$ against L (we use the absolute value of Δm_B since the S-wave mass shift is negative). For both S- and P-waves, the expected linear dependence is clearly visible.

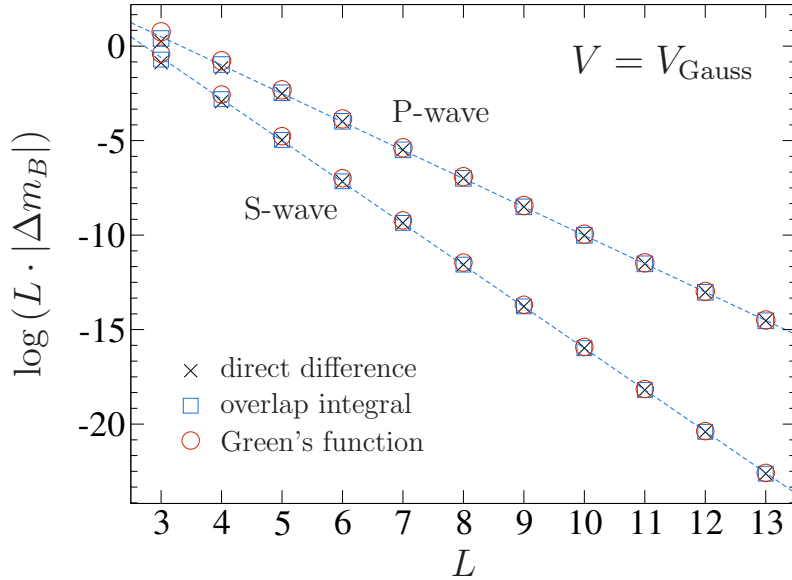


Figure 3.2: S-wave and P-wave mass shifts $\log(L \cdot |\Delta m_B|)$ as functions of the box size L (in lattice units) for a Gaussian potential. We show the results obtained from the direct difference Eq. (3.12) (crosses), evaluation of the overlap integral Eq. (3.30) (squares), and discretized versions of Eqs. (3.35), (3.45) (circles). The dashed lines show linear fits to the overlap integral results.

When we perform a linear fit to the overlap integral data (dashed lines in Fig. 3.2) we obtain $\kappa = 2.198 \pm 0.005$, $|A_\kappa| = 11.5 \pm 0.2$ for the S-wave results and $\kappa = 1.501 \pm 0.004$, $|A_\kappa| = 7.0 \pm 0.1$ for the P-wave results. The values for the asymptotic normalization constants are in good agreement with the results $|A_\kappa| \sim 11.5$ (S-wave) and $|A_\kappa| \sim 7.2$ (P-wave) that are obtained directly from the $L_\infty = 40$ data. Inserting the corresponding energy eigenvalue into the lattice dispersion relation (3.76), we find $\kappa \sim 2.211$ (S-wave) and $\kappa \sim 1.501$ (P-wave), again in very good agreement with the fit results. The remaining small discrepancies can be attributed to the mixing with higher partial waves induced by the lattice discretization and the fact that we have not performed a continuum extrapolation to vanishing lattice spacing.

Simple step potential

For a simple step potential,

$$V_{\text{step}}(r) = -V_0 \theta(R - r), \quad (3.84)$$

which we use with $R = 2$ and $V_0 = 3$, the numerical calculation becomes more difficult because the discontinuous shape introduces considerable lattice artifacts. Still, we discuss it here due to its strict finite range and since we find that for a small lattice spacing of $a = 0.2$ the results are satisfactory. In Fig. 3.3 we show a plot analogous to the one presented for the Gaussian potential. Again, the results from the different methods agree well and the expected linear behavior is clearly visible. Furthermore, the results from the three methods agree well with each other already for smaller L (compared to the results for the Gaussian potential), as expected from the fact that the step potential does not have a tail.

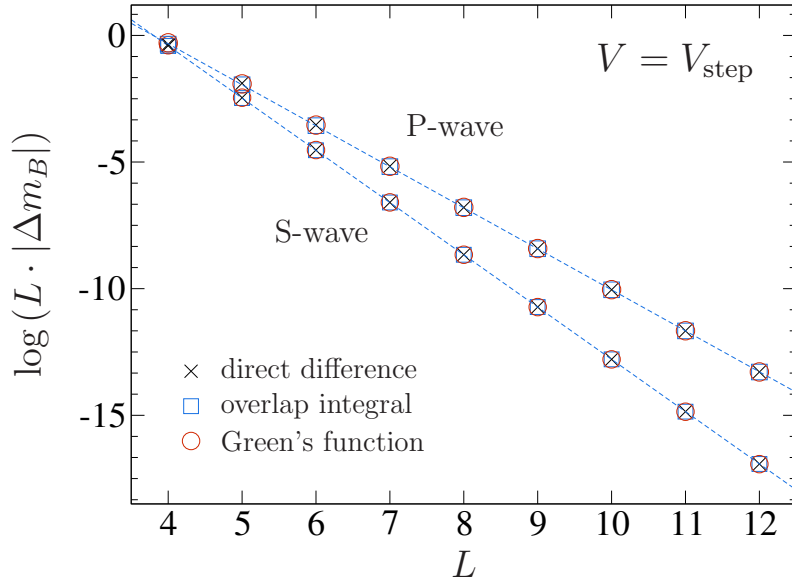


Figure 3.3: S-wave and P-wave mass shifts $\log(L \cdot |\Delta m_B|)$ as functions of the box size L (in lattice units) for a simple step potential. The symbols are as in Fig. 3.2.

From fitting to the overlap integral data (dashed lines in Fig. 3.3) we obtain $\kappa = 2.0636 \pm 0.0005$, $|A_\kappa| = 29.17 \pm 0.06$ for the S-wave results and $\kappa = 1.6192 \pm 0.0009$, $|A_\kappa| = 12.48 \pm 0.05$ for the P-wave results. From the $L_\infty = 40$ data we find $\kappa \sim 2.0666$, $|A_\kappa| \sim 29.6$ (S-wave) and $\kappa \sim 1.6242$, $|A_\kappa| \sim 12.8$ (P-wave). Given that we do not have error estimates for the $L_\infty = 40$ results, the overall agreement is quite good.

Finally, we also check our result for the D-wave mass splittings, using again the step potential with $a = 0.2$. In Fig. 3.4 we show the mass shift for the D-wave states in both the T_2^+ and the E^+ representation. Due to the polynomial coefficients $\alpha\left(\frac{1}{\kappa L}\right)$ —see Eq. (3.58) and Table 3.1—one does not expect a linear dependence on L for $\log(L \cdot |\Delta m_B|)$. Hence, we simply plot Δm_B as a function of L directly and do not perform a fit. Nevertheless, we see that (except for very small L , where obviously the condition $L \gg R$ is not satisfied) the agreement between the three methods to calculate Δm_B is very good and hence conclude that our mass-shift formula indeed gives the right result also for $\ell = 2$.

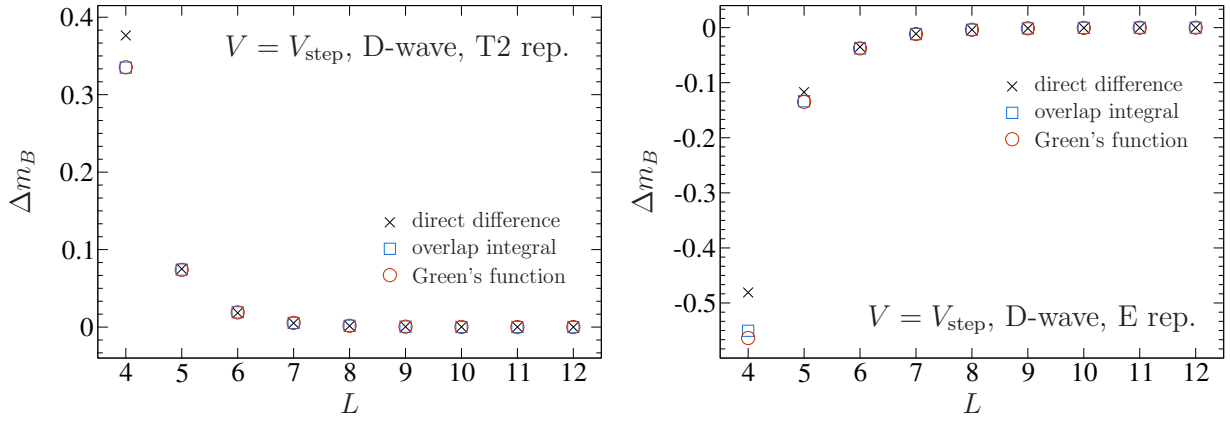


Figure 3.4: D-wave, mass shift Δm_B for T_2^+ rep. (left panel) and E^+ rep. (right panel) as a function of the box size L (in lattice units) for a simple step potential. The symbols are as in Fig. 3.2.

3.6 Two-dimensional systems

In this section we derive a formula for the finite-volume (or rather finite-area) mass shift of bound states in two-dimensional systems. The results can be used, for example, in lattice simulations of cold atomic systems, which can be prepared experimentally to be effectively two-dimensional [105, 106]. We note that the S-wave case in two dimensions was previously investigated in Ref. [107].

In two dimensions, the Schrödinger equation is

$$-\frac{1}{2\mu}\Delta_r^{2D}\psi_B(\mathbf{r}) + \int d^2r' V(\mathbf{r}, \mathbf{r}')\psi_B(\mathbf{r}') = -E_B\psi_B(\mathbf{r}) \quad (3.85)$$

with

$$\Delta_r^{2D}\psi_B(\mathbf{r}) = \left[\frac{1}{r}\frac{\partial}{\partial r} + \frac{\partial^2}{\partial r^2} + \frac{1}{r^2}\frac{\partial^2}{\partial\theta^2} \right]\psi_B(\mathbf{r}) \quad (3.86)$$

in polar coordinates. States are described by a single angular momentum quantum number $m = 0, \pm 1, \pm 2, \dots$, and for the wave function we have the separation

$$\psi_B(\mathbf{r}) = u_m(r)Y_m(\theta) \quad (3.87)$$

with

$$Y_m(\theta) = \frac{e^{im\theta}}{\sqrt{2\pi}}. \quad (3.88)$$

The two linearly independent solutions of the free radial equation

$$\left(\frac{d^2}{dr^2} + \frac{1}{r}\frac{d}{dr} - \frac{m^2}{r^2} + p^2 \right) u_m(r) = 0, \quad (3.89)$$

are just the Bessel and Neumann functions $J_m(pr)$ and $N_m(pr)$. For a bound state, we have $p^2 = -\kappa^2 = -2\mu E_B$, and the wave function has the asymptotic form

$$u_m(r) = A_\kappa K_m(\kappa r) \quad \text{for } r > R, \quad (3.90)$$

where K_m is the modified Bessel function of the second kind. It is related to the Hankel function of the first kind,

$$H_m^{(1)}(z) = J_m(z) + iN_m(z), \quad (3.91)$$

via

$$K_m(x) = \frac{\pi}{2} i^{m+1} H_m^{(1)}(ix). \quad (3.92)$$

As in the three-dimensional case, A_κ is the asymptotic normalization constant. Inserting Eq. (3.92) into Eq. (3.90) yields a form which is more similar to the three-dimensional expression. To render the analogy to the calculations in Section 3.4 as explicit as possible, we will use the Hankel function in the following intermediate steps and only express the final results in terms of the modified Bessel function.

Nearly all of the three-dimensional calculation carries over if we just replace all exponential terms with Hankel functions. The overlap integral for the mass shift is now

$$\Delta m_B^{(m)} = \sum_{|\mathbf{n}|=1} \int d^2r \int d^2r' \psi_{B,m}^*(\mathbf{r}) V(\mathbf{r}, \mathbf{r}') \psi_{B,m}(\mathbf{r}' + \mathbf{n}L) + \mathcal{O}\left(iH_m^{(1)}(\sqrt{2}\kappa L)\right). \quad (3.93)$$

From the asymptotic form of the Hankel function,

$$H_m^{(1)}(z) \sim \sqrt{\frac{2}{\pi z}} e^{i(z - \frac{m}{2}\pi - \frac{\pi}{4})} \quad \text{as } |z| \rightarrow \infty, \quad (3.94)$$

it is clear that in principle we still have an exponential behavior. In deriving Eq. (3.93) we have used this to write

$$\mathcal{O}\left(H_m^{(1)}(i\kappa L)^2\right) \sim \mathcal{O}\left(H_m^{(1)}(2i\kappa L)\right) \ll \mathcal{O}\left(H_m^{(1)}(\sqrt{2}i\kappa L)\right). \quad (3.95)$$

In the following we will simply write the correction terms as $\mathcal{O}(e^{-\sqrt{2}\kappa L})$, as in the three-dimensional case.

The two-dimensional analog of the relation (3.38) is

$$Y_m(\theta) H_m^{(1)}(i\kappa r) = (-i)^m R_m \left(-\frac{1}{\kappa} \nabla_r^{2D} \right) H_0^{(1)}(i\kappa r), \quad (3.96)$$

where $R_m(r, \theta) = r^m Y_m(\theta)$. This follows from

$$R_m(\nabla_r^{2D}) f(r) = R_m(\mathbf{r}) \left(\frac{1}{r} \frac{d}{dr} \right)^m f(r) \quad (3.97)$$

and

$$\left(\frac{1}{z} \frac{d}{dz} \right)^m H_0^{(1)}(z) = (-1)^m z^{-m} H_m^{(1)}(z). \quad (3.98)$$

The derivation of Eq. (3.97) can be carried out in the same manner as the three-dimensional proof of Lemma B.1 in [102], using the expansion of $e^{i\mathbf{p}\cdot\mathbf{r}}$ (2D vectors) in terms of Bessel functions. As the final ingredient we have

$$\left[\Delta_r^{2D} - \kappa^2 \right] \frac{i}{4} H_0^{(1)}(i\kappa r) = -\delta^{(2)}(\mathbf{r}). \quad (3.99)$$

Using all this in steps completely analogous to those in three dimensions, we get

$$\Delta m_B^{(m)} = (-1)^{m+1} \cdot \frac{\pi A_\kappa}{\mu} \sum_{|\mathbf{n}|=1} R_m \left(-\frac{1}{\kappa} \nabla_r^{2D} \right) \psi_{B,m}^*(\mathbf{r} - \mathbf{n}L) \Big|_{\mathbf{r}=0} + \mathcal{O}(e^{-\sqrt{2}\kappa L}). \quad (3.100)$$

For $m = 0$ (two-dimensional S-waves), this directly yields

$$\Delta m_B^{(0)} = -2 \frac{|A_\kappa|^2}{\mu} K_0(\kappa L) + \mathcal{O}(e^{-\sqrt{2}\kappa L}). \quad (3.101)$$

In fact, Eq. (3.100) can be simplified further. Inserting the asymptotic form for the wave function for $\psi_{B,m}^*$ and using (3.96) a second time gives

$$\Delta m_B^{(m)} = (-1)^{m+1} \cdot \frac{\pi |A_\kappa|^2}{\mu} \sum_{|\mathbf{n}|=1} R_m \left(-\frac{1}{\kappa} \nabla_r^{2D} \right) R_m^* \left(-\frac{1}{\kappa} \nabla_r^{2D} \right) \left[i \frac{\pi}{2} H_0^{(1)}(i\kappa r) \right] \Big|_{\mathbf{r}=\mathbf{n}L} + \mathcal{O}(e^{-\sqrt{2}\kappa L}). \quad (3.102)$$

From Eq. (3.88) and $R_m(\mathbf{r}) = r^m Y_m(\theta)$ it is clear that

$$R_m(\theta) R_m^*(\theta) = \frac{(r^2)^m}{2\pi}, \quad (3.103)$$

which then yields

$$R_m \left(-\frac{1}{\kappa} \nabla_r^{2D} \right) R_m^* \left(-\frac{1}{\kappa} \nabla_r^{2D} \right) f(r) = \frac{1}{\kappa^{2m}} \cdot \frac{1}{2\pi} (\Delta_r^{2D})^m f(r) \quad (3.104)$$

for any sufficiently smooth $f(r)$. This is essentially the same relation that we used to derive the trace formula in the three-dimensional case, only that here we do not have to sum over different m . Together with the two-dimensional analog of Eq. (3.68),

$$(\Delta_r^{2D})^m H_0^{(1)}(i\kappa r) = \kappa^{2m} H_0^{(1)}(i\kappa r) \quad (r \neq 0), \quad (3.105)$$

we then get

$$\begin{aligned} \Delta m_B^{(m)} &= (-1)^{m+1} \cdot \frac{|A_\kappa|^2}{2\mu} \sum_{|\mathbf{n}|=1} \frac{1}{\kappa^{2m}} (\Delta_r^{2D})^m \left[i \frac{\pi}{2} H_0^{(1)}(i\kappa r) \right] \Big|_{\mathbf{r}=\mathbf{n}L} + \mathcal{O}(e^{-\sqrt{2}\kappa L}) \\ &= (-1)^{m+1} \cdot \frac{2|A_\kappa|^2}{\mu} K_0(\kappa L) + \mathcal{O}(e^{-\sqrt{2}\kappa L}). \end{aligned} \quad (3.106)$$

As we shall see in the following, this is the final result for $m = 0$ and any odd m , whereas for even $m \neq 0$ things become slightly more complicated.

In general, we have to take into account that the finite volume breaks the original planar rotational symmetry of the system down to the symmetry group of a square. We find

that states with the same absolute value of m may mix to form good eigenstates in the finite volume. More precisely, we have the symmetric and antisymmetric combinations

$$|m, \pm\rangle = \frac{1}{\sqrt{2}}(|m\rangle \pm |-m\rangle) \quad (3.107)$$

for $m \neq 0$. When we calculate the mass shift for these states (in the same way as described in Section 3.4.1), we get mixing terms of the form

$$\Delta m_B^{(m, \text{mixed})} = (-1)^{m+1} \cdot \frac{\pi A_\kappa}{\mu} \sum_{|\mathbf{n}|=1} R_m \left(-\frac{1}{\kappa} \nabla_{\mathbf{r}}^{2D} \right) \psi_{B, -m}^*(\mathbf{r}) \Big|_{\mathbf{r}=\mathbf{n}L} + \mathcal{O}(e^{-\sqrt{2}\kappa L}). \quad (3.108)$$

Since the condition for the mixing of states is

$$2m \equiv 0 \pmod{4}, \quad (3.109)$$

they do not play a role for odd m (in fact, they vanish in this case). For even m , however, we have to take them into account and find

$$\Delta m_B^{(m, \pm)} = \frac{1}{2} \left(\Delta m_B^{(m)} \pm 2\Delta m_B^{(m, \text{mixed})} + \Delta m_B^{(-m)} \right) \quad (3.110)$$

as our final result. As an illustration, we give the explicit results for $|m| = 2$:

$$\Delta m_B^{(2, +)} = -4 \frac{|A_\kappa|^2}{\mu} \left[\left(1 + \frac{12}{\kappa^2 L^2}\right) K_0(\kappa L) + \left(\frac{4}{\kappa L} + \frac{24}{\kappa^3 L^3}\right) K_1(\kappa L) \right] + \mathcal{O}(e^{-\sqrt{2}\kappa L}), \quad (3.111a)$$

$$\Delta m_B^{(2, -)} = 16 \frac{|A_\kappa|^2}{\mu} \left[\frac{3}{\kappa^2 L^2} K_0(\kappa L) + \left(\frac{1}{\kappa L} + \frac{6}{\kappa^3 L^3}\right) K_1(\kappa L) \right] + \mathcal{O}(e^{-\sqrt{2}\kappa L}). \quad (3.111b)$$

3.7 Twisted boundary conditions

In this section, we go back to the three-dimensional case and discuss a generalization of the mass-shift formula obtained by changing the boundary condition imposed on the finite-volume wave function. Instead of the periodicity (3.11) we now require that

$$\psi(\mathbf{r} + \mathbf{n}L) = \psi(\mathbf{r}) e^{-i\boldsymbol{\theta} \cdot \mathbf{n}} \quad (3.112)$$

for all $\mathbf{n} \in \mathbb{Z}^3$, where $\boldsymbol{\theta}$ is an arbitrary vector of phases. It is clear that setting $\boldsymbol{\theta} = \mathbf{0}$ in this so-called *twisted boundary condition* gives back Eq. (3.11). As we will discuss in more detail shortly in Section 3.7.2, a boundary condition of this form arises when one considers a system of more than two particles, two of which form the bound state whose mass shift we are interested in. In such a setup one has to consider the full two-particle wave function

$$\Psi(\mathbf{r}_1, \mathbf{r}_2) = \Psi(\mathbf{R}, \mathbf{r}) = e^{i\mathbf{P} \cdot \mathbf{R}} \psi(\mathbf{r}), \quad (3.113)$$

where

$$\mathbf{r} = \mathbf{r}_1 - \mathbf{r}_2 \quad \text{and} \quad \mathbf{R} = \eta_1 \mathbf{r}_1 + \eta_2 \mathbf{r}_2 \quad (3.114)$$

are the relative and center-of-mass coordinates, respectively, and $\eta_{1,2}$ are the mass ratios

$$\eta_1 = \frac{m_1}{m_1 + m_2} \quad , \quad \eta_2 = 1 - \eta_1 . \quad (3.115)$$

If one demands that $\Psi(\mathbf{r}_1, \mathbf{r}_2)$ is periodic in both coordinates, *e.g.*,

$$\Psi(\mathbf{r}_1 + \mathbf{n}L, \mathbf{r}_2) = e^{i\mathbf{P}\cdot\mathbf{R}} e^{i\eta_1 L\mathbf{P}\cdot\mathbf{n}} \psi(\mathbf{r} + \mathbf{n}L) = \Psi(\mathbf{r}_1, \mathbf{r}_2) , \quad (3.116)$$

one finds that the behavior of $\psi(\mathbf{r} + \mathbf{n}L)$ has to cancel the additional phase,

$$\psi(\mathbf{r} + \mathbf{n}L) = e^{-i\eta_1 L\mathbf{P}\cdot\mathbf{n}} \psi(\mathbf{r}) . \quad (3.117)$$

This is just Eq. (3.112) with $\boldsymbol{\theta} = \eta_1 L\mathbf{P}$. More generally, one can of course write the boundary condition in the form

$$\begin{aligned} \Psi(\mathbf{r}_1 + \mathbf{n}_1 L, \mathbf{r}_2 + \mathbf{n}_2 L) \\ = e^{i\mathbf{P}\cdot\mathbf{R}} e^{i\eta_1 L\mathbf{P}\cdot\mathbf{n}_1} e^{i\eta_2 L\mathbf{P}\cdot\mathbf{n}_2} \psi(\mathbf{r} + (\mathbf{n}_1 - \mathbf{n}_2)L) \\ = \Psi(\mathbf{r}_1, \mathbf{r}_2) , \end{aligned} \quad (3.118)$$

but this again gives Eq. (3.117) since

$$e^{i\eta_1 L\mathbf{P}\cdot\mathbf{n}_1} e^{i\eta_2 L\mathbf{P}\cdot\mathbf{n}_2} = e^{i\eta_1 L\mathbf{P}\cdot\mathbf{n}_1} e^{i(1-\eta_1)L\mathbf{P}\cdot\mathbf{n}_2} = e^{i\eta_1 L\mathbf{P}\cdot(\mathbf{n}_1 - \mathbf{n}_2)} , \quad (3.119)$$

where the last equality follows by noting that the total momentum for the center-of-mass movement \mathbf{P} is quantized in the finite volume,

$$\mathbf{P} = \frac{2\pi}{L} \mathbf{K} \quad , \quad \mathbf{K} \in \mathbb{Z}^3 . \quad (3.120)$$

Keeping in mind these considerations as a motivation, we now derive the the finite-volume mass shift for a the two-particle system with twisted boundary conditions—without writing $\boldsymbol{\theta}$ in terms of the momentum \mathbf{P} , however, but rather keeping it as an arbitrary parameter.

3.7.1 Generalized derivation

We carry out the derivation along the lines laid out in Section 3.2 and start by making an ansatz $|\psi_\theta\rangle$ for the finite-volume wave function of the form

$$\langle \mathbf{r} | \psi_\theta \rangle = \psi_\theta(\mathbf{r}) = \sum_{\mathbf{n}} \psi_B(\mathbf{r} + \mathbf{n}L) e^{i\boldsymbol{\theta}\cdot\mathbf{n}} . \quad (3.121)$$

Like the $|\psi_0\rangle$ defined in Eq. (3.13), this has at least the correct boundary behavior:

$$\begin{aligned} \psi_\theta(\mathbf{r} + \mathbf{n}L) &= \sum_{\mathbf{n}'} \psi_B(\mathbf{r} + \mathbf{n}'L + \mathbf{n}L) e^{i\boldsymbol{\theta}\cdot\mathbf{n}'} \\ &= \sum_{\mathbf{n}''=\mathbf{n}'+\mathbf{n}} \psi_B(\mathbf{r} + \mathbf{n}''L) e^{i\boldsymbol{\theta}\cdot(\mathbf{n}''-\mathbf{n})} = \psi_\theta(\mathbf{r}) e^{-i\boldsymbol{\theta}\cdot\mathbf{n}} . \end{aligned} \quad (3.122)$$

Acting on this state with the finite-volume Hamiltonian, we get

$$\begin{aligned}
H_L \psi_\theta(\mathbf{r}) &= H_0 \sum_{\mathbf{n}'} \psi_B(\mathbf{r} + \mathbf{n}'L) e^{i\boldsymbol{\theta} \cdot \mathbf{n}'} + \sum_{\mathbf{n}', \mathbf{n}} \int d^3 r' V(\mathbf{r} + \mathbf{n}L, \mathbf{r}' + \mathbf{n}L) \psi_B(\mathbf{r}' + \mathbf{n}'L) e^{i\boldsymbol{\theta} \cdot \mathbf{n}'} \\
&= \sum_{\mathbf{n}'} \left\{ \left[H_0 \psi_B(\mathbf{r} + \mathbf{n}'L) + \int d^3 r' V(\mathbf{r} + \mathbf{n}'L, \mathbf{r}' + \mathbf{n}'L) \psi_B(\mathbf{r}' + \mathbf{n}'L) \right] e^{i\boldsymbol{\theta} \cdot \mathbf{n}'} \right. \\
&\quad \left. + \sum_{\mathbf{n} \neq \mathbf{n}'} \int d^3 r' V(\mathbf{r} + \mathbf{n}L, \mathbf{r}' + \mathbf{n}L) \psi_B(\mathbf{r}' + \mathbf{n}'L) e^{i\boldsymbol{\theta} \cdot \mathbf{n}'} \right\} \\
&= -E_B(\infty) \sum_{\mathbf{n}'} \psi_B(\mathbf{r} + \mathbf{n}'L) e^{i\boldsymbol{\theta} \cdot \mathbf{n}'} \\
&\quad + \sum_{\mathbf{n}'} \sum_{\mathbf{n} \neq \mathbf{n}'} \int d^3 r' V(\mathbf{r} + \mathbf{n}L, \mathbf{r}' + \mathbf{n}L) \psi_B(\mathbf{r}' + \mathbf{n}'L) e^{i\boldsymbol{\theta} \cdot \mathbf{n}'}, \quad (3.123)
\end{aligned}$$

which analogously to Eq. (3.15) we write as

$$\hat{H}_L |\psi_\theta\rangle = -E_B(\infty) |\psi_\theta\rangle + |\eta_\theta\rangle \quad (3.124)$$

with

$$\eta_\theta(\mathbf{r}) = \sum_{\mathbf{n}'} \sum_{\mathbf{n} \neq \mathbf{n}'} \int d^3 r' V(\mathbf{r} + \mathbf{n}L, \mathbf{r}' + \mathbf{n}L) \psi_B(\mathbf{r}' + \mathbf{n}'L) e^{i\boldsymbol{\theta} \cdot \mathbf{n}'}. \quad (3.125)$$

We see that in the end the phase factor $e^{i\boldsymbol{\theta} \cdot \mathbf{n}'}$ is simply carried through the whole calculation. Since furthermore it does not depend on the variable \mathbf{r} , we can now conclude that all steps carried out in Section 3.2.2 remain valid in spite of its presence and directly arrive at the integral formula for the finite-volume mass shift with twisted boundary conditions:

$$\Delta m_B(\boldsymbol{\theta}) = \sum_{|\mathbf{n}|=1} \int d^3 r \psi_B^*(\mathbf{r}) V(\mathbf{r}) \psi_B(\mathbf{r} + \mathbf{n}L) e^{i\boldsymbol{\theta} \cdot \mathbf{n}} + \mathcal{O}(e^{-\sqrt{2}\kappa L}). \quad (3.126)$$

For S-wave states, the final result then is

$$\Delta m_B^{(0)}(\boldsymbol{\theta}) = -|A_\kappa|^2 \frac{e^{-\kappa L}}{\mu L} \times \sum_{\mathbf{n}=\hat{\mathbf{e}}_x, \hat{\mathbf{e}}_y, \hat{\mathbf{e}}_z} \cos(\boldsymbol{\theta} \cdot \mathbf{n}) + \mathcal{O}(e^{-\sqrt{2}\kappa L}), \quad (3.127)$$

i.e., the phases from pairs of opposite directions combine to give cosine factors. Again, it is clear that setting $\boldsymbol{\theta} = \mathbf{0}$ gives back the old result (3.35) for periodic boundary conditions. For P-wave states, there is now a dependence on the quantum number m :

$$\Delta m_B^{(1,0)}(\boldsymbol{\theta}) = |A_\kappa|^2 \frac{e^{-\kappa L}}{\mu L} \times \frac{-(1 + \kappa L)(\cos \theta_x + \cos \theta_y) + (2 + \kappa L(2 + \kappa L)) \cos \theta_z}{\kappa^2 L^2}, \quad (3.128a)$$

$$\Delta m_B^{(1,\pm 1)}(\boldsymbol{\theta}) = |A_\kappa|^2 \frac{e^{-\kappa L}}{\mu L} \times \frac{(1 + \kappa L(1 + \kappa L))(\cos \theta_x + \cos \theta_y) - 2(1 + \kappa L) \cos \theta_z}{2\kappa^2 L^2}. \quad (3.128b)$$

However, this goes away as it should if one sends $\boldsymbol{\theta} \rightarrow \mathbf{0}$. For $m = 0$, for example, one finds that

$$\begin{aligned} & - (1 + \kappa L)(\cos \theta_x + \cos \theta_y) + (2 + \kappa L(2 + \kappa L)) \cos \theta_z \\ & = -2(1 + \kappa L)2 + (2 + \kappa L(2 + \kappa L)) = \kappa^2 L^2, \end{aligned} \quad (3.129)$$

cancelling the additional factor in the denominator and thus giving back the old result.

Improved volume dependence

Already in the two-body sector the results given above are actually quite interesting. From Eq. (3.127), for example, one can see that for a bound state with equal mass constituents (such that the mass ratios are $\eta_1 = \eta_2 = 1/2$), the leading finite-volume mass shift can be made to vanish if one chooses to perform the calculation in a “boosted” frame with $\mathbf{K} = (1, 1, 1)/2$ rather than in the rest frame of the bound state, which would be the naïve choice.

In Ref. [3] it was argued and demonstrated numerically that this procedure can be generalized to bound states of more than two particles if one assumes that there is no cluster substructure. Furthermore, in Ref. [90] Davoudi and Savage discuss a general method for reducing finite-volume corrections in two-body calculations by choosing appropriate combinations of boosted frames.

3.7.2 Topological volume factors

As mentioned at the outset, the mass shift for twisted boundary conditions is important for systems of more than two particles in a finite volume, two of which form a dimer bound state. In the following, we will discuss how these shifts yield correction factors that have to be taken into account in finite-volume determinations of scattering phase shifts where one or more of the particles is composite.⁴

To this end, consider the scattering at low energies of two particles labeled A and B , both of which can be either elementary (pointlike) or composite bound states. For the sake of definiteness we take A to be a pointlike “atom” and B to be a dimer bound state.

In order to extract the S-wave scattering phase shift $\delta_0(p)$ from finite-volume calculations, a popular strategy is to apply Lüscher’s formula

$$p \cot \delta_0(p) = \frac{1}{\pi L} S(\eta) \quad , \quad \eta = \left(\frac{Lp}{2\pi} \right)^2, \quad (3.130)$$

where p is the center-of-mass momentum of the A - B system and

$$S(\eta) = \sqrt{4\pi} \cdot \mathcal{Z}_{00}(1, \eta) = \lim_{s \rightarrow 1} \sum_{\mathbf{n} \in \mathbb{Z}^3} \frac{1}{(\mathbf{n}^2 - \eta)^s} \quad (3.131)$$

⁴The relations presented in the following, published in Ref. [3], were derived by D. Lee [108]. The present author’s main contribution to Ref. [3] was the derivation of the twisted-boundary mass-shift formula.

is the Lüscher Zeta-function (see, *e.g.*, Ref. [102]).⁵

The crucial point here is that the momentum p is determined from energy levels of the A - B system in the finite volume which, in turn, are functions of the box size L , *i.e.*

$$p = p(E_{AB}(L)). \quad (3.132)$$

If now at least one of the particles A and B is a composite bound state, there will be a contribution to the volume dependence of the total energy that is solely due to the mass shift of the bound state. In order to apply Lüscher's formula (3.130), this contribution has to be determined and subtracted.

Turning back to our atom-dimer example, we assume that the underlying interactions between the atoms has a finite range R and impose periodic boundary conditions. We denote an A - B scattering state with momentum $p = |\mathbf{p}|$ in the center-of-mass frame by Ψ_p and write it as

$$\langle \mathbf{r} | \Psi_p \rangle = c \cdot \sum_{\mathbf{k} \in \mathbb{Z}^3} \frac{e^{i \frac{2\pi \mathbf{k}}{L} \cdot \mathbf{r}}}{(2\pi \mathbf{k}/L)^2 - p^2} \quad (3.133)$$

in configuration space, with some normalization constant c . In writing this expression, which corresponds to a pure S-wave, we have assumed that contributions from higher partial waves can be neglected. It is then valid as an approximation for all \mathbf{r} outside shifted copies of the finite-range interaction if we neglect exponentially-suppressed contributions in the effective interaction between composite particles that are introduced by the bound-state wave functions. As discussed in Ref. [3], this is valid because for the current derivation we are only interested in the contributions due to the shifts in the binding energies. According to the formulas derived above, these are also exponentially small, but their contributions to the scattering are suppressed further by inverse powers of L . Note that upon discretization the expression in Eq. (3.133) essentially goes over into the lattice Green's function defined in Section 3.5.1.

Let \hat{H} denote the Hamiltonian for the system we are considering. Acting with this on the state $|\Psi_p\rangle$ then gives

$$\langle \mathbf{r} | \hat{H} | \Psi_p \rangle = c \cdot \left(\frac{L}{2\pi} \right)^2 \sum_{\mathbf{k} \in \mathbb{Z}^3} \frac{e^{i \frac{2\pi \mathbf{k}}{L} \cdot \mathbf{r}} \left[\frac{p^2}{2\mu_{AB}} + E_A^{2\pi \mathbf{k}/L}(L) + E_B^{-2\pi \mathbf{k}/L}(L) \right]}{\mathbf{k}^2 - \eta} \quad (3.134)$$

in configuration space [108], where μ_{AB} is the reduced mass of the A - B system and with η as defined in Eq. (3.130). In this expression, $E_{A,B}^{\pm 2\pi \mathbf{k}/L}(L)$ are the energy contributions (at volume L) due to the binding of the states A and B , moving with momentum $\pm 2\pi \mathbf{k}/L$. By definition, they are zero for point particles. In particular, for our specific example here we have $E_A^{2\pi \mathbf{k}/L}(L) = 0$ for all L , but we keep it in the equations in order to give a more general result. The total energy of the A - B system is then

$$E_{AB}(p, L) = \frac{\langle \Psi_p | \hat{H} | \Psi_p \rangle}{\langle \Psi_p | \Psi_p \rangle} = \frac{1}{\mathcal{N}} \sum_{\mathbf{k} \in \mathbb{Z}^3} \frac{\frac{p^2}{2\mu_{AB}} + E_A^{2\pi \mathbf{k}/L}(L) + E_B^{-2\pi \mathbf{k}/L}(L)}{(\mathbf{k}^2 - \eta)^2} \quad (3.135)$$

⁵As discussed in Ref. [102], $\mathcal{Z}_{00}(s, \eta)$ is initially defined by the sum in Eq. (3.131) for $\text{Re}(s) > 3/2$ and then extended to the whole complex plane by analytic continuation; this is what we express with the limit in Eq. (3.131).

with the normalization factor

$$\mathcal{N} = \sum_{\mathbf{k}} (\mathbf{k}^2 - \eta)^{-2}. \quad (3.136)$$

The volume dependence of $E_B^{-2\pi\mathbf{k}/L}(L)$ is known from the derivation in Section 3.7.1. According to Eq. (3.127), it is given as

$$\begin{aligned} \Delta E_B(\mathbf{k}, L) &\equiv E_B^{-2\pi\mathbf{k}/L}(L) - E_B^{-2\pi\mathbf{k}/L}(\infty) \\ &= \Delta m_B^{(0)}(\boldsymbol{\theta} = -2\pi\eta_B\mathbf{k}) = -|A_\kappa|^2 \frac{e^{-\kappa L}}{\mu_B L} \times \sum_{i=x,y,z} \cos(2\pi\eta_B k_i) + \mathcal{O}(e^{-\sqrt{2}\kappa L}), \end{aligned} \quad (3.137)$$

where μ_B and η_B are the reduced mass and mass ratio of the constituents comprising the state B . If the state A is composite as well, one has an analogous expression for the contribution $E_A^{2\pi\mathbf{k}/L}(L)$. The total volume dependence of the energy E_{AB} can then be written as

$$E_{AB}(p, L) - E_{AB}(p, \infty) = \tau_A(\eta) \cdot \Delta E_A(\mathbf{0}, L) + \tau_B(\eta) \cdot \Delta E_B(\mathbf{0}, L) \quad (3.138)$$

with the *topological volume factors*

$$\tau_{A,B}(\eta) = \frac{1}{\mathcal{N}} \sum_{\mathbf{k}} \frac{\sum_{i=1,2,3} \cos(2\pi\eta_{A,B} k_i)}{3(k^2 - \eta)^2}. \quad (3.139)$$

They are obtained by inserting the expressions for $\Delta E_{A,B}(\mathbf{k}, L)$ into the sum over all \mathbf{k} in Eq. (3.135) and factoring out the volume dependence of the states A and B at rest. Eq. (3.138) is the desired contribution to the volume dependence of the energy levels E_{AB} (determined in numerical calculations) that should be subtracted before applying Lüscher's formula (3.130) for an extraction of the scattering phase shift.

Figure 3.5 demonstrates the importance of this procedure. For the atom–dimer (more generally called “fermion–dimer” here) system it shows lattice results for the scattering length and effective range calculated from S-wave phase shifts that were extracted using Lüscher's finite-volume formula (3.130). The results shown in the plot were obtained in a calculation by Bour *et al.*, the full details of which can be found in Ref. [109]. They are shown here with the kind permission of the authors.

Using dimensionless units obtained by rescaling all quantities with the dimer binding momentum κ_D , both the scattering length a_{FD} and the effective range r_{FD} are plotted against different values of the lattice spacing a_{latt} on the x -axis, such that a continuum extrapolation can be performed. The two data sets shown in the plots were obtained using two different lattice Hamiltonians that yield the same continuum limit.

One clearly sees that the correct values (indicated by the blue triangles in Fig. 3.5) are only reached when the topological corrections factors are included in the calculation. The effect is particularly prominent for the effective range, where otherwise the result is completely off.

It should be pointed out here that the effect of the topological volume contributions is so strong in the chosen example because the dimer was tuned to be very shallow and

the volumes used in the numerical calculation were not very large. Together, these two factors enhance the relative importance of the binding-energy shifts. In a calculation with deeper dimers and/or larger volumes, the effect can be much weaker or even negligible. However, in general it is always there and should be taken into account, especially when the exact situation is *a priori* unknown.

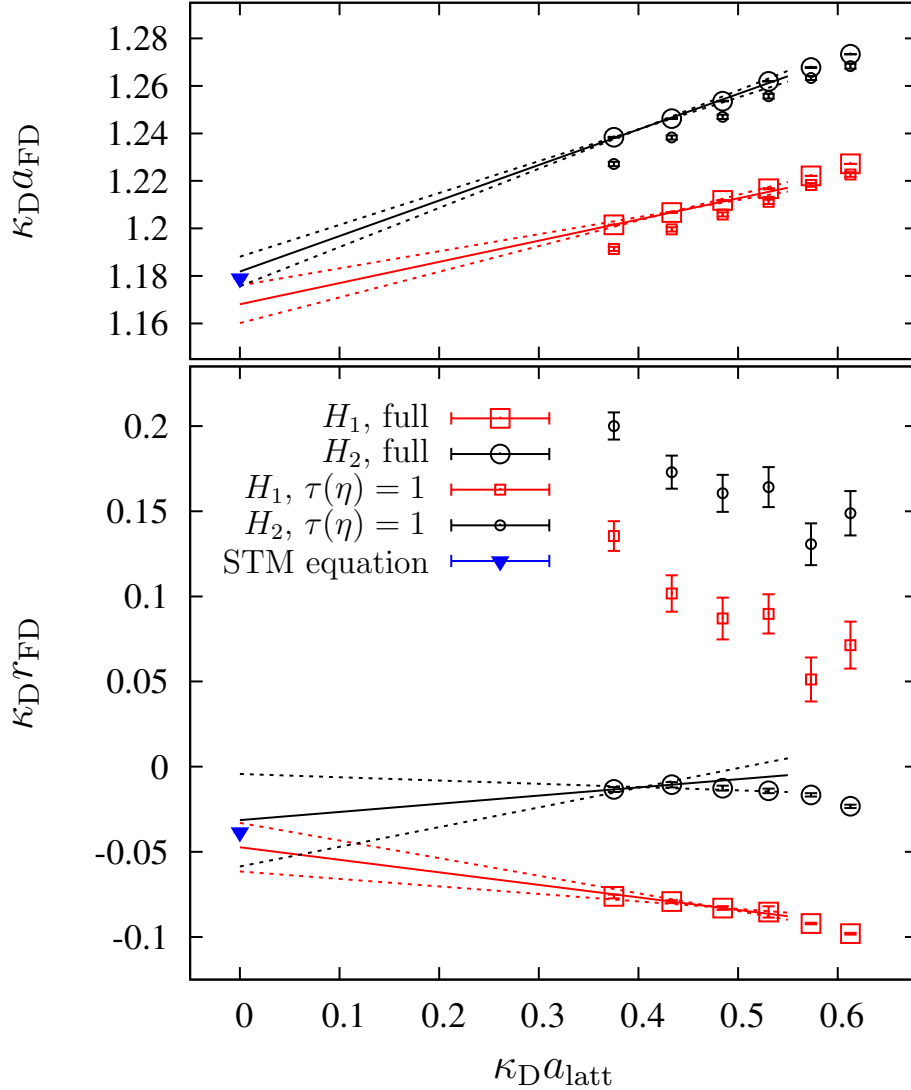


Figure 3.5: Lattice results and continuum extrapolation with error estimates for the fermion–dimer scattering length (top) and effective range parameter (bottom). For comparison we show the continuum results obtained via the Skorniakov–Ter-Martirosian equation.

3.8 Summary and outlook

In this chapter we have derived explicit formulae for the mass shift of P- and higher-wave bound states in a finite volume and discussed their decomposition into states transforming according to the representations of the cubic group. We have compared our numerical

results for $\ell \leq 2$ with numerical calculations of the finite-volume dependence for lattice Gaussian and step potentials and found good agreement with the predictions. For $\ell \geq 2$, the mass shift of a given state (ℓ, m) depends on the angular momentum projection m due to the breaking of rotational symmetry. Averaged over all m in a multiplet, however, the absolute value of the mass shift is even independent of ℓ . The mass shift for states in representations of the cubic group is the same for all states, and its sign can be understood from the leading parity of the representations. We have furthermore derived corresponding expressions for the finite-volume mass shift in two-dimensional systems.

With the known volume dependence, lattice calculations provide a method to extract asymptotic normalization coefficients of bound state wave functions, which are of interest, for example, in low-energy astrophysical capture reactions. Using a relation that will be discussed in more detail in Chapter 5, the asymptotic normalization and binding momentum of a shallow bound state can be used to extract the effective range from a simulation.

Furthermore, we have shown how twisted boundary conditions arise if one studies dimer states in moving frames and how the mass shift for this case leads to topological correction factors that have to be taken into account in finite-volume calculations of composite-particle scattering. A precise knowledge of these corrections is particularly important for processes involving shallow dimer states in volumes that are not very large.

Our work provides a general framework for future lattice studies of molecular states with angular momentum in systems with short-range interactions. Applications to nuclear halo systems and molecular states in atomic and hadronic physics appear promising. An important next step would be to include Coulomb effects into the framework in order to investigate the volume dependence of bound states of charged particles, which are much easier to treat experimentally. In particular, this extension of the formalism is important if one wants to describe proton-halo nuclei. Another interesting direction would be to analyze the volume dependence of resonances along the lines of Refs. [104, 110].

Chapter 4

The Coulomb force

Overview

The Coulomb potential, although notoriously difficult to handle due to its long-range nature, is one of the most important and probably most thoroughly investigated interactions in quantum mechanics. We review here results from the vast literature on the subject with a focus on aspects that will be important for the following two chapters of this thesis. The first part, where we introduce the Coulomb wave functions and the modified effective range expansion, is based largely on the introductory section of Ref. [5], but provides some additional details. In the second part we discuss the full off-shell Coulomb T-matrix. In particular, we give an approximate expression for this function in the case of a Yukawa-screened Coulomb potential, originally derived by Gorshkov [111]. This section contains, at least to the author’s best knowledge, some results that have not previously been published.

4.1 Coulomb wave functions

For a pure Coulomb interaction the radial Schrödinger equation for two particles carrying electromagnetic charges Z_1e and Z_2e reads

$$p^2 w_\ell(r) = -\frac{d^2}{dr^2} w_\ell(r) + \frac{\ell(\ell+1)}{r^2} w_\ell(r) + \frac{\gamma}{r} w_\ell(r) \quad (4.1)$$

with the Coulomb parameter

$$\gamma = 2\mu \alpha Z_1 Z_2, \quad (4.2)$$

and the fine-structure constant

$$\alpha = \frac{e^2}{4\pi} \approx \frac{1}{137}. \quad (4.3)$$

We use here the letter w to denote the wave functions in order to distinguish them from the $u_\ell(r)$ describing the asymptotically non-interacting “neutral” system discussed in Chapter 2.

The solutions of (5.29) are the so-called *Coulomb wave functions*, and their properties are well-known. We use here the conventions introduced by Yost, Breit and Wheeler in Ref. [112] and summarize some important relations in the following. For a more comprehensive discussion we refer to the review article by Hull and Breit [113].

Explicitly, we write the wave functions as [114, 115]

$$F_\ell^{(p)}(r) = \frac{1}{2} \left| \frac{e^{i\frac{\pi}{2}k} \Gamma(\frac{1}{2} + m - k)}{\Gamma(2m + 1)} \right| e^{-i\frac{\pi}{2}(\frac{1}{2}+m)} M_{k,m}(z) \quad (4.4a)$$

$$G_\ell^{(p)}(r) = \frac{\Gamma(\frac{1}{2} + m - k)}{|\Gamma(\frac{1}{2} + m - k)|} e^{-i\frac{\pi}{2}(\frac{1}{2}-m+k)} W_{k,m}(z) + iF_\ell^{(p)}(r), \quad (4.4b)$$

where

$$\rho = pr \quad , \quad \eta = \frac{\gamma}{2p}, \quad (4.5)$$

and

$$z = 2i\rho \quad , \quad k = i\eta \quad , \quad m = \ell + \frac{1}{2}. \quad (4.6)$$

The functions $M_{k,m}$ and $W_{k,m}$ are Whittaker functions, which can be expressed in terms of hypergeometric functions as

$$M_{k,m}(z) = e^{-\frac{1}{2}z} z^{\frac{1}{2}+m} {}_1F_1\left(\frac{1}{2} + m - k, 1 + 2m; z\right), \quad (4.7)$$

$$W_{k,m}(z) = e^{-\frac{1}{2}z} z^{\frac{1}{2}+m} U\left(\frac{1}{2} + m - k, 1 + 2m; z\right). \quad (4.8)$$

${}_1F_1(a, b; z)$ is Kummer's function of the first kind,

$${}_1F_1(a, b; z) = \sum_{n=0}^{\infty} \frac{a^{(n)} z^n}{b^{(n)} n!}, \quad a^{(n)} = a(a+1) \cdots (a+n-1), \quad (4.9)$$

and

$$U(a, b; z) = \frac{\Gamma(1-b)}{\Gamma(1+a-b)} {}_1F_1(a, b; z) + \frac{\Gamma(b-1)}{\Gamma(a)} z^{1-b} {}_1F_1(a-b+1, 2-b; z). \quad (4.10)$$

Due to their behavior in the limit $\rho = pr \rightarrow 0$,

$$F_\ell^{(p)}(r) \sim C_{\eta,\ell} \rho^{\ell+1}, \quad (4.11a)$$

$$G_\ell^{(p)}(r) \sim \frac{\rho^{-\ell}}{C_{\eta,\ell}(2\ell+1)}, \quad (4.11b)$$

$F_\ell^{(p)}$ and $G_\ell^{(p)}$ are commonly called the regular and irregular Coulomb wave functions, respectively. The factor $C_{\eta,\ell}$, which in the following we refer to as the *Gamow factor*,¹ is given by

$$C_{\eta,0}^2 = \frac{2\pi\eta}{e^{2\pi\eta} - 1}, \quad (4.12)$$

¹Note that there is no general agreement about the name of $C_{\eta,\ell}$ in the literature. It is sometimes also referred to as the *Sommerfeld factor* or, perhaps introduced as a sort of compromise, *Gamow-Sommerfeld factor*.

and

$$C_{\eta,\ell}^2 = \frac{2^{2\ell}}{[(2\ell+1)!]^2} \prod_{s=1}^{\ell} (s^2 + \eta^2) \cdot C_{\eta,0}^2. \quad (4.13)$$

Sometimes it is convenient to write it in the more general form [103]

$$C_{\eta,\ell} = \frac{2^\ell e^{-\frac{\pi\eta}{2}} [\Gamma(\ell+1+i\eta)\Gamma(\ell+1-i\eta)]^{\frac{1}{2}}}{\Gamma(2\ell+2)}. \quad (4.14)$$

For asymptotically large $\rho = pr$, on the other hand the Coulomb wave functions behave as

$$F_\ell^{(p)}(r) \sim \sin(\rho - \ell\pi/2 - \eta \log(2\rho) + \sigma_\ell), \quad (4.15a)$$

$$G_\ell^{(p)}(r) \sim \cos(\rho - \ell\pi/2 - \eta \log(2\rho) + \sigma_\ell) \quad (4.15b)$$

with the *Coulomb phase shift*

$$\sigma_\ell = \arg \Gamma(\ell+1+i\eta). \quad (4.16)$$

From Eqs. (4.11) and (4.15) it is clear that $F_\ell^{(p)}(r)$ and $G_\ell^{(p)}(r)$ are the direct analogues of the Riccati–Bessel functions $S_\ell(pr)$ and $C_\ell(pr)$ that solve the free radial Schrödinger equation. The key differences to point out are the presence of the factors of $C_{\eta,\ell}$ in (4.11) and of the additional phases $\eta \log(2pr)$ σ_ℓ in (4.15). The latter—in particular the logarithmically-divergent term—reflect the inherent long-range nature of the Coulomb potential: no matter how large the separation r of two charged particles becomes, the phase of their relative-motion wave function (determined solely by the regular function $F_\ell^{(p)}(r)$ for a pure Coulomb interaction) never goes to a constant, and the particles are thus never free [116].

4.1.1 The Gamow factor

The factor $C_{\eta,0}^2$ has a direct physical interpretation. To see this, note first that the full three-dimensional continuum Coulomb wave function (with outgoing asymptotics for the spherical wave and normalized such that the incoming plane-wave component $\sim \exp(i\mathbf{p}\cdot\mathbf{r})$ has unit amplitude) can be written in terms of a confluent hypergeometric function as [117]

$$\psi_{\mathbf{p}}^{(+)}(\mathbf{r}) = e^{-\frac{\pi\eta}{2}} \Gamma(1+i\eta) e^{i\mathbf{p}\cdot\mathbf{r}} {}_1F_1(i\eta, 1; ipr - i\mathbf{p}\cdot\mathbf{r}). \quad (4.17)$$

Its partial-wave expansion is given in terms of the regular Coulomb wave functions as (see Refs. [118, 119] and *cf.* also Ref. [120])

$$\psi_{\mathbf{p}}^{(+)}(\mathbf{r}) = \sum_{\ell=0}^{\infty} (2\ell+1) i^\ell e^{i\sigma_\ell} \frac{F_\ell^{(p)}(r)}{pr} P_\ell(\cos\theta). \quad (4.18)$$

It is clear that only the S-wave term contributes in the limit $r \rightarrow 0$, such that by inserting the threshold behavior of $F_\ell^{(p)}(r)$ from Eq. (4.11a) we find that

$$\lim_{|\mathbf{r}|\rightarrow 0} \psi_{\mathbf{p}}^{(+)}(\mathbf{r}) = e^{i\sigma_\ell} C_{\eta,0}. \quad (4.19)$$

Alternatively, one can derive directly from Eq. (4.17) that

$$|\psi_{\mathbf{p}}^{(+)}(\mathbf{0})|^2 = e^{-\pi\eta}\Gamma(1+i\eta)\Gamma(1-i\eta) = C_{\eta,0}^2, \quad (4.20)$$

where the last equality follows from Eq. (4.14). As pointed out in Ref. [117] (for example) this means that the S-wave Gamow factor (squared) is the probability of two charged particles to be found at zero separation.²

4.1.2 Analytic wave functions

Of all possible linearly independent pairs of solutions for the Schrödinger equation (5.29), the Coulomb wave functions $F_\ell^{(p)}(r)$ and $G_\ell^{(p)}(r)$ are convenient to use because with their behavior at the origin and for asymptotically large distances, given in Eqs. (4.11) and (4.15), respectively, they correspond most directly to the solutions of the free Schrödinger equation discussed in Chapter 2. In contrast to those functions, however, $F_\ell^{(p)}(r)$ and $G_\ell^{(p)}(r)$ cannot directly be used in order to obtain expressions that are analytic in p^2 . Rather, the fact that they are expressed in terms of the variables $\rho = pr$ and $\eta \sim 1/p$ yields series expansions [112, 113] with a complicated “entanglement” of terms in p and r .

As first done by Lambert in Ref. [121], it is possible to define Coulomb wave functions that are directly analytic in p^2 . Lambert’s result was later generalized by Bollé and Gesztesy in Ref. [122]. Their pair of analytic wave functions, which we denote by $F_n^{(0)}(p, r)$ and $\tilde{G}_n^{(0)}(p, r)$ and discuss in more detail in Appendix A, will be very useful in the following Chapter 5. Here, we note for completeness that Coulomb wave functions analytic in the energy are also discussed in a more recent publication by Seaton [123].

4.2 Modified effective range expansion

Analogous to the discussion in Section 2.1.4 we now consider the case where a finite-range interaction $V(r, r')$ is present in addition to the Coulomb potential. We again assume that the interaction allows for a solution that is regular at the origin, and the finite-range condition (5.1) implies that $V(r, r')$ vanishes if $r > R$ or $r' > R$ for some fixed but arbitrary range R . The radial Schrödinger equation now reads

$$p^2 w_\ell(r) = -\frac{d^2}{dr^2} w_\ell(r) + \frac{\ell(\ell+1)}{r^2} w_\ell(r) + 2\mu \int_0^R dr' V(r, r') w_\ell(r') + \frac{\gamma}{r} w_\ell(r). \quad (4.21)$$

A general solution of Eq. (4.21) for momentum p can be written as a linear combination of the regular and irregular Coulomb wave functions $F_\ell^{(p)}$ and $G_\ell^{(p)}$ defined in the previous section,

$$w_\ell^{(p)}(r) \propto \left[\cot \tilde{\delta}_\ell(p) F_\ell^{(p)}(r) + G_\ell^{(p)}(r) \right] \quad \text{for } r > R, \quad (4.22)$$

²In particular, the wave function at the origin stays finite although the Coulomb potential diverges for $r \rightarrow 0$. The latter is only a mathematical pathology that is always regulated by screening effects in a real physical system.

with an arbitrary overall normalization, and where $\tilde{\delta}_\ell$ is the phase shift of the full solution $w_\ell^{(p)}$ compared to the regular Coulomb function $F_\ell^{(p)}$ [13]. Since it can be related to the partial-wave expansion of a function T_{SC} defined by [124, 125]

$$T = T_{SC} + T_C \iff T_{SC} = T - T_C, \quad (4.23)$$

where T is the full T-matrix corresponding to the combined interaction $\hat{V} + \hat{V}_C$ and T_C is the pure Coulomb T-matrix (see Section 4.4), $\tilde{\delta}_\ell$ is called the ‘‘Coulomb-modified’’ or ‘‘Coulomb-subtracted’’ scattering phase shift.

Instead of the ordinary effective range expansion (2.19) we now have the more complicated expression

$$C_{\eta,\ell}^2 p^{2\ell+1} \cot \tilde{\delta}_\ell(p) + \gamma h_\ell(p) = -\frac{1}{a_\ell^C} + \frac{1}{2} r_\ell^C p^2 + \dots, \quad (4.24)$$

where

$$h_\ell(p) = p^{2\ell} \frac{C_{\eta,\ell}^2}{C_{\eta,0}^2} h(\eta), \quad (4.25)$$

$$h(\eta) = \operatorname{Re} \psi(i\eta) - \log |\eta|, \quad (4.26)$$

and the *digamma function* $\psi(z) = \Gamma'(z)/\Gamma(z)$ is the logarithmic derivative of the Gamma function. It means that in order to get an expression that is analytic in p^2 , one has to multiply $p^{2\ell+1} \cot \tilde{\delta}_\ell(p)$ by the Gamow factor squared and add an additional function that cancels the remaining non-analytic terms.

Eq. (4.24) is called the *Coulomb-modified effective range expansion*. For $\ell = 0$, it simplifies to

$$C_{\eta,0}^2 p \cot \tilde{\delta}_0(p) + \gamma h(\eta) = -\frac{1}{a_0^C} + \frac{1}{2} r_0^C p^2 + \dots. \quad (4.27)$$

A derivation of Eq. (4.27) for the case of proton–proton scattering can be found, for example, in Ref. [13].³ See also Ref. [11] for a detailed discussion. The analytic properties of the $\ell = 0$ modified effective range function are investigated in Ref. [126].

In Ref. [122], Bollé and Gesztesy derived a very general form of the Coulomb-modified effective range expansion for an arbitrary number of spatial dimensions. Specializing their result to the three-dimensional case, a version of Eq. (4.24) can be written as

$$C_{\eta,\ell}^2 p^{2\ell+1} \left(\cot \tilde{\delta}_\ell(p) - i \right) + \gamma \tilde{h}_\ell(p) = -\frac{1}{a_\ell^C} + \frac{1}{2} r_\ell^C p^2 + \dots \quad (4.28)$$

with⁴

$$\tilde{h}_\ell(p) = \frac{(2p)^{2\ell}}{\Gamma(2\ell+2)^2} \frac{|\Gamma(\ell+1+i\eta)|^2}{|\Gamma(1+i\eta)|^2} \left(\psi(i\eta) + \frac{1}{2i\eta} - \log(i\eta) \right). \quad (4.29)$$

³As a remark we note that on first sight the expansion given in Eq. (51) of Bethe’s paper [13] seems to be different from the one given here in Eq. (4.27), which is the same as given in later publications referring to Bethe’s result. The η -dependent function on the left hand side of Bethe’s expansion appears to differ from our $h(\eta)$ by two times the Euler-Mascheroni constant γ_E . This apparent conflict can be resolved by noting that the $g(\eta)$ in Eq. (51) of Ref. [13] is *not* the function defined in Eq. (47a) of the same paper, but rather given by $\lim_{\eta_1 \rightarrow \infty} [g(\eta) - g(\eta_1)]$, where in this latter expression the g from Eq. (47a) is meant. The limiting process then yields exactly the term $-2\gamma_E$.

⁴This definition essentially comes from combining Eqs. (4.1) and (4.2) of Ref. [122], with the correction that the exponent in Eq. (4.2) should be -2 rather than 2 .

The latter function can be rewritten using

$$C_{\eta,\ell}^2 = \frac{2^{2\ell}}{\Gamma(2\ell+2)^2} \frac{|\Gamma(\ell+1+i\eta)|^2}{|\Gamma(1+i\eta)|^2} C_{\eta,0}^2, \quad (4.30)$$

with $C_{\eta,0}^2$ as defined in Eq. (4.12). The expressions given here reproduce Eqs. (4.24) and (4.13) when one explicitly assumes that the momentum p is real. In fact, one has to rewrite Eq. (4.29) in this manner in order to get an effective range function that is analytic in p^2 around threshold.

The form of the Coulomb-modified effective range expansion for general ℓ that we have given in Eqs. (4.24) and (4.28) is the same as in Ref. [122]. Note that sometimes another convention, differing from ours by an overall momentum-independent factor, is used in the literature. The effective range expansion given in Refs. [124, 127, 128] can be written as

$$\left(\frac{\Gamma(2\ell+2)}{2^\ell \Gamma(\ell+1)} \right)^2 \left[C_{\eta,\ell}^2 p^{2\ell+1} \left(\cot \tilde{\delta}_\ell(p) - i \right) + \gamma \tilde{h}_\ell(p) \right] = -\frac{1}{\tilde{a}_\ell^C} + \frac{1}{2} \tilde{r}_\ell^C p^2 + \dots \quad (4.31)$$

This expression has the advantage of having a more direct connection to the ordinary effective range expansion without Coulomb effects. For $\ell = 0$, both our choice and the form in Eq. (4.31) give the same expression. In this work we will, because of its simpler form, primarily use the convention of Eqs. (4.24) and (4.28).

4.3 Bound-state regime

In order to discuss the bound-state regime for systems of charged particles we need to know the solutions of Eq. (5.29) with the appropriate (exponentially decaying) behavior. In other words, we need the Coulomb analogs of the Hankel functions H_ℓ^\pm .

4.3.1 Asymptotic wave function

Essentially, this role is played by the Whittaker functions $W_{\mp i\eta, \ell + \frac{1}{2}}$. From the definitions (4.4) one directly sees that

$$G_\ell^{(p)}(r) - iF_\ell^{(p)}(r) = e^{-i\sigma_\ell} e^{i\frac{\pi}{2}(\ell-i\eta)} W_{i\eta, \ell + \frac{1}{2}}(2ipr) \quad (4.32)$$

where the prefactor is found by noting that with m and k as in Eq. (4.6) we have

$$\frac{\Gamma(\frac{1}{2} + m - k)}{|\Gamma(\frac{1}{2} + m - k)|} = e^{i \arg \Gamma(\ell+1-i\eta)} = e^{-i\sigma_\ell} \quad (4.33)$$

due to the property $\overline{\Gamma(z)} = \Gamma(\bar{z})$ of the Gamma function. Using this, one can also write the Coulomb phase shift in the form

$$e^{i\sigma_\ell} = \left(\frac{\Gamma(\ell+1+i\eta)}{\Gamma(\ell+1-i\eta)} \right)^{\frac{1}{2}}, \quad (4.34)$$

which is useful for showing that furthermore

$$G_\ell^{(p)}(r) + iF_\ell^{(p)}(r) = e^{i\sigma_\ell} e^{-i\frac{\pi}{2}(\ell+i\eta)} W_{-i\eta, \ell+\frac{1}{2}}(-2ipr). \quad (4.35)$$

More precisely, this follows from the definitions (4.4) after a short calculation involving the relation [114]

$$M_{k,m}(z) = e^{-i\pi k} \frac{\Gamma(2m+1)}{\Gamma(\frac{1}{2}+m-k)} W_{-k,m}(-z) - e^{i\pi(m-\frac{1}{2}+k)} \frac{\Gamma(2m+1)}{\Gamma(\frac{1}{2}+m+k)} W_{k,m}(z), \quad (4.36)$$

the second term of which cancels the $W_{k,m}(z)$ from $G_\ell^{(p)}(r)$ after simplifying the prefactors with the help of (4.34). These and further relations for Coulomb wave functions with complex arguments and/or parameters can also be found in the articles by Humblet [129] and Dzieciol *et al.* [130].

According to Hull and Breit [113], the asymptotic behavior of the Whittaker functions for large $|z|$ is

$$W_{k,m}(z) \sim e^{-z/2} z^k, \quad W_{-k,m}(-z) \sim e^{z/2} (-z)^{-k}, \quad (4.37)$$

such that the normalizable bound-state solution is given by

$$W_{-i\eta, \ell+\frac{1}{2}}(-2ipr) \propto \frac{e^{-\kappa r}}{r^{|\eta|}} \quad \text{as } |z| \rightarrow \infty \quad (4.38)$$

for bound-state momenta $p = i\kappa$, $\kappa > 0$.

4.3.2 Bound-state condition and ANC

We now go back to the case where a finite-range interaction is present in addition to the Coulomb tail and consider solutions $w_\ell^{(p)}(r)$ of Eq. (4.21) with the asymptotic form as given in Eq. (4.22). Inverting Eqs. (4.32) and (4.35) in order to express $W_{\pm i\eta, \ell+\frac{1}{2}}$ in terms of $F_\ell^{(p)}$ and $G_\ell^{(p)}$ and inserting the result into Eq. (4.22) gives

$$w_\ell^{(p)}(r) \propto [\cot \tilde{\delta}_\ell(p) - i] W_{i\eta, \ell+\frac{1}{2}}(2ipr) - [\cot \tilde{\delta}_\ell(p) + i] e^{2i\sigma_\ell} e^{-i\pi\ell} W_{-i\eta, \ell+\frac{1}{2}}(-2ipr) \quad (4.39)$$

for $r > R$, in direct analogy to Eq. (2.18) that describes the case without Coulomb interaction (see Section 2.1.3). Repeating the argument that for a bound state the component representing the incoming wave—given by the $W_{i\eta, \ell+\frac{1}{2}}$ —has to vanish, one finds that the condition for the existence of a bound state with binding momentum κ is

$$\cot \tilde{\delta}_\ell(p = i\kappa) = i. \quad (4.40)$$

In other words, one simply has to replace the scattering phase shift $\delta_\ell(p)$ in Eq. (2.21) with its Coulomb-modified analog $\tilde{\delta}_\ell(p)$. Furthermore, we define a bound-state solution $w_{A,\ell}^{(i\kappa)}(r)$ that behaves exactly like the Whittaker function,

$$w_{A,\ell}^{(i\kappa)}(r) = \tilde{A}_\kappa \cdot W_{-i\eta, \ell+\frac{1}{2}}(2\kappa r) \quad \text{for } r > R, \quad (4.41)$$

where \tilde{A}_κ denotes the asymptotic normalization constant (ANC) for a bound state of charged particles.

4.4 The Coulomb T-matrix

For the pure Coulomb interaction it is possible to write down a closed expression for the full off-shell T-matrix (see Section 2.2.2). If we write the Coulomb interaction as an operator \hat{V}_C with

$$\langle \mathbf{r} | \hat{V}_C | \mathbf{r}' \rangle = \delta^{(3)}(\mathbf{r} - \mathbf{r}') V_C(\mathbf{r}) \quad \text{with} \quad V_C(\mathbf{r}) = V_C(r) \equiv \frac{\gamma}{2\mu r}, \quad (4.42)$$

$$\langle \mathbf{p} | \hat{V}_C | \mathbf{q} \rangle = \frac{2\pi\gamma}{\mu} \frac{1}{(\mathbf{p} - \mathbf{q})^2} \equiv V_C(\mathbf{p}, \mathbf{q}), \quad (4.43)$$

the Lippmann-Schwinger equation (2.46) for the Coulomb T-matrix T_C reads

$$\hat{T}_C(E) = \hat{V}_C + \hat{V}_C \hat{G}_0^{(+)}(E) \hat{T}_C(E), \quad (4.44)$$

where the energy E is a free (complex) parameter.

Slightly altering our notation for the rest of this chapter, we introduce the center-of-mass momentum scale k (instead of denoting it by p as done so far) and write

$$E = \frac{k^2}{2\mu}, \quad \eta = \frac{\gamma}{2k}. \quad (4.45)$$

With this, a solution of Eq. (4.44) in momentum space can be written in the Hostler form⁵ [131–133]

$$T_C(k; \mathbf{p}, \mathbf{q}) = V_C(\mathbf{p}, \mathbf{q}) \left\{ 1 - 2i\eta \int_1^\infty \left(\frac{s+1}{s-1} \right)^{-i\eta} \frac{ds}{s^2 - 1 - \epsilon} \right\}, \quad (4.46)$$

where

$$\epsilon = \frac{(p^2 - k^2)(q^2 - k^2)}{k^2(\mathbf{p} - \mathbf{q})^2}. \quad (4.47)$$

Alternatively, it can be recast in terms of hypergeometric functions as

$$T_C(k; \mathbf{p}, \mathbf{q}) = V_C(\mathbf{p}, \mathbf{q}) \left\{ 1 - \Delta^{-1} \left[{}_2F_1 \left(1, i\eta, 1 + i\eta; \frac{\Delta - 1}{\Delta + 1} \right) - {}_2F_1 \left(1, i\eta, 1 + i\eta; \frac{\Delta + 1}{\Delta - 1} \right) \right] \right\}, \quad (4.48)$$

with the new variable Δ defined via

$$\Delta^2 = 1 + \epsilon. \quad (4.49)$$

For future reference we note that this can be shown by using the integral representation [103]

$${}_2F_1(a, b; c; z) = \frac{\Gamma(c)}{\Gamma(b)\Gamma(c-b)} \int_0^1 t^{b-1} (1-t)^{c-b-1} (1-tz)^{-a} dt \quad (4.50)$$

⁵Up to a prefactor $(e^{2\pi\eta} - 1)^{-1}$ in front of the integral, this is the form given in Eq. (90) of Ref. [131]. Note, however, that the additional factor should actually not be there, which can be seen by starting from Eq. (86) in the same reference.

for the hypergeometric function to obtain first

$${}_2F_1\left(1, i\eta; 1 + i\eta; \frac{\Delta - 1}{\Delta + 1}\right) = \frac{\Gamma(1 + i\eta)}{\Gamma(i\eta)} \int_0^1 \frac{t^{i\eta-1} dt}{1 - t \frac{\Delta-1}{\Delta+1}} = i\eta \int_1^\infty \frac{t^{-i\eta} dt}{t - \frac{\Delta-1}{\Delta+1}}, \quad (4.51)$$

and subsequently, using the transformation

$$t = \frac{s+1}{s-1}, \quad dt = \frac{2 ds}{(s-1)^2} \quad (4.52)$$

to arrive at

$$\begin{aligned} {}_2F_1\left(1, i\eta; 1 + i\eta; \frac{\Delta - 1}{\Delta + 1}\right) - {}_2F_1\left(1, i\eta; 1 + i\eta; \frac{\Delta + 1}{\Delta - 1}\right) \\ = i\eta \int_1^\infty \left(\frac{s+1}{s-1}\right)^{-i\eta} \frac{2\Delta ds}{s^2 - \Delta^2}. \end{aligned} \quad (4.53)$$

This gives back the integral form (4.46) of $T_C(k; \mathbf{p}, \mathbf{q})$ when inserted into Eq. (4.48).

4.4.1 Yukawa screening

In many situations, most notably in numerical calculations, it is necessary to suppress the long range of the Coulomb potential by *screening* it at large distances. A popular choice to implement this is to replace the plain Coulomb interaction with a Yukawa potential,

$$V_C(\mathbf{r}) \longrightarrow V_{C,\lambda}(\mathbf{r}) = \frac{\gamma}{2\mu} \frac{e^{-\lambda r}}{r}, \quad (4.54)$$

where the screening parameter λ can be interpreted as a photon mass. In momentum space, the Yukawa potential is given by

$$V_{C,\lambda}(\mathbf{p}, \mathbf{q}) = \frac{2\pi\gamma}{\mu} \frac{1}{(\mathbf{p} - \mathbf{q})^2 + \lambda^2}. \quad (4.55)$$

In fact, the Coulomb potential in momentum space is usually defined by taking the limit $\lambda \rightarrow 0$ in this expression because the Fourier transform of $1/r$ is not immediately well-defined. From the above expression it is clear that the photon mass regulates the singularity that otherwise occurs in forward direction ($\mathbf{q} = \mathbf{p}$, *i.e.*, for vanishing momentum transfer).

Ref. [131] gives an expression for what we in the following call the “partially screened” Coulomb T-matrix $\hat{T}_{C,\lambda}$, originally derived by Gorshkov [111]. It is defined by the relation

$$\hat{T}_{C,\lambda} = \hat{V}_{C,\lambda} + \hat{V}_{C,\lambda} \hat{G}_0^{(+)} \hat{T}_C, \quad (4.56)$$

where we have not written out the energy dependence of the functions for notational convenience.

Note that this is not a Lippmann–Schwinger equation because the operator that appears on the right-hand side is the unscreened Coulomb T-matrix \hat{T}_C . Still, $\hat{T}_{C,\lambda}$ is an interesting

object to study because it can be written down as a closed expression that converges to the unscreened Coulomb T-matrix \hat{T}_C in the limit $\lambda \rightarrow 0$. Due to this property it is useful in numerical calculations where the the Coulomb interaction—with its pole at vanishing momentum transfer that would otherwise create problems—has to be regulated. Ideally, one would of course like to use an expression for the exact Yukawa T-matrix in such an approach, but no closed solution for that quantity is known so far. We thus propose here to use $\hat{T}_{C,\lambda}$ as a pragmatic alternative and will discuss its application to the low-energy proton–deuteron system in Chapter 6. Since it has the right behavior in the limit $\lambda \rightarrow 0$, we expect it to adequately describe most of the nonperturbative Coulomb effects.

Unfortunately, the expression given for $T_{C,\lambda}(k; \mathbf{p}, \mathbf{q})$ in Eqs. (246) and (247) of Ref. [131] is not fully correct.⁶ Since in the original paper by Gorshkov [111] the limit $\lambda \rightarrow 0$ is taken without first giving the explicit form of the partially screened T-matrix, we will derive it here in the following.

To this end we start from Eq. (244) of Ref. [131], which in our notation reads

$$T_{C,\lambda}(k; \mathbf{p}, \mathbf{q}) = V_{C,\lambda}(\mathbf{p}, \mathbf{q}) - i\eta \int_0^1 \frac{dx}{\Lambda_0(x)} V_{C,\lambda-ik\Lambda_0(x)}(x\mathbf{p}, \mathbf{q}) \times \exp \left\{ -i\eta \int_x^1 \frac{dx_1}{x_1\Lambda_0(x_1)} \right\}, \quad (4.57)$$

where $\Lambda_0(x)$ is defined as the positive root of

$$\Lambda_0^2(x) = [1 - (p/k)^2 x] (1 - x), \quad (4.58)$$

and $V_{C,\lambda-ik\Lambda_0(x)}$ is just the Yukawa potential (4.55) with the substitution $\lambda \rightarrow \lambda - ik\Lambda_0(x)$.

We now consider the integral in Eq. (4.57). With the substitution [111]

$$x = \frac{s^2 - 1}{s^2 - (p/k)^2}, \quad \frac{dx}{ds} = \frac{2s(1 - (p/k)^2)}{(s^2 - (p/k)^2)^2} \quad (4.59)$$

one finds that

$$\Lambda_0(x) = s(1 - x), \quad (4.60)$$

and since furthermore

$$1 - x = \frac{1 - (p/k)^2}{s^2 - (p/k)^2}, \quad (4.61)$$

the integral in the exponent is just

$$\int_x^1 \frac{dx_1}{x_1\Lambda_0(x_1)} = \int_s^\infty \frac{2ds_1}{s_1^2 - 1} = \log\left(\frac{s+1}{s-1}\right). \quad (4.62)$$

For the potential term under the integral we find

$$V_{C,\lambda-ik\Lambda_0(x)}(x\mathbf{p}, \mathbf{q}) = \frac{2\pi\gamma}{\mu} \times \frac{(s^2 - (p/k)^2)}{(s^2 - 1)(\mathbf{q} - \mathbf{p})^2 + \frac{1}{k^2} \left[\lambda^2(k^2 s^2 - p^2) - 2i\lambda k s(k^2 - p^2) - (k^2 - q^2)(k^2 - p^2) \right]} \quad (4.63)$$

⁶This can be seen by a straightforward dimensional analysis of Eq. (247) in Ref. [131]. Furthermore, the prefactor in Eq. (246) is written in terms of the unscreened Coulomb potential, which is clearly not correct.

after a lengthy but straightforward calculation. Adding

$$0 = \lambda^2(s^2 - 1) - \lambda^2 s^2 + \lambda^2 \quad (4.64)$$

in the denominator, we can rewrite this as

$$V_{C,\lambda-ik\Lambda_0(x)}(x\mathbf{p}, \mathbf{q}) = \frac{2\pi\gamma}{\mu} \times \frac{(s^2 - (p/k)^2)}{(s^2 - 1)[(\mathbf{q} - \mathbf{p})^2 + \lambda^2] - \frac{1}{k^2}[(k^2 - q^2)(k^2 - p^2)] + \frac{1}{k^2}[(k^2 - p^2)(\lambda^2 - 2i\lambda ks)]}. \quad (4.65)$$

Finally, noting that the term in the numerator cancels against the same factor in

$$\frac{dx}{\Lambda_0(x)} = \frac{2 ds}{s^2 - (p/k)^2}, \quad (4.66)$$

and factoring out the Yukawa potential, we arrive at

$$T_{C,\lambda}(k; \mathbf{p}, \mathbf{q}) = V_{C,\lambda}(\mathbf{p}, \mathbf{q}) \left\{ 1 - 2i\eta \int_1^\infty \left(\frac{s+1}{s-1} \right)^{-i\eta} \frac{ds}{s^2 - 1 - \epsilon_\lambda + \zeta_\lambda(s)} \right\} \quad (4.67)$$

with

$$\epsilon_\lambda = \frac{(k^2 - p^2)(k^2 - q^2)}{k^2 [(\mathbf{q} - \mathbf{p})^2 + \lambda^2]} \quad (4.68)$$

and

$$\zeta_\lambda(s) = \frac{(k^2 - p^2)(\lambda^2 - 2i\lambda ks)}{k^2 [(\mathbf{q} - \mathbf{p})^2 + \lambda^2]}. \quad (4.69)$$

This expression is very similar to the integral form of the unscreened Coulomb T-matrix. The only differences are given by the new term $\zeta_\lambda(s)$ in the denominator and the fact that all singularities, both in the overall prefactor and under the integral, are now regulated by adding λ^2 . In fact, one directly sees that in the limit $\lambda \rightarrow 0$, Eq. (4.67) converges to the unscreened expression given in Eq. (4.46).

4.4.2 Expression in terms of hypergeometric functions

Something that is not noted in Refs. [131] and [111] is that—just like the unscreened Coulomb T-matrix— $T_{C,\lambda}(k; \mathbf{p}, \mathbf{q})$ can also be expressed in terms of hypergeometric functions. To obtain this expression we first note that the denominator in Eq. (4.67) can be written as

$$s^2 - 1 - \epsilon_\lambda + \zeta_\lambda(s) = s^2 - (1 + d_1 \cdot D^2) - (d_2 \cdot D^2)s \quad (4.70)$$

with

$$d_1 = k^2 - q^2 - \lambda^2, \quad d_2 = 2i\lambda k \quad (4.71)$$

and

$$D^2 = \frac{k^2 - p^2}{k^2 [(\mathbf{q} - \mathbf{p})^2 + \lambda^2]}. \quad (4.72)$$

After making the transformation

$$s = \frac{t+1}{t-1}, \quad \int_1^\infty ds = 2 \int_1^\infty \frac{dt}{(t-1)^2} \quad (4.73)$$

we get

$$T_{C,\lambda}(k; \mathbf{p}, \mathbf{q}) = V_{C,\lambda}(\mathbf{p}, \mathbf{q}) \times \left\{ 1 - 4i\eta \int_1^\infty \frac{t^{-i\eta} dt}{-D^2(d_1 + d_2)t^2 + (4 + 2D^2 \cdot d_1)t - D^2(d_1 - d_2)} \right\}. \quad (4.74)$$

To proceed further, we use the indefinite integral⁷

$$\int \frac{t^\nu dt}{x_2 t^2 + x_1 t + x_0} = \frac{1}{X_1} \frac{2^{-\nu} t^\nu}{\nu} \left\{ {}_2F_1(-\nu, -\nu; 1-\nu; X_2^+(t)) \cdot X_3^+(t)^{-\nu} - {}_2F_1(-\nu, -\nu; 1-\nu; X_2^-(t)) \cdot X_3^-(t)^{-\nu} \right\}, \quad (4.75)$$

where

$$X_1 = \sqrt{x_1^2 - 4x_0x_2}, \quad X_2^\pm(t) = \frac{x_1 \mp X_1}{x_1 + 2tx_2 \mp X_1}, \quad X_3^\pm(t) = \frac{tx_2}{x_1 + 2tx_2 \mp X_1}. \quad (4.76)$$

Evaluating this at $t = 1$ is straightforward, but considering $t \rightarrow \infty$ requires a little more care. From Eq. (4.76) one sees that $X_2^\pm(t)$ goes to zero like $1/t$ as $t \rightarrow \infty$, such that the hypergeometric functions simply yield one in this limit. Since the potentially problematic (because $\nu = -i\eta$) prefactor t^ν is cancelled by the numerator of $X_3^\pm(t)^{-\nu}$ with the remainder then going to zero as $t \rightarrow \infty$, we can conclude that there is actually no contribution to the integral from the upper boundary in Eq. (4.74) and that its value is hence given by the right-hand side of Eq. (4.82) with $t = 1$.

Before inserting this into Eq. (4.74), we subsequently apply the identities [103]

$${}_2F_1(a, b; c; z) = (1-z)^{c-a-b} {}_2F_1(c-a, c-b; c; z) \quad (4.77)$$

and

$${}_2F_1(a, b; c; z) = (1-z)^{-a} {}_2F_1\left(a, c-b; c; \frac{z}{z-1}\right) \quad (4.78)$$

to rewrite

$$\begin{aligned} {}_2F_1(-\nu, -\nu; 1-\nu; z) &= (1-z)^{1+\nu} {}_2F_1(1, 1; 1-\nu; z) \\ &= (1-z)^\nu {}_2F_1\left(1, -\nu; 1-\nu; \frac{z}{z-1}\right). \end{aligned} \quad (4.79)$$

This is useful because from Eq (4.76) one finds that for $z = X_2^\pm(t)$,

$$(1-z)^\nu = 2^\nu X_3^\pm(t)^\nu, \quad (4.80)$$

⁷This result has been obtained with the help of computer algebra software (Wolfram Mathematica).

canceling the inverse factors of this in Eq. (4.82). Moreover, the arguments simplify to

$$\frac{z}{z-1} = -\frac{1}{2} \frac{X_2^\pm(t)}{X_3^\pm(t)} = -\frac{x_1 \mp X_1}{2tx_2}. \quad (4.81)$$

With this, we then have

$$\int_1^\infty \frac{t^\nu dt}{x_2 t^2 + x_1 t + x_0} = \frac{1}{\nu X_1} \left\{ {}_2F_1\left(1, -\nu; 1 - \nu; -\frac{x_1 + X_1}{2x_2}\right) - {}_2F_1\left(1, -\nu; 1 - \nu; -\frac{x_1 - X_1}{2x_2}\right) \right\}. \quad (4.82)$$

Finally, applying the above result to Eq. (4.74), we can write the partially-screened Coulomb T-matrix as

$$T_{C,\lambda}(k; \mathbf{p}, \mathbf{q}) = V_C(\mathbf{p}, \mathbf{q}) \left\{ 1 - \Delta_\lambda^{-1} [{}_2F_1(1, i\eta, 1 + i\eta; X_\lambda^-) - {}_2F_1(1, i\eta, 1 + i\eta; X_\lambda^+)] \right\}, \quad (4.83)$$

with

$$\Delta_\lambda^2 = 1 + \frac{(k^2 - p^2)(k^2 - q^2 - \lambda^2)}{k^2 [(\mathbf{q} - \mathbf{p})^2 + \lambda^2]} - \frac{\lambda^2(k^2 - p^2)^2}{k^2 [(\mathbf{q} - \mathbf{p})^2 + \lambda^2]^2} \quad (4.84)$$

and

$$X_\lambda^\pm = \frac{2k^2 [(\mathbf{q} - \mathbf{p})^2 + \lambda^2] (1 \pm \Delta_\lambda) + (k^2 - p^2)(k^2 - q^2 - \lambda^2)}{(k^2 - p^2) [(k + i\lambda)^2 - q^2]}. \quad (4.85)$$

As it should, this reduces to the hypergeometric expression (4.48) for the unscreened Coulomb T-matrix in the limit $\lambda \rightarrow 0$. It is directly clear from Eqs. (4.84) and (4.49) that

$$\lim_{\lambda \rightarrow 0} \Delta_\lambda^2 = \Delta^2, \quad (4.86)$$

and a straightforward calculation then furthermore shows that

$$\lim_{\lambda \rightarrow 0} X_\lambda^\pm = \frac{\Delta \pm 1}{\Delta \mp 1}. \quad (4.87)$$

Chapter 5

Causality bounds for charged particles

Overview

In this chapter, we derive a generalization of the so-called Wigner causality bound for a system of charged particles, where the Coulomb force determines the long-range interactions. The majority of the material presented in the following sections has been published in Ref. [5]. The review of Coulomb wave functions and the modified effective range expansion from that reference have already been given in the preceding chapter; the remaining parts are included here in a slightly re-arranged and amended form. A part of Section 5.7 is based on results from Ref. [4] that have been omitted in Chapter 3 to put them in a more suitable context here. Finally, the discussion of causality bounds for van der Waals tails in Section 5.8 is summarized from Ref. [7], which was mainly worked out by S. Elhatisari.

5.1 Introduction

The constraints of causality for two-body scattering with finite-range interactions were first derived by Wigner [134]. The causality bound can be understood as a lower bound on the time delay Δt between the incoming and outgoing wave packets. When Δt is negative, the outgoing wave packet departs earlier than for the non-interacting system. However, the incoming wave must first reach the interaction region before the outgoing wave can leave. In low-energy scattering this manifests itself as an upper bound on the effective range parameter. In Ref. [135], Phillips and Cohen derived this bound for S-wave scattering with finite-range interactions. Some constraints on nucleon–nucleon scattering and the chiral two-pion exchange potential were considered in Ref. [136], and relations between the scattering length and effective range have been explored for one-boson exchange potentials [137] and van der Waals potentials [138]. In Refs. [10, 139] the causality bounds for finite-range interactions were extended to an arbitrary number of space-time dimensions and arbitrary angular momentum. The extension to systems with

partial-wave mixing was first studied in Ref. [140].

Here, we consider the causality constraints for the scattering of two charged particles with an arbitrary finite-range interaction. This analysis, published in Ref. [4], is the first study of causality bounds that takes into account the long-range Coulomb force. The results presented here are relevant to studies of low-energy scattering of nuclei and nucleons using effective field theory (EFT), in particular for the application of effective field theory to the nuclear halo systems discussed in Section 2.4.3.

There is an important connection between causality bounds and the convergence of effective-field-theory calculations with increasing order [140]. For local contact interactions, the range of the effective interaction is controlled by the momentum cutoff scale of the effective theory. In effective theories with non-perturbative renormalization, which typically occur in nuclear physics, exact cutoff-independence can generally not be achieved. There is a “natural” value of the cutoff at which all higher-order corrections scale as expected from dimensional analysis. If the cutoff is taken larger, “new physics” intervenes, the corrections scale unnaturally, and unitarity violations may occur. This is different from what one encounters in high-energy particle physics where the renormalization is typically perturbative and cutoff momenta can be chosen arbitrarily large. For calculations using dimensional regularization, the renormalization scale plays a similar role in regulating ultraviolet physics.

The term “new physics,” in the above context, refers to details left out (integrated out) in the effective theory. In the case of halo EFT, these details are the finite size of the core nucleus and its internal excitations as well as the exponential tail of the pion-exchange interaction. Problems with convergence of the effective theory can occur if the cutoff scale is set higher than the scale of the new physics. It is desirable to have a more quantitative measure of when problems may appear, and this is where the causality bound provides a useful diagnostic tool. For each scattering channel we use the physical scattering parameters to compute a quantity called the causal range, R_c . It is the minimum range for finite-range interactions consistent with the requirements of causality and unitarity. For any fixed cutoff scale, the causality bound marks a branch cut of the effective theory when viewed as a function of physical scattering parameters [140]. The coupling constants of the effective theory become complex when scattering parameters violating the causality bound are enforced. These branch cuts do not appear in perturbation theory; however, a nearby branch point can spoil the absolute convergence of the perturbative expansion.

Our results can be viewed as a guide for improving the convergence of halo-EFT calculations. In particular, if the cutoff momentum used in a calculation is too high, then problems with convergence may appear in some observables. Consequently, the causal range can be used to estimate the “natural” ultraviolet cutoff Λ of the effective theory as R_c^{-1} . The natural cutoff is optimal in the sense that no known infrared physics is left out of the theory and that all corrections involving the ultraviolet cutoff scale naturally [141, 142]. Increasing the cutoff beyond the natural value will not improve the accuracy of the calculation.

The causality bounds also have an impact in the regime of bound states. For two-body halo states—or more generally whenever there is a shallow two-body bound state close to threshold—the same integral identity that yields the causality bound for the effective

range can be used to derive a relation between the asymptotic normalization constant (ANC) of the bound-state wave function, the binding momentum, and the effective range for the scattering of the two halo constituents. This relation can be shown to be equivalent to a result previously derived by Sparenberg *et al.* [143]. Its significance lies in the fact that the ANC is an important input parameter for the calculation of near-threshold radiative capture and photodissociation reactions. The causality bounds also constrain the range of model potentials that are fitted to scattering data in order to extract ANCs.

The organization of this chapter is as follows. After briefly reviewing in Section 5.2 the theoretical setup for two charged particles with additional short-range interactions (discussed in detail in Chapter 4), we derive the charged-particle causality bounds for arbitrary values of the orbital angular momentum in Section 5.3. This analysis includes both attractive and repulsive Coulomb forces. In Section 5.4 we define the causal range and then extract and discuss this quantity in Section 5.5 for several nuclear scattering processes including proton–proton, proton–deuteron, proton– ^3He , proton–alpha, and alpha–alpha scattering. Some numerical calculations are given in Section 5.6. In Section 5.7, we elucidate the relation for asymptotic normalization constants mentioned above and extract, as an application, the ANCs of the excited 2^+ and 1^- states in ^{16}O from α – ^{12}C scattering data. Before briefly touching the subject of causality bounds for other long-range forces (in particular, for a van der Waals potential) in Section 5.8, we then conclude with a summary of the main results and provide an outlook.

5.2 Setup and preliminaries

We consider a two-particle system with reduced mass μ interacting via a finite-range potential with range R . As already done in the previous chapters, we write the interaction as a real symmetric operator with kernel $V(r, r')$ satisfying the finite-range condition,

$$V(r, r') = 0 \quad \text{if } r > R \text{ or } r' > R. \quad (5.1)$$

In particular, we assume that the interaction is energy-independent. After giving a detailed formal derivation of the causality bounds in the following sections, we will come back to the question what the above assumptions mean for the application to (halo) EFT calculations in Section 5.5.

In the absence of Coulomb interactions the system with (fixed but arbitrary) angular momentum ℓ is described by the radial Schrödinger equation,

$$p^2 u_\ell^{(p)}(r) = -\frac{d^2}{dr^2} u_\ell^{(p)}(r) + \frac{\ell(\ell+1)}{r^2} u_\ell^{(p)}(r) + 2\mu \int_0^R dr' V(r, r') u_\ell^{(p)}(r'). \quad (5.2)$$

As done in Chapter 2, we adopt the conventions of Ref. [10] and choose the normalization of $u_\ell^{(p)}$ that for $r \geq R$ we have

$$u_\ell^{(p)}(r) = p^\ell [\cot \delta_\ell(p) S_\ell(pr) + C_\ell(pr)], \quad (5.3)$$

where S_ℓ and C_ℓ are the Riccati-Bessel functions and $\delta_\ell(p)$ is the scattering phase shift.

If the particles carry electromagnetic charges Z_1e and Z_2e , respectively, there is a Coulomb potential in addition to the finite-range interaction. As done in Chapter 4, we write this as

$$V_C(r) = \frac{\gamma}{2\mu r} = \frac{\alpha Z_1 Z_2}{r}, \quad (5.4)$$

such that in the radial Schrödinger equation we simply get a term $\sim \gamma/r$ because the factor of 2μ in the denominator cancels out. From Section 4.2 we quote it in the form

$$p^2 w_\ell^{(p)}(r) = -\frac{d^2}{dr^2} w_\ell^{(p)}(r) + \frac{\ell(\ell+1)}{r^2} w_\ell^{(p)}(r) + 2\mu \int_0^R dr' V(r, r') w_\ell^{(p)}(r') + \frac{\gamma}{r} w_\ell^{(p)}(r), \quad (5.5)$$

where again we use the superscript “ (p) ” to denote the solution for a given center-of-mass momentum p . We choose the normalization of $w_\ell^{(p)}$ such that for $r \geq R$ we have¹

$$w_\ell^{(p)}(r) = p^\ell C_{\eta, \ell} \left[\cot \tilde{\delta}_\ell(p) F_\ell^{(p)}(r) + G_\ell^{(p)}(r) \right], \quad (5.6)$$

with the Coulomb-subtracted phase shift $\tilde{\delta}_\ell$ and the regular and irregular Coulomb wave functions $F_\ell^{(p)}$ and $G_\ell^{(p)}$ as defined in Chapter 4. The inclusion of the Gamow factor in the normalization $C_{\eta, \ell}$ will be convenient later, when we rewrite Eq. (5.6) in terms of a different pair of functions and relate it to the Coulomb-modified effective range expansion (4.24), rearranged in the form

$$C_{\eta, \ell}^2 p^{2\ell+1} \cot \tilde{\delta}_\ell(p) = -\gamma h_\ell(p) - \frac{1}{a_\ell^C} + \frac{1}{2} r_\ell^C p^2 + \dots, \quad (5.7)$$

with $h_\ell(p)$ as defined in Chapter 4.

5.3 Derivation of the causality bound

With the Coulomb wave functions and Coulomb-modified effective range expansion at our hands, we can now closely follow the derivation presented in Ref. [10] for scattering in the absence of Coulomb interactions.

5.3.1 Wronskian identities

We consider solutions of the radial Schrödinger equation (4.21) for two different momenta p_A and p_B . Introducing the short-hand notation

$$w_{A,B}(r) = w_\ell^{(p_{A,B})}(r), \quad (5.8)$$

i.e., suppressing the angular-momentum subscript ℓ for convenience, we get

$$\begin{aligned} (p_B^2 - p_A^2) \int_\epsilon^r dr' w_A(r') w_B(r') &= (w_B w'_A - w_A w'_B) \Big|_\epsilon^r \\ &\quad - 2\mu \int_\epsilon^r dr' \int_0^R dr [w_B(r) V(r, r') w_A(r') - w_A(r) V(r, r') w_B(r')] \end{aligned} \quad (5.9)$$

¹Note that for $\ell = 0$ our normalization is the same as chosen in Ref. [13], *i.e.*, for $r \geq R$ our solution $w_0^{(p)}$ coincides with the function φ defined in Eq. (42) of that paper.

by subtracting w_A times the equation for w_B from that for w_B multiplied by w_A , as it is done in Ref. [10], and integrating from some small radius ϵ to r .

We assume that our interaction $V(r, r')$ is such that it alone (without the additional Coulomb potential) permits a solution that is sufficiently regular at the origin, *i.e.*, $u_\ell(0) = 0$ and $\partial_r u_\ell$ stays finite as $r \rightarrow 0$, where u_ℓ is a solution of Eq. (5.2). As boundary condition for the solutions $w_{A,B}$ of the full radial Schrödinger equation we can then demand as well that they vanish with finite derivative at the origin. If we only had the Coulomb potential and no additional interaction, this is fulfilled by the regular Coulomb function $F_\ell^{(p)}(r)$, *cf.* Eq. (4.11a). We can thus take the limit $\epsilon \rightarrow 0$ in Eq. (5.9) and get the relation

$$W[w_B, w_A](r) = (p_B^2 - p_A^2) \int_0^r dr' w_A(r') w_B(r'), \quad (5.10)$$

where the Wronskian $W[w_B, w_A]$ is defined as

$$W[w_B, w_A](r) = w_B(r) w_A'(r) - w_A(r) w_B'(r). \quad (5.11)$$

5.3.2 Rewriting the wave functions

Following further the derivation presented in Ref. [10], we re-express the solutions $w_\ell^{(p)}(r)$ in terms of functions $f(p, r)$ and $g(p, r)$ such that

$$w_\ell^{(p)}(r) = p^{2\ell+1} C_{\eta, \ell}^2 \cot \tilde{\delta}_\ell(p) f(p, r) + g(p, r) \quad (5.12)$$

for $r \geq R$, with $f(p, r)$ analytic in p^2 ,

$$f(p, r) = f_0(r) + f_2(r) p^2 + \mathcal{O}(p^4), \quad (5.13)$$

and

$$g(p, r) = \tilde{g}(p, r) + \phi(p) \cdot f(p, r). \quad (5.14a)$$

The $g(p, r)$ contains a term which is non-analytic in p^2 and is proportional to $f(p, r)$. The remainder $\tilde{g}(p, r)$, however, is analytic in p^2 ,

$$\tilde{g}(p, r) = g_0(r) + g_2(r) p^2 + \mathcal{O}(p^4). \quad (5.14b)$$

Combining Eqs. (5.6) and (5.12), we find

$$f(p, r) = \frac{1}{p^{\ell+1} C_{\eta, \ell}} F_\ell^{(p)}(r) \quad (5.15a)$$

and

$$g(p, r) = p^\ell C_{\eta, \ell} G_\ell^{(p)}(r). \quad (5.15b)$$

These functions are directly related to the analytic Coulomb wave functions of Bollé and Gesztesy [122] mentioned in Section 4.1.2 and discussed further in Appendix A. In fact, one simply has that $f(p, r)$ is exactly the $F_n^{(0)}(p, r)$ defined in Eq. (A.3a), whereas comparison of Eqs. (5.15b) and (A.3b) shows that

$$g(p, r) = \tilde{G}_n^{(0)}(p, r) + \left(\gamma \tilde{h}_\ell(p) - i p^{2\ell+1} C_{\eta, \ell}^2 \right) \cdot F_n^{(0)}(p, r) \quad (5.16)$$

with $\tilde{G}_n^{(0)}(p, r)$ as defined in Eq. (A.4). This implies that

$$\tilde{g}(p, r) = \tilde{G}_n^{(0)}(p, r) \quad (5.17)$$

and

$$\phi(p) = \gamma \tilde{h}_\ell(p) - ip^{2\ell+1} C_{n,\ell}^2 = \gamma h_\ell(p), \quad (5.18)$$

where the last step follows from the combination of Eqs. (4.29) and (A.4) after a short calculation.

When we insert now the modified effective range expansion (4.24) into the asymptotic Coulomb wave function (5.12), the non-analytic term involving $h_\ell(p)$ conveniently drops out and we are left with

$$w_\ell^{(p)}(r) = \left(-\frac{1}{a_\ell^C} + \frac{1}{2} r_\ell^C p^2 + \dots \right) f(p, r) + \tilde{g}(p, r) \quad \text{for } r \geq R. \quad (5.19)$$

Thus, it is possible to choose a normalization such that $w_\ell^{(p)}(r)$ is analytic in p^2 . Combining this with the expansions (5.13) and (5.14), we arrive at

$$w_\ell^{(p)}(r) = -\frac{1}{a_\ell^C} f_0(r) + g_0(r) + p^2 \left[\frac{1}{2} r_\ell^C f_0(r) - \frac{1}{a_\ell^C} f_2(r) + g_2(r) \right] + \mathcal{O}(p^4). \quad (5.20)$$

5.3.3 The causality-bound function

From here we can proceed exactly as in Ref. [10]. For the Wronskian of two solutions w_A and w_B for $r \geq R$ we find

$$\begin{aligned} W[w_B, w_A](r) = (p_B^2 - p_A^2) & \left\{ \frac{1}{2} r_\ell^C W[f_0, g_0](r) + \left(\frac{1}{a_\ell^C} \right)^2 W[f_2, f_0](r) \right. \\ & \left. - \frac{1}{a_\ell^C} [W[f_2, g_0](r) - W[g_2, f_0](r)] + W[g_2, g_0](r) \right\} + \mathcal{O}(p_{A,B}^4). \end{aligned} \quad (5.21)$$

Note that in the $\mathcal{O}(p_{A,B}^4)$ we have also included terms of the form $p_A^2 p_B^2$. We set $p_A = 0$ in Eq. (5.10) and furthermore take the limit $p_B \rightarrow 0$. Using the expansion (5.21), we get

$$-r_\ell^C W[f_0, g_0](r) = b_\ell^C(r) - 2 \int_0^r dr' \left[w_\ell^{(0)}(r') \right]^2 \quad (5.22)$$

for $r \geq R$, with $w_\ell^{(0)}(r) = \lim_{p \rightarrow 0} w_\ell^{(p)}(r)$ and the *causality-bound function*

$$b_\ell^C(r) = 2W[g_2, g_0](r) - \frac{2}{a_\ell^C} \{W[f_2, g_0](r) + W[g_2, f_0](r)\} + \frac{2}{(a_\ell^C)^2} W[f_2, f_0](r). \quad (5.23)$$

Written as a function of $\rho = p \cdot r$, the Wronskian of the Coulomb wave functions is²

$$W[F_\ell^{(p)}, G_\ell^{(p)}](\rho) = -W[G_\ell^{(p)}, F_\ell^{(p)}](\rho) = -1. \quad (5.24)$$

²See, for example, Eq. (14.2.4) in Ref. [103].

Since $d/dr = p \cdot d/d\rho$ and $W[f, f] \equiv 0$, we also have

$$W[f, g](r) = W[f, \tilde{g}](r) = -1. \quad (5.25)$$

Plugging in the expansions (5.13) and (5.14), we see that $W[f_0, g_0](r) = -1$ for the leading-order functions, and $W[f_2, g_0](r) = W[g_2, f_0](r)$ for the terms at $\mathcal{O}(p^2)$. Inserting these relations into Eq. (5.22), we get

$$r_\ell^C = b_\ell^C(r) - 2 \int_0^r dr' \left[w_\ell^{(0)}(r') \right]^2, \quad (5.26)$$

where $b_\ell^C(r)$ has been simplified to

$$b_\ell^C(r) = 2W[g_2, g_0](r) - \frac{4}{a_\ell^C} W[f_2, g_0](r) + \frac{2}{(a_\ell^C)^2} W[f_2, f_0](r). \quad (5.27)$$

Since the integral in Eq. (5.26) is positive definite, the resulting causality bound is

$$r_\ell^C \leq b_\ell^C(r), \quad \forall r \geq R. \quad (5.28)$$

5.3.4 Calculating the Wronskians

We now derive the explicit form of the function $b_\ell^C(r)$. To do this, we need expressions for the Wronskians that appear in Eq. (5.27). We can obtain them by first noting that $f(p, r)$ and $\tilde{g}(p, r)$, being linear combinations of Coulomb wave functions (with p -dependent coefficients), are solutions of the Coulomb Schrödinger equation,

$$\left[-\frac{d^2}{dr^2} + \frac{\ell(\ell+1)}{r^2} + \frac{\gamma}{r} - p^2 \right] x(p, r) = 0, \quad (5.29)$$

which, of course, corresponds to setting $V(r, r') = 0$ in Eq. (4.21). Here and in the following, x stands for either f or \tilde{g} . Inserting the expansion

$$x(p, r) = x_0(r) + p^2 x_2(r) + \mathcal{O}(p^4) \quad (5.30)$$

into Eq. (5.29) and comparing orders in p^2 , we find that

$$\left[-\frac{d^2}{dr^2} + \frac{\ell(\ell+1)}{r^2} + \frac{\gamma}{r} \right] x_0(r) = 0, \quad (5.31)$$

i.e., x_0 is a solution of the zero-energy Coulomb Schrödinger equation, and

$$\left[-\frac{d^2}{dr^2} + \frac{\ell(\ell+1)}{r^2} + \frac{\gamma}{r} \right] x_2(r) = x_0(r). \quad (5.32)$$

From this we readily obtain the differential equations

$$\frac{d}{dr} W[f_2, f_0](r) = [f_0(r)]^2, \quad (5.33a)$$

$$\frac{d}{dr} W[g_2, g_0](r) = [g_0(r)]^2, \quad (5.33b)$$

$$\frac{d}{dr} W[f_2, g_0](r) = f_0(r)g_0(r) \quad (5.33c)$$

for the desired Wronskians. Put together, this yields a simple first-order differential equation for $b_\ell^C(r)$,

$$\frac{d}{dr} b_\ell^C(r) = 2 \left(g_0(r) - \frac{1}{a_\ell^C} f_0(r) \right)^2. \quad (5.34)$$

From Eqs. (A.7) and (A.8) in Ref. [122] we have the explicit expressions

$$f_0(r) = \frac{(2l+1)!}{\sqrt{\gamma^{2l+1}}} \sqrt{r} I_{2l+1}(2\sqrt{\gamma r}), \quad (5.35a)$$

$$g_0(r) = \frac{2\sqrt{\gamma^{2l+1}}}{(2l+1)!} \sqrt{r} K_{2l+1}(2\sqrt{\gamma r}) \quad (5.35b)$$

for $\gamma > 0$, where I_α and K_α are modified Bessel functions, and

$$f_0(r) = \frac{(2l+1)!}{\sqrt{(-\gamma)^{2l+1}}} \sqrt{r} J_{2l+1}(2\sqrt{-\gamma r}), \quad (5.36a)$$

$$g_0(r) = \frac{-\pi \sqrt{(-\gamma)^{2l+1}}}{(2l+1)!} \sqrt{r} N_{2l+1}(2\sqrt{-\gamma r}) \quad (5.36b)$$

for $\gamma < 0$, where J_α and Y_α are the ordinary Bessel functions.^{3,4}

Using these expressions for f_0 and g_0 and Eq. (5.34) we can determine $b_\ell^C(r)$ up to an integration constant. In order to fix this constant, we must work directly with the Wronskians in Eq. (5.23). Before we do that, however, we first discuss the general form of $b_\ell^C(r)$. We break apart the function as a sum of two functions, $X_\ell(r)$ and $Y_\ell(r)$, and a constant term Z_ℓ ,

$$b_\ell^C(r) = X_\ell(r) + Y_\ell(r) + Z_\ell. \quad (5.37)$$

We take $X_\ell(r)$ to be a function consisting entirely of a sum of terms that have a pole at $r = 0$, ranging from order 1 to ℓ ,

$$X_\ell(r) = \sum_{m=1}^{\ell} X_{\ell,m} r^{-m}. \quad (5.38)$$

By furthermore requiring the function $Y_\ell(r)$ to vanish at $r = 0$, the decomposition in Eq. (5.37) is unique.

Where exactly the contributions to the three terms in the decomposition originate from can be inferred from the behavior of $f(p, r)$ and $g(p, r)$ at the origin. From Eq. (4.11a) combined with Eq. (5.15) we find that

$$f(p, r) \sim r^{\ell+1} \quad \text{as } r \rightarrow 0. \quad (5.39)$$

³From Eq. (9.1.50) and the remark above Eq. (9.6.41) in Ref. [103] it is clear that these f_0 and g_0 are indeed solutions of Eq. (5.31).

⁴Bollé and Gesztesy actually give an expression for g_0 in the attractive case ($\gamma < 0$) that involves the Hankel function $H_\alpha^{(2)}$ times i instead of the Neumann function N_α (also called Bessel function of the second kind and denoted then by Y_α). With that, however, g_0 would not be real, which it should be. Our g_0 as in Eq. (5.36b) is taken from the results of Lambert [121].

This implies that every term in the expansion of $f(p, r)$ is $\mathcal{O}(r^{\ell+1})$. Therefore,

$$\lim_{r \rightarrow 0} W[f_2, f_0](r) = 0 \quad (5.40)$$

for all ℓ , which means that this Wronskian only yields contributions to the $Y_\ell(r)$.

Furthermore, from Eq. (17) in Ref. [112] we know that the irregular Coulomb wave function has the asymptotic behavior

$$G_\ell^{(p)} \sim D_{\eta, \ell} \rho^{-\ell} \quad \text{as } \rho \rightarrow 0, \quad (5.41)$$

with $D_{\eta, \ell}$ fulfilling $C_{\eta, \ell} D_{\eta, \ell} = 2\ell + 1$. Using Eq. (5.15b) then yields

$$g(p, r) \sim \frac{r^{-\ell}}{2\ell + 1} \quad \text{as } r \rightarrow 0. \quad (5.42)$$

We note that $g_0(r)$ has exactly the same behavior near $r = 0$ and can thus show that $g_2(r)$ is subleading as $r \rightarrow 0$, $g_2(r) \sim r^{-\ell+c}$ for $c > 0$. From this we infer that

$$\lim_{r \rightarrow 0} W[f_0, g_2](r) = 0 \quad (5.43)$$

for all ℓ , so also from this Wronskian we only get contributions to $Y_\ell(r)$. Both the singular $X_\ell(r)$ and the constant Z_ℓ , therefore, only come from the Wronskian $W[g_2, g_0](r)$.

For $\ell = 0$ the situation is still simple because the above analysis also tells us that

$$\lim_{r \rightarrow 0} W[g_2, g_0](r) = 0 \quad \text{for } \ell = 0, \quad (5.44)$$

i.e., $b_0^C(r)$ is given entirely by $Y_0(r)$. With the knowledge that it vanishes at the origin, it is actually straightforward to give an explicit expression for $b_0^C(r)$ in terms of antiderivatives of the right hand side of Eq. (5.34), where one has to insert the $f_0(r)$ and $g_0(r)$ from Eqs. (5.35) and (5.36). The result, obtained by integrating from 0 to r , is

$$\begin{aligned} b_0^C(r) = & \frac{2r^3}{3} (a_0^C)^{-2} {}_1F_2 \left(\frac{3}{2}; 2, 4; 4\gamma r \right) - \frac{4r^2}{\sqrt{\pi}} (a_0^C)^{-1} G_{1,3}^{2,1} \left(4\gamma r \left| \begin{matrix} \frac{1}{2} \\ 0, 1, -2 \end{matrix} \right. \right) \\ & + 4\sqrt{\pi}\gamma r^2 G_{2,4}^{3,1} \left(4\gamma r \left| \begin{matrix} -1, \frac{1}{2} \\ -1, 0, 1, -2 \end{matrix} \right. \right) \end{aligned} \quad (5.45)$$

for the repulsive case, and

$$\begin{aligned} b_0^C(r) = & \frac{2r^3}{3} (a_0^C)^{-2} {}_1F_2 \left(\frac{3}{2}; 2, 4; 4\gamma r \right) + 4\sqrt{\pi}r^2 (a_0^C)^{-1} G_{2,4}^{2,1} \left(-4\gamma r \left| \begin{matrix} \frac{1}{2}, -\frac{1}{2} \\ 0, 1, -2, -\frac{1}{2} \end{matrix} \right. \right) \\ & + 2\pi^2 \left[\frac{\gamma^2 r^3}{3} {}_1F_2 \left(\frac{3}{2}; 2, 4; 4\gamma r \right) - \frac{2\gamma r^2}{\sqrt{\pi}} G_{3,5}^{3,1} \left(-4\gamma r \left| \begin{matrix} -1, \frac{1}{2}, -\frac{1}{2} \\ -1, 0, 1, -2, -\frac{1}{2} \end{matrix} \right. \right) \right] \end{aligned} \quad (5.46)$$

for an attractive Coulomb interaction. In the above equations, ${}_pF_q$ and $G_{p,q}^{m,n}$ denote the (generalized) hypergeometric and Meijer G -functions, respectively.

For general $\ell \geq 1$, $W[g_2, g_0](r)$ is singular at $r = 0$ and the analysis becomes more complicated. For practical purposes one can simply use power-series expansions for the Bessel functions that appear in the expressions for the zero-energy functions and integrate these term by term until a desired precision is reached. The only additional ingredients needed are the values for the constant terms Z_ℓ because these are obviously not generated by the integration.

5.3.5 Constant terms in the causality-bound function

Obtaining these constants turns out to be the central difficulty in the derivation of the causality bound for the charged-particle system, which so far—apart from having to cope with more complicated expressions—very closely followed the path laid out for the neutral system in Ref. [10].

In order to determine the Z_ℓ we consider the explicit form of $\tilde{g}(p, r)$. From the results of Bollé and Gesztesy [122], we have⁵

$$\begin{aligned} \tilde{g}(p, r) = & \mathcal{N}_\ell(p) \cdot \gamma \log(|\gamma|r) \cdot f(p, r) \\ & + \gamma \operatorname{Re} \left\{ \mathcal{N}_\ell(p) \cdot r^{\ell+1} e^{-ipr} \cdot \sum_{n=0}^{\infty} [a_{\ell,n}(p) + b_{\ell,n}(p)] r^n \right\} \\ & + \operatorname{Re} \left\{ \frac{r^{-\ell}}{2\ell+1} e^{-ipr} \cdot \sum_{n=0}^{2\ell} d_{\ell,n}(p) r^n \right\}, \end{aligned} \quad (5.47)$$

where

$$\mathcal{N}_\ell(p) = \frac{(2p)^{2\ell}}{\Gamma(2\ell+2)^2} \prod_{s=1}^{\ell} (s^2 + \eta^2), \quad (5.48)$$

$$a_{\ell,n}(p) = \frac{-\Gamma(2\ell+2)}{\Gamma(n+1)\Gamma(n+2\ell+2)} (2ip)^n \prod_{s=1}^n (s+\ell-i\eta) \cdot [\psi(n+1) + \psi(n+2\ell+2)], \quad (5.49a)$$

$$b_{\ell,n}(p) = \frac{\Gamma(2\ell+2)}{\Gamma(n+1)\Gamma(n+2\ell+2)} (2ip)^n \prod_{s=1}^n (s+\ell-i\eta) \cdot \sum_{j=1}^{n+\ell} \frac{1}{j-i\eta}, \quad (5.49b)$$

and

$$d_{\ell,n}(p) = \frac{1}{\Gamma(n+1)} (2ip)^n \prod_{s=1}^n \left(\frac{s-\ell-1-i\eta}{s-2\ell-1} \right). \quad (5.50)$$

With this result and the appropriate expression for $g_0(r)$ from Eq. (5.35) or (5.36) one can use the following procedure to calculate the Z_ℓ , *i.e.*, the terms of order r^0 in the Wronskian $W[g_2, g_0](r)$.

1. Note that

$$W[\tilde{g}, g_0](r) = p^2 W[g_2, g_0](r) + \mathcal{O}(p^4) \quad (5.51)$$

and calculate this Wronskian using a truncated version of $\tilde{g}(p, r)$ as given in Eq. (5.47). Including terms up to the order $2\ell+1$ in r is sufficient.

2. From the result, extract the terms that are of the order r^0 .
3. From that expression then extract the terms that are of the order p^2 . They constitute the $\mathcal{O}(r^0)$ contributions in a series expansion of $W[g_2, g_0](r)$ which cannot be obtained from a term-by-term integration of $g_0(r)^2$.

⁵One gets this form from Eq. (A.5) in Appendix A by inserting $n = 2\ell + 3$, $\eta = \gamma/(2p)$ and assuming that the momentum p is real and positive.

With the help of computer algebra software, this prescription is straightforward to implement. The results for $\ell = 0, \dots, 2$ are shown in Table 5.1.

ℓ	0	1	2
Z_ℓ	0	$\gamma \left(\frac{1}{6} - \frac{2\gamma_E}{9} \right)$	$\gamma^3 \left(\frac{79}{21600} - \frac{\gamma_E}{360} \right)$

Table 5.1: Constant term Z_ℓ in Eq. (5.37) for $\ell = 0, 1, 2$. $\gamma_E = 0.577216\dots$ is the Euler-Mascheroni constant. The values are the same for repulsive ($\gamma > 0$) and attractive ($\gamma < 0$) Coulomb potentials.

At this point we remark that, in principle, it is also possible to use the wave functions defined by Seaton [123] to get explicit expressions for $f_2(r)$ and $g_2(r)$ (in addition to the already known zero-energy functions), and then simply calculate all the Wronskians directly. However, the analytic irregular Coulomb function defined by Seaton is slightly different from our $\tilde{g}(p, r)$. More importantly, not all coefficients needed for the expansions are given explicitly. Finally, writing everything in terms of the wave functions of Bollé and Gesztesy paves the way for a generalization of the results presented here to an arbitrary number of spatial dimensions.

Knowing now what the constant terms Z_ℓ , it is possible to write down explicit expressions for the causality-bound functions $b_\ell^C(r)$ also for $\ell > 0$. To do that we use that the antiderivative of the right-hand side of Eq. (5.34) can be expressed in terms of (generalized) hypergeometric functions ${}_pF_q$ and Meijer G -functions $G_{p,q}^{m,n}$. The only additional point to be taken into account is that the antiderivative of $g_0(r)^2$ in general includes a constant term that is different from the desired Z_ℓ . Hence, one has to determine this term and add another constant such that their sum is exactly equal to the Z_ℓ given in Table 5.1.

We have carried out this procedure explicitly for $\ell = 1$ and $\ell = 2$. Since the results are rather lengthy, we give the complete expressions for $b_1^C(r)$ and $b_2^C(r)$ in Appendix B.

5.4 The causal range

The causality-bound equation (5.28) can be rewritten as

$$b_\ell^C(r) - r_\ell^C \geq 0 \quad \forall r \geq R. \quad (5.52)$$

In cases where the details of the interaction (in particular its range, assuming that a description with finite-range potentials is applicable) is not known, one can use Eq. (5.52) to define the *causal range* R_c of a scattering system as that value of r for which the bound is just satisfied, *i.e.*,

$$b_\ell^C(R_c) - r_\ell^C = 0. \quad (5.53)$$

We note from Eq. (5.34) that the derivative of $b_\ell^C(r)$ is non-negative,

$$\frac{d}{dr} b_\ell^C(r) = 2 \left(g_0(r) - \frac{1}{a_\ell^C} f_0(r) \right)^2 \geq 0. \quad (5.54)$$

Hence, b_ℓ^C is an increasing function of r and the causal range is defined uniquely. For the case that Eq. (5.53) does not have a solution (*i.e.*, if $b_\ell^C(r)$ is positive already for $r = 0$) we define the causal range to be zero. Note that the causal range is a function only of the scattering length and the effective range. It can thus be calculated from observables in a well-defined way.

The importance of the causal range is given by the fact that it can be interpreted as the minimum range a potential is allowed to have to be consistent with causality. If, for a given system, the values in individual partial waves differ significantly, the maximum value should be taken as the causal range of the underlying potential. Alternatively, one can model the interaction with an ℓ -dependent potential. For effective field theories with short-range interactions such as halo EFT, the causal range constrains the allowed values of the momentum-space cutoff or the lattice spacing used in numerical calculations.

5.4.1 Practical considerations

At this point we recall that our derivation of the causality bounds was based on the assumption that the concrete system under consideration is described by a finite-range (though possibly non-local) two-body interaction which is energy-independent. In EFT calculations one frequently obtains effective interactions that explicitly depend on the energy. We note that this energy dependence can be traded for momentum dependence at any given order in the power counting (EFT expansion) by using the equations of motion obtained from the effective Lagrangian. However, the energy dependence introduces another length scale into the system, and so the conversion to momentum-dependent interactions could produce an interaction range so large that the causality bounds may not be useful in practice.

There are also other theoretical frameworks, *e.g.*, Feshbach reaction theory, that explicitly use energy-dependent interactions. Here again the energy dependence introduces a length scale which acts as an interaction range. This can be seen from the time delay of the scattered wavepacket, which is proportional to the derivative of the phase shift with respect to energy. By setting up a very strong energy dependence for the interactions it is possible to produce a time delay which is arbitrarily large and negative. This has the same effect as interactions at arbitrarily large separations.

Furthermore, the assumption of a strict finite range certainly is an idealization that is only applicable to a varying degree of validity to concrete physical systems. For example, there can be exchange forces arising from the Pauli principle. Consider, for example, nuclear halo systems with a tightly bound core and a halo nucleon which is only weakly bound to the core. The exchange of a nucleon from the core and the halo nucleon that is necessary to anti-symmetrize the system can only give a sizable contribution if there is spatial overlap between the wave function of the core and the wave function of the halo nucleon. This yields a short-range exponential tail that, within the domain of validity of the effective theory, can be subsumed in the effective range parameters of the halo-core interaction. The same analysis would apply to low-energy nucleon-nucleus scattering upon the core nucleus. Another more prominent effect is given by exponential tails generated by simple pion-exchange contributions; *cf.* Ref. [140] and the discussion in the following section.

5.5 Examples and results

We now calculate explicit values for causal ranges in few-nucleon systems. In Fig. 5.1 we plot the left-hand side of Eq. (5.52) as a function of r for the case of proton–proton S-wave scattering. The causal range can then be read off as the point where the function becomes zero. Fig. 5.2 shows analogous plots for α – α S- and D-wave scattering. In this system, there are visible error bands due to the larger uncertainties in the effective range parameters.

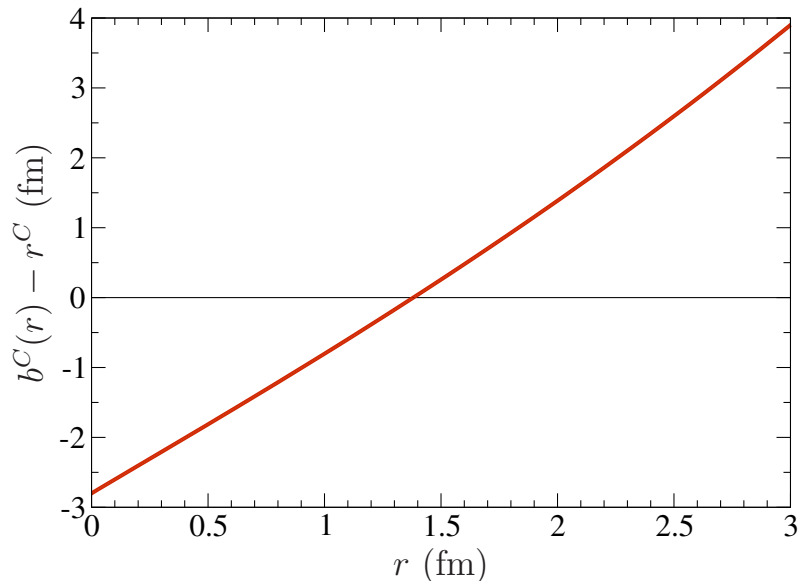


Figure 5.1: Causal range plot for S-wave proton–proton scattering.

In Table 5.2 we give a summary of the causal ranges that one finds for various two-body systems of light nuclei where low-energy scattering parameters and/or phase shifts are available from experiments. The results are briefly discussed in the following subsections.

5.5.1 Proton–proton scattering

For p – p S-wave scattering one finds a causal range of about 1.38 fm. This value is very close to the range estimate obtained by assuming that the typical length scale of the N – N interaction is set by the inverse pion mass, $\hbar c/M_\pi \approx 1.4$ fm. The value one finds in the 3P_0 channel is somewhat larger ($R_c \approx 2.3$ fm), whereas the 3P_1 effective range parameters impose almost no constraint on the range of the nuclear potential in this channel. As we will discuss in more detail below, this suggests some significant differences in the radial dependence of the interactions for the 3P_1 channel.

For effective-field-theory calculations with purely local interactions (*e.g.*, pionless effective field theory), our results suggest to keep the cutoff momentum smaller than M_π for the 1S_0 and 3P_0 channel. However, there is more freedom to take a higher cutoff for the 3P_1 channel.

In Ref. [140], causality bounds were investigated for neutron–proton scattering. The

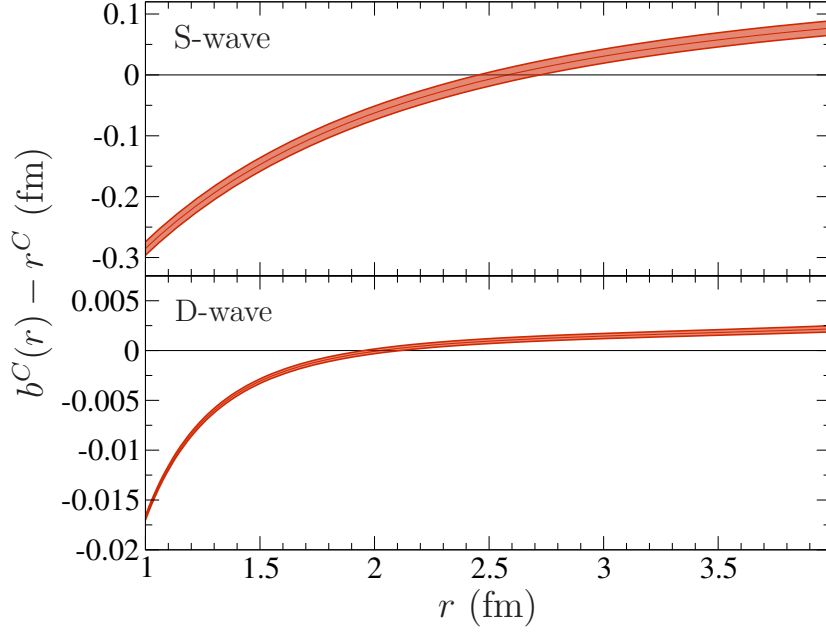


Figure 5.2: Causal range plot for S-wave α - α scattering.

System	Reference	Channel	$a^C / \text{fm}^{2\ell+1}$	$r^C / \text{fm}^{-2\ell+1}$	R_c / fm
p - p	[144]	1S_0	-7.828 ± 0.008	2.80 ± 0.02	1.38 ± 0.01
p - p	[145]	3P_0	-3.03 ± 0.11	4.22 ± 0.11	2.33 ± 0.05
p - p	[145]	3P_1	2.013 ± 0.053	-7.92 ± 0.17	≈ 0.03
p - d	[146]	$^2S_{1/2}$	2.73 ± 0.10	2.27 ± 0.12	3.90 ± 0.15
p - d	[147]	$^2S_{1/2}$	4	-2.8	0
p - d	[146]	$^4S_{3/2}$	11.88 ± 0.40	2.63 ± 0.02	$2.20^{+0.07}_{-0.06}$
p - d	[147]	$^4S_{3/2}$	11.11	2.64	2.29
p - ^3He	[148]	1S_0	11.1 ± 0.4	1.58 ± 0.12	$1.32^{+0.21}_{-0.17}$
p - ^3He	[148]	3S_1	9.04 ± 0.14	1.50 ± 0.06	$1.27^{+0.10}_{-0.09}$
p - α	[149]	$S_{1/2}$	4.97 ± 0.12	1.295 ± 0.082	$1.32^{+0.40}_{-0.21}$
p - α	[149]	$P_{1/2}$	-19.36 ± 0.50	0.349 ± 0.021	2.65 ± 0.07
p - α	[149]	$P_{3/2}$	-44.83 ± 0.51	-0.365 ± 0.113	$0.49^{+0.17}_{-0.10}$
α - α	[62]	S	$(-1.65 \pm 0.17) \cdot 10^3$	1.084 ± 0.011	$2.58^{+0.14}_{-0.13}$
α - α	[150]	D	$(-7.23 \pm 0.61) \cdot 10^3$	$(-1.31 \pm 0.22) \cdot 10^{-3}$	$2.03^{+0.09}_{-0.07}$

Table 5.2: Summary of causal-range results obtained from experimental input for various few-nucleon systems.

results ($R_c = 1.27$ fm for 1S_0 , $R_c = 3.07$ fm for 3P_0 , and $R_c = 0.23$ fm for 3P_1) are qualitatively very similar to what we find for the p - p system. This would indicate only a moderate amount of isospin breaking.

In the same publication [140], the influence of the shape of the potential upon the neutron–proton causal range was also studied numerically. When the potential is repulsive at shorter distances (less than ~ 1 fm) and attractive at larger distances (greater than ~ 1 fm), the causal range comes out on the larger side, about 2 fm or more. When the potential is attractive at intermediate distances and repulsive at larger distances, then the causal range is smaller, about 1 fm or less. The pion tail determines the sign of the potential at larger distances. For both the n - p and the p - p interaction, the one-pion exchange tail is repulsive in the 3P_1 -channel while it is attractive in the 3P_0 -channel.

Note that causality bounds in the presence of pion-exchange contributions were also discussed by Phillips and Cohen in Ref. [135]. Ideally, one would account for the one-pion-exchange tail explicitly in the calculation of the causal range, as it was done in this work for the long-range Coulomb potential. Without knowing analytical solutions of the Schrödinger equation involving a Yukawa-like potential (plus a Coulomb part, in the p - p case), however, such a procedure can at best be implemented numerically. For an example, see Ref. [151].

5.5.2 Proton–deuteron scattering

There are several experimental determinations of p - d effective range parameters. In Table 5.2 we have included results from Arvieux [146] and Huttel *et al.* [147]. While for the quartet-channel there is a good agreement between the scattering lengths and effective ranges (and, of course, of the resulting causal ranges, which come out as 2.2–2.3 fm), there is a large discrepancy for the doublet-channel results.

The difficulty of determining the proton–deuteron doublet-channel scattering length has previously been discussed by Orlov and Orevkov [152]. Comparing different models, the authors conclude that 0.024 fm is currently the best theoretical estimate for the doublet-channel p - d scattering length. From Table 3 in Ref. [152] one reads off that the corresponding value for the Coulomb-modified effective range is as huge as $8.23 \cdot 10^5$ fm. Inserting these numbers into the causal-range calculation one gets a very large value of $R_c \approx 8.15$ fm. As a consequence, no definite conclusion can be reached with the currently available data.

Note that three-body forces have been found to be very important for theoretical calculations of the p - d (and n - d) threshold scattering parameters. Our analysis here, however, is independent of the microscopic origin of the effective interaction between proton and deuteron. In a detailed picture, the force might arise from two-nucleon forces or three-nucleon forces, but the result is always some effective two-body interaction between the proton and the deuteron. The causal range we calculate is the minimum range that this effective interaction has to have in order to be able to reproduce the experimentally determined scattering parameters.

5.5.3 Proton–helion scattering

For the scattering of protons off a helium nucleus we were able to find data for both p - ${}^3\text{He}$ and p - α scattering. In the first case, there was only enough data available to calculate the causal range for the S-wave channels. Since both the scattering lengths and effective ranges are very similar for the singlet and the triplet channel, so are the resulting causal ranges, which come out as approximately 1.3 fm.

Incidentally, one finds almost the same value for the S-wave in p - α scattering. For this system, it is interesting to compare to the neutron–alpha system, where there is no Coulomb repulsion in the scattering process. Results for the n - α causal ranges can be read off from Fig. 5 in Ref. [10] (obtained using effective range parameters from Ref. [149]). Even though from the plot one only gets quite rough estimates, one clearly sees that the results for the $S_{1/2}$ and $P_{1/2}$ channels agree very well between p - α and n - α scattering, which as in the nucleon–nucleon case discussed above could be interpreted as only a moderate amount of isospin breaking. However, the causal ranges for the $P_{3/2}$ channels are very different (~ 0.5 fm for p - α , ~ 2 fm for n - α). It is an interesting question if this discrepancy hints at an error in the extraction of the effective range parameters (either for one of the systems or possibly both), or if there actually is a physical reason behind the difference in the causal ranges.

5.5.4 Alpha–alpha scattering

For α - α S-wave scattering we use the values given by Higa *et al.* (see Ref. [62] and experimental references therein), $a_0^C = (-1.65 \pm 0.17) \cdot 10^3$ fm and $r_0^C = (-1.084 \pm 0.011)$ fm to find a causal range of about 2.58 fm.

For the $\ell = 2$ channel, no effective range parameters could be found in the literature. We have thus used the phase-shift data collected in the review article by Afzal *et al.* [150] to perform the fit to the effective range expansion (Eq. (4.24) with $\ell = 2$) ourselves. By including the phase-shift data up to $E_{\text{lab}} \approx 6.5$ MeV we find $a_2^C = (-7.23 \pm 0.61) \cdot 10^3$ fm⁵ and $r_2^C = (-1.31 \pm 0.22) \cdot 10^{-3}$ fm⁻³. However, the fit is strongly dominated by the $\mathcal{O}(p^4)$ shape parameter, so the actual uncertainties of a_2^C and r_2^C should probably be somewhat larger. For the causal range in this channel we find a value of about 2 fm, which is just slightly smaller than the S-wave result.

5.6 Numerical calculations

In order to check our relations and to get a better understanding of the values for the causal range, we now present some explicit numerical calculations.

By cutting off the singular parts of the potential (*i.e.*, the Coulomb potential and the angular momentum term for $\ell \geq 0$) at very small distances, it is a simple task to numerically solve the radial Schrödinger equation (4.21) in configuration space. From the radial wave functions one can extract the Coulomb-modified phase shifts by looking for a zero

at some large (*i.e.*, much larger than the range R of the short-range potential) distance,

$$w_\ell^{(p)}(r_0) = 0 \quad , \quad r_0 \gg R, \quad (5.55)$$

and then calculating

$$\cot \tilde{\delta}_\ell(p) = -\frac{G_\ell(p)(r_0)}{F_\ell(p)(r_0)}. \quad (5.56)$$

For the simplest case of a local step potential,

$$V(r, r') = V_{\text{step}}(r) \cdot \delta(r - r') \equiv V_0 \theta(R - r) \cdot \delta(r - r'), \quad (5.57)$$

one can of course also obtain the phase shift directly by matching the wave functions at $r = R$. The effective range parameters are then obtained by repeating the calculation for several (small) momenta and fitting Eq. (4.24) to the results.

In order to test Eq. (5.26) directly one needs the wave function to calculate the integral

$$\int_0^r dr' \left[w_\ell^{(0)}(r') \right]^2 = \lim_{p \rightarrow 0} \int_0^r dr' \left[w_\ell^{(p)}(r') \right]^2. \quad (5.58)$$

Even if we do not actually take the limit $p \rightarrow 0$ but rather just insert some small $p_0 = 0.1$ (in units of an arbitrary inverse length scale), we find that the relation

$$r_\ell^C \approx b_\ell^C(R) - 2 \int_0^R dr' \left[w_\ell^{(p_0)}(r') \right]^2 \quad (5.59)$$

is typically fulfilled to better than one-percent accuracy for the simple step potential defined above.

For illustration, in the following we choose units where the radial distance is measured in fm. The potential range is set to 1 fm and its strength is measured in MeV.⁶ Furthermore, the reduced mass and Coulomb parameter are set to the values for the proton–proton system, *i.e.*, $2\mu = m_N \approx 940$ MeV and $\gamma = \gamma_{p-p} \approx 0.035$ fm⁻¹.

In Figs. 5.3 and 5.4 we show the results (for $\ell = 0, 1, 2$) for both repulsive and attractive step potentials. Quite interestingly, the $\ell = 0$ causal range for the repulsive potential stays at zero (meaning that one could reproduce the same values of the scattering length and the effective range also with a contact interaction) until a potential strength of about 100 MeV. For higher partial waves the causal range takes a nonzero value for much weaker potentials, but the rise is less steep. In general, it is remarkable that the causal range is typically considerably smaller than the actual potential range ($R = 1$ fm).

For attractive potentials the causal range grows much faster as the potential strength (now negative) increases. In contrast to what one might expect, no special features are seen in the causal ranges as the potential becomes strong enough to support a new bound state close to threshold, *i.e.*, when there is a pole in the scattering length parameter.

To conclude this section, we show the general dependence of the causal range on both the scattering length and the effective range, which has the advantage of not depending on a

⁶Note that with these conventions, the quantity that is used in the numerical calculation is $v_0 \equiv 2\mu V_0 / (\hbar c)^2$, where $\hbar c \approx 197.33$ MeV · fm is used for the unit conversion.

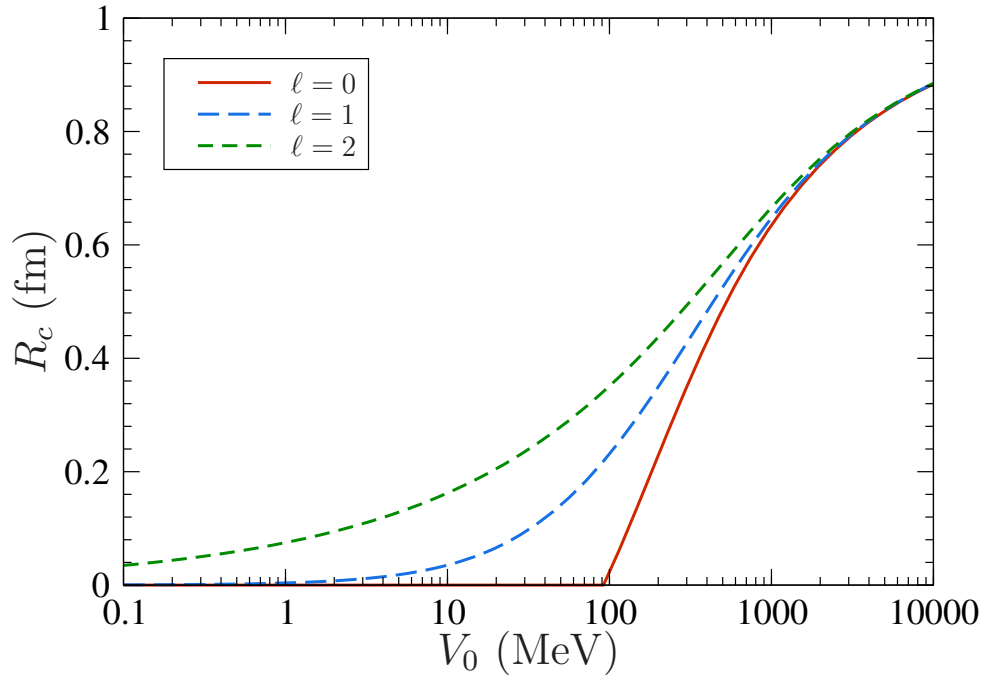


Figure 5.3: Causal range for a repulsive step potential and $\gamma = \gamma_{p-p}$.

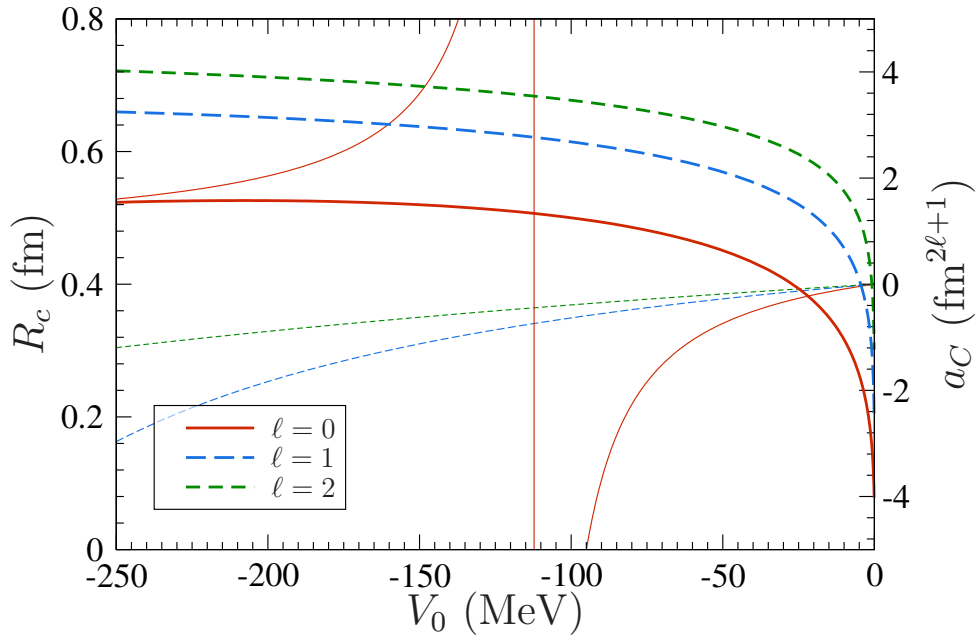


Figure 5.4: Causal range (thick lines) for an attractive step potential and $\gamma = \gamma_{p-p}$. The thin lines show the corresponding scattering lengths.

certain model potential. For illustration, we again measure distances in fm and set the Coulomb parameter to the value of the proton–proton system. In Figs. 5.5 and 5.6 we show the results for $\ell = 0$ and $\ell = 1$. For negative r^C , the causal range stays essentially zero. For positive effective ranges, it increases as the absolute value of a^C becomes larger. If one gradually turns off the Coulomb interaction by letting $\gamma \rightarrow 0$, the $\ell = 1$ plot stays almost unchanged, whereas the $\ell = 0$ result remains qualitatively the same, but with a much steeper rise in the quadrant where $a^C > 0$ and $r^C > 0$.

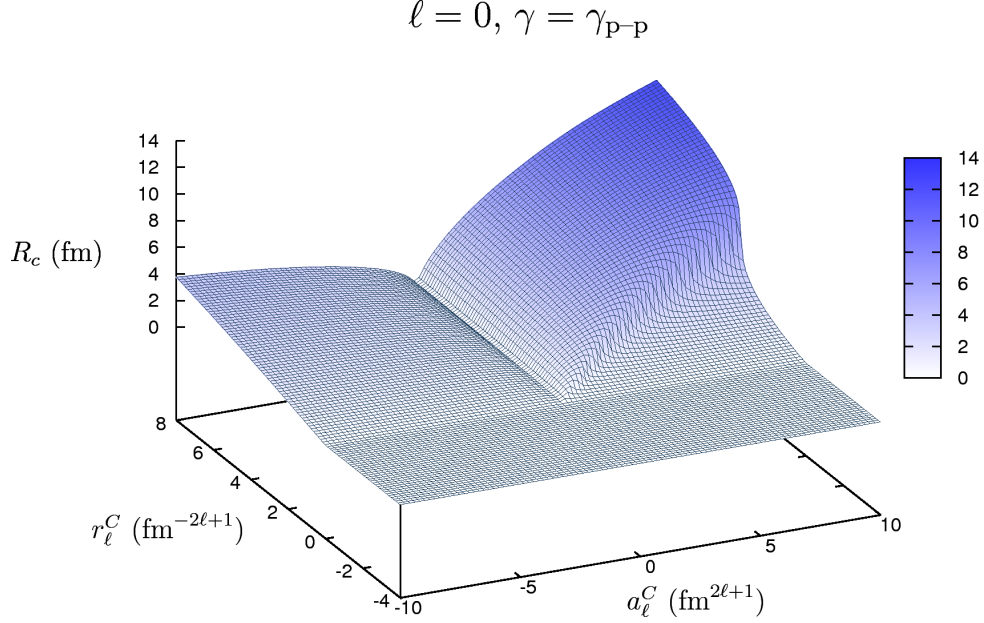


Figure 5.5: Causal range for $\gamma = \gamma_{\text{p-p}}$ and $\ell = 0$ in dependence of a_0^C and r_0^C , both measured in fm.

5.7 Relation for asymptotic normalization constants

The formalism that has been used so far in this chapter in order to derive the causality bound for the effective range can be extended to the bound-state regime to derive a relation between the asymptotic normalization of the bound state wave function and the effective range of the corresponding two-particle scattering process.

It is well-known [9] and was, as noted already in Chapter 3, also pointed out by Lüscher [8] that the asymptotic normalization constant (ANC) of the bound-state wave function is related to scattering parameters. More precisely, the residue of the bound-state pole in the analytically-continued elastic scattering amplitude (the $f_\ell(p)$ defined in Eqs. (2.22) and (2.23) in Chapter 2) is proportional to $|A_\kappa|^2$. In the limit of shallow bound states, $\kappa \rightarrow 0$, it is possible to make a more direct connection to the effective range in the corresponding scattering channel. Ultimately, however, it can be viewed again as a manifestation of the analyticity of the scattering amplitude as a function defined on the complex energy plane.

Before we discuss the relation for our system of charged particles, we first present its

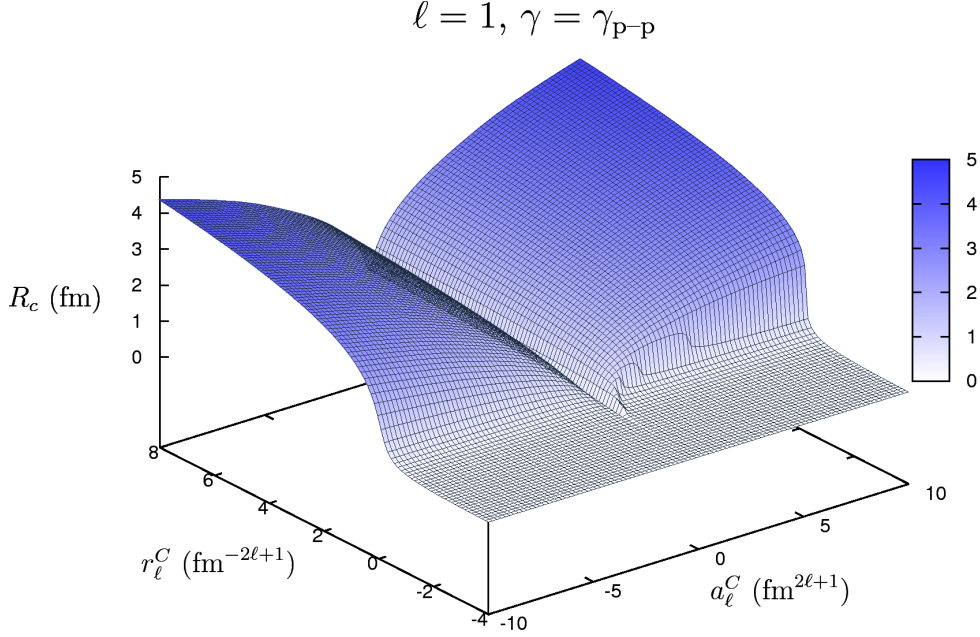


Figure 5.6: Causal range for $\gamma = \gamma_{\text{p-p}}$ and $\ell = 1$ in dependence of a_1^C and r_1^C , measured in fm^3 and fm^{-1} , respectively.

derivation for the simpler case without Coulomb interaction.

5.7.1 Derivation for the neutral system

As a starting point we quote the neutral version of our “master equation” (5.26) from Ref. [10],

$$r_\ell = b_\ell(R) - \int_0^R dr \left[u_\ell^{(0)}(r) \right]^2, \quad (5.60)$$

where r_ℓ is the effective range as defined by Eq. (2.19) and

$$u_\ell^{(0)}(r) = \lim_{p \rightarrow 0} u_\ell^{(p)}(r) \quad (5.61)$$

is the zero-energy limit of the scattering wave function for the uncharged system, normalized as in Eq. (5.3). The neutral version of the causality-bound function, $b_\ell(R)$, can be given in closed form for arbitrary angular momentum. Specializing the general formula given in Ref. [10] to the three-dimensional case one finds

$$\begin{aligned} b_\ell(R) &= -\frac{2\Gamma(\ell - \frac{1}{2})\Gamma(\ell + \frac{1}{2})}{\pi} \left(\frac{R}{2}\right)^{-2\ell+1} \\ &\quad - \frac{4}{\ell + \frac{1}{2}} \frac{1}{a_\ell} \left(\frac{R}{2}\right)^2 + \frac{2\pi}{\Gamma(\ell + \frac{3}{2})\Gamma(\ell + \frac{5}{2})} \frac{1}{a_\ell^2} \left(\frac{R}{2}\right)^{2\ell+3} \\ &= -\frac{2\Gamma(\ell - \frac{1}{2})\Gamma(\ell + \frac{1}{2})}{\pi} \left(\frac{R}{2}\right)^{-2\ell+1} + \mathcal{O}(a_\ell^{-1}). \end{aligned} \quad (5.62)$$

For $\ell = 0$, this simply gives

$$b_0 = 2R + \mathcal{O}(a_\ell^{-1}). \quad (5.63)$$

Note that $a_\ell^{-1} \rightarrow 0$ as $\kappa \rightarrow 0$, and since we only consider finite-range potentials, we can in fact write $\mathcal{O}(a_\ell^{-1}) = \mathcal{O}(\kappa)$.

Recall now that following the conventions of Section 2.1.3 we use the explicitly momentum-dependent normalization condition (5.3) for the scattering wave functions $u_\ell^{(p)}(r)$. Upon going to the bound-state pole,

$$p \rightarrow i\kappa \quad , \quad \cot \delta_\ell(p \rightarrow i\kappa) = i, \quad (5.64)$$

we get the wave function $u_\ell^{(i\kappa)}(r)$ with the asymptotic form as given in Eq. (2.30). By comparison with Eq. (2.29) one directly finds that its relation to the unit-normalized $u_{A,\ell}^{(i\kappa)}(r)$ is simply

$$u_\ell^{(i\kappa)}(r) = \frac{\kappa^\ell}{A_\kappa} u_{A,\ell}^{(i\kappa)}(r), \quad (5.65)$$

where A_κ is the ANC. Writing the normalization condition for $u_{A,\ell}^{(i\kappa)}(r)$ in the form

$$1 = \left(\int_0^R dr + \int_R^\infty dr \right) |u_{A,\ell}^{(i\kappa)}(r)|^2 \quad (5.66)$$

and using the relation (5.65), we can rewrite Eq. (5.60) as

$$r_\ell = b_\ell(R) - 2 \lim_{\kappa \rightarrow 0} \left\{ \frac{\kappa^{2\ell}}{A_\kappa^2} - \int_R^\infty dr \left[u_\ell^{(i\kappa)}(r) \right]^2 \right\}. \quad (5.67)$$

According to Eq. (2.30), the remaining integral is

$$\int_R^\infty dr \left[u_\ell^{(i\kappa)}(r) \right]^2 = \kappa^{2\ell} \int_R^\infty dr \left[i^\ell H_\ell^+(i\kappa r) \right]^2. \quad (5.68)$$

For $\ell = 0$, we get

$$\int_R^\infty dr \left[u_\ell^{(i\kappa)}(r) \right]^2 = \frac{e^{-2\kappa R}}{2\kappa} = \frac{1}{2\kappa} - R + \mathcal{O}(\kappa) \quad \text{as } \kappa \rightarrow 0. \quad (5.69)$$

Together with Eq. (5.63) this yields

$$r_0 + \frac{2}{A_\kappa^2} - \frac{1}{\kappa} = \mathcal{O}(\kappa), \quad (5.70)$$

which is, up to the given order, equivalent to the relation

$$A_\kappa^2 = \frac{2\kappa}{1 - \kappa r_0} \quad (5.71)$$

from Ref. [14]. For $\ell \geq 1$, the integral is [153]

$$\int_R^\infty dr \left[u_\ell^{(i\kappa)}(r) \right]^2 = \frac{\Gamma(\ell - \frac{1}{2}) \Gamma(\ell + \frac{1}{2})}{\pi} \left(\frac{R}{2} \right)^{-2\ell+1} + \mathcal{O}(\kappa) \quad \text{as } \kappa \rightarrow 0. \quad (5.72)$$

We see that the leading term exactly cancels the one in Eq. (5.62) and thus arrive at

$$r_\ell + \frac{2\kappa^{2\ell}}{A_\kappa^2} = \mathcal{O}(\kappa). \quad (5.73)$$

There are two things to point out about the cancellation of terms encountered above. Firstly, it is clear that Eq. (5.67) can be rigorously valid only for zero-energy bound states, *i.e.*, if one strictly considers the limit $\kappa \rightarrow 0$. Since the left-hand side is a constant, the R -dependence of $b_\ell(R)$ has to cancel that of the integral. In the scattering regime this is ensured by taking the zero-energy limit, *i.e.*, considering scattering directly at threshold. In the bound-state regime, on the other hand, one is of course interested in finding a relation for the case of a bound state close to threshold, where κ is small but finite. It is obvious that in principle this poses a problem because the $b_\ell(R)$ in Eq. (5.67) is a strictly increasing function of R , whereas the integral is always bounded and in fact becomes smaller with increasing R . The key observation is that for finite binding momenta, the cancellation of the R -dependence is valid only *up to higher orders in κ* . In other words, the terms subsumed as $\mathcal{O}(\kappa)$ in Eqs. (5.70) and (5.73) are still functions of R .

Secondly, however, the cancellation of the leading R -dependent terms is by no means a coincidence, but can—as we shall do in the next section when we derive the relation for a system of charged particles—be proven on more general grounds. Upon doing that one finds that Eq. (5.73) is in fact true in a stronger form with only terms of the order κ^2 on the right-hand side.

5.7.2 Derivation for charged particles

We now derive the analogous relation for a system of charged particles. The appropriate starting point is Eq. (5.26) derived in Section 5.3, from which we already obtained the causality bounds for the effective range parameter. For bound-state momenta, we write it as

$$r_\ell^C = b_\ell^C(r) - 2 \lim_{\kappa \rightarrow 0} \int_0^r dr' \left[w_\ell^{(i\kappa)}(r') \right]^2 \quad \text{for all } r > R, \quad (5.74)$$

with $b_\ell^C(r)$ now as defined in Eq. (5.27). In order to proceed we need again the precise connection between the radial wave functions $w_\ell^{(i\kappa)}$ appearing in Eq. (5.74) and the unit-normalized proper bound-state wave functions $w_{A,\ell}^{(i\kappa)}(r)$ defined in Eq. (4.41). Formally, we can write

$$w_\ell^{(i\kappa)}(r) = (i\kappa)^\ell C_{\eta,\ell} \left[\cot \tilde{\delta}_\ell(i\kappa) F_\ell^{(i\kappa)}(r) + G_\ell^{(i\kappa)}(r) \right] \quad \text{for } r > R, \quad (5.75)$$

but we need to be careful with the way the analytic continuation to the bound-state regime is done. In Section 4.3 we showed that in complete analogy to the neutral case, $\cot \tilde{\delta}_\ell(i\kappa) = i$ for a bound state and that the resulting linear combination $G_\ell^{(p)}(r) + iF_\ell^{(p)}(r)$ of Coulomb wave functions is proportional to the Whittaker function $W_{-i\eta,\ell+\frac{1}{2}}(-2ipr)$. More precisely, from Eq. (4.35) we have that

$$C_{\eta,\ell} \left[G_\ell^{(p)}(r) + iF_\ell^{(p)}(r) \right] = C_{\eta,\ell} e^{i\sigma_\ell} e^{-i\frac{\pi}{2}(\ell+i\eta)} W_{-i\eta,\ell+\frac{1}{2}}(-2ipr). \quad (5.76)$$

The combination of prefactors in this turns out to be crucial to get a well-behaved expression in the limit $p \rightarrow i\kappa$. Combining Eqs. (4.14) and (4.34), we have

$$C_{\eta,\ell} e^{i\sigma_\ell} = \frac{2^\ell e^{-\frac{\pi\eta}{2}} [\Gamma(\ell+1+i\eta)\Gamma(\ell+1-i\eta)]^{\frac{1}{2}}}{\Gamma(2\ell+2)} \left(\frac{\Gamma(\ell+1+i\eta)}{\Gamma(\ell+1-i\eta)} \right)^{\frac{1}{2}}. \quad (5.77)$$

Note that $i\eta$ will be real for bound-state momenta, and in the following, where we only consider the case of a repulsive Coulomb potential⁷ (*i.e.*, $\gamma > 0$), it is in fact a positive number. Conveniently, the term $\Gamma(\ell+1-i\eta)$, which might hit a pole in the Gamma function, cancels in Eq. (5.77). Noting that also the phase $\exp(\pi\eta/2)$ drops out, we can finally write

$$w_\ell^{(i\kappa)}(r) = \kappa^\ell \tilde{C}_{\eta,\ell} W_{-i\eta,\ell+\frac{1}{2}}(2\kappa r) \quad \text{for } r > R, \quad (5.78)$$

where we have defined

$$\tilde{C}_{\eta,\ell} = \frac{2^\ell \Gamma(\ell+1+i\eta)}{\Gamma(2\ell+2)}. \quad (5.79)$$

Comparing this with Eq. (4.41) we readily infer that

$$w_\ell^{(i\kappa)}(r) = \frac{\kappa^\ell}{\tilde{A}_\kappa} \tilde{C}_{\eta,\ell} \cdot w_{A,\ell}^{(i\kappa)}(r) \quad (5.80)$$

with the asymptotic normalization constant \tilde{A}_κ . Following now the same steps as in Section 5.7.1, we can rewrite Eq. (5.74) as

$$r_\ell^C = b_\ell^C(r) - 2 \lim_{\kappa \rightarrow 0} \left\{ \frac{\kappa^{2\ell}}{\tilde{A}_\kappa^2} \tilde{C}_{\eta,\ell}^2 - \int_r^\infty dr' \left[w_\ell^{(i\kappa)}(r') \right]^2 \right\} \quad \text{for } r > R. \quad (5.81)$$

Canceling the r -dependence

We now show that the r -dependence in Eq. (5.81) drops out up to corrections of higher order in κ . When we derived the relation for the neutral case we established the cancellation of the leading term by analytically carrying out the integral over the asymptotic wave function (which was just a simple Riccati–Hankel function in that case) and then expanding the result in powers of κ . Since the asymptotic wave function is now given by a Whittaker function, the situation for the charged case is much more complicated. However, as already mentioned at the end of Section 5.7.1, the cancellation can in fact be established in a more general way.

To this end we recall from Eq. (5.20) that

$$w_\ell^{(p)}(r) = -\frac{1}{a_\ell^C} f_0(r) + g_0(r) + \mathcal{O}(p^2). \quad (5.82)$$

It is straightforward to assume that this is valid also in the bound-state regime since we are working with a wave function explicitly analytic in p^2 . Hence,

$$\left[w_\ell^{(i\kappa)}(r) \right]^2 = \left(-\frac{1}{a_\ell^C} f_0(r) + g_0(r) \right)^2 + \mathcal{O}(\kappa^2) = \frac{1}{2} \frac{d}{dr} b_\ell^C(r) + \mathcal{O}(\kappa^2), \quad (5.83)$$

⁷Considering attractive Coulomb potentials does not make much sense in the present context because it would create an infinite tower of bound states arbitrarily close to threshold.

where in the last step we have inserted Eq. (5.34). This directly tells us that $b_\ell^C(r)$ in Eq. (5.81) cancels with the integral up to higher-order terms in κ (which are still functions of r) and, possibly, an integration constant. This situation is already familiar from the calculation of the Wronskian $W[g_2, g_0](r)$. Again the constant term can only come from the integral over $g_0(r)^2$. To determine it, we note that

$$\int_r^\infty dr' [g_0(r')]^2 < \infty \text{ if } r > 0, \quad (5.84)$$

i.e., the integral is actually convergent and gives a Meijer G -function, as already encountered in Section 5.3.4. The constant term coming from this function has to be combined with the already known Z_ℓ in $b_\ell^C(r)$. We define

$$\Delta Z_\ell = W[g_2, g_0](r) + \int_r^\infty dr' [g_0(r')]^2, \quad (5.85)$$

which is explicitly r -independent, to finally arrive at

$$r_\ell^C + \frac{2\kappa^{2\ell}}{\tilde{A}_\kappa^2} \tilde{C}_{\eta,\ell}^2 + 2 \Delta Z_\ell = \mathcal{O}(\kappa^2) \quad (5.86)$$

or, equivalently,⁸

$$|\tilde{A}_\kappa| = \kappa^\ell \tilde{C}_{\eta,\ell} \left(-\frac{r_\ell^C}{2} - \Delta Z_\ell + \mathcal{O}(\kappa^2) \right)^{-1/2}, \quad (5.87)$$

both valid in the limit where $\kappa \rightarrow 0$.

In Table 5.3 we give the resulting values for the ΔZ_ℓ for $\ell = 0, 1, 2$. Note that up to a minus sign, these are exactly the correction terms mentioned at the end of Section 5.3.5. This means that the antiderivative used to obtain the explicit expressions for the $\ell = 1$ and $\ell = 2$ causality-bound functions given in Appendix B corresponds essentially to the definite integral in Eq. (5.84), at least for the case of a repulsive Coulomb interaction, where this is convergent.

ℓ	0	1	2
ΔZ_ℓ	$-1/(3\gamma)$	$-\gamma/108$	$-17\gamma^3/10800$

Table 5.3: Integration constant ΔZ_ℓ in Eqs. (5.86) and (5.87) for $\ell = 0, 1, 2$.

Finally, we note that Sparenberg *et al.* [143] have previously derived an ANC relation equivalent to ours, but written in terms of the scattering length instead of the effective range parameter. The equivalence of the two relations up to the contributions of higher-order shape parameters is shown in Appendix C.

5.7.3 Application to the oxygen-16 system

The ^{16}O nucleus has two excited states lying just below the α - ^{12}C threshold, a 2^+ at about -245 keV and an even more shallow 1^- at only -45 keV. The properties of these

⁸Note that in Ref. [5] there was a typo that accidentally put the $\tilde{C}_{\eta,\ell}$ in Eq. (5.87) in the denominator.

states play an important role in astrophysical helium burning processes [154–156]. In the following, we calculate asymptotic normalization constants for both states under the assumption that they can be described in a $\alpha + {}^{12}\text{C}$ halo picture.

We use the recent data obtained by Tischhauser *et al.* [157] (for the actual phase shifts see their Ref. [32]) in order to extract the Coulomb-modified effective range for the $\alpha-{}^{12}\text{C}$ P- and D-wave channels. Focussing first on the D-wave, we note that the combination of the strong Coulomb repulsion and the $\ell = 2$ centrifugal barrier makes the low-energy phase shifts very small over a wide energy range. Moreover, there is a narrow resonance at a center-of-mass energy of about 2.7 MeV, which strongly constrains the energy region for a straightforward fit to the effective range function. From a simple fit to the data up to the narrow resonance one only obtains an effective range parameter with an uncertainty too large (50%) to allow an extraction of the ANC because the latter depends on r^C very sensitively.

To mitigate this problem, we use the position of the 2^+ oxygen state as an additional input parameter for a self-consistent extraction of the effective range. In the following, we describe this procedure in more detail.

At the position of the bound state, where $\cot \tilde{\delta}_\ell(i\kappa) = i$, the Coulomb-modified effective range expansion (4.28) reduces to

$$\gamma \tilde{h}_\ell(i\kappa) = -\frac{1}{a_\ell^C} - \frac{1}{2} r_\ell^C \kappa^2 + \dots, \quad (5.88)$$

where now

$$\tilde{h}_\ell(i\kappa) = \frac{(2i\kappa)^{2\ell}}{(2\ell + 1)!^2} \prod_{s=1}^{\ell} (s^2 + \eta^2) \times \left(\psi(i\eta) + \frac{1}{2i\eta} - \log(i\eta) \right), \quad \eta = \frac{\gamma}{2i\kappa}. \quad (5.89)$$

A straightforward calculation shows that for the prefactor we have

$$\frac{(2i\kappa)^{2\ell}}{(2\ell + 1)!^2} \prod_{s=1}^{\ell} (s^2 + \eta^2) = \frac{\gamma^{2\ell}}{(2\ell + 1)!^2} + \mathcal{O}(\kappa^2). \quad (5.90)$$

Furthermore, for the digamma function we have the asymptotic expansion (Eq. (6.3.18) in Ref. [103])

$$\psi(z) = \log z - \frac{1}{2z} - \sum_{n=1}^{\infty} \frac{B_{2n}}{2n z^{2n}} \quad (5.91)$$

for $|z| \rightarrow \infty$, where the B_{2n} are the Bernoulli numbers,

$$B_0 = 1, \quad B_1 = -\frac{1}{2}, \quad B_2 = \frac{1}{6}, \quad \dots \quad (5.92)$$

Noting that the sum in Eq. (5.91) only starts at $n = 1$, we find that $\gamma \tilde{h}_\ell(i\kappa)$ only starts at order κ^2 , and inserting the precise relation into Eq. (5.88), we arrive at

$$\frac{1}{a_\ell^C} = \left(-\frac{1}{2} r_\ell^C + \frac{\gamma^{2\ell-1}}{3(2\ell + 1)^2} \right) \kappa^2 + \mathcal{O}(\kappa^4). \quad (5.93)$$

Neglecting the effective-range contribution at leading order, we insert the binding momentum $\kappa \approx 0.187 \text{ fm}^{-1}$ of the 2^+ state to get a first approximation for the scattering length parameter. This is then used to constrain a subsequent fit to the phase-shift data up to about 2.6 MeV, *i.e.*, just below the narrow resonance. We include a single $\mathcal{O}(p^4)$ shape parameter in the fit since some curvature is clearly necessary. The r_2^C obtained from this is then used in Eq. (5.93) to get a better result for $1/a_2^C$, which, in turn, is fed back into the fit. Iterating this procedure a couple of times yields a well-converged self-consistent result for r_2^C . After eight iterations, we find

$$r_2^C = (5.94 \pm 0.35) \cdot 10^{-4} \text{ fm}^{-3} \quad (5.94)$$

for the α - ^{12}C D-wave. Including a second shape parameter in the fitting procedure only changes this result within the given uncertainty, so we conclude that for the energy range we have been fitting, a single shape parameter really is sufficient to account for the curvature. Inserting the fit result into Eq. (5.87) yields

$$|A(2^+)| = (2.41 \pm 0.38) \cdot 10^4 \text{ fm}^{-1/2} \quad (5.95)$$

for the 2^+ state in ^{16}O . Here and in the following, we simply write A instead of \tilde{A}_κ to keep the notation simple. Including in Eq. (5.86) an $\mathcal{O}(\kappa^4)$ term of the order of the shape parameter gives a consistent result for $|A(2^+)|$ within the error given above.

When we apply the same procedure to the 1^- state just 45 keV below the α - ^{12}C threshold, we also see a nice convergence and obtain the results

$$r_1^C = (4.546 \pm 0.002) \cdot 10^{-2} \text{ fm}^{-1} \quad (5.96)$$

and

$$|A(1^-)| = (1.188 \pm 0.024) \cdot 10^{14} \text{ fm}^{-1/2}. \quad (5.97)$$

The overall picture for the 1^- state is somewhat more complicated, however. On the one hand, the extraction of the effective range parameters is easier in this case because there is no narrow resonance limiting the fit range (we have used the data up to $E_{\text{cm}} = 3.75 \text{ MeV}$). By doing a simple fit without the self-consistent iteration we get values for the effective range and the ANC that are slightly smaller but overlap with the results given above when the respective uncertainties are taken into account. On the other hand, allowing for a second shape parameter changes the value of the effective range quite dramatically to 0.046 fm^{-1} , which leads to an imaginary ANC. This could indicate that the effective range parameters from the simple fit violate the causality bound. The fact that r^C has to be such that Eq. (5.86) yields a real value for the ANC can be interpreted as a weaker remnant of the original causality-bound relation. Alternatively, the cluster picture might not be applicable for the shallow 1^- state in ^{16}O .

Our result for the ANC of the 2^+ state is about a factor five smaller than the value $|A(2^+)| = (1.11 \pm 0.11) \cdot 10^5 \text{ fm}^{-1/2}$ obtained by Brune *et al.* [154], while the value for $|A(1^-)|$ is about a factor two smaller. Other, more recent determinations [158, 159] have found even larger values. For the interpretation of this discrepancy, note that our calculations are predictions of the ANCs based only on alpha-carbon elastic scattering data and the assumption that the system can be approximately described in an effective

two-body picture with a finite-range interaction. In the references mentioned above, the ANCs are extracted from alpha-carbon transfer measurements. Note furthermore that a comparison of the experimental extractions in Ref. [158] exhibits quite some discrepancy (factors of two up to roughly an order of magnitude) also between the cited individual experimental determinations of the ANCs.

Sparenberg *et al.* [160] have carried out a similar analysis for the 2^+ state based on their ANC relation (*cf.* Ref. [143]). They subtracted the narrow resonance from the α - ^{12}C D-wave phase shift data in order to extract a set of higher-order shape parameters and concluded that present-day data are not sufficient to constrain the ANC strongly. As discussed above, our approach of performing a self-consistent fit to the data below the resonance constrained by the separation energy and using the effective range instead of the scattering length as input in the ANC relation improves the stability of the extraction. However, compared to other determinations our ANC values are generally smaller by a factor two to five. We thus conclude that this issue requires further study.

5.8 Other long-range forces

The causality bounds derived above for the system with Coulomb interactions are, despite being quite involved due to the complicated nature of the Coulomb wave functions, not fundamentally different from the result that one obtains in the purely finite-range case. In Section 5.7.1 we have already quoted the causality-bound function for this case from Ref. [10]. According to Eq. (5.62), its behavior is

$$b_\ell(r) = -\frac{2\Gamma(\ell - \frac{1}{2})\Gamma(\ell + \frac{1}{2})}{\pi} \left(\frac{r}{2}\right)^{-2\ell+1} + \mathcal{O}(r^2). \quad (5.98)$$

From the explicit results for the Coulomb causality-bound functions, given in Eqs. (5.45) and (5.46) for $\ell = 0$, and in Appendix B for $\ell = 1, 2$, one finds that

$$b_\ell^C(r) = -\left(\frac{2^\ell \Gamma(\ell + 1)}{\Gamma(2\ell + 2)}\right)^2 \times \frac{2\Gamma(\ell - \frac{1}{2})\Gamma(\ell + \frac{1}{2})}{\pi} \left(\frac{r}{2}\right)^{-2\ell+1} + \mathcal{O}(r^{-2\ell+2}). \quad (5.99)$$

Up to an additional prefactor and the subleading pole terms (if $\ell \geq 2$) in Eq. (5.99), the leading behavior is exactly the same as for pure finite-range interactions.⁹ The overall prefactor goes away if one uses the conventions of Eq. (4.31) for the Coulomb-modified effective range expansion.

In both cases, the S-wave causality-bound function vanishes at the origin, whereas for all $\ell \geq 1$ it has a pole. It is this pole that requires the effective range parameter to tend towards negative infinity in the limit where the range of the potential goes to zero and therefore prevents one from tuning the effective range parameter for P- and higher partial wave to zero in a calculations with exact zero-range interactions [10, 139].

⁹Strictly, we have explicitly derived this only for $\ell = 0, 1, 2$. We assume here, however, that Eq. (5.99) is true in general.

5.8.1 Singular potentials

The above comparison has been given in Ref. [7], where we have just corrected a minor typo¹⁰ here. As furthermore discussed there, the situation changes significantly for interactions with long-range tails of the form

$$V_\alpha(r) = \frac{g}{r^\alpha} \quad \text{with } \alpha > 2, \quad (5.100)$$

where g denotes the coupling strength.

The properties of such so-called *singular potentials* have been reviewed in detail by Frank *et al.* in Ref. [161]. They are particularly peculiar if they are attractive ($g < 0$) because in that case there always exists an infinite spectrum of bound states that is not bounded from below. Obviously, this situation is unphysical.

Still, it is interesting to study such singular potentials if one assumes that they only determine the long-range *tail* of a given interaction and are, by some mechanism, cut off at small distances. For an analysis of systems with this kind of behavior, it is important to study solutions of the Schrödinger equation with pure inverse-power-law interactions. For the $1/r^4$ potential, for example, such solutions have been known for a long time and can be written in terms of Mathieu functions [162]. At zero energy, it is possible to write down the general solution of the radial Schrödinger equation with a potential of the form (5.100). From Ref. [161] we quote the result that the physical solution (vanishing at the origin) is given by

$$u_{\alpha,\ell}(r) \propto r^{1/2} K_n(\beta r^\sigma) \quad \text{with } n = \frac{2\ell + 1}{\alpha - 2}, \quad (5.101)$$

where $K_n(z)$ is a modified Bessel function, and

$$\beta = \frac{2g^{1/2}}{\alpha - 2}, \quad \sigma = 1 - \frac{\alpha}{2}. \quad (5.102)$$

A second linearly-independent solution is given by inserting the modified Bessel function $I_n(z)$ in Eq. (5.101). From this one already sees that the highly singular nature of the potential leads to a peculiar behavior of the wave function. For an attractive potential ($g < 0$), Eq. (5.102) implies that the parameter β becomes purely imaginary. Although in that case the amplitude of $u_{\alpha,\ell}(r)$ still goes to zero in the limit $r \rightarrow 0$, at the same time it oscillates more and more rapidly and in fact has an essential singularity at the origin. We will come back to this point and discuss its implication for the causality bound in the next section.

Of particular physical importance is the attractive van der Waals potential,

$$V_{\text{vdW}}(r) = -\frac{C_6}{r^6}, \quad C_6 > 0, \quad (5.103)$$

because it describes the long-range interaction of neutral atoms (or molecules) due to their mutual polarization [28]. For example, it determines the attractive part of the phenomenological Lennard–Jones potential [161].

¹⁰The subleading pole terms were given in Ref. [7] as $\mathcal{O}(r^{-2\ell})$ instead of $\mathcal{O}(r^{-2\ell+2})$, which obviously made them not subleading but rather more singular than the first term.

Based on explicit solutions derived by Gao [163], causality bounds for this kind of potential have been studied in Ref. [7]. In the following we summarize the central results of that publication.

5.8.2 Causality bounds for van der Waals interactions

Introducing the van der Waals length scale

$$\beta_6 = (2\mu C_6)^{1/4}, \quad (5.104)$$

the Schrödinger equation for a two-particle system with a (non-local) finite-range interaction $V(r, r')$ and an additional van der Waals tail of the form (5.103) can be written as

$$p^2 v_\ell^{(p)}(r) = -\frac{d^2}{dr^2} v_\ell^{(p)}(r) + \frac{\ell(\ell+1)}{r^2} v_\ell^{(p)}(r) + 2\mu \int_0^R dr' V(r, r') v_\ell^{(p)}(r') + \theta(r-R) \frac{\beta_6^4}{r^6} v_\ell^{(p)}(r). \quad (5.105)$$

We use the letter v here to denote the radial wave functions in order to distinguish them from those for the asymptotically non-interacting (u) and the Coulomb (w) case. As usual, we denote a solution for momentum p with a corresponding superscript. Due to its highly singular behavior, the van der Waals potential has to be cut off at small distances. In Eq. (5.105) we have conveniently done this with the step function $\theta(r-R)$. In principle, other methods (and cut-off radii) can be used, but it is always possible to absorb the difference into $V(r, r')$, which we have not specified explicitly. The only important point here is that for $r > R$ the interaction is given exactly and explicitly by the van der Waals tail because that is the setup we are interested in.

Asymptotic wave functions

It is convenient to introduce the rescaled variables

$$r_s = r/\beta_6 \quad \text{and} \quad p_s = p\beta_6. \quad (5.106)$$

In the outer region ($r > R$), the Schrödinger equation (5.105) then reduces to

$$\left[\frac{d^2}{dr_s^2} - \frac{\ell(\ell+1)}{r_s^2} + \frac{1}{r_s^6} + p_s^2 \right] v_\ell^{(p)}(r) = 0. \quad (5.107)$$

The exact solutions of this equation (valid for all $r_s > 0$) have been derived by Gao in Ref. [163] and are given in terms of infinite sums of Bessel functions. Up to a minor

change in notation,¹¹ we quote them here in the form used in Ref. [7],

$$F_\ell^{\text{vdW}}(p, r) = \frac{r_s^{1/2}}{X_\ell^2(p_s) + Y_\ell^2(p_s)} \left[X_\ell(p_s) \sum_{m=-\infty}^{\infty} b_m(p_s) J_{\nu+m}(\rho_s) - Y_\ell(p_s) \sum_{m=-\infty}^{\infty} b_m(p_s) N_{\nu+m}(\rho_s) \right], \quad (5.108a)$$

$$G_\ell^{\text{vdW}}(p, r) = \frac{r_s^{1/2}}{X_\ell^2(p_s) + Y_\ell^2(k_s)} \left[X_\ell(p_s) \sum_{m=-\infty}^{\infty} b_m(p_s) N_{\nu+m}(\rho_s) + Y_\ell(p_s) \sum_{m=-\infty}^{\infty} b_m(p_s) J_{\nu+m}(\rho_s) \right], \quad (5.108b)$$

with the radial variable

$$\rho_s = \frac{1}{2r_s^2}, \quad (5.109)$$

and with the momentum-dependent coefficients $X_\ell(p_s)$, $Y_\ell(p_s)$ —not to be confused with the functions introduced in Section 5.3.4—and $b_m(p_s)$ as defined in the appendix of Ref. [7]. The variable ν that appears in the indices of the Bessel functions is determined as the root of a (transcendental) equation that again involves the momentum p_s . As such, it is also a momentum-dependent function, but for simplicity we have not indicated this explicitly in Eqs. (5.108).

Both van der Waals wave functions defined above have an essential singularity at the origin which lets their amplitude vanish in the limit $r \rightarrow 0$ with infinitely-rapid oscillations. This is the same behavior that was mentioned above for the general zero-energy solutions of attractive singular power-law potentials. An important consequence is that there is no singled-out regular solution defined by its vanishing at the origin and thus no obvious choice for the definition of a scattering phase shift. Rather, one has an infinite number of linearly-independent pairs of solutions that can, in principle, all be used to express the asymptotic wave function of the system.

As already mentioned in Section 2.1.4 in Chapter 2, Gao has extended the formalism of quantum defect theory to describe systems with tails of the singular power-law type (5.100) in Ref. [21]. The application to the special case of a van der Waals potential is discussed in Ref. [164]. By writing the general solution of Eq. (5.105) for $r > R$ as

$$v_\ell^{(p)}(r) = F_\ell^{\text{vdW}}(p, r) - \tan \delta_\ell^{(\text{short})}(p) G_\ell^{\text{vdW}}(p, r), \quad (5.110)$$

we define the *short-range K-matrix*¹²

$$\tan \delta_\ell^{(\text{short})}(p) = \hat{K}_\ell(p). \quad (5.111)$$

¹¹In Ref. [7], these solutions are called F_L and G_L , where L denotes the angular momentum. They are related to the functions f_l^{c0} and g_l^{c0} defined in Ref. [21] by the normalization factors $F_\ell^{\text{vdW}} = f_\ell^{c0}/\sqrt{2}$ and $G_\ell^{\text{vdW}} = -g_\ell^{c0}/\sqrt{2}$, with $l = \ell$.

¹²Note that our \hat{K}_ℓ is called K_ℓ^0 in Refs. [163, 165] and corresponds to $-K_\ell^{c0}$ of Refs. [21, 164].

Other choices for the basis pair of van der Waals wave functions correspond to different K-matrices. The $\hat{K}_\ell(p)$ defined above in terms of $F_\ell^{\text{vdW}}(p, r)$ and $G_\ell^{\text{vdW}}(p, r)$ is the most convenient choice to describe the system near the zero-energy threshold [21]. In particular, it is an analytic function of p^2 [165],

$$\hat{K}_\ell(p) = \sum_{n=0}^{\infty} K_{\ell,2n} p^{2n}. \quad (5.112)$$

The parameters appearing in this expansion characterize the low-energy physics of the system, which means that Eq. (5.112) can be seen as analog of the ordinary effective range expansion. $K_{\ell,0}$ is, essentially, an inverse scattering length parameter, and $K_{\ell,2}$ plays the role of the effective range. Note, however, that this is just an approximate correspondence, which can already be seen from looking at the dimensions of these quantities ($K_{\ell,0}$ is dimensionless whereas $K_{\ell,2}$ has the dimension of an inverse momentum squared, corresponding to an area). The short-range K-matrix \hat{K}_ℓ has been used by Gao to define so-called *generalized* scattering lengths and effective ranges [164]. An important quantity that enters in these relations is the van der Waals length scale β_6 defined in Eq. (5.104). In fact, as discussed in Ref. [7], for almost all scattering systems of alkali atoms that have been studied experimentally so far one finds that β_6^2 dominates the generalized effective range compared to the parameter $K_{\ell,2}$.

Despite their complicated nature, the van der Waals wave functions are analytic functions of p^2 [163] and thus possess expansions

$$F_\ell^{\text{vdW}}(p, r) = f_{\ell,0}^{\text{vdW}}(r) + f_{\ell,2}^{\text{vdW}}(r) p^2 + \mathcal{O}(p^4), \quad (5.113a)$$

$$G_\ell^{\text{vdW}}(p, r) = g_{\ell,0}^{\text{vdW}}(r) + g_{\ell,2}^{\text{vdW}}(r) p^2 + \mathcal{O}(p^4). \quad (5.113b)$$

With

$$\nu_0 = (2\ell + 1)/4, \quad (5.114)$$

the leading-order functions are simply

$$f_{\ell,0}^{\text{vdW}}(r) = r_s^{1/2} J_{\nu_0}(\rho_s), \quad (5.115a)$$

$$g_{\ell,0}^{\text{vdW}}(r) = r_s^{1/2} N_{\nu_0}(\rho_s), \quad (5.115b)$$

where $J_n(z)$ and $N_n(z)$ are Bessel functions of the first and second kind, respectively. Of course, these are just linear combinations of the general zero-energy solutions mentioned in Section 5.8.1. The quadratic terms in Eqs. (5.113) are somewhat more involved, but can also be written down explicitly [7].

The van der Waals causality bound

With the ingredients given in the previous section one has everything at hand to derive the van der Waals causality bound exactly as in Ref. [10] and done for the Coulomb potential in this chapter. In fact, the derivation here is almost as simple as in the purely finite-range case because the quadratic radial functions $f_{\ell,2}$ and $g_{\ell,2}$ —and thus the Wronskians appearing in the causality-bound function—are known explicitly. The result is

$$K_{\ell,2} = b_\ell^{\text{vdW}}(r) - \frac{\pi}{4} \int_0^r dr' \left[v_\ell^{(0)}(r') \right]^2, \quad (5.116)$$

with

$$b_\ell^{\text{vdW}}(r) = \frac{\pi}{4} \left\{ W[f_{\ell,2}^{\text{vdW}}, f_{\ell,0}^{\text{vdW}}](r) + K_{\ell,0}^2 W[g_{\ell,2}^{\text{vdW}}, g_{\ell,0}^{\text{vdW}}](r) - K_{\ell,0} \left(W[g_{\ell,2}^{\text{vdW}}, f_{\ell,0}^{\text{vdW}}](r) + W[f_{\ell,2}^{\text{vdW}}, g_{\ell,0}^{\text{vdW}}](r) \right) \right\}. \quad (5.117)$$

In the well-known fashion, the positive-definiteness of the integral term in Eq. (5.116) yields a causality bound of the form

$$K_{\ell,2} \leq b_\ell^{\text{vdW}}(r) \quad \text{for all } r > R, \quad (5.118)$$

and the van der Waals causal range R_c^{vdW} is defined by

$$K_{\ell,2} = b_\ell^{\text{vdW}}(R_c^{\text{vdW}}). \quad (5.119)$$

The Wronskians in Eq. (5.117) are given explicitly in Ref. [7]. They have the important property that for all angular momenta ℓ they vanish in the limit $r \rightarrow 0$, which implies the same for the van der Waals causality-bound function $b_\ell^{\text{vdW}}(r)$. This stands in clear contrast to the behavior found for the asymptotically non-interacting system and for interactions with Coulomb tails. As summarized in Eqs. (5.98) and (5.99), in both these cases the causality-bound function for $\ell \geq 1$ diverges at the origin.

This important difference can be traced back to the behavior of the wave functions. Since both van der Waals wave functions vanish as $r \rightarrow 0$ (faster than a power law), the same is true for the coefficient functions in Eqs. (5.113) and, in turn, for the Wronskians. At the same time this means that the latter can be calculated as straightforward integrals from 0 to r over products of the zero-energy solutions (5.115), *cf.* Section 5.3.4. Since all functions vanish in the limit $r \rightarrow 0$, there are no peculiar integration constants as encountered for Coulomb tails. In Ref. [7] it is argued further that this should also be true for other singular-potential tails that lead to the same behavior of the wave functions.

The fact that the van der Waals causality-bound function $b_\ell^{\text{vdW}}(r)$ does not diverge at $r = 0$ is quite significant. It means that as long as the short-range K-matrix parameter $K_{\ell,2}$ is less than or equal to zero, there is no real constraint on the interaction range from the causality-bound relation (5.118). As a consequence, in an effective field with contact interactions that incorporates a van der Waals tail of the interaction, the causality bound does not induce convergence problems when the cutoff is taken to infinity, provided that $K_{\ell,2} \leq 0$ holds for the angular-momentum channel one is interested in.

However, the van der Waals length scale apparently plays quite an important role. As already pointed out, it is found to be the dominant scale when $K_{\ell,2}$ is expressed in terms of Gao's generalized effective range parameters [7, 164]. Furthermore, causal ranges that were calculated in Ref. [7] for systems of alkali atoms where scattering parameters could be found in the literature¹³ all came out significantly smaller than β_6 .

¹³Unfortunately, only S-wave parameters could be found. It would be very interesting to see if the reported result persists for higher partial waves.

Causal range near an S-wave magnetic Feshbach resonance

Since their first experimental observation in 1998 [166], Feshbach resonances have become a popular tool to tune the interactions in cold atomic systems by varying an externally applied magnetic field [167] (see also K. Helfrich's doctoral thesis [56] and references therein). It is thus interesting to study the impact of the van der Waals causality bound in this context.

In Ref. [168] the multi-channel problem of scattering around a magnetic Feshbach resonance is reduced to a description by an effective single-channel K-matrix that depends on the applied magnetic field B . The behavior around the resonance is described by several parameters. $B_{0,\ell}$ is the position of the Feshbach resonance, while g_{res} parametrizes its width. K_{ℓ}^{bg} is a background value for the K-matrix, and a scale $d_{B,\ell}$ is introduced in order to define a dimensionless magnetic field. With these parameters, we write the effective single-channel K-matrix as

$$\hat{K}_{\ell}^{\text{eff}}(p, B) = -K_{\ell}^{\text{bg}} \left[1 + \frac{g_{\text{res}}}{p^2 \beta_6^2 - g_{\text{res}} (B_s + 1)} \right], \quad (5.120)$$

with

$$B_s = \frac{(B - B_{0,\ell})}{d_{B,\ell}}. \quad (5.121)$$

The parametrization given above corresponds to Eq. (18) in Ref. [168]. Note that we have slightly changed the notation and are using a different sign convention for the K-matrix.

By expanding the right-hand side of Eq. (5.120) in p^2 it is straightforward to determine the K-matrix expansion parameters $K_{\ell,0}$ and $K_{\ell,2}$. A short calculation yields that

$$K_{\ell,0}^{\text{eff}} = -K_{\ell}^{\text{bg}} \left(1 + \frac{1}{B_s + 1} \right) \quad (5.122)$$

and

$$K_{\ell,2}^{\text{eff}} = \frac{\beta_6^2 K_{\ell}^{\text{bg}}}{g_{\text{res}} (B_s + 1)^2}. \quad (5.123)$$

As noted in Ref. [168], the parameters K_{ℓ}^{bg} and g_{res} are constrained by the condition

$$K_{\ell}^{\text{bg}} g_{\text{res}} < 0. \quad (5.124)$$

This implies that $K_{\ell,2}^{\text{eff}}$ as given by Eq. (5.123) is always negative. From the causality bound in Eq. (5.118) it then follows that wherever the effective single-channel description considered here is applicable and correctly captures the entire energy-dependence of the short-range K-matrix, the causal range will be zero when the interaction is tuned close to a Feshbach resonance.

5.9 Summary and outlook

In this chapter, we have investigated the constraints imposed by causality on the low-energy scattering parameters of charged particles interacting via a short-range interaction

and a long-range Coulomb potential. Similar to the case of neutral particles without Coulomb interaction [10, 135–140], our considerations yield a constraint on the maximum value of the Coulomb-modified effective range.

While conceptually straightforward, the calculation of the Wronskians required for the derivation of the bound function is intricate. We have calculated them through term-by-term integration of the power-series expansion of the zero-energy wave functions and additionally determining the integration constants that are not generated by this process.

We define the causal range as the minimum value of the interaction range consistent with the causality bound. In effective field theories with contact interactions such as halo EFT, the natural momentum cutoff is of the order of the inverse of the causal range. If the natural cutoff is not known from other considerations, its size can be estimated from the causal range. If the momentum cutoff used in a calculation is too high, then problems with convergence of higher order corrections can appear. For example, the convergence pattern might be such that an improvement in higher orders of the EFT can only be sustained through large cancellations between individual terms. Such an unnatural pattern would be especially undesirable for the stability of numerical (lattice) calculations. Our results can thus be viewed as a guide for improving the convergence pattern of EFT calculations with contact interactions. In lattice simulations of halo EFT, the lattice spacing should not be taken smaller than the causal range.

We have analyzed the causal ranges for a variety of systems ranging from proton–proton scattering to alpha–alpha scattering. Our results for causal ranges in different partial waves in these systems typically vary by factors of 2–3. The precise values are quite sensitive to small uncertainties in the effective range parameters. In channels with a large negative effective range the causal range is very close to zero, which implies that causality provides almost no constraints on the range of the interaction in this case. Thus, the causal range provides a good order-of-magnitude estimate of the range of interaction, but drawing more quantitative conclusions about the structure of the underlying potentials is difficult. In order to illustrate the dependence of the causal range on scattering parameters, we have performed explicit numerical calculations for a simple step potential with a Coulomb tail.

After an analytic continuation to the bound state regime, the integral relations for the causality bound can also be used to derive a model-independent expression for the ANC of shallow bound states. If the state is a two-body halo state, the relation can be used to extract the ANC from low-energy scattering parameters. Up to higher-order shape parameters, our relation is equivalent to the one previously derived by Sparenberg *et al.* in Ref. [143] (see Appendix C for details). One difference is that we express the ANC in terms of the binding momentum and the effective range rather than the binding momentum and the scattering length. We find this form more suitable for the extraction of ANCs from scattering data since the effective range is typically more precisely determined than the scattering length for shallow states. Moreover, extracting the effective range in a self-consistent fit from the scattering data that reproduces the correct separation energy improves the stability of the extraction.

We have illustrated our relation by extracting the ANCs of the excited 2^+ and 1^- states in ^{16}O from α – ^{12}C scattering data. Compared to previous extractions [154, 158, 159], our values are generally smaller. Whether this difference is physically significant requires

further study. The application of our relation to other shallow cluster states and a benchmark against model calculations would also be very interesting.

Finally, we have discussed causality bounds for systems where the long-range interaction is given by a singular potential. In particular, we have reviewed the case of an attractive van der Waals tail as it appears in the scattering of neutral atoms. In this case, the situation is fundamentally different from the systems of charged or asymptotically non-interacting particles. Due to the behavior of the singular-potential wave functions, the causality-bound function never has a pole at the origin, which implies that there is no constraint on the interaction range as long as the short-range parameter $K_{\ell,2}$ is negative or zero. We have shown that this is always the case for scattering around a magnetic Feshbach resonance provided that the effective single-channel description of Ref. [164] is applicable. These results can be useful in developing an EFT for systems zero-range interactions and an attractive van der Waals tail.

Chapter 6

The proton–deuteron system revisited

Overview

In this chapter we consider the S-wave proton–deuteron system in pionless effective field theory, a project already started in the present author’s diploma thesis [169]. The first part of what follows is largely based on a subsequent publication [1] (a summary of which appeared in the APFB2011 conference proceedings [6]), with a few details changed, added, and corrected. The material presented in the second part (Section 6.5.2 and beyond), however, is new and has not previously been published.

6.1 Introduction

In Section 2.4 we introduced effective field theories as a powerful tool that can be used to carry out calculations in a formalism involving directly the “correct” degrees of freedom for the physical system under consideration. In particular, in nuclear systems at very low energies and momenta, pion-exchange effects cannot be resolved and one can hence use the *pionless effective field theory* introduced in Section 2.4.2. This approach only includes short-range contact interactions between nucleons [49, 52] and is constructed to reproduce the effective range expansion [13] in the two-body system. It furthermore recovers Efimov’s universal approach to the three-nucleon problem [170, 171].

The extension of pionless EFT to include the long-range Coulomb interaction was first discussed by Kong and Ravndal for the proton–proton channel [117, 172]. In Ref. [173], this analysis was extended to next-to-next-to-leading order. A renormalization-group analysis of proton–proton scattering in a distorted wave basis was carried out in Refs. [174, 175]. Moreover, the theory was applied to proton–proton fusion in Refs. [176, 177].

Here, we are interested in the nuclear three-body system with two charged particles, *i.e.*, protons. Although the Coulomb interaction can be treated as a perturbative correction for intermediate and higher energies, it becomes strong close to threshold and has to

be treated nonperturbatively there. In Ref. [178], Rupak and Kong have formulated a power counting that takes into account such strong Coulomb contributions in the quartet channel of proton–deuteron (p – d) scattering. They calculated the phase shifts to next-to-next-to-leading order (N²LO) in the pionless EFT and included Coulomb effects to next-to-leading order (NLO) [178]. However, they were not able to extend their calculation to the threshold region below center-of-mass momenta of 20 MeV. Furthermore, they did not consider the doublet channel and the ${}^3\text{He}$ bound state.

A leading order calculation of the ${}^3\text{He}$ nucleus including nonperturbative Coulomb interactions has been carried out by Ando and Birse [179]. Including isospin breaking effects in the nucleon–nucleon scattering lengths, they obtained a good description of the ${}^3\text{He}$ – ${}^3\text{H}$ binding energy difference, but they did not consider scattering observables. A similar study at next-to-leading order in the pionless EFT was carried out using the resonating group method [180]. Those results do not include isospin breaking and are consistent with other determinations of the ${}^3\text{He}$ – ${}^3\text{H}$ binding energy difference.

In this chapter, we apply the power counting of Rupak and Kong to study the S-wave p – d system in both the quartet and the doublet channel. Focussing first on results already published in Ref. [1], we show how by using a special integration mesh we are able to calculate scattering phase shifts in both channels down to very small momenta of the order 3 MeV. After reviewing the formalism of pionless EFT in Section 6.2, we discuss these results in Section 6.3. Amending then our previous work, we consider in Sections 6.4 and 6.5 both a perturbative evaluation of the Coulomb contribution to the ${}^3\text{He}$ – ${}^3\text{H}$ binding-energy difference as well as a nonperturbative calculation of the ${}^3\text{He}$ binding energy and wave function. Although our calculation only includes Coulomb photons, it gives almost the same result as found by Ando and Birse [179].

From the nonperturbative bound-state calculation we find that the doublet-channel system beyond leading order does not seem to be renormalized correctly when Coulomb contributions are taken into account. We discuss this in some detail in Section 6.6 and also critically review the situation in the scattering regime. As a further new result we present in Section 6.7 a first preliminary calculation of proton–deuteron scattering lengths in pionless EFT. We then conclude with a brief summary and an outlook.

6.2 Formalism and building blocks

We write the effective Lagrangian in the form

$$\begin{aligned} \mathcal{L} = & N^\dagger \left(iD_0 + \frac{\mathbf{D}^2}{2M_N} \right) N - d^{i\dagger} \left[\sigma_d + \left(iD_0 + \frac{\mathbf{D}^2}{4M_N} \right) \right] d^i - t^{A\dagger} \left[\sigma_t + \left(iD_0 + \frac{\mathbf{D}^2}{4M_N} \right) \right] t^A \\ & + y_d [d^{i\dagger} (N^T P_d^i N) + \text{h.c.}] + y_t [t^{A\dagger} (N^T P_t^A N) + \text{h.c.}] + \mathcal{L}_{\text{photon}} + \mathcal{L}_3, \end{aligned} \quad (6.1)$$

with the nucleon field N and two dibaryon fields d^i (with spin 1 and isospin 0) and t^A (with spin 0 and isospin 1), corresponding to the deuteron and the spin-singlet isospin-triplet virtual bound state in S-wave nucleon–nucleon scattering. Both dibaryon fields are formally ghosts since their kinetic terms have a negative sign. This is required to

reproduce the positive values of the effective ranges with short-range interactions [135]. Despite these “wrong” signs, the Lagrangian (6.1) can be shown to be equivalent to the most general version including only nucleon fields (see, for example, Ref. [181]). One can interpret the choice of signs in Eq. (6.1) as “avoiding” the Wigner bound (*cf.* Chapter 5), but since the effective N – N interactions (obtained by eliminating the dibaryon fields with the kinetic energy terms included) become energy-dependent, this is not a rigorous statement.

Spin and isospin degrees of freedom are included by treating the field N as a doublet in both spaces, but for notational convenience we usually suppress the spin and isospin indices of N . The operators

$$P_d^i = \frac{1}{\sqrt{8}} \sigma^2 \sigma^i \tau^2 \quad , \quad P_t^A = \frac{1}{\sqrt{8}} \sigma^2 \tau^2 \tau^A \quad , \quad (6.2)$$

with the Pauli matrices $\vec{\sigma}$ and $\vec{\tau}$ operating in spin and isospin space, respectively, project out the 3S_1 and 1S_0 nucleon–nucleon partial waves.

The covariant derivative

$$D_\mu = \partial_\mu + ieA_\mu \hat{Q} \quad , \quad (6.3)$$

where \hat{Q} is the charge operator, includes the coupling to the electromagnetic field. Furthermore, we have the kinetic and gauge fixing terms for the photons,

$$\mathcal{L}_{\text{photon}} = -\frac{1}{4} F_{\mu\nu} F^{\mu\nu} - \frac{1}{2\xi} (\partial_\mu A^\mu - \eta_\mu \eta_\nu \partial^\nu A^\mu)^2 \quad , \quad (6.4)$$

of which we only keep contributions from Coulomb photons. These correspond to a static Coulomb potential between charged particles, but for convenience we introduce Feynman rules for a Coulomb-photon propagator,

$$\Delta_{\text{Coulomb}}(k) = \frac{i}{\mathbf{k}^2 + \lambda^2} \quad , \quad (6.5)$$

which we draw as a wavy line, and factors $(\pm ie \hat{Q})$ for the vertices.¹ Following Ref. [178], we have regulated the singularity of the Coulomb-photon propagator at zero momentum transfer by introducing a photon mass λ in Eq. (6.5). This corresponds to a screening of the Coulomb interaction in configuration space by writing it as a Yukawa potential $\sim e^{-\lambda r}/r$. In the numerical calculations that will be discussed later on, λ is always taken to be small (typically well below 1 MeV). In fact, by choosing a mesh-point distribution dense around the Coulomb peak it is possible to numerically take the zero-screening limit $\lambda \rightarrow 0$ [169].

S-wave nucleon–deuteron scattering can take place in either a spin-3/2 (quartet channel) or spin-1/2 (doublet channel) configuration. In the doublet channel, a three-body contact interaction is required for renormalization already at leading order in the EFT [54]. We

¹Due to the sign convention chosen in the Lagrangian (6.1), dibaryon–photon vertices get an additional minus sign.

write it here in the form given by Ando and Birse [179],

$$\mathcal{L}_3 = \frac{M_N H(\Lambda)}{3\Lambda^2} \left(y_d^2 N^\dagger (\vec{d} \cdot \vec{\sigma})^\dagger (\vec{d} \cdot \vec{\sigma}) N + y_t^2 N^\dagger (\vec{t} \cdot \vec{\tau})^\dagger (\vec{t} \cdot \vec{\tau}) N - y_d y_t \left[N^\dagger (\vec{d} \cdot \vec{\sigma})^\dagger (\vec{t} \cdot \vec{\tau}) N + \text{h.c.} \right] \right), \quad (6.6)$$

where Λ is a momentum cutoff applied in the three-body equations discussed below and $H(\Lambda)$ a known log-periodic function of the cutoff that depends on a three-body parameter Λ_* . The Lagrangian in Eq. (6.6) differs slightly from the one quoted in Refs. [1, 169], which was taken over from Ref. [55]. The version given above corrects a mistake in the old expression and has also been used in Ref. [182]. Fortunately, the results in the older publications were not actually affected by this problem (see Section 6.2.4 for details).

6.2.1 Full dibaryon propagators

In the strong sector, we adopt the standard power counting for large S-wave scattering length [49, 52]. A nucleon bubble together with a bare dibaryon propagator scales as $\mathcal{O}(1)$. The bare dibaryon propagators therefore are dressed by nucleon bubbles to all orders, giving the geometric series for the full propagators that are shown diagrammatically in Fig. 6.1.

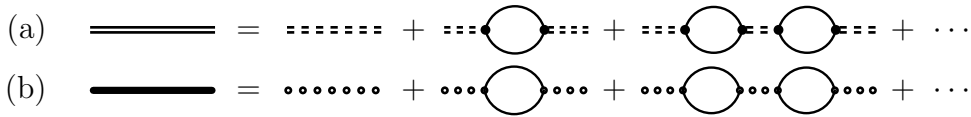


Figure 6.1: Full dibaryon propagators in (a) the 3S_1 state (*i.e.* the deuteron) and (b) the 1S_0 state.

For convenience, we also resum the effective range corrections that arise when the dibaryons in the theory are promoted to dynamical fields by including their kinetic terms. We do not go into the details of the calculations here and simply quote the results for the renormalized propagators. They are obtained by demanding that the (S-wave) effective range expansions

$$k \cot \delta_d = -\kappa_d + \frac{\rho_d}{2}(k^2 + \kappa_d^2) + \dots \quad (6.7)$$

around the deuteron pole² at $k = i\kappa_d = i\sqrt{M_N E_d}$, and

$$k \cot \delta_t = -\frac{1}{a_t} + \frac{\rho_t}{2}k^2 + \dots \quad (6.8)$$

²The notation ρ_d is used in the quadratic term of Eq. (6.7) because the expansion is not around zero momentum. The difference of ρ_d to the effective range in a standard expansion around zero momentum is smaller than 1% [16]. Note furthermore that in Ref. [1] we used the more common (at least in the context of pionless EFT) notation γ_d for the deuteron binding momentum. We changed it here to instead of κ_d in order to be consistent with the conventions used throughout the present work.

for the singlet channel are reproduced. The expansion for the singlet channel is around zero momentum; alternatively one could also expand here around the position of the virtual bound state. In writing Eq. (6.8), however, we have used that $\rho_t = r_{0t}$ to the order we are working at and will in the following also identify $\kappa_t \equiv 1/a_t$ to make the notation more symmetric. After renormalization (using the PDS scheme [50]), the fully resummed propagators are

$$\Delta_d^{ij}(p) \equiv \delta^{ij} \Delta_d(p) = -\frac{4\pi i}{M_N y_d^2} \cdot \frac{\delta^{ij}}{-\kappa_d + \sqrt{\frac{\mathbf{p}^2}{4} - M_N p_0 - i\varepsilon - \frac{\rho_d}{2} \left(\frac{\mathbf{p}^2}{4} - M_N p_0 - \kappa_d^2 \right)}} \quad (6.9)$$

and

$$\Delta_t^{AB}(p) \equiv \delta^{AB} \Delta_t(p) = -\frac{4\pi i}{M_N y_t^2} \cdot \frac{\delta^{AB}}{-\kappa_t + \sqrt{\frac{\mathbf{p}^2}{4} - M_N p_0 - i\varepsilon - \frac{\rho_t}{2} \left(\frac{\mathbf{p}^2}{4} - M_N p_0 \right)}} \quad (6.10)$$

which means that we have fixed the parameters appearing in the effective Lagrangian according to³

$$\sigma_{d,t} = \frac{2}{M_N} \frac{\mu - \kappa_{d,t}}{\rho_{d,t}} \quad , \quad y_{d,t}^2 = \frac{8\pi}{M_N^2} \frac{1}{\rho_{d,t}} \quad (6.11)$$

These expressions are valid up to N²LO since the resummation of the effective-range contributions only includes a subset of higher-order (N³LO etc.) terms. At leading order, range corrections are not included and the dibaryon kinetic terms do not contribute. The corresponding propagators are obtained by setting $\rho_t = 0$ and $\rho_d = 0$ in Eqs. (6.9) and (6.10), while perturbative expressions for the NLO and N²LO propagators can be obtained by expanding the equations up to linear and quadratic order in ρ_d and ρ_t , respectively. For each expression, the corresponding deuteron wave function renormalization constant is given by the residue at the bound state pole:

$$Z_0^{-1} = i \frac{\partial}{\partial p_0} \frac{1}{\Delta_d(p)} \Big|_{p_0 = -\frac{\kappa_d^2}{M_N}, \mathbf{p}=0} \quad (6.12)$$

At leading order, one simply has

$$Z_0^{\text{LO}} = \kappa_d \rho_d \quad (6.13)$$

whereas the result from the fully resummed expression (6.9) is

$$Z_0^{\text{N}^2\text{LO}} = \frac{\kappa_d \rho_d}{1 - \kappa_d \rho_d} \quad (6.14)$$

The expressions for the perturbatively expanded propagators can then simply be read off from the geometric series

$$\frac{1}{1 - \kappa_d \rho_d} = 1 + \kappa_d \rho_d + (\kappa_d \rho_d)^2 + \dots \quad (6.15)$$

³Choosing the normal positive signs for the dibaryon kinetic energy terms in the Lagrangian (6.1) would have given a minus sign in the expression for $y_{d,t}^2$ and thus made the coupling constants purely imaginary. This situation is avoided with the choice of the negative signs.

Note that since $\kappa_d \rho_d \approx 0.4$, the above series converges only rather slowly. This fact can be taken into account by choosing an alternative renormalization scheme, called *Z-parametrization* [183], that is constructed in such a way that it produces the fully resummed Z_0 as given in Eq. (6.14) already at NLO. In Ref. [184] the approach has been applied to the three-nucleon system in pionless EFT and shown to improve the overall convergence of the theory. In the present work, however, where we are primarily interested in the inclusion of Coulomb effects, we use the simpler scheme with the propagators as given in Eqs. (6.9) and (6.10).

6.2.2 Coulomb contributions in the proton–proton system

The Coulomb interaction breaks the isospin symmetry that is implicit in the dibaryon propagators considered so far. For the p - p part of the singlet dibaryon we can also have Coulomb-photon exchanges inside the nucleon bubble. These can be resummed to all orders, yielding a dressed nucleon bubble [117, 172] that is subsequently used to calculate the full singlet-dibaryon propagator in the p - p channel. This is shown in Fig. 6.2. The result for the leading order propagator is [179]

$$\Delta_{t,pp}^{AB}(p) \equiv \delta^{AB} \Delta_{t,pp}(p) = -\frac{4\pi i}{M_N y_t^2} \cdot \frac{\delta^{AB}}{-1/a^C - \gamma \tilde{h}_0(p')} \quad (6.16)$$

with

$$\gamma = \gamma_{p-p} = \alpha M_N \quad , \quad \alpha = \frac{e^2}{4\pi} \approx \frac{1}{137} \quad , \quad p' = i\sqrt{\mathbf{p}^2/4 - M_N p_0 - i\varepsilon} \quad , \quad (6.17)$$

and function $\tilde{h}_\ell(p)$ as defined in Eq. (4.29), giving

$$\tilde{h}_0(p') = \psi(i\eta) + \frac{1}{2i\eta} - \log(i\eta) \quad , \quad \eta = \eta(p') = \frac{\gamma}{2p'} \quad . \quad (6.18)$$

This means, of course, that the Coulomb-modified effective range expansion (4.28) discussed in Chapter 4 has been used for renormalization. We denote here the p - p S-wave scattering length simply as a_C . Corrections due to the corresponding Coulomb-modified effective range r_C can be included in the same way as described in the preceding section by first resumming insertions of the kinetic energy operators to all orders and then matching the result to reproduce the modified effective range expansion up to quadratic order.

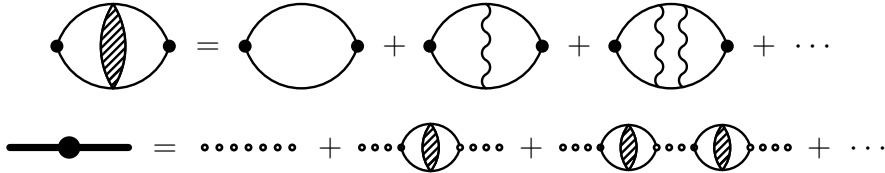


Figure 6.2: Dressed nucleon bubble and full singlet dibaryon propagator in the p - p channel.

To simplify the equations that we give later on, we introduce here the propagator functions

$$D_{d,t}(E; q) \equiv (-i) \cdot \Delta_{d,t} \left(E - \frac{q^2}{2M_N}, q \right) \quad (6.19)$$

and

$$D_t^{pp}(E; q) \equiv (-i) \cdot \Delta_{t,pp} \left(E - \frac{q^2}{2M_N}, q \right). \quad (6.20)$$

6.2.3 Power counting

The power counting of pionless effective field theory has been extensively discussed in the literature (see the reviews [43, 47, 185] and references therein), such that we can be rather brief on this subject here. We will, however, elaborate a bit on the power counting for the Coulomb sector of the theory as it was introduced by Rupak and Kong in Ref. [178].

Strong sector

Without electromagnetic effects, the most relevant low-energy scale Q of the theory is set by the deuteron binding momentum $\kappa_d \approx 45$ MeV. We can formally count the external momenta k, p to be of the same order. Since we are working in a setup without explicit pions, the natural ultraviolet cutoff of our theory is of the order of the pion mass, $\Lambda \sim M_\pi$. Which cutoff is best to use in practice depends on whether one discusses the quartet-channel or the doublet-channel system. In the first case short-range effects are suppressed by the Pauli principle and one finds that already $\Lambda = M_\pi \approx 140$ MeV is sufficient for an accurate description. In the doublet channel, on the other hand, the cutoff must be set to a few hundred MeV to get converged results. In either case, the combination of the two scales yields the expansion parameter $\mathcal{O}(Q/\Lambda) \sim 1/3$ of pionless EFT.

A further relevant scale in our system is the nucleon mass M_N . It appears explicitly in kinetic energies, which scale as $\mathcal{O}(Q^2/M_N)$. As a consequence, the nucleon propagator scales as $\mathcal{O}(M_N/Q^2)$ and the loop integration measure $d^4q = d^3q dq_0$ scales as $\mathcal{O}(Q^5/M_N)$. Note, however, that in each loop the dq_0 -integration can be carried out by picking up the residue from one nucleon propagator, so loops with one of the involved nucleon propagators canceled simply scale as $\mathcal{O}(Q^3)$.

We assume $y_d^2 \sim y_t^2 \sim \Lambda/M_N^2$ for the nucleon–dibaryon coupling constants and $\sigma_d \sim \sigma_t \sim Q\Lambda/M_N$ for the bare dibaryon-propagator terms. Together with the scaling of loops as discussed in the previous paragraph it then follows that in order to get the strong ($n-d$) scattering amplitude, one has to iterate the leading one-nucleon exchange diagram to all orders. The result can be written as an integral equation and will be discussed in Section 6.2.4.

Including Coulomb photons

The power counting has to be adapted when Coulomb effects are included. From the form of the (Yukawa-screened) Coulomb potential in momentum space,

$$V_{c,\lambda}(q) \sim \frac{\alpha}{q^2 + \lambda^2}, \quad (6.21)$$

it is clear that Coulomb contributions dominate for small momentum transfers. As noted in Ref. [178], they enter $\sim \alpha M_N/q$, *i.e.*, proportional to the Coulomb parameter η intro-

duced in Chapter 4. This behavior is not captured by the power counting for the strong sector, which consequently has to be modified in order to perform calculations including Coulomb effects for small external momenta.

Most importantly, one can no longer simply assume that the scale of all momenta is set by the deuteron binding momentum, $Q \sim \kappa_d$. Instead, one has to keep track of the new scale introduced by the external momenta separately. We generically denote this scale by p and assume $p \ll Q$ for the power counting. This means that we make a simultaneous expansion in *two* small parameters Q/Λ and $p/(\alpha M_N)$ [178].⁴ For $p \gtrsim Q$, the Coulomb contributions are small and the results in both schemes agree.

With this modified counting, it is not straightforward to deduce the scaling of loops anymore. Kinetic energies always scale like Q , so the scaling of dq_0 and the nucleon propagator is not modified in the presence of Coulomb effects. However, where before we could simply assume that all loop momenta are dominated by the scale $Q \sim \kappa_d$, we now have to check first which contribution is picked up (or rather enhanced) after carrying out the dq_0 -integral. In the following we illustrate this by deducing the scaling of a few selected diagrams.

Selected diagrams

In Fig. 6.3 we show all diagrams contributing to p - d scattering that involve a single Coulomb-photon exchange and are thus of the order α . The last one, diagram (d) has the most straightforward behavior since it simply scales as α/p^2 . Diagram (a) has the same factor because also here the Coulomb-photon propagator involves the external momentum scale p , but it is further enhanced a factor Λ/Q from the nucleon bubble, which is easy to count as there are no Coulomb-photon exchanges inside the bubble. This is of course in perfect agreement with the fact that the direct coupling of the photon to the dibaryon—generated by gauging the dibaryon kinetic energy operators—only enters at NLO in the EFT counting. This makes diagram (d) both $\mathcal{O}(\alpha)$ and an effective-range correction $\sim \rho_{d,t}$.

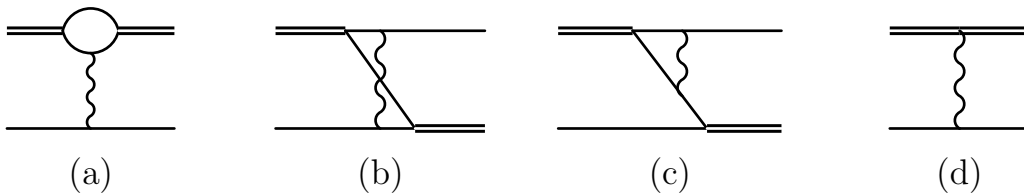


Figure 6.3: Leading $\mathcal{O}(\alpha)$ diagrams involving Coulomb photons.

Since diagram (b) is more complicated to count, we first consider diagram (c), where clearly the loop does not involve the external momentum p but is rather dominated by the deuteron binding momentum flowing into the triangle loop. This yields then that compared to the simple one-nucleon exchange diagram (without a photon) it is suppressed by a factor $\alpha M_N/Q$. Consistent with this one finds by a direct numerical evaluation that at threshold (vanishing p - d center-of-mass momentum) it is a 15% effect.

⁴For a related approach in the pionful theory, see also Ref. [186].

Finally, although it is not straightforward to see due to the non-planar topology of diagram (b), one can argue also here that the deuteron binding momentum flowing into the loop sets the scale there and thus take all momenta to scale like Q . Following Rupak and Kong [178] in doing this, we get the same $\alpha M_N/Q$ suppression factor as for diagram (c). A direct numerical calculation shows that it is a 7% effect at threshold.

We can summarize the findings so far by saying that unless a diagram directly exhibits the (regulated) Coulomb pole, it is not enhanced and thus a small electromagnetic correction to the same diagram topology without Coulomb-photon exchange. The enhanced Coulomb contributions are particularly large in the threshold region (where p is very small) and should thus be iterated to all orders. In our calculation of scattering phase shifts we neglect both diagrams (b) and (c). Their relative size at threshold mentioned above gives an *a priori* uncertainty of 7–15 percent, from which we conclude that Coulomb effects are included in the calculation at an accuracy corresponding to the typical NLO uncertainty from the EFT expansion.

What we have stepped over so far are diagrams like Fig. 6.3a with more than one Coulomb photon attached to the nucleon bubble. For the diagram with two photons (and thus two loops that share a nucleon propagator) one finds a total scaling $\sim \alpha^2 M_N \Lambda / (Q^3 p)$ which means that compared to diagram (b) it is suppressed by a factor $\alpha M_N p / Q^2$. In Ref. [178] it is argued that the diagram with three photons could contribute with a factor $\sim \log(p/Q)$, which is already small for $p \geq 1$ MeV, and that the diagrams with $n > 3$ photons attached to the bubble are even infrared finite and suppressed by factors of α^n . Neglecting all these contributions is thus consistent with not including diagrams (b) and (c).

To conclude this section we point out again that the power counting established here is specifically designed to account for Coulomb contributions that become strong in the scattering at low momenta. At larger momenta, where the Coulomb parameter $\alpha M_N / p$ becomes small, it would suffice to not iterate any Coulomb diagrams but rather include them strictly perturbatively. However, exactly because they become small we assume that it also does not spoil the calculation to iterate them everywhere.

The above discussion clearly shows that the counting scheme employed here is rather complicated and, except for the simplest diagrams, certainly not unambiguous. As we will discuss in Section 6.5.2, for calculations in the bound-state regime the counting definitely has to be modified because there all loop-momentum scales are set by the binding momentum of the bound state. Based on the findings there, we will then argue in Section 6.6.5 that the same counting, which is actually simpler, should also be used in the scattering regime. For the moment, however, we proceed as in Ref. [1] and apply the counting as described above.

6.2.4 Integral equations

From the preceding section it follows that certain diagrams have to be resummed to all orders in order to calculate N - d scattering amplitudes in pionless EFT. We now discuss how this is done by constructing and solving integral equations for the corresponding half off-shell T-matrices in momentum space. We start again by first discussing the strong sector (neutron–deuteron scattering) and then subsequently include Coulomb contributions

to get the desired proton–deuteron equations.

The integral equations are essentially Lippmann–Schwinger equations written out in momentum space. In the following, we generically use the calligraphic letter \mathcal{T} to denote their solutions and use appropriate subscripts to indicate which system we are referring to. This choice of notation indicates that we adopt the standard convention in the field, where the T-matrix differs from the one defined in Chapter 2 by an overall minus sign, and that in order to obtain the physical T-matrix one also has to include the deuteron wave function renormalization factor. The exact relation is

$$T(E; \mathbf{k}, \mathbf{p}) = -Z_0 \mathcal{T}(E, \mathbf{k}, \mathbf{p}). \quad (6.22)$$

Throughout the text, we write “ \mathcal{T} -matrix” (or simply “amplitude”) to indicate this distinction.

Strong sector

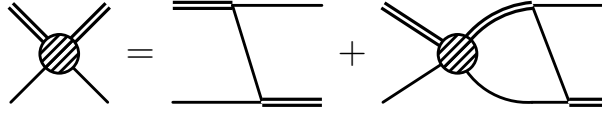


Figure 6.4: Integral equation for the strong scattering amplitude \mathcal{T}_s in the quartet channel.

Figure 6.4 shows a diagrammatic representation of the quartet-channel n - d amplitude, which is the simplest case one can have. The only interaction occurring here is the one-nucleon exchange diagram with deuteron legs on both sides. Including all spin-, isospin- and symmetry factors, it is given by

$$\text{Diagram} = -\frac{iM_N y_d^2}{2} \cdot (\sigma^j \sigma^i)_\alpha^\beta \delta_a^b \cdot \frac{1}{\mathbf{k}^2 + \mathbf{k} \cdot \mathbf{p} + \mathbf{p}^2 - M_N E - i\varepsilon}. \quad (6.23)$$

Since the spins of all three nucleons taking part in the reaction have to be aligned to produce a total spin- $3/2$ state, the Pauli principle prohibits here a three-nucleon contact interaction for which the particles have to occupy the same point in space. Furthermore, only the dibaryon field representing the deuteron can appear in the intermediate state.

Generically, we define the S-wave projected amplitude as

$$\mathcal{T}(E; k, p) = \frac{1}{2} \int_{-1}^1 d\cos\theta \mathcal{T}(E; \mathbf{k}, \mathbf{p}) \quad , \quad \theta = \theta_{\mathbf{k}, \mathbf{p}}. \quad (6.24)$$

Applying this to the one-nucleon exchange shown in Eq. (6.23) yields the projected interaction kernel

$$K_s(E; k, p) \equiv \frac{1}{kp} Q_0 \left(\frac{k^2 + p^2 - M_N E - i\varepsilon}{kp} \right) \quad (6.25)$$

with the Legendre function of the second kind

$$Q_0(a) = \frac{1}{2} \int_{-1}^1 \frac{dx}{x+a} = \frac{1}{2} \log \left(\frac{a+1}{a-1} \right). \quad (6.26)$$

The unprojected \mathcal{T} -matrix has the same spin-isospin indices as the kernel function shown in Eq. (6.23), $\mathcal{T} = (\mathcal{T}^{ij})_{\alpha a}^{\beta b}$. The n - d quartet channel is chosen by inserting $i = (1 - i2)/\sqrt{2}$ and $j = (1 + i2)/\sqrt{2}$ for the deuteron spin-1 indices, $\alpha = \beta = 1$ for the nucleon spins, and $a = b = 2$ to select the neutron in isospin space. As done in Refs. [55, 181], we have used here a short-hand notation for the spin-1 indices i and j that includes prefactors to be used in a linear combination. Written out explicitly, the strong quartet-channel amplitude is accordingly given by

$$\mathcal{T}_s^q = \frac{1}{2} \left(\mathcal{T}_s^{11} + i (\mathcal{T}_s^{12} - \mathcal{T}_s^{21}) + \mathcal{T}_s^{22} \right)_{12}^{12} \quad (6.27)$$

and fulfills the integral equation

$$\mathcal{T}_s^q = -M_N y_d^2 K_s + \mathcal{T}_s^q \otimes [M_N y_d^2 D_d K_s] . \quad (6.28)$$

As in Ref. [1] we have introduced here the short-hand notation

$$A \otimes B \equiv \frac{1}{2\pi^2} \int_0^\Lambda dq q^2 A(\dots, q) B(q, \dots) \quad (6.29)$$

and used the propagator function D_d as defined in Eq. (6.19). As indicated in Eq. (6.29), we regulate all loop integrations with an explicit momentum cutoff Λ .

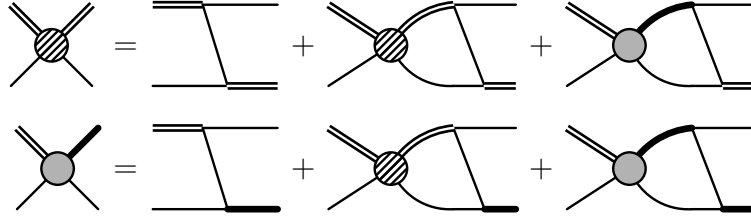


Figure 6.5: Coupled-channel integral equation for the strong scattering amplitude \mathcal{T}_s in the doublet channel. The diagrams involving the three-body force have been omitted.

The equation for the doublet-channel amplitude is shown in Fig. 6.5. Since the spin-singlet dibaryon is now allowed to appear in the intermediate state, we have a coupled-channel system of two amplitudes that we call $\mathcal{T}_s^{d,a}$ and $\mathcal{T}_s^{d,b}$. Of these, the “upper part” $\mathcal{T}_s^{d,a}$ corresponds directly to the n - d scattering process we are interested in, whereas $\mathcal{T}_s^{d,b}$ only enters as an off-shell quantity because the spin-singlet dibaryon, being only a virtual bound state, cannot appear as a true asymptotic state.

Furthermore, with the spins coupled to a total spin $1/2$, the Pauli principle no longer prohibits a three-nucleon interaction, and indeed such a term is needed already at leading order to renormalize the system [54]. The corresponding diagrams have, however, been omitted Fig. 6.5 for simplicity. They can be reinstated by supplementing every one-nucleon exchange with a matching N - d contact interaction from Eq. (6.6). With the n - d doublet-channel projection,

$$\mathcal{T}_s^{d,a} = \frac{1}{3} (\sigma^i)_{\alpha}^{\alpha'} (\mathcal{T}_s^{a,ij})_{\alpha'a}^{\beta'b} (\sigma^j)_{\beta'}^{\beta} \Big|_{\substack{a=b=2 \\ \alpha=\beta=1}} , \quad (6.30a)$$

$$\mathcal{T}_s^{d,b} = \frac{1}{3} (\sigma^i)_{\alpha}^{\alpha'} (\mathcal{T}_s^{b,iB})_{\alpha'a}^{\beta\beta'} (\tau^B)_{\beta'}^b \Big|_{\substack{a=b=2 \\ \alpha=\beta=1}} , \quad (6.30b)$$

and introducing furthermore the abbreviations

$$g_{dd} = \frac{M_N y_d^2}{2}, \quad g_{dt} = \frac{M_N y_d y_t}{2}, \quad g_{tt} = \frac{M_N y_t^2}{2}, \quad (6.31)$$

the result can be written as

$$\begin{aligned} \begin{pmatrix} \mathcal{T}_s^{\text{d,a}} \\ \mathcal{T}_s^{\text{d,b}} \end{pmatrix} &= \begin{pmatrix} g_{dd} \left(K_s + \frac{2H(\Lambda)}{\Lambda^2} \right) \\ -g_{dt} \left(3K_s + \frac{2H(\Lambda)}{\Lambda^2} \right) \end{pmatrix} \\ &+ \begin{pmatrix} -g_{dd} D_d \left(K_s + \frac{2H(\Lambda)}{\Lambda^2} \right) & g_{dt} D_t \left(3K_s + \frac{2H(\Lambda)}{\Lambda^2} \right) \\ g_{dt} D_d \left(3K_s + \frac{2H(\Lambda)}{\Lambda^2} \right) & -g_{tt} D_t \left(K_s + \frac{2H(\Lambda)}{\Lambda^2} \right) \end{pmatrix} \otimes \begin{pmatrix} \mathcal{T}_s^{\text{d,a}} \\ \mathcal{T}_s^{\text{d,b}} \end{pmatrix}. \end{aligned} \quad (6.32)$$

For a more detailed derivation of the equations above we refer to Refs. [1, 169].⁵ Although, as pointed out in Section 6.2, a different three-nucleon Lagrangian has been quoted in those works, the doublet-channel equation found there is the same as in Eq. (6.32) due an incorrect derivation of the corresponding Feynman rules that compensated the problem. Presumably, the same was done by the authors of Ref. [55], which the results were compared to.

Including Coulomb effects

As discussed in Section 6.2.3, the dominant Coulomb contribution is the bubble diagram shown Fig. 6.3a. Its energy and momentum dependence is given by

$$K_{\text{bubble}}(E; \mathbf{k}, \mathbf{p}) = \frac{\mathcal{I}_{\text{bubble}}(E; \mathbf{k}, \mathbf{p})}{(\mathbf{k} - \mathbf{p})^2 + \lambda^2}, \quad (6.33)$$

where

$$\mathcal{I}_{\text{bubble}}(E; \mathbf{k}, \mathbf{p}) = \frac{\arctan\left(\frac{2\mathbf{p}^2 - \mathbf{k}^2 - \mathbf{k} \cdot \mathbf{p}}{\sqrt{3\mathbf{k}^2 - 4M_N E - i\epsilon} \sqrt{(\mathbf{k} - \mathbf{p})^2}}\right) + \arctan\left(\frac{2\mathbf{k}^2 - \mathbf{p}^2 - \mathbf{k} \cdot \mathbf{p}}{\sqrt{3\mathbf{p}^2 - 4M_N E - i\epsilon} \sqrt{(\mathbf{k} - \mathbf{p})^2}}\right)}{\sqrt{(\mathbf{k} - \mathbf{p})^2}} \quad (6.34)$$

is the expression for the bubble loop integral. It can be simplified by noting that due to the denominator in Eq. (6.33) the whole expression is dominated by terms with $\mathbf{p}^2 \approx \mathbf{k}^2$. When the expression appears under the dq integral, we analogously get $\mathbf{p}^2 \approx \mathbf{k}^2$ and can furthermore assume that $\mathbf{q}^2 \approx \mathbf{k}^2$ because of the pole at this position in the deuteron propagator. Inserting then the total center-of-mass energy,

$$E = E(k) = \frac{3k^2}{4M_N} - \frac{\kappa_d^2}{M_N}, \quad k = |\mathbf{k}|, \quad (6.35)$$

we get

$$\frac{\mathcal{I}_{\text{bubble}}(E; \mathbf{k}, \mathbf{p})}{(\mathbf{k} - \mathbf{p})^2 + \lambda^2} \approx \frac{1}{2|\kappa_d|} \frac{1}{(\mathbf{k} - \mathbf{p})^2 + \lambda^2} \quad (6.36a)$$

⁵In particular, a comprehensive discussion of the spin-isospin projections can be found in Appendix B of Ref. [169].

and

$$\Delta_d \left(E - \frac{\mathbf{q}^2}{2M_N}, \mathbf{q} \right) \cdot \frac{\mathcal{I}_{\text{bubble}}(E; \mathbf{q}, \mathbf{p})}{(\mathbf{q} - \mathbf{p})^2 + \lambda^2} \approx \Delta_d \left(E - \frac{\mathbf{q}^2}{2M_N}, \mathbf{q} \right) \cdot \frac{1}{2|\kappa_d|} \frac{1}{(\mathbf{q} - \mathbf{p})^2 + \lambda^2}, \quad (6.36b)$$

by using the expansion $\arctan(x) = x + \mathcal{O}(x^3)$ in Eq. (6.34). The same simplifications, which effectively amount to keeping only loop contributions with $q \sim p$, have also been used in Ref. [178]. Note that they explicitly rely on the energy being given by Eq. (6.35) and are thus not valid in the bound-state regime, where $E < -E_d = -\kappa_d^2/M_N$.

For diagrams with the spin-singlet dibaryon in the intermediate state, as they appear in the doublet-channel calculation, the argument based on the deuteron pole is actually not true. However, for energies in the scattering regime, Eq. (6.36) is still a good approximation (numerically, a 15% effect at threshold and thus compatible with neglecting the diagram shown in Fig. 6.3c).

A more subtle point is that the above approximation also changes the ultraviolet scaling of the diagram, an effect for which it is difficult to judge *a priori* how important it is. Since the only true advantage of the approximation is that it (quite significantly) simplifies the calculation, but certainly does not improve it in any physical sense, it is probably best to not use it if possible. After first giving the results obtained *with* the approximation in Section 6.3 (as reported in Ref. [1]), we will come back to discussing its impact in Section 6.6.5.

Three-channel formalism

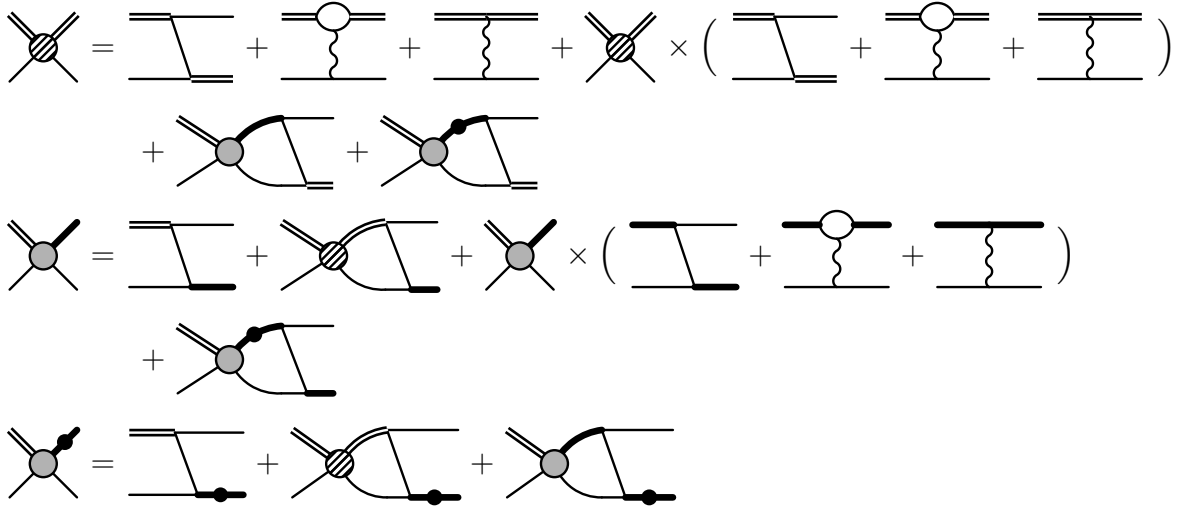


Figure 6.6: Coupled-channel integral equation for the full (*i.e.* strong + Coulomb) scattering amplitude $\mathcal{T}_{\text{full}}$ in the doublet channel. The diagrams representing the three-nucleon force have been omitted.

Due to the fact that the electromagnetic interaction does not couple to isospin eigenstates we now need two different projections for the amplitude \mathcal{T}^b with the outgoing spin-singlet

dibaryon:

$$\mathcal{T}_{\text{full}}^{\text{d,b1}} = \frac{1}{3}(\sigma^i)_{\alpha}^{\alpha'} (\mathcal{T}_{\text{full}}^{\text{b,iB}})^{\beta\beta'} (\mathbf{1} \cdot \delta^{B3})_{b'}^b \Big|_{\substack{a=b=1 \\ \alpha=\beta=1}}, \quad (6.37\text{a})$$

$$\mathcal{T}_{\text{full}}^{\text{d,b2}} = \frac{1}{3}(\sigma^i)_{\alpha}^{\alpha'} (\mathcal{T}_{\text{full}}^{\text{b,iB}})^{\beta\beta'} (\mathbf{1} \cdot \delta^{B1} + i\mathbf{1} \cdot \delta^{B2})_{b'}^b \Big|_{\substack{a=1, b=2 \\ \alpha=\beta=1}}. \quad (6.37\text{b})$$

The latter corresponds to the amplitude with the outgoing spin-singlet dibaryon in a pure p - p state. For the diagrams where this component appears in the intermediate state we have to insert the p - p propagator (6.16).

Diagrammatically, the resulting three-channel integral equation is shown in Fig. 6.6. It is given by

$$\begin{aligned} \begin{pmatrix} \mathcal{T}_{\text{full}}^{\text{d,a}} \\ \mathcal{T}_{\text{full}}^{\text{d,b1}} \\ \mathcal{T}_{\text{full}}^{\text{d,b2}} \end{pmatrix} &= \begin{pmatrix} g_{dd} \left(K_s + \frac{2H(\Lambda)}{\Lambda^2} \right) \\ -g_{dt} \left(K_s + \frac{2H(\Lambda)}{3\Lambda^2} \right) \\ -g_{dt} \left(2K_s + \frac{4H(\Lambda)}{3\Lambda^2} \right) \end{pmatrix} + \begin{pmatrix} g_{dd} K_c^{(d)} \\ 0 \\ 0 \end{pmatrix} \\ &+ \begin{pmatrix} -g_{dd} D_d \left(K_s + \frac{2H(\Lambda)}{\Lambda^2} \right) & g_{dt} D_t \left(3K_s + \frac{2H(\Lambda)}{\Lambda^2} \right) & 0 \\ g_{dt} D_d \left(K_s + \frac{2H(\Lambda)}{3\Lambda^2} \right) & g_{tt} D_t \left(K_s - \frac{2H(\Lambda)}{3\Lambda^2} \right) & 0 \\ g_{dt} D_d \left(2K_s + \frac{4H(\Lambda)}{3\Lambda^2} \right) & -g_{tt} D_t \left(2K_s + \frac{4H(\Lambda)}{3\Lambda^2} \right) & 0 \end{pmatrix} \otimes \begin{pmatrix} \mathcal{T}_{\text{full}}^{\text{d,a}} \\ \mathcal{T}_{\text{full}}^{\text{d,b1}} \\ \mathcal{T}_{\text{full}}^{\text{d,b2}} \end{pmatrix} \\ &+ \begin{pmatrix} -g_{dd} D_d K_c^{(d)} & 0 & g_{dt} D_t^{pp} \left(3K_s + \frac{2H(\Lambda)}{\Lambda^2} \right) \\ 0 & -g_{tt} D_t K_c^{(t)} & -g_{tt} D_t^{pp} \left(K_s + \frac{2H(\Lambda)}{3\Lambda^2} \right) \\ 0 & 0 & -g_{tt} D_t^{pp} \times \frac{4H(\Lambda)}{3\Lambda^2} \end{pmatrix} \otimes \begin{pmatrix} \mathcal{T}_{\text{full}}^{\text{d,a}} \\ \mathcal{T}_{\text{full}}^{\text{d,b1}} \\ \mathcal{T}_{\text{full}}^{\text{d,b2}} \end{pmatrix} \quad (6.38) \end{aligned}$$

with the Coulomb kernel functions

$$\begin{aligned} K_c^{(d,t)}(E; k, p) &= -\alpha M_N \times \left[\underbrace{\int_{-1}^1 d \cos \theta \frac{\mathcal{I}_{\text{bubble}}(E; \mathbf{k}, \mathbf{p})}{(\mathbf{k} - \mathbf{p})^2 + \lambda^2}}_{\text{LO}} + \underbrace{\frac{\rho_{d,t}}{2kp} Q \left(-\frac{k^2 + p^2 + \lambda^2}{2kp} \right)}_{\text{NLO}} \right] \\ &\approx \frac{\alpha M_N}{2kp} Q \left(-\frac{k^2 + p^2 + \lambda^2}{2kp} \right) \left(\frac{1}{|\kappa_d|} - \rho_{d,t} \right). \quad (6.39) \end{aligned}$$

In writing Eq. (6.38) we have separated the terms in such a way that the Coulomb contributions can be easily identified.

Note that the terms involving $H(\Lambda)$ in Eq. (6.38) differ slightly from the version given in Refs. [1, 169] due to the incorrect Feynman rules used in those works. Still, this turns out not to be a serious problem because both the old expressions and Eq. (6.38) are such that they reduce to the two-channel n - d equation (6.32) when all Coulomb effects are switched off and one considers the sum $\mathcal{T}^{\text{d,b}} = \mathcal{T}^{\text{d,b1}} + \mathcal{T}^{\text{d,b2}}$. As a consequence, one finds the same $H(\Lambda)$ in a numerical fit to the triton binding energy as with the old expression, and all observables are unaffected.

In order to calculate Coulomb-subtracted phase shifts, we also need the amplitude for pure Coulomb scattering. Since the electromagnetic interaction in our approximation does not couple the different channels, for both quartet-channel and doublet-channel p - d scattering is given by the simple equation

$$\mathcal{T}_c = g_{dd} K_c^{(d)} - \mathcal{T}_c \otimes [g_{dd} D_d K_c^{(d)}] . \quad (6.40)$$

Higher-order corrections

From Eq. (6.39) one directly sees that the diagram with the photon coupled directly to a dibaryon (Fig. 6.3d and its analog with a spin-singlet dibaryon) is proportional to the effective range (ρ_d or ρ_t) and thus a correction that enters at next-to-leading order in the EFT power counting. This has already been mentioned in Section 6.2.3. Apart from that, the order of our calculation is determined by the expressions used for the dibaryon propagators.

The fully resummed propagators given in Eqs. (6.9) and (6.10) have spurious deep poles that do not correspond to actual physical bound states. In the quartet channel, the cutoff can be chosen low enough to avoid that pole. Due to the larger cutoff needed in the doublet channel, however, we cannot use the resummed propagators here. Instead, we follow the approach of Ref. [187] and use the perturbative expansions (more appropriately called “partially resummed propagators”) mentioned in Section 6.2.1. This still resums some higher-order effective-range contributions, but removes the unphysical pole.⁶

More precisely, at next-to-leading order we always use propagators $D_{d,t}^{\text{N}^2\text{LO}}$ that include a single insertion of the dibaryon kinetic energy operator and are thus linear in the effective range. At next-to-next-to leading order (N²LO) the propagators $D_{d,t}^{\text{N}^2\text{LO}}$ for the doublet-channel calculation include corrections quadratic in the effective ranges, whereas in the quartet-channel we use the fully-resummed expression given by Eq. (6.9) together with a cutoff low enough to avoid the unphysical pole.

Since the publication of Ref. [1] an agreement has been reached in the literature [187–189] that in the doublet channel, a second (energy-dependent) three-nucleon interaction is needed at N²LO for consistent renormalization. As in Ref. [1], we do not include such a term here for simplicity and thus obtain only a partial N²LO result. In fact, as we will discuss in Section 6.6.5, with Coulomb effects included, the question of correct renormalization in the double channel might have to be reconsidered already at next-to-leading order.

6.2.5 Numerical implementation

The integral equations presented in the previous sections have to be solved numerically. We do so by discretizing the integrals, using Gaussian quadrature, principal value inte-

⁶Note that the resummation procedure also affects the ultraviolet behavior of the propagators. The fully resummed expressions fall off faster than the leading-order propagators, whereas the perturbative expansions do not go to zero anymore for large p . This point will become important in Section 6.6.

gration to deal with the singularity of the deuteron propagator, and appropriate transformations of the integration domain.

The latter are especially important to deal with the numerical difficulties caused by the Coulomb-photon propagators. Even though we have regulated the singularity with an artificial photon mass λ , the latter has to be kept small in order to not modify the theory too much. This then yields strongly peaked functions. As shown in Ref. [169], the Coulomb peaks in the inhomogeneous parts the integral equations are the major numerical difficulty. It can be overcome by concentrating the quadrature points around the peak and always putting half of the quadrature points into the low-momentum region. With this procedure it is then possible to (linearly) extrapolate the results back to the physical case $\lambda = 0$. The error introduced by this extrapolation can in general be neglected compared to the theoretical uncertainty from the EFT expansion discussed below.

We use the experimental input parameters shown in Table 6.1 for the numerical calculation.

Parameter	Value	Ref.	Parameter	Value	Ref.
κ_d	45.701 MeV	[48]	ρ_d	1.765 fm	[16]
a_t	−23.714 fm	[47]	ρ_t	2.73 fm	[47]
a_C	−7.8063 fm	[145]	r_C	2.794 fm	[145]

Table 6.1: Parameters used for the numerical calculation.

6.3 Scattering phase shifts

From the solutions of the integral equations we can obtain the S-wave scattering phase shifts as

$$\delta(k) = \frac{1}{2i} \log \left(1 + \frac{2ikM_N}{3\pi} Z_0 \mathcal{T}(E_k; k, k) \right). \quad (6.41)$$

In order to account for the deuteron as a composite asymptotic state, the \mathcal{T} -matrix is multiplied by the wave function renormalization Z_0 defined in Eq. (6.12). This procedure also removes the dependence of the amplitude on the coupling constant y_d , which so far we have kept in all equations. We call $Z_0 \mathcal{T}(E_k; k, k)$ the *renormalized amplitude*.

For the p - d system, what we compare to experimental data are the Coulomb-subtracted phase shifts already introduced in Chapter 4. We calculate them here as

$$\tilde{\delta}(k) \approx \delta_{\text{diff}}(k) \equiv \delta_{\text{full}}(k) - \delta_c(k), \quad (6.42)$$

where $\delta_{\text{full}}(k)$ is obtained from the full integral equation including both Coulomb and strong interactions and $\delta_c(k)$ is obtained from Eq. (6.40) which only includes the Coulomb interaction. This procedure (as opposed to calculating the pure Coulomb phase shift analytically) has the advantage of properly taking into account of the finite cutoff, the EFT expansion, and the regulating photon mass λ .

In the following, we report the results as given in Ref. [1].

6.3.1 Quartet channel

In Fig. 6.7 we show the phase shift results for both neutron–deuteron and proton–deuteron scattering as functions of the center-of-mass momentum k . The error bands are generated by varying the cutoff within a range of 120 to 160 MeV. Since the cutoff variation is small, we conclude that the calculation is well converged at these cutoffs. This finding is important because it allows us to use the fully resummed deuteron propagator (6.9) at N²LO, which would be problematic numerically for cutoffs $\Lambda \gtrsim 200$ MeV due to the unphysical second pole introduced by the resummation. For the n – d curve in Fig. 6.7 we have used a single cutoff $\Lambda = 140$ MeV since we only include this result here for comparison and because its band produced by the cutoff variation would be as narrow as that of the p – d result at N²LO.

The fact that the error bands do not overlap is no point of concern since they only give a lower bound on the uncertainty of the calculation. From the expansion parameter $Q/\Lambda \sim \kappa_d \rho_d \approx 1/3$ of the EFT, the error can be estimated as 30%, 10%, and 3% at LO, NLO, and N²LO, respectively. Thus, at LO, the 30% uncertainty from the expansion parameter clearly dominates. At NLO and N²LO, however, the band from the cutoff variation gives a reasonable estimate of the total error in the calculation.

Our N²LO band agrees very well with the results of Rupak and Kong [178] and also with the experimental data included in the plot. Due to our improved numerical procedure we were able to extend the calculation of Ref. [178] into the threshold region below $k = 20$ MeV (indicated by the dotted line in Fig. 6.7), where Rupak and Kong could not obtain convergent results for small photon masses.

6.3.2 Doublet channel

The doublet-channel results for the p – d scattering phase shifts as functions of the center-of-mass momentum k are shown in Fig. 6.8. As in the quartet channel, the p – d curve lies above the n – d curve and at least at N²LO it agrees quite well with the experimental data. A more quantitative comparison is, unfortunately, not possible since there are no errors given for the data points. The error bands were generated here by varying the cutoff within a natural range of 200 to 600 MeV (*i.e.*, a few times the pion mass).

Note that according to the power counting of Ref. [187] our N²LO calculation is incomplete since we did not include a subleading three-body force at this order. Figure 6.8 nevertheless shows how the results improve from order to order. Despite the fact that we omitted the subleading three-body force, our partial N²LO result is stable to within about ten percent under the cutoff variation, which is consistent with the 7–15% error estimate based on the neglected Coulomb diagrams (see Section 6.2.3 and Ref. [178]). This stability suggests that the scattering is relatively insensitive to the subleading three-body interaction. At higher energies, however, there is some room for such a contribution as our partial result consistently lies two to four degrees above the experimental data.

We observe that the shift from LO to NLO is of the same order of magnitude as the shift from NLO to N²LO, a behavior that is typical for effective-range corrections in the doublet channel [191]. The smallness of the NLO corrections can be understood as a

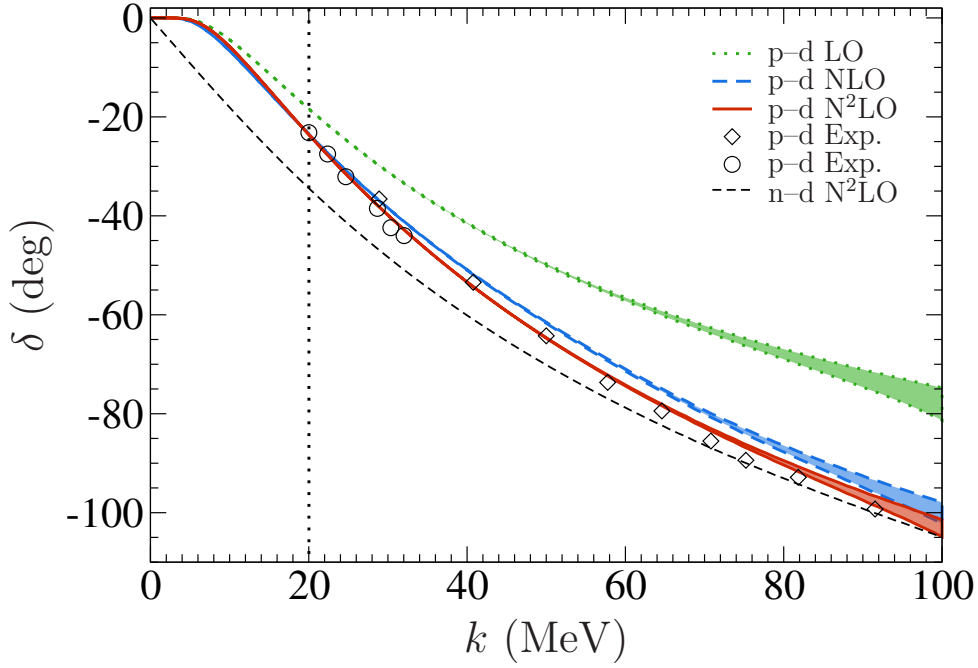


Figure 6.7: N - d quartet-channel S-wave scattering phase shifts as functions of the center-of-mass momentum k . Error bands generated by cutoff variation from 120 to 160 MeV. Experimental p - d phase shift data taken from Refs. [146] (diamonds) and [190] (circles).

cancellation between two different contributions to this correction, proportional to $\kappa\rho_d$ and $\kappa_d\rho_d$, respectively, where κ is the typical momentum scale of the process. Furthermore, it is known that at LO observables are often described better than expected from the power counting once the exact pole position of the two-body propagator is reproduced [28]. As a consequence, the shifts in observables from LO to NLO can be small and of a size comparable to the corresponding shifts from NLO to N²LO, which more directly reflect the uncertainty due to the EFT expansion.

Upon closer examination it turns out that the above results should actually be taken with a grain of salt. This has already been hinted at when we discussed the power counting in Section 6.2.3 and the approximation made in Eq. (6.36). Indeed, a more careful analysis of the bound-state regime that has been carried out since the publication of Ref. [1] also sheds some new light on the scattering calculation. After first giving a detailed discussion of the new bound-state results in the following sections, we will thus revisit this issue in Section 6.6.5.

6.4 Trinucleon wave functions

In order to calculate the ${}^3\text{H}$ - ${}^3\text{He}$ binding-energy shift in perturbation theory we need the wave functions that describe the trinucleon (triton) bound state. As illustrated diagram-

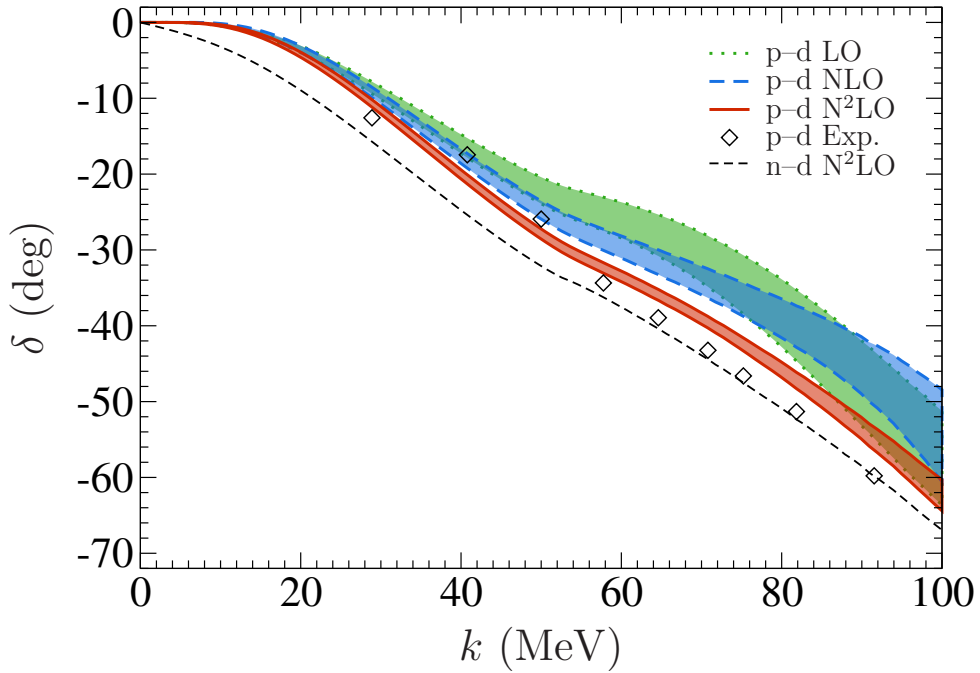


Figure 6.8: N - d doublet channel S-wave scattering phase shifts as functions of the center-of-mass momentum k . Error bands generated by cutoff variation from 200 to 600 MeV. Experimental p - d phase shift data taken from Ref. [146].

matically in Fig. 6.9, at the bound-state pole the \mathcal{T} -matrix factorizes as

$$\mathcal{T}(E; k, p) = -\frac{\mathcal{B}^\dagger(k)\mathcal{B}(p)}{E + E_B} + \text{terms regular at } E = -E_B, \quad (6.43)$$

where the $\mathcal{B}(p)$ are what we call *amputated* wave functions or vertex factors. For a derivation of this relation, including the sign, see Section D.4.3 in Appendix D.

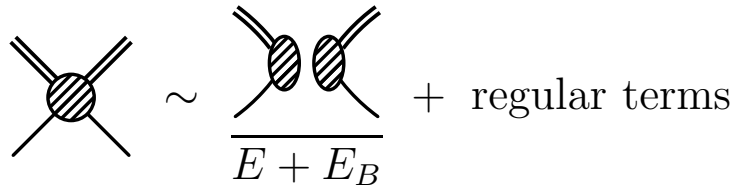


Figure 6.9: Diagrammatic representation of the factorization of \mathcal{T} -matrix at the bound-state pole.

6.4.1 Homogeneous equation

For our coupled-channel problem, $\mathcal{T}(E; k, p)$ is a matrix in channel-space, and the wave functions will thus be vectors. Since the Coulomb repulsion does not act in the channel where the spin-singlet dibaryon is in a pure p - p or n - n state, we use here the three-channel equation structure introduced for the p - d scattering equations, but with all Coulomb

contributions switched off. Our interaction kernel is then given by

$$\hat{K} \equiv \begin{pmatrix} -g_{dd} \left(K_s + \frac{2H(\Lambda)}{\Lambda^2} \right) & g_{dt} \left(3K_s + \frac{2H(\Lambda)}{\Lambda^2} \right) & g_{dt} \left(3K_s + \frac{2H(\Lambda)}{\Lambda^2} \right) \\ g_{dt} \left(K_s + \frac{2H(\Lambda)}{3\Lambda^2} \right) & g_{tt} \left(K_s - \frac{2H(\Lambda)}{3\Lambda^2} \right) & -g_{tt} \left(K_s + \frac{2H(\Lambda)}{3\Lambda^2} \right) \\ g_{dt} \left(2K_s + \frac{4H(\Lambda)}{3\Lambda^2} \right) & -g_{tt} \left(2K_s + \frac{4H(\Lambda)}{3\Lambda^2} \right) & -g_{tt} \times \frac{4H(\Lambda)}{3\Lambda^2} \end{pmatrix}, \quad (6.44)$$

which is found from Eq. (6.38) by factoring out all propagators and omitting the $K_c^{(d,t)}$ entries. Inserting the factorization at the pole (6.43) into the Lippmann-Schwinger equation and taking the limit $E \rightarrow -E_B$ gives a homogeneous equation of the form

$$\vec{\mathcal{B}}_s = (\hat{K} \hat{D}) \otimes \vec{\mathcal{B}}_s \quad (6.45)$$

with

$$\vec{\mathcal{B}}_s \equiv (\mathcal{B}_s^{d,a}, \mathcal{B}_s^{d,b1}, \mathcal{B}_s^{d,b2})^T, \quad \hat{D} = \text{diag}(D_d, D_t, D_t), \quad (6.46)$$

The inhomogeneous interaction terms have dropped out here since they are regular as $E = -E_B$, and we have canceled the overall \mathcal{B}^\dagger terms from the factorization.

6.4.2 Normalization condition

In order to calculate quantities based on the wave functions \mathcal{B}_s it is important to normalize them correctly. To this end one has to take into account that the ‘‘potential’’ derived from the EFT we are using here, *i.e.*, the one-nucleon exchange kernel as given in Eqs. (6.23) and (6.25), is effectively energy-dependent. The normalization condition is

$$\left(\hat{D} \vec{\mathcal{B}}_s \right)^T \otimes \frac{d}{dE} \left(\hat{I} - \hat{K} \right) \Big|_{E=-E_B^{3H}} \otimes \left(\hat{D} \vec{\mathcal{B}}_s \right) = 1, \quad (6.47)$$

where we have defined the matrix of inverse propagators $\hat{I} = \text{diag}(I_d, I_t, I_t)$ with

$$I_{d,t}(E, q, q') = \frac{2\pi^2}{q^2} \delta(q - q') D_{d,t}(E; q)^{-1}. \quad (6.48)$$

A detailed derivation of this can be found in Appendix D, in particular in Section D.4. Note, however, that the insight that energy-dependent interactions imply a nontrivial normalization condition for bound-state wave functions is not new at all but has been known for a long time (see, for example, the overview by Agrawala *et al.* [192] and references therein).

Numerical verification

The normalization condition derived above can be checked by considering the residue of the \mathcal{T} -matrix at the bound-state pole. Following Hagen *et al.* [68] we define

$$Z = \lim_{E \rightarrow -E_B} (E + E_B) \int_0^\Lambda \frac{dq q^2}{2\pi^2} \int_0^\Lambda \frac{dq' q'^2}{2\pi^2} D(E, q) \mathcal{T}(E; q, q') D(E, q') \quad (6.49)$$

and call this quantity the Z -factor of the trinucleon state, or simply *trimer Z -factor*. As we will discuss shortly, for our coupled-channel system we need to sum over all components of the \mathcal{T} -matrix. In Eq. (6.49) we have written $D(E, q)$ to denote a generic dibaryon propagator.

Inserting the factorization of the \mathcal{T} -matrix at the pole as given in Eq. (6.43), we find that

$$Z = \int_0^\Lambda \frac{dq q^2}{2\pi^2} \int_0^\Lambda \frac{dq' q'^2}{2\pi^2} D(-E_B, q) \mathcal{B}^\dagger(q) \mathcal{B}(q') D(-E_B, q') \\ = \left| \int_0^\Lambda \frac{dq q^2}{2\pi^2} D(-E_B, q) \mathcal{B}(q) \right|^2, \quad (6.50)$$

where the last equality follows by noting that the propagators are real in the bound-state regime. Of course, it is crucial here that the wave functions $\mathcal{B}(q)$ are normalized correctly, so numerically calculating Z from both Eqs. (6.49) and (6.50) and showing that the results agree provides the means to verify our normalization condition (6.47) with an explicit calculation.

We now carry out this procedure for the triton wave functions in the two-channel formalism. In order to implement Eq. (6.49) we also need the part of the amplitude that describes the (unphysical) scattering of a spin-singlet dibaryon and a nucleon. The complete \mathcal{T} -matrix for the system is then given by

$$\hat{\mathcal{T}}_s^d = \begin{pmatrix} \mathcal{T}_s^{d,a} & \mathcal{T}_s^{d,c} \\ \mathcal{T}_s^{d,b} & \mathcal{T}_s^{d,d} \end{pmatrix}, \quad (6.51)$$

where the first column is determined by Eq. (6.32) and the second column is a solution of the analogous equation

$$\begin{pmatrix} \mathcal{T}_s^{d,c} \\ \mathcal{T}_s^{d,d} \end{pmatrix} = \begin{pmatrix} -g_{dt} \left(3K_s + \frac{2H(\Lambda)}{\Lambda^2} \right) \\ g_{tt} \left(K_s + \frac{2H(\Lambda)}{\Lambda^2} \right) \end{pmatrix} \\ + \begin{pmatrix} -g_{dd} D_d \left(K_s + \frac{2H(\Lambda)}{\Lambda^2} \right) & g_{dt} D_t \left(3K_s + \frac{2H(\Lambda)}{\Lambda^2} \right) \\ g_{dt} D_d \left(3K_s + \frac{2H(\Lambda)}{\Lambda^2} \right) & -g_{tt} D_t \left(K_s + \frac{2H(\Lambda)}{\Lambda^2} \right) \end{pmatrix} \otimes \begin{pmatrix} \mathcal{T}_s^{d,c} \\ \mathcal{T}_s^{d,d} \end{pmatrix}. \quad (6.52)$$

The expression for the trimer Z -factor in terms of the \mathcal{T} -matrix is then

$$Z_{\mathcal{T}} = \lim_{E \rightarrow -E_B} (E + E_B) \sum_{i,j=1}^2 \left[\hat{D}_{ii} \otimes (\hat{\mathcal{T}}_s^d)_{ij} \otimes \hat{D}_{jj} \right], \quad (6.53)$$

where we have switched back to the short-hand notation of Section 6.2.4 (with the modification that $\hat{D} = \text{diag}(D_d, D_t)$ is only a 2×2 matrix here) and inserted a subscript \mathcal{T} in order to distinguish it from the expression in terms of the wave functions, which we write as

$$Z_{\mathcal{B}} = \sum_{i=1}^2 \left| \hat{D}_{ii} \otimes (\vec{\mathcal{B}}_s)_i \right|^2. \quad (6.54)$$

Numerically calculating Z_B is straightforward since it is just a simple integral over the normalized wave functions. Implementing the procedure to calculate $Z_{\mathcal{T}}$, on the other hand, is more delicate since in order to numerically obtain the residue one has to rely on cancellations between large numbers. If, however, we approach the bound-state pole exponentially, *i.e.*, set

$$E(x) = -E_B + (E_B - E_0) \cdot \exp(-x), \quad (6.55)$$

where E_0 is some energy between the deuteron binding energy E_d and E_B , we find that indeed $Z_{\mathcal{T}}$ converges to Z_B as a function of the parameter x .⁷

We show this in Figs. 6.10 and 6.11 for two different cutoffs $\Lambda = 1000$ MeV and $\Lambda = 377.69$ MeV, where the latter value is approximately the first zero of the three-nucleon force $H(\Lambda)$.⁸ In both calculations we have used $E_0 = 1.1 \times E_d$, which means that at $x = 20$ the distance to the pole (which is always fixed to be exactly at $E_B = 8.4818$ MeV) is only about 10^{-8} MeV. Only if one goes even closer to the pole ($x \gtrsim 25$), numerical difficulties become significant and $Z_{\mathcal{T}}$ starts to visibly deviate from Z_B . At $x = 20$, $Z_{\mathcal{T}}$ still agrees with Z_B to within about 1.5% for $\Lambda = 1000$ MeV and with better than 0.05% accuracy for $\Lambda = 377.69$ MeV.⁹ Altogether, we take the above findings as a clear numerical verification underlining the correctness of our normalization condition (6.47).

Note that the value of the Z -factor varies significantly for different cutoffs. This can be understood by noting that the way we have defined it in Eqs. (6.49) and (6.50), Z is an *unrenormalized* quantity. For the current discussion where we are only interested in establishing the agreement of $Z_{\mathcal{T}}$ and Z_B , however, this is of no importance.

6.5 Helium-3 properties

We are now finally in a position to discuss the Helium-3 system. In the first part of this section we will describe how to obtain the ${}^3\text{H}$ – ${}^3\text{He}$ binding energy shift in a perturbative approach based the normalized trinucleon wave functions \mathcal{B}_s . The results presented here correct and thus supersede those given in Ref. [1]. We will additionally describe how to obtain the ${}^3\text{He}$ binding energy nonperturbatively by locating the pole in the full \mathcal{T} -matrix. The results of both calculations will be shown and discussed in Subsec. 6.5.3.

⁷The author would like to thank P. Hagen for suggesting this approach.

⁸This selection of cutoffs is mostly arbitrary. The reason for choosing the latter cutoff was to investigate if the three-nucleon force has any significant influence on the numerical convergence. Comparison with Fig. 6.10 shows that this does not seem to be the case. We have checked that also at other cutoffs the overall behavior is the same.

⁹The better agreement for $\Lambda = 377.69$ MeV is most probably due to the absolute value of the Z -factor being much smaller there than at $\Lambda = 1000$ MeV, which makes it easier to accurately determine a numerical result originating from the cancellation between large numbers.

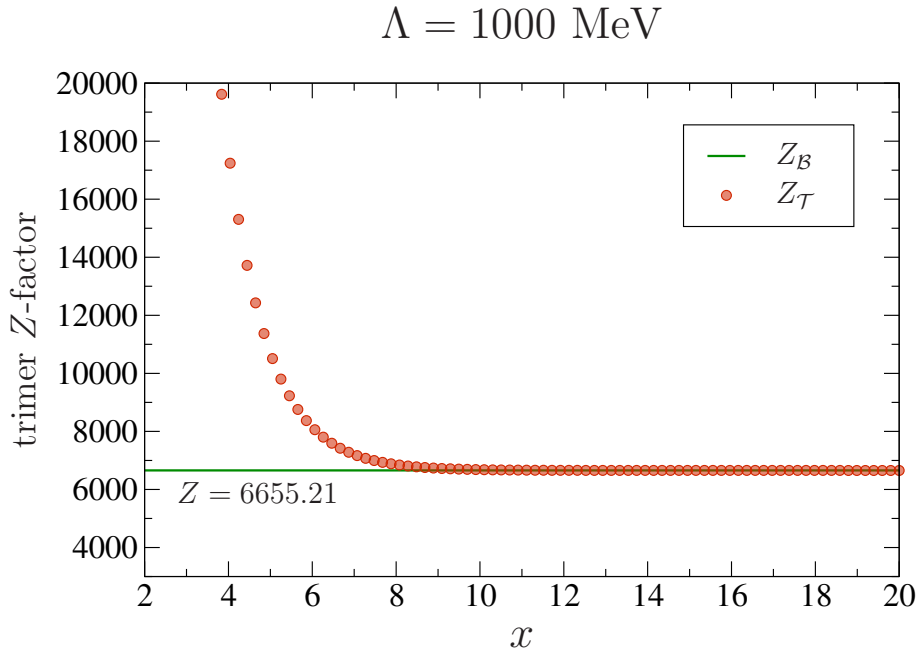


Figure 6.10: Triton trimer Z factor for cutoff $\Lambda = 1000 \text{ MeV}$. x is the parameter in Eq. (6.55).

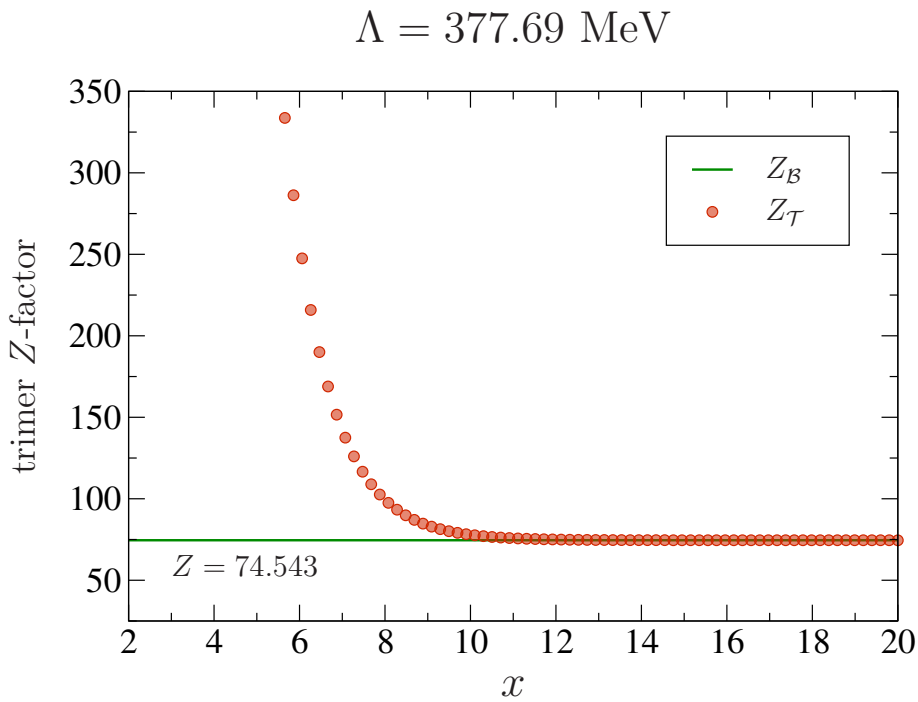


Figure 6.11: Triton trimer Z factor for cutoff $\Lambda = 377.69 \text{ MeV}$, where $H(\Lambda) \approx 0$. x is the parameter in Eq. (6.55).

6.5.1 Energy shift in perturbation theory

In Ref. [1] the ${}^3\text{H}$ – ${}^3\text{He}$ binding-energy difference was calculated using

$$\Delta E_C^{\text{old}} = \left(\hat{D}\vec{\mathcal{B}}_s \right)^T \otimes \text{diag}(V_C, V_C, 0) \otimes \left(\hat{D}\vec{\mathcal{B}}_s \right) \quad (6.56)$$

with the S-wave projected Coulomb potential

$$V_C(E; q, q') = -\frac{4\pi\alpha}{2qq'} Q \left(-\frac{q^2 + q'^2 + \lambda^2}{2qq'} \right) \quad (6.57)$$

in momentum space. The prediction for the ${}^3\text{He}$ binding energy is then given by

$$-E_B^{{}^3\text{He}} = -E_B^{{}^3\text{H}} + \Delta E_C^{\text{old}}. \quad (6.58)$$

However, the naïve approach in Eq. (6.56) is actually not correct. By taking the simple matrix elements of the Coulomb potential between the wave functions $\vec{\mathcal{B}}_s$ in the nucleon–dibaryon formalism, one effectively couples the photon directly to the dibaryon. However, as discussed in Section 6.2.3, this coupling only enters at next-to-leading order in the EFT power counting.

More subtle, but no less important, is to realize that the expression in Eq. (6.56) is not renormalized correctly. By considering the terms that enter in the normalization condition (6.47) we find that formally the wave functions $\vec{\mathcal{B}}_s$ are proportional to the EFT coupling constants y_d and y_t . In the results for physical quantities this dependence has to drop out, just as it does in the scattering calculation where the deuteron wave function renormalization constant cancels the y_d -dependence of the \mathcal{T} -matrix.

In fact, Eq. (6.56) neglects the three-body nature of the problem. To correct this, what should be done is to calculate the diagram shown in Fig. 6.12a at leading order and only add the contribution shown Fig. 6.12b as an NLO-correction. Effectively, this amounts to calculating

$$\Delta E_C^{\text{new}} = \left(\hat{D}\vec{\mathcal{B}}_s \right)^T \otimes \hat{K}_C \otimes \left(\hat{D}\vec{\mathcal{B}}_s \right) \quad (6.59)$$

with the matrix

$$\hat{K}_C = \text{diag}(-g_{dd}K_c^{(d)}, -g_{tt}K_c^{(t)}, 0). \quad (6.60)$$

The kernel functions K_c here are the same that appear in the integral equation for the full scattering amplitude, with the leading-order contribution given by the bubble diagram, Fig. 6.3a, and the direct coupling to the dibaryon only entering at next-to-leading order. As we will discuss in more detail in the next section, it is important here to not use the approximation (6.36) for the bubble diagram but rather include the full expression given in the first line of Eq. (6.39).

The new procedure takes into account the EFT expansion and, since \hat{K}_C is proportional to $y_{d,t}^2$, ΔE_C^{new} is also renormalized correctly. However, the picture is still not complete. As shown in Fig. 6.13, there are also contributions to the energy shift that arise from Coulomb-photon diagrams not taken into account so far. For the scattering calculation we argued that they can be neglected, but we already mentioned at the end of Section 6.2.3 that the power counting has to be modified in the bound-state regime. As we will discuss shortly, these additional diagrams actually are important and should be taken into account in the energy-shift calculation. The complete \hat{K}_C then becomes a non-diagonal matrix.



Figure 6.12: Diagrams contributing to the ${}^3\text{H}$ - ${}^3\text{He}$ binding energy difference in perturbation theory. (a) Leading-order diagram. (b) NLO-correction.



Figure 6.13: Additional diagrams contributing to the ${}^3\text{H}$ - ${}^3\text{He}$ binding energy difference in perturbation theory. (a) Box diagram. (b) Triangle diagram.

6.5.2 Nonperturbative calculation

In Ref. [179], Ando and Birse calculate the ${}^3\text{He}$ binding energy in pionless EFT by using a nonperturbative framework that involves the full off-shell Coulomb T-matrix. As already discussed by Kok *et al.* in Refs. [193, 194], the latter complication is not actually necessary in the bound-state regime. In this section we carry out a calculation analogous to that of Ando and Birse, but only involving Coulomb photons. The resulting equation structure is still quite complex, but much simpler and in particular easier to handle numerically than that of Ref. [179].

Diagram scaling in the bound-state regime

At this point it is important to recall from Section 6.2.3 that the Coulomb diagrams in Figs. 6.3b and 6.3c, which in the following we simply refer to as the *box* and *triangle* diagrams, respectively, are not small *per se*, but rather that the bubble diagram, Fig. 6.3a, is enhanced in the low-energy scattering regime due to the Coulomb singularity at zero momentum transfer. That effect is particularly prominent in the inhomogeneous part of the integral equation, where in the on-shell limit one directly hits the Coulomb pole and the expression is only rendered finite by the regulating photon mass λ .

In the bound-state regime this is no longer the case. There are no inhomogeneous terms that could exhibit a Coulomb peak, and since all loops are dominated by the binding momentum of the bound-state under consideration, the dibaryon propagators do not further enhance integration domains of small momentum transfer.

The consequence of all this is that in a nonperturbative calculation of the Helium-3 binding energy all $\mathcal{O}(\alpha)$ Coulomb diagrams should be treated on an equal footing and included

in the calculation. Furthermore, for the integral in the bubble diagram we have to use the full expression as given by Eq. (6.34) since the argument allowing the approximation given in Eq. (6.36) is not valid in the bound-state regime.

Full equation structure

The resulting full equation structure is shown diagrammatically in Fig. 6.14 and given by the expression

$$\begin{aligned}
\begin{pmatrix} \mathcal{T}_{\text{full}'}^{\text{d,a}} \\ \mathcal{T}_{\text{full}'}^{\text{d,b1}} \\ \mathcal{T}_{\text{full}'}^{\text{d,b2}} \end{pmatrix} &= \begin{pmatrix} g_{dd} \left(K_s + \frac{2H(\Lambda)}{\Lambda^2} \right) \\ -g_{dt} \left(K_s + \frac{2H(\Lambda)}{3\Lambda^2} \right) \\ -g_{dt} \left(2K_s + \frac{4H(\Lambda)}{3\Lambda^2} \right) \end{pmatrix} + \begin{pmatrix} g_{dd} \left(K_c^{(d)} + K_{\text{box}} \right) \\ -g_{dt} K_{\text{box}} \\ -2g_{dt} K_{\text{tri}}^{(\text{in})} \end{pmatrix} \\
&+ \begin{pmatrix} -g_{dd} D_d \left(K_s + \frac{2H(\Lambda)}{\Lambda^2} \right) & g_{dt} D_t \left(3K_s + \frac{2H(\Lambda)}{\Lambda^2} \right) & 0 \\ g_{dt} D_d \left(K_s + \frac{2H(\Lambda)}{3\Lambda^2} \right) & g_{tt} D_t \left(K_s - \frac{2H(\Lambda)}{3\Lambda^2} \right) & 0 \\ g_{dt} D_d \left(2K_s + \frac{4H(\Lambda)}{3\Lambda^2} \right) & -g_{tt} D_t \left(2K_s + \frac{4H(\Lambda)}{3\Lambda^2} \right) & 0 \end{pmatrix} \otimes \begin{pmatrix} \mathcal{T}_{\text{full}'}^{\text{d,a}} \\ \mathcal{T}_{\text{full}'}^{\text{d,b1}} \\ \mathcal{T}_{\text{full}'}^{\text{d,b2}} \end{pmatrix} \\
&+ \begin{pmatrix} -g_{dd} D_d \left(K_c^{(d)} + K_{\text{box}} \right) & 3g_{dt} D_t K_{\text{box}} & g_{dt} D_t^{pp} \left(3K_s + 3K_{\text{tri}}^{(\text{out})} + \frac{2H(\Lambda)}{\Lambda^2} \right) \\ g_{dt} D_d K_{\text{box}} & -g_{tt} D_t \left(K_c^{(t)} - K_{\text{box}} \right) & -g_{tt} D_t^{pp} \left(K_s + K_{\text{tri}}^{(\text{out})} + \frac{2H(\Lambda)}{3\Lambda^2} \right) \\ 2g_{dt} D_d K_{\text{tri}}^{(\text{in})} & -2g_{dt} D_t K_{\text{tri}}^{(\text{in})} & -g_{tt} D_t^{pp} \times \frac{4H(\Lambda)}{3\Lambda^2} \end{pmatrix} \\
&\otimes \begin{pmatrix} \mathcal{T}_{\text{full}'}^{\text{d,a}} \\ \mathcal{T}_{\text{full}'}^{\text{d,b1}} \\ \mathcal{T}_{\text{full}'}^{\text{d,b2}} \end{pmatrix}, \quad (6.61)
\end{aligned}$$

which, albeit quite complex, is a direct extension of Eq. (6.38). We use a prime in the subscript to indicate the inclusion of the additional Coulomb contributions. The first of these, K_{box} , is initially given by a rather complicated expression but can be simplified to [195]

$$\begin{aligned}
K_{\text{box}}(E; k, p) &= -\alpha M_N \\
&\times \frac{1}{2} \int_{-1}^1 d\cos\theta \left\{ \frac{\arctan \left(\frac{2\mathbf{p}^2 - \mathbf{k}^2 - \mathbf{k} \cdot \mathbf{p}}{\sqrt{3\mathbf{k}^2 - 4M_N E - i\epsilon} \sqrt{(\mathbf{k} - \mathbf{p})^2}} \right) + \arctan \left(\frac{2\mathbf{k}^2 - \mathbf{p}^2 - \mathbf{k} \cdot \mathbf{p}}{\sqrt{3\mathbf{p}^2 - 4M_N E - i\epsilon} \sqrt{(\mathbf{k} - \mathbf{p})^2}} \right)}{(\mathbf{k}^2 + \mathbf{p}^2 + \mathbf{k} \cdot \mathbf{p} - M_N E - i\epsilon) \sqrt{(\mathbf{k} - \mathbf{p})^2}} \right. \\
&\quad \left. - \frac{\lambda}{(\mathbf{k}^2 + \mathbf{p}^2 + \mathbf{k} \cdot \mathbf{p} - M_N E - i\epsilon)^2} \right\}, \quad (6.62)
\end{aligned}$$

which is valid up to (negligible) corrections of order λ^2 . For the triangle-diagram contributions one furthermore finds

$$K_{\text{tri}}^{(\text{out})}(E; k, p) = -\alpha M_N \times \frac{1}{2} \int_{-1}^1 d\cos\theta \frac{\mathcal{I}_{\text{tri}}(E; \mathbf{k}, \mathbf{p})}{\mathbf{k}^2 + \mathbf{p}^2 + \mathbf{k} \cdot \mathbf{p} - M_N E - i\epsilon}, \quad (6.63a)$$

$$K_{\text{tri}}^{(\text{in})}(E; k, p) = K_{\text{tri}}^{(\text{out})}(E; k, p), \quad (6.63b)$$

where the superscripts indicate whether the Coulomb-photon exchange is on the incoming (left) or outgoing (right) side of the diagram. The loop function appearing in Eq. (6.63a) is given by

$$\begin{aligned} \mathcal{I}_{\text{tri}}(E; \mathbf{k}, \mathbf{p}) &= \frac{i}{2\sqrt{\mathbf{k}^2/4 + \mathbf{k} \cdot \mathbf{p} + \mathbf{p}^2}} \\ &\times \left\{ \log \left(\frac{i(\mathbf{k}^2/2 - \mathbf{k} \cdot \mathbf{p} - \mathbf{p}^2 - \lambda^2 - M_N E - i\varepsilon)}{\sqrt{\mathbf{k}^2/4 + \mathbf{k} \cdot \mathbf{p} + \mathbf{p}^2}} + 2\sqrt{\lambda^2 + 3\mathbf{k}^2/4 - M_N E - i\varepsilon} \right) \right. \\ &\quad \left. - \log \left(\frac{i(\mathbf{k}^2 + \mathbf{p}^2 + \mathbf{k} \cdot \mathbf{p} - \lambda^2 - M_N E - i\varepsilon)}{\sqrt{\mathbf{k}^2/4 + \mathbf{k} \cdot \mathbf{p} + \mathbf{p}^2}} + 2\lambda \right) \right\}. \quad (6.64) \end{aligned}$$

The spin and isospin projections for both diagrams are completely analogous to those for the simple one-nucleon exchange diagram, with additional projection operators from the photon vertices ensuring that contributions forbidden by charge conservation vanish as they should.

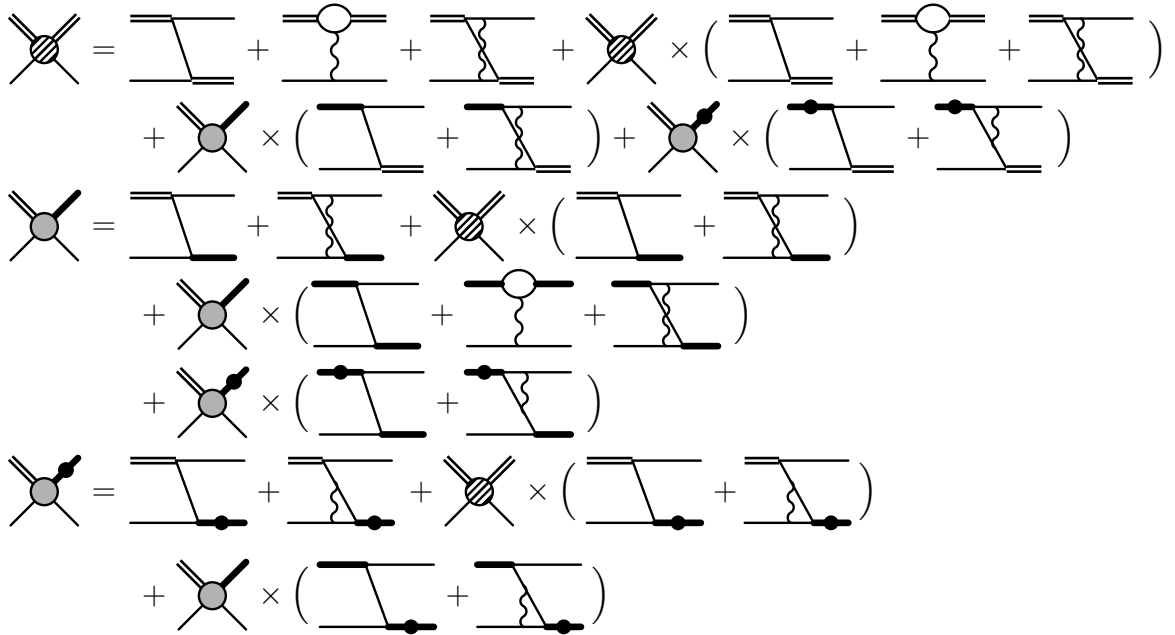


Figure 6.14: Coupled-channel integral equation for the full scattering amplitude $\mathcal{T}_{\text{full}}$ used for the nonperturbative ${}^3\text{He}$ calculation. The diagrams representing the three-nucleon force have been omitted.

6.5.3 Leading-order results

The leading-order results for the ${}^3\text{He}$ binding energy are summarized in Fig. 6.15. The lower dashed curve shows the result of the naïve calculation reported in Ref. [1]. The upper dashed curve is the corrected result according to Eq. (6.59), where only the bubble diagram

is taken into account at leading order. The effect of including all $\mathcal{O}(\alpha)$ Coulomb diagrams (that are leading order in the EFT counting) is shown by the lower solid curve, whereas the upper solid curve shows the result obtained from the nonperturbative calculation described in Section 6.5.2. For comparison, the experimental ${}^3\text{He}$ and ${}^3\text{H}$ binding energies are indicated as dotted lines and the cutoff dependence of the three-nucleon force $H(\Lambda)$ is shown as a thin dashed curve.

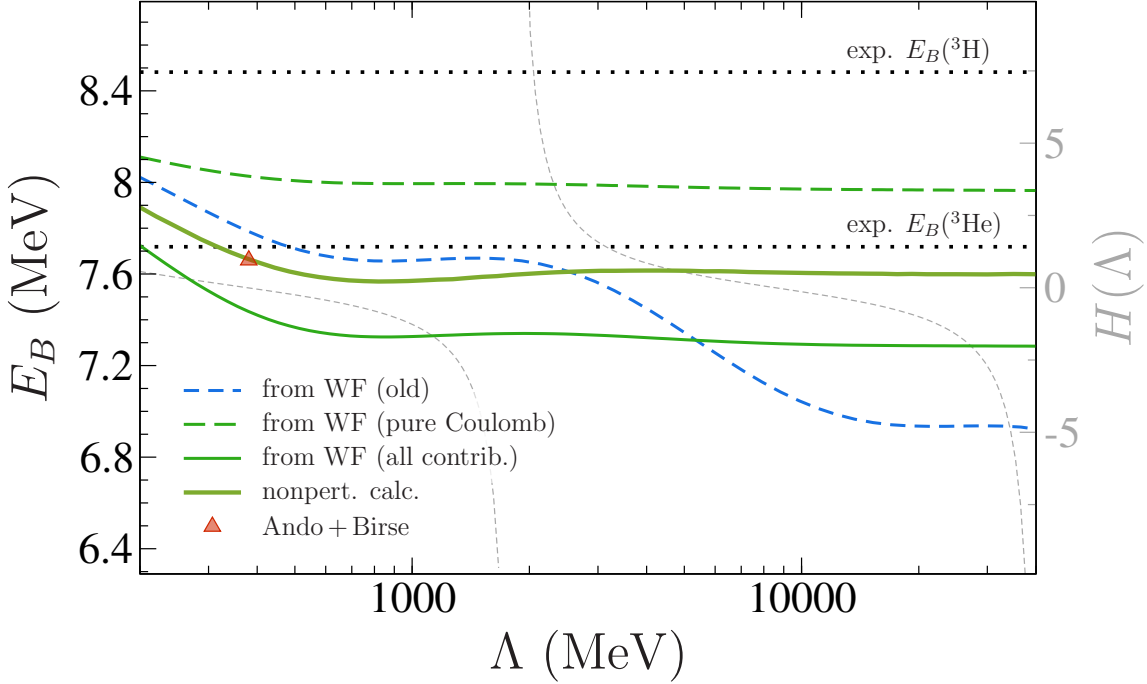


Figure 6.15: Leading-order predictions for the ${}^3\text{He}$ binding energy as a function of the cutoff. Lower dashed curve: result from the naïve calculation reported in Ref. [1]. Upper dashed curve: corrected result according to Eq. (6.59). Lower solid curve: corrected result including all $\mathcal{O}(\alpha)$ Coulomb diagrams. Upper solid curve: nonperturbative result according to Section 6.5.2. Red triangle: result from Ref. [179]. Dotted lines: experimental values for the ${}^3\text{H}$ and ${}^3\text{He}$ binding energies. Thin dashed curve: cutoff-dependence of three-nucleon force.

The most striking feature is that the new results, both from the perturbative and the nonperturbative calculation, do not show the fall-off at large cutoffs that was reported in Ref. [1] and is shown here by the lower dashed curve. An explanation for why this effect occurs in the naïve calculation will be given below in Section 6.6.

In fact, the new results are both essentially stable beyond cutoffs of about 500 MeV. From Fig. 6.15 we furthermore see clearly that it is important to take into account all $\mathcal{O}(\alpha)$ Coulomb diagrams in the perturbative calculation. Comparing it with the result from the bubble diagram alone shows that the box and triangle diagrams together give more than half of the total energy shift (with the larger part coming from the triangle contributions). The nonperturbative result comes out closer to the experimental value than the perturbative one, as should be expected from that more complete calculation. Within the typical 30% uncertainty of a leading-order calculation in pionless EFT, however, they agree both with one another and with the experimental Helium-3 binding energy of about

7.72 MeV.¹⁰

Finally, the result obtained by Ando and Birse in Ref. [179] by using the full off-shell Coulomb T-matrix lies almost directly on our curve. The small energy difference of about 0.004 MeV that we obtain at their cutoff $\Lambda = 380.689$ MeV is well below the accuracy of the calculation and cannot be resolved in the plot.¹¹ This is in perfect agreement with the conclusion of Kok *et al.* [193, 194] that a Coulomb-photon approximation should be well justified in the bound-state regime.

Wave functions

From the new equation structure (6.61) we can also obtain Helium-3 wave functions. In Fig. 6.16 we show a representative plot, calculated at a cutoff $\Lambda = 400$ MeV. The solid curves indicate the result obtained from the full equation including all leading Coulomb diagrams, whereas the dashed curves are obtained by calculating simple trinucleon wave functions (without Coulomb effects) for a system with the three-nucleon force was fixed to reproduce the experimental ${}^3\text{He}$ binding energy. Both are normalized according to the condition (6.47) with the interaction \hat{K} set to the appropriate form.

Comparing the two results one finds that low-momentum modes are suppressed in the wave functions from the full calculation compared to the simple trinucleon result. This is in good agreement with what one naïvely expects from the repulsive Coulomb force: it is particularly strong for small relative momenta of the charged subsystems, thus lowering the probability of the system to be in such a state. For the wave function component where the dibaryon is in a pure p - p state, this does not apply because in that case there is no Coulomb repulsion between the dibaryon and the third nucleon. Indeed, exactly this can also be seen in Fig. 6.16.

The wave functions obtained in this manner can be used as nonperturbative input quantities for other calculations, *e.g.*, a consistent determination of the Helium-3 photodisintegration in pionless EFT, which is currently work in progress.

6.6 The Coulomb problem at next-to-leading order

From the promising results at leading order one might to expect that going to next-to-leading order gives both more precision and better agreement with the experimental Helium-3 energy. However, as shown in Fig. 6.17, exactly the opposite is the case. The results from both the perturbative and the nonperturbative calculation are now closer to—or even above—the triton binding energy, which certainly does not make sense physically. Moreover, the results are strongly cutoff-dependent again and rise to even larger

¹⁰For the perturbative calculation this statement of course refers to the result where all $\mathcal{O}(\alpha)$ diagrams are included. The error estimate should in this case be taken as 30% of the *energy shift* (since that is what is calculated), which then gives a marginal agreement with the experimental value.

¹¹Ando and Birse use the single cutoff $\Lambda = 380.689$ MeV for their calculation because they find that the three-nucleon vanishes there. We find this zero of $H(\Lambda)$ at $\Lambda \approx 377.69$ MeV instead. This small discrepancy is most likely due to differences in the numerical implementation and negligible here.

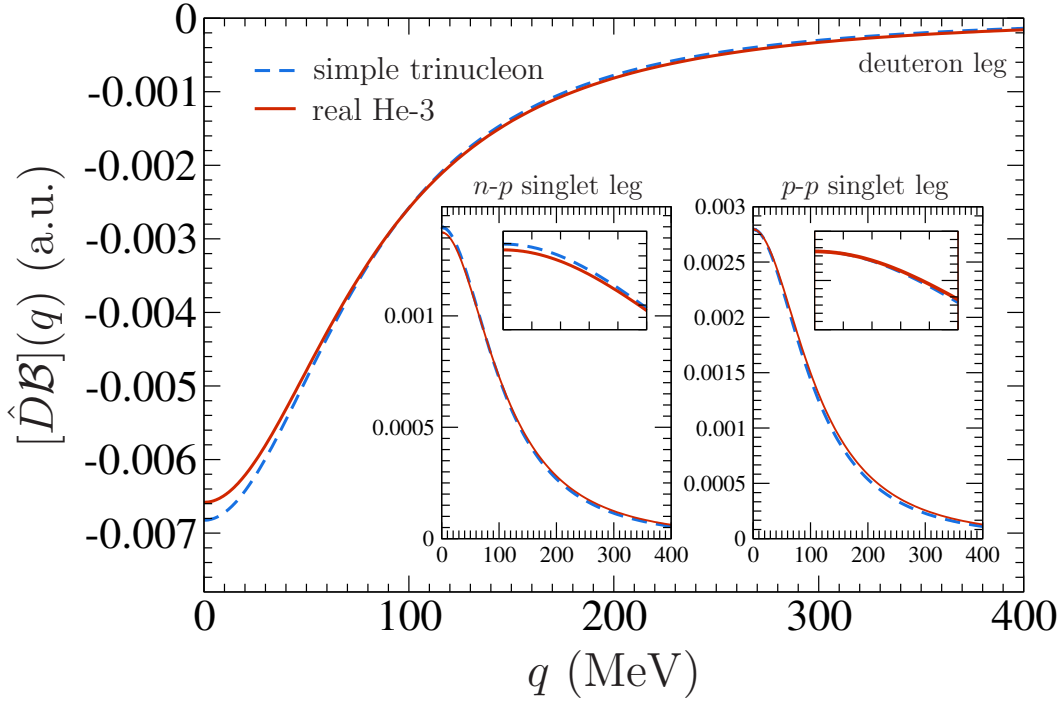


Figure 6.16: Three-component Helium-3 wave functions calculated for a cutoff $\Lambda = 400$ MeV. Solid curves: result from full calculation involving all leading Coulomb diagrams. Dashed curves: result from simple trinucleon calculation with the three-nucleon force fixed to give the experimental Helium-3 binding energy.

binding energies as the cutoff is increased. From these findings we suspect that our next-to-leading order calculation is not renormalized properly and that a new counterterm might be needed to renormalize the system at this order when Coulomb effects are included. In the following we investigate the situation in more detail by analyzing the large-momentum (ultraviolet) behavior of the components that enter in the expression (6.59) for the perturbative energy shift.

6.6.1 Scaling of the dibaryon propagators

The ultraviolet scaling of the dibaryon propagators can be directly inferred from looking at their expressions. We consider here the deuteron propagator D_d as a representative example. At leading order, its scaling is

$$D_d^{\text{LO}}(E; q) \propto \frac{1}{-\kappa_d + \sqrt{\frac{3}{4}q^2 - M_N E - i\varepsilon}} \sim \frac{1}{q} \text{ as } q \rightarrow \infty. \quad (6.65)$$

Upon going to next-to-leading order, this is multiplied by a factor proportional to the effective range,

$$D_d^{\text{NLO}}(E; q) = D_d^{\text{LO}}(E; q) \left[1 + \frac{\rho_d}{2} \cdot \frac{3q^2/4 - M_N E - \kappa_d^2}{-\kappa_d + \sqrt{\frac{3}{4}q^2 - M_N E - i\varepsilon}} \right], \quad (6.66)$$

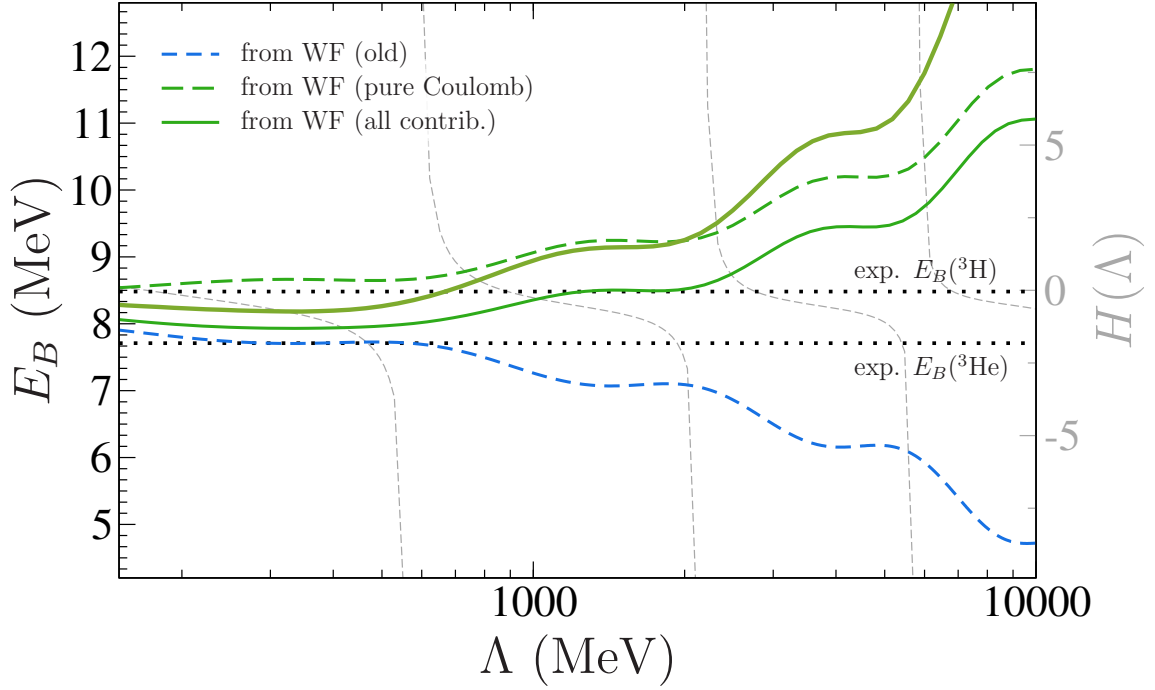


Figure 6.17: NLO results for the ${}^3\text{He}$ binding energy as a function of the cutoff. The curves are as in Fig. 6.15

such that the asymptotic behavior is changed to

$$D_d^{\text{NLO}}(E; q) \sim \text{const. as } q \rightarrow \infty. \quad (6.67)$$

Repeating this procedure in order to get the N²LO and higher-order propagators one even gets functions that are divergent ($\sim q$, $\sim q^2$, etc.) in the ultraviolet.

6.6.2 Ultraviolet behavior of the amplitude

In order to find the behavior of the wave functions $\mathcal{B}(p)$ introduced in Section 6.4, we first go back to the corresponding \mathcal{T} -matrix. As discussed, for example, in Ref. [187], for fixed E and k the n - d doublet channel amplitude $\mathcal{T}_s^d(E; k, p)$ has an asymptotic behavior determined by linear combinations of $p^{\pm i s_0 - 1}$ in the limit $p \rightarrow \infty$. It is the imaginary parts with $s_0 \approx 1.0064$ that give rise to the log-periodic behavior of the three-nucleon force $H(\Lambda)$ necessary to renormalize the system. What is important for the discussion here is the modulus of the scaling:

$$|\mathcal{T}_s^d(E; k, p)| \sim \frac{1}{p} \text{ as } p \rightarrow \infty. \quad (6.68)$$

Since the derivation of this is independent of the energy E , the same scaling also applies in the bound-state regime. In particular, it is inherited by the wave functions, such that also

$$|\mathcal{B}_s(p)| \sim \frac{1}{p} \text{ as } p \rightarrow \infty. \quad (6.69)$$

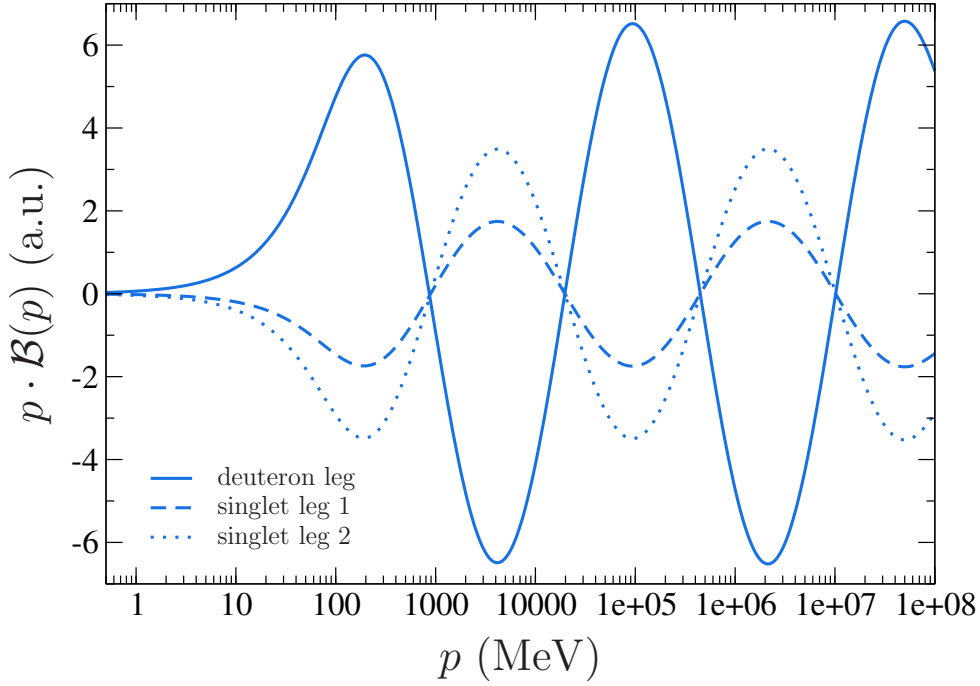


Figure 6.18: Rescaled leading order trinucleon wave function $p \cdot \mathcal{B}_s(p)$ (in arbitrary units) as a function of the momentum p .

Indeed, as shown in Fig. 6.18, one also finds numerically that a plot of $p \cdot \mathcal{B}_s(p)$ against p shows a log-periodic behavior for large p with constant amplitude.

The analysis above is true at leading order. Numerically, we find the approximate scaling

$$|\mathcal{B}_s(p)| \sim |\mathcal{T}_s^d(E; k, p)| \sim \frac{1}{p^{3/2}} \text{ as } p \rightarrow \infty \quad (\text{NLO}) \quad (6.70)$$

for the wave functions (and the corresponding \mathcal{T} -matrix) at next-to-leading order. This behavior is illustrated in Fig. 6.19, where we show the NLO wave functions up to large p , rescaled with a factor $p^{3/2}$. As in the leading-order case, this gives an oscillating function with approximately constant amplitude. Note that the oscillations are more rapid than at leading order and that the exact log-periodicity is broken at NLO. This is consistent with the behavior of the three-nucleon force $H(\Lambda)$ at next-to-leading order (*cf.* Fig. 6.17). The $p^{-3/2}$ fall-off can be seen more clearly in the inlay shown in Fig. 6.19, where the deuteron-leg component of the wave function (without rescaling) is plotted in a double-logarithmic scale. The same scaling behavior as reported here was found—and explained based on analytical considerations—for the scattering amplitude in Ref. [196].

To some extent this faster fall-off at next-to-leading order compensates the scaling of the dibaryon propagators, but, as we shall discuss below, not by enough to render the result convergent.

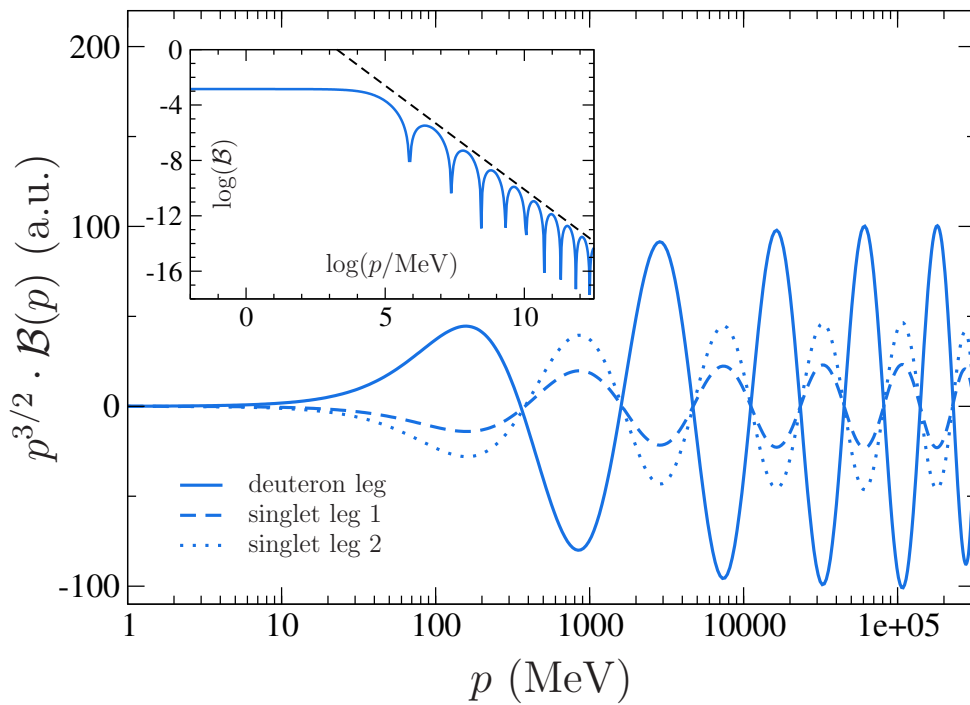


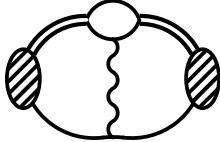
Figure 6.19: Rescaled NLO trinucleon wave function $p^{3/2} \cdot \mathcal{B}_s(p)$ (in arbitrary units) as a function of the momentum p . The inlay shows the deuteron-leg component (without rescaling) in a double-logarithmic plot; the dashed line included there has a slope of exactly $-3/2$. For the other two components not included in the double-logarithmic plot, one finds exactly the same behavior.

6.6.3 Consequences

We first consider the situation in the leading-order case. The scaling of the Coulomb kernel in Eq. (6.59) is determined there by the large-momentum behavior of the bubble diagram without the approximation (6.36). From Eqs. (6.39) and (6.34) we then have

$$K_c^{\text{LO}}(E; k, q) \sim \frac{1}{q^3} \text{ as } q \rightarrow \infty. \quad (6.71)$$

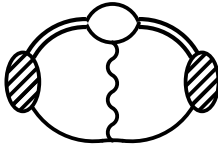
Denoting in the following all loop momenta generically by q , we find



$$\sim \left(\frac{1}{q}\right)_B^2 \times (q^3)_{\text{loops}}^2 \times \left(\frac{1}{q}\right)_D^2 \times \left(\frac{1}{q^3}\right)_{\text{kernel}} \sim \frac{1}{q} \quad (\text{LO}) \quad (6.72)$$

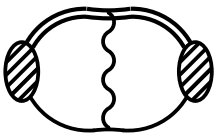
for the total scaling of the matrix element. Since this is the only contribution at leading order, the result for the energy shift converges as the cutoff is increased. From the same kind of analysis we can understand what led to the cutoff dependence in the result of Ref. [1]: the kernel V_C as defined in Eq. (6.57) only falls off like $1/q^2$ asymptotically such that the corresponding matrix element is logarithmically divergent.¹²

Considering finally the situation at next-to-leading order, we find that we can no longer avoid a divergent result. For the contribution of the bubble diagram we now obtain



$$\sim \left(\frac{1}{q^{3/2}}\right)_B^2 \times (q^3)_{\text{loops}}^2 \times (q^0)_D^2 \times \left(\frac{1}{q^3}\right)_{\text{kernel}} \sim q^0 \quad (\text{NLO}), \quad (6.73)$$

which gives a logarithmic divergence. Even more problematic is the additional contribution entering at this order. For the kernel with the photon coupled directly to the dibaryon we have the scaling



$$\sim \left(\frac{1}{q^{3/2}}\right)_B^2 \times (q^3)_{\text{loops}}^2 \times (q^0)_D^2 \times \left(\frac{1}{q^2}\right)_{\text{kernel}} \sim q, \quad (6.74)$$

and thus a linear divergence. This again also applies to the old calculation involving V_C , which has the same scaling and thus diverges linearly as well. Indeed, by comparing the dashed curves in Figs. 6.15 and 6.17 we see that the NLO result has a much stronger cutoff dependence than at leading order, and can understand this now from the analysis carried out above.

Furthermore, we can explain as well why the new perturbative result at NLO looks almost like a mirror image of the old one. If we rewrite V_C in Eq. (6.57) by factoring out a $y_{d,t}^2$, the result is just the next-to-leading order contribution to $K_c^{(d,t)}$, but with the sign reversed. Due to the faster divergence of this term we barely see the effect of the “leading” bubble diagram at all.

¹²The same kind of divergence occurs if the bubble diagram is approximated as in Eq. (6.36). However, as already mentioned repeatedly, the approximation is not valid in the bound-state regime, and the divergence that would appear if we were to use it there is just another manifestation of this fact.

6.6.4 Nonperturbative calculation

Also the result found from the nonperturbative calculation exhibits a strong cutoff dependence at next-to-leading order, with the corresponding curve in Fig. 6.17 even rising somewhat faster than the perturbative result. From the analysis above one is led to suspect that again the scaling of the involved diagrams is the origin of this effect. In order to show this, we look at what kind of diagrams are generated when the bound-state integral equation is iterated.



Figure 6.20: Two diagrams generated by iterating the bound-state integral equation.

Figure 6.20a shows a two-loop diagram with a Coulomb-photon exchange that is generated by iterating the equation once. Since the one-nucleon exchange also scales like $1/q^2$, we find a total scaling $\sim q^{1/2}$ for the diagram by applying the same kind of analysis as in the sections above. This indeed indicates a divergence.

However, the answer cannot be quite so simple in this case because one directly sees that the diagram with two subsequent nucleon exchanges actually has the same kind of behavior. The important point here is that exactly the same situation also occurs in the system without Coulomb effects, but that every nucleon-exchange is always accompanied by a vertex from the three-nucleon force. Since according to the renormalization prescription this three-nucleon force is adjusted at each cutoff in order to reproduce a three-body experimental input (the triton binding energy, in our case) one effectively also absorbs the divergence into $H(\Lambda)$. By adding then afterwards the Coulomb contributions into the equation, the problem is reintroduced.

At leading order, the situation is different because there the $1/q$ -scaling of the dibaryon propagators ensures that additional loops generated by iterating the integral equation do not create divergences, neither due to Coulomb photons nor due to the nucleon-exchange interaction. The three-nucleon force is needed in this case only to fix the oscillating behavior of the scattering amplitude [54].

6.6.5 Back to the scattering regime

The above findings also raise some questions concerning the NLO scattering calculation in the doublet channel. If the assertion that the system is not renormalized correctly is true, the effect should also show up in the cutoff-variation of the scattering phase shifts. Indeed, this is what we find. If we perform the phase-shift calculation with cutoffs of the same size as in Fig. 6.17 (up to $\Lambda \approx 10000$ MeV), the result does not seem to converge. Instead, the curves shown for four different cutoffs in the upper panel of Fig. 6.21 move upwards with increasing Λ .

One can of course take the stance, as we have done in Section 6.3 by varying the cutoff only between 200 and 600 MeV, that the cutoff in an EFT calculation should be taken of a natural order of magnitude (defined by the scale of physics left out from the theory). According to Fig. 6.15, the leading-order Helium-3 results are indeed converged at these cutoffs. At next-to-leading order, however, the results are problematic already in that regime. With this in mind, considering cutoffs far beyond the natural size here and in the preceding sections is primarily a tool to expose and analyze this behavior more clearly.

Using the full equation structure (6.61) to fit the three-nucleon force such that it reproduces the experimental ${}^3\text{He}$ energy turns out to remove the strong cutoff dependence of the p - d results (without affecting the results for lower cutoffs very much), just as it does in the n - d system when $H(\Lambda)$ is fixed to reproduce the triton binding energy. This is shown in the lower panel of Fig. 6.21, where we plot the curves analogous to those in the upper panel obtained by re-fitting the three-nucleon force. For consistency we have used the same equation structure as in the bound-state regime—including the box and triangle diagrams and without the approximation of the bubble diagram—in the calculations of all phase-shift results shown in Fig. 6.21.

We interpret these findings as a further indication that in the p - d system there is a new three-body counterterm, which at least numerically can be absorbed by refitting $H(\Lambda)$. Such a situation could be accounted for by adding to the three-body Lagrangian (6.6) a piece proportional to the charge operator (making it vanish in the triton system). Since it is not forbidden by symmetry, such a term should be there, and the only question is at which order in the EFT counting it enters. Our results strongly suggest that it is necessary for correct renormalization at NLO.

This conclusion, however, comes with a caveat. We cannot rule out here that the whole problem might be due to using the partially resummed propagators in the integral equations. If there truly is a new counterterm at NLO in the system with Coulomb effects, it should also show up in a fully perturbative calculation that only includes range corrections up to a fixed order instead of resumming a subset of higher-order contributions. For the related system of three uncharged bosons this procedure has been implemented in Ref. [188]. In the charged system, the situation becomes more involved because the photon coupling directly to the dibaryon introduces a new type of range correction that has to be treated on an equal footing with kinetic-energy insertions in the propagators. The new efficient implementation of perturbative range corrections recently presented in Ref. [197] might be a useful tool to do this.

One contribution entering in such a calculation at next-to-leading order would be the diagram shown on the left-hand side of Eq. (6.74), but with all propagators and amplitudes given by their leading-order versions. Counting powers of loop momenta indicates a logarithmic divergence for this. However, since in principle there could be cancellations of divergences between different contributions, one cannot draw definite conclusions here without carrying out the calculation. It will certainly be interesting to investigate this issue further.

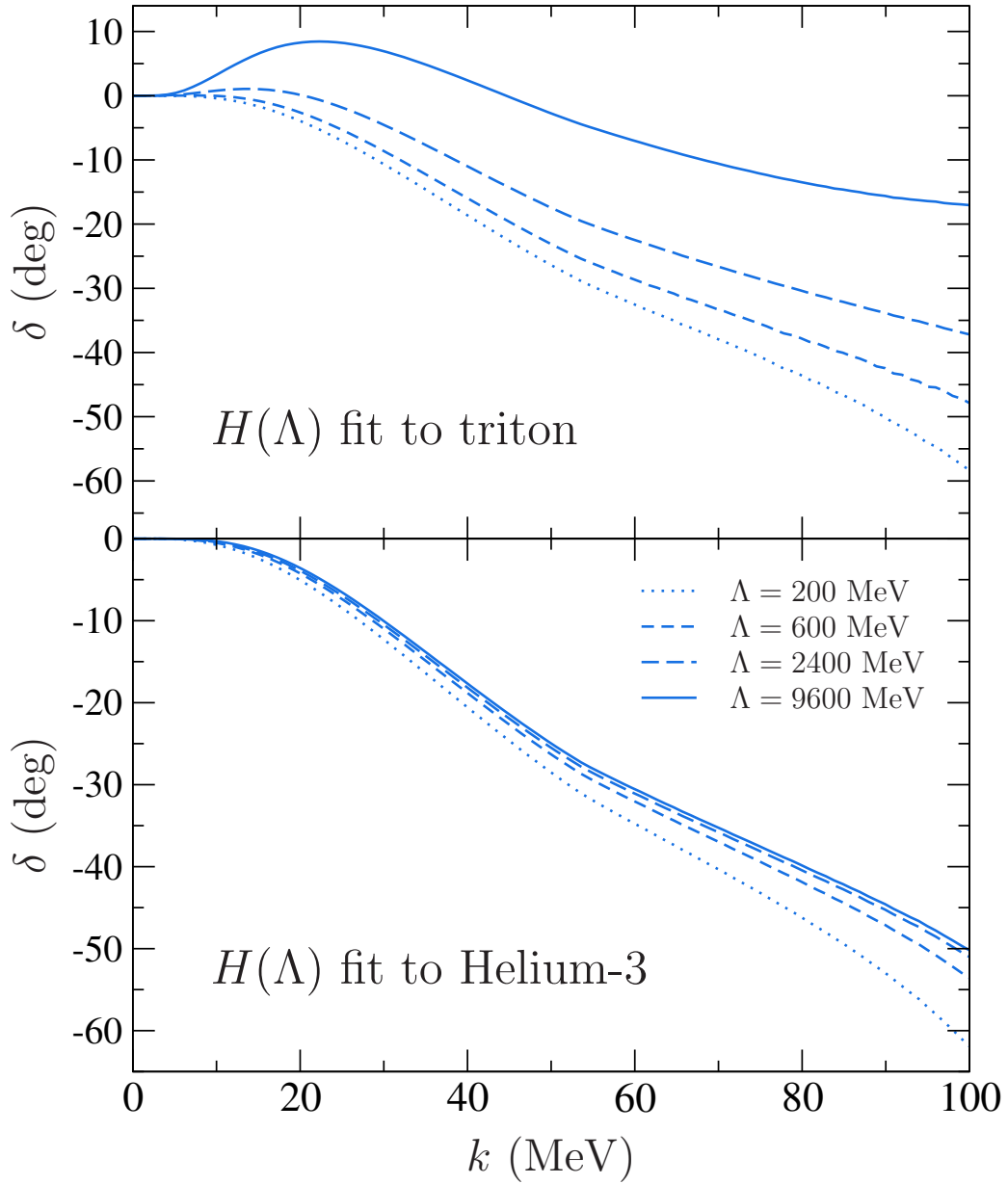


Figure 6.21: NLO p - d scattering phase shifts for large cutoffs obtained using Eq. (6.61). Upper panel: $H(\Lambda)$ fit to reproduce triton binding energy in the n - d system. Lower panel: $H(\Lambda)$ fit to reproduce ${}^3\text{He}$ binding energy in the p - d system.

Neglected diagrams and the bubble approximation

Although the main motivation for deriving the full equation structure (6.61) with the box and triangle diagrams included was the nonperturbative Helium-3 calculation, with the complete expression at hand we are now also in a position to directly check the approximations made in the scattering regime. Based on the power counting described in Section 6.2.3, we neglected there the contributions from the box and triangle diagrams, and furthermore used the approximation given in Eq. (6.36) for the bubble diagram.

To avoid interference with the problematic situation at NLO discussed in the previous section, we go back to the leading-order calculation and show in Fig. 6.22 the old band (as given in Fig. 6.8) together with the result obtained without approximating the bubble diagram (dashed curve) and furthermore what we get from the full equation with also the box and triangle contributions included (solid curve). As before, all error bands were generated by varying the cutoff between 200 and 600 MeV, which is certainly sufficient at leading order.

The band from the full calculation overlaps well with the old result. In fact, if one takes the real uncertainty to be the typical 30% of a leading-order pionless EFT calculation, the two bands are almost indistinguishable. It would be tempting to interpret this as an *a posteriori* confirmation of both the Coulomb power counting for the scattering regime and the approximation used for the bubble diagram, for if it were not for the result with only the bubble approximation turned off. Since the corresponding band in Fig. 6.22 is broader and consistently shifted upwards (for momenta k below about 70 MeV), it turns out that really the combination of both things—approximating the bubble diagram and neglecting the additional contributions—is important to get the same result as from the full calculation. This indicates that in the latter case there are some substantial cancellations between the effects of the individual Coulomb diagrams.

A similar effect occurs in the quartet channel. In this case we have additionally calculated the result with the bubble diagram still approximated, but the box diagram¹³ already included. Overall, the results from the individual calculations shown in Fig. 6.7 differ now not so much at low center-of-mass momenta, but quite substantially above the deuteron break-up threshold ($k \gtrsim 52$ MeV). Since the error bands would be as narrow as in Fig. 6.7 and are not essential for what we want to show here, we have used a single cutoff $\Lambda = 140$ MeV to generate the curves.

The cancellation between the two effects is particularly striking here: the result obtained with both the bubble-diagram approximation turned off and the box diagram included at the same time (solid curve) is almost identical to the old result (dotted curve). The same pattern is found also in the higher-order calculations.

Altogether, these findings cast some doubt on the Coulomb power counting as discussed in Section 6.2.3. In particular, the good agreement of the N²LO quartet-channel phase shifts with experimental data that was found based on this counting scheme already in Ref. [178] appears now to be somewhat accidental, at least at higher energies. Based on the findings obtained here we propose that instead of using the old counting one should—

¹³Note that the triangle diagram does not appear in the quartet channel since there are never two protons in the intermediate dibaryon.

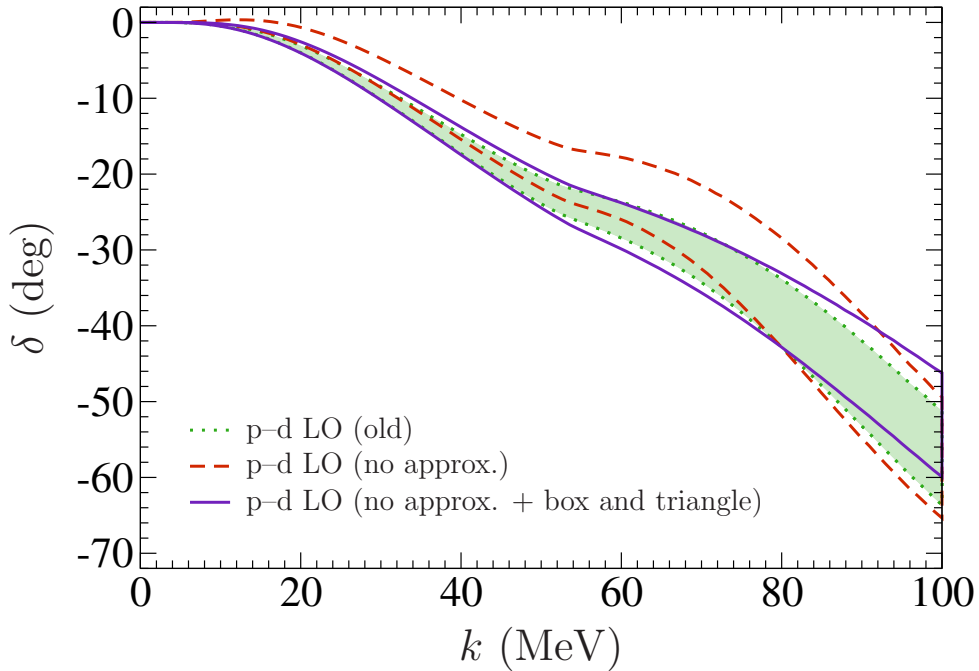


Figure 6.22: Leading order p - d doublet channel S-wave scattering phase shifts as functions of the center-of-mass momentum k . Dotted curve: old result as shown in Fig. 6.8. Dashed curve: result without approximating the bubble diagram. Solid curve: same as dashed curve with additional Coulomb diagrams (box and triangle) included. Error bands generated by cutoff variation within 200–600 MeV.

also in the scattering regime—simply include all $\mathcal{O}(\alpha)$ Coulomb diagrams. At the same time, as already alluded to below Eq. (6.36), one should not use the approximation for the bubble diagram because it has no physical justification and turns out to have a more significant impact on the result than naïvely expected.

This new scheme¹⁴ has the advantage of being much more straightforward and at the same time completely consistent throughout both the scattering and the bound-state regime. The price to be paid for this is that the calculations to be carried out are quite a bit more involved. With suitable adaptive integration routines to carry out the S-wave projections of the Coulomb diagrams numerically, however, the integral equations can still be solved on ordinary desktop computers.

Having concluded that the original Coulomb counting scheme should be modified raises the question how important higher-order contributions (in α) really are. Very close to the zero-momentum threshold they could in principle be quite important. As a first step to tackle this problem, we will in the next section discuss the calculation of (Coulomb-modified) proton–deuteron scattering lengths within the current framework.

¹⁴We would like to emphasize here that the new scheme does not imply to do strict perturbation theory in α . The included Coulomb diagrams are still iterated nonperturbatively to all orders, which means that the perturbation expansion up to $\mathcal{O}(\alpha)$ is applied to the *kernels* used in the Lippmann–Schwinger equations.

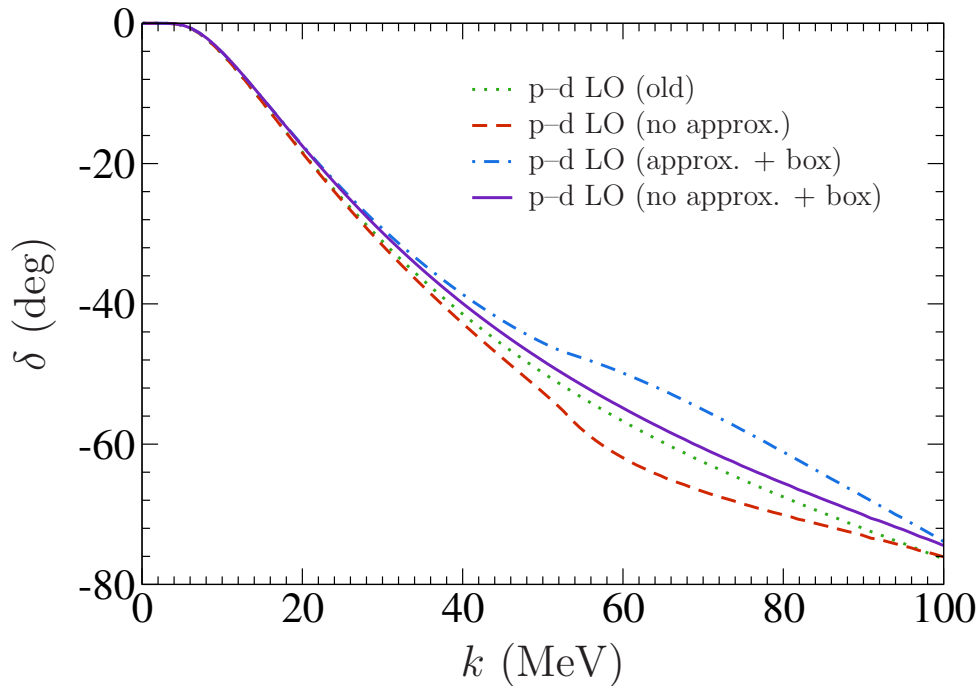


Figure 6.23: Leading order p - d quartet channel S-wave scattering phase shifts as functions of the center-of-mass momentum k . Dotted curve: old result as shown in Fig. 6.7. Dashed curve: result without approximating the bubble diagram. Dash-dotted curve: result with the additional Coulomb box diagram box included (but the bubble diagram still approximated). Solid curve: same as dash-dotted curve, but without approximating the bubble diagram. All curves were calculated at a cutoff $\Lambda = 140$ MeV.

6.7 Proton–deuteron scattering lengths

The optimized numerical procedure outlined in Section 6.2.5 allows us to calculate the p – d scattering phase shifts down to very low center-of-mass momenta k and at the same time effectively remove the regulating photon mass λ from the calculation. Yet, due to the absence of experimental phase shift data below $k \lesssim 20$ MeV there is no real test for the phase-shift calculation in that regime.

It is thus interesting to extend the calculation to the direct extraction of threshold parameters, *i.e.*, proton–deuteron scattering (S-wave) scattering lengths. They are defined by the Coulomb-modified effective range expansion (4.24), which we write here in the form

$$C_{\eta,0}^2 k \cdot \cot \delta_{\text{diff}}(k) + \gamma h(\eta) = -\frac{1}{a_0^C} + \mathcal{O}(k^2) \quad (6.75)$$

with

$$\gamma = \gamma_{p-d} = 4\alpha M_N/3 \quad \text{and} \quad \eta = \frac{\gamma_{p-d}}{2k}. \quad (6.76)$$

In the following, since we are only considering S-waves, we will omit all $\ell = 0$ indices. For clarity, we furthermore denote the scattering length as a_{p-d} and use superscripts “4” and “2” to indicate the quartet- and doublet channel results, respectively.

The first approach that comes to mind for applying Eq. (6.75) is to simply insert Coulomb-subtracted phase shifts $\delta_{\text{diff}}(k)$ in with the photon mass already extrapolated to zero. However, this is not a very good idea. To see this note that the use of the regulating photon mass is not the only approximation in the calculation. There is also the finite cutoff and, more importantly, the fact that following the EFT power counting we only include a certain set of Coulomb contributions in the calculation. Effectively this means that our calculation does not directly correspond to using the Coulomb potential α/r in configuration space. To solve this problem we propose that it is better to first calculate scattering lengths from Eq. (6.75) for several finite photon masses and then use those results to extrapolate a_{p-d} to $\lambda \rightarrow 0$.

6.7.1 Numerical calculation of the Gamow factor

The Gamow factor $C_{\eta,0}$ entering in Eq. (6.75) is quite strongly affected by the photon-mass screening. Using the analytic formula for the unscreened Coulomb potential given in Eq. (4.12) would result in a values that are far too small. Therefore, in order to carry out the procedure just described we need to extract the correct approximation for the Gamow factor from the numerical calculation in a consistent way. To this end it is useful to recall from Chapter 4 that, if $\psi_{\mathbf{k}}^{(+)}(\mathbf{r})$ denotes the exact three-dimensional scattering wave function for the pure Coulomb potential, then

$$C_{\eta,0}^2 = C_{\eta,0}^2(k) = |\psi_{\mathbf{k}}^{(+)}(\mathbf{r} = \mathbf{0})|^2. \quad (6.77)$$

This means that it should be possible to calculate the appropriate expression for the Gamow directly from the scattering wave function (for a given center-of-mass momentum k) corresponding to our approximate Coulomb potential.

In fact, this is exactly what one should do. In Ref. [17], van Haeringen and Kok give a general version of the modified effective range expansion for systems where the interaction is given by the sum of a long-range potential V_L and a short-range interaction V_S . It can be written in the form

$$|\mathcal{F}_\ell(k)|^{-2} k^{2\ell+1} (\cot \delta_\ell^M(k) - i) + M_\ell(k), \quad (6.78)$$

where $\delta_\ell^M(k)$ is the subtracted phase shift

$$\delta_\ell^M = \delta_\ell^S - \delta_\ell^L. \quad (6.79)$$

This is just what we obtain from the numerical calculation, where V_L is given by the approximate Coulomb potential and V_S is the short-range EFT interaction.

Furthermore, $\mathcal{F}_\ell(k)$ in Eq. (6.78) is the Jost function associated with V_L , whereas $M_\ell(k)$ is a rather complicated expression that involves derivatives of the corresponding Jost solution.¹⁵ The important point is now that for $\ell = 0$ we simply have [24]

$$|\mathcal{F}_0(k)|^{-2} = \lim_{r \rightarrow 0} |\psi_{\mathbf{k},0}^{(+)}(r)|^2, \quad (6.80)$$

where $\psi_{\mathbf{k},0}^{(+)}(r)$ is the S-wave component of the scattering wave function, *cf.* Eq. (2.37).

From Chapter 2, Eq. (2.49), we recall that the momentum-space scattering wave function can be expressed in terms of the T-matrix. In our present conventions (see the remark at the beginning of Section 6.2.4), we have

$$\psi_{\mathbf{k},0}^{(+)}(p) = \frac{2\pi^2}{k^2} \delta(k-p) - \frac{2\mu Z_0 \mathcal{T}(E; p, k)}{k^2 - p^2 + i\varepsilon}, \quad E = E(k), \quad (6.81)$$

where $\mathcal{T}(E; p, k)$ is the S-wave projected \mathcal{T} -matrix. Fortunately, this is exactly what we already calculated in order to obtain the Coulomb-subtracted phase shifts. From the expansion of the plane wave $e^{i\mathbf{k}\cdot\mathbf{r}}$ in terms of Legendre polynomials,

$$e^{i\mathbf{k}\cdot\mathbf{r}} = e^{ikr \cos \theta} = \sum_{\ell=0}^{\infty} (2\ell+1) i^\ell j_\ell(kr) P_\ell(\cos \theta), \quad (6.82)$$

where $j_\ell(z)$ is the spherical Bessel function of order ℓ , one finds that the partial-wave projected wave function in configuration space can be obtained from the momentum-space version as¹⁶

$$\psi_{\mathbf{k},\ell}^{(+)}(r) = \frac{1}{2\pi^2} \int_0^\infty dp p^2 i^\ell j_\ell(pr) \psi_{\mathbf{k},\ell}^{(+)}(p). \quad (6.83)$$

We only need this here for $\ell = 0$, of course. Using $\lim_{r \rightarrow 0} j_0(pr) = 1$ and cutting off the momentum-space integral at $p = \Lambda$ (since we only know the \mathcal{T} -matrix up to that value), we arrive at

$$\mathcal{F}_0(k)^{-1} = \psi_{\mathbf{k},0}^{(+)}(r=0) \approx 1 + \frac{\mu}{\pi^2} \int_0^\Lambda \frac{dp p^2}{p^2 - k^2 - i\varepsilon} Z_0 \mathcal{T}(E; p, k), \quad (6.84)$$

¹⁵The Jost solution $f(k, r)$ is a solution of the radial Schrödinger equation involving V_L that fulfills the boundary condition $\lim_{r \rightarrow \infty} e^{ikr} f(k, r) = 1$. The Jost function $\mathcal{F}_\ell(k)$ is then defined as the Wronskian $W(f, \varphi)$, where φ is a solution determined by $\varphi(0) = 0$ and $\varphi'(0) = 1$. For details see, for example, Ref. [24].

¹⁶The inverse transformation is $\psi_{\mathbf{k},\ell}^{(+)}(r) = 4\pi \int_0^\infty dr r^2 (-i)^\ell j_\ell(pr) \psi_{\mathbf{k},\ell}^{(+)}(r)$.

which is straightforward to evaluate by numerical principal-value integration. Inserting for \mathcal{T} the result of the calculation involving only the pure Coulomb diagrams and squaring the right-hand side of Eq. (6.84) gives the desired Gamow factor consistently extracted from the numerical EFT calculation. Summarizing the above results, we write it as

$$C_{\eta,\lambda}^2 = \left| 1 + \frac{2M_N}{3\pi^2} \int_0^\Lambda \frac{dp p^2}{p^2 - k^2 - i\varepsilon} Z_0 \mathcal{T}_c(E; p, k) \right|^2, \quad (6.85)$$

where we have added the additional subscript “ λ ” to distinguish it from the expression for the unscreened Coulomb potential. In writing Eq. (6.85) we have inserted the reduced mass $\mu = 2M_N/3$ for the p - d system and set $\mathcal{T} = \mathcal{T}_c$, where the latter is defined by Eq. (6.40). With this, the final form of the Coulomb-modified effective-range expansion that we use for the numerical calculation reads

$$C_{\eta,\lambda}^2 k \cdot \cot \delta_{\text{diff}}(k) + \gamma h(\eta) = -\frac{1}{a_{p-d}} + \mathcal{O}(k^2). \quad (6.86)$$

Note that in principle also the term involving $h(\eta)$ should be modified due to the screening. Unfortunately, this quantity cannot be extracted from the numerical calculation in the same simple way as the Gamow factor. Lacking a better expression, we will thus use $h(\eta)$ as defined in Eq. (4.26). Since it vanishes at $k = 0$, this is not a problem for the extraction of the scattering length, but it means that we cannot consistently extract effective ranges at the same time.

6.7.2 Bubble diagram with full off-shell Coulomb T-matrix

Since the Coulomb interaction is strongest directly at threshold, the scattering-length calculation should be a good testing ground for checking the influence of higher-order Coulomb diagrams that we have not taken into account so far. Rather than simply including $\mathcal{O}(\alpha^2)$ diagrams (with two Coulomb-photon exchanges) to estimate the effect of higher-order terms, we adopt the approach of Ando and Birse [179] and directly include the full off-shell Coulomb T-matrix in the diagrams. Effectively, this resums all subsequent Coulomb-photon exchanges for a given topology. The resulting diagrams are shown in Fig. 6.24.

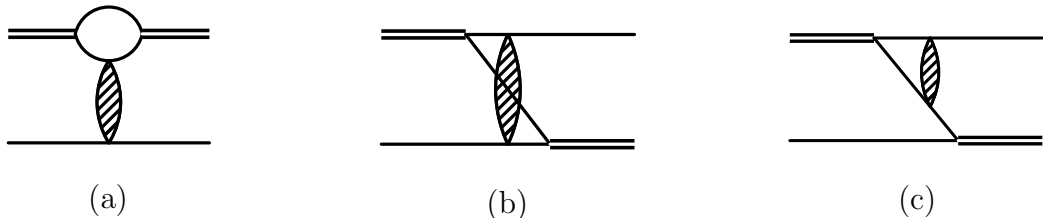


Figure 6.24: Diagrams involving the full off-shell Coulomb T-matrix (indicated by the blob).

In Ref. [179], Ando and Birse only consider the bound-state regime. Without going into further details, they argue that the finite extent of the wave functions helps to regularize

the Coulomb singularity and thus use an unscreened interaction. Since we cannot apply this approach in the scattering regime, we use here the partially screened Coulomb T-matrix $T_{C,\lambda}$ introduced in Section 4.4.1. We assume that this gives an appropriate description for small photon masses λ because in the limit $\lambda \rightarrow 0$, $T_{C,\lambda}$ converges to the exact (unscreened) Coulomb T-matrix T_C .

The most important contribution is again given by the “full bubble diagram” shown in Fig. 6.24a. Its spin- and isospin structure is exactly the same as for the leading expression with just a single Coulomb-photon exchange. Only the loop integral, which before could be evaluated analytically, now has the more complicated form

$$\mathcal{I}_{\text{bubble}}^{\text{full}}(E; \mathbf{k}, \mathbf{p}) = \int_0^\infty dq q^2 T_{C,\lambda}(i\sqrt{3q^2/4 - M_N E}; \mathbf{k}, \mathbf{p}) \times \int_{-1}^1 d\cos\theta' \int_0^{2\pi} \frac{d\phi'}{a(b + c \cdot \cos\phi')} \quad (6.87)$$

with

$$a = k^2 + kq \cos\theta' + q^2 - M_N E, \quad (6.88a)$$

$$b = p^2 + pq \cos\theta \cos\theta' + q^2 - M_N E, \quad (6.88b)$$

$$c = pq \sin\theta \sin\theta'. \quad (6.88c)$$

Here, as in Eqs. (6.62) and (6.63a), θ is the angle between the vectors \mathbf{k} and \mathbf{p} , whereas θ' denotes the angle between \mathbf{k} and the loop momentum \mathbf{q} , and the azimuthal angle ϕ' enters through rewriting the angle between \mathbf{p} and \mathbf{q} . It can be integrated over analytically with the result

$$\int_0^{2\pi} \frac{d\phi'}{b + c \cdot \cos\phi'} = \frac{2\pi}{\sqrt{b^2 - c^2}} \quad (6.89)$$

for $b > c$, which, according to Eqs. (6.88) is certainly fulfilled for the scattering-length calculation we are interested in. Only for calculations above the deuteron breakup threshold, where the energy E is positive, one would have to be more careful here.

Setting

$$\cos\theta' \equiv x \Rightarrow \sin\theta' = \sqrt{1 - x^2}, \quad (6.90)$$

the remaining angular integral has the form

$$\int_{-1}^1 \frac{dx}{(A + B \cdot x)\sqrt{C + D \cdot x + E \cdot x^2}} \quad (6.91)$$

with

$$A = k^2 + q^2 - M_N E, \quad (6.92a)$$

$$B = kq, \quad (6.92b)$$

$$C = (p^2 + q^2 - M_N E)^2 - p^2 q^2 (1 - \cos^2\theta) \quad (6.92c)$$

$$D = (p^2 + q^2 - M_N E) \times 2pq \cos\theta \quad (6.92d)$$

$$E = p^2 q^2. \quad (6.92e)$$

Using integration by parts, this can be done analytically. The final result for the full-bubble kernel function is then¹⁷

$$K_{\text{bub}}^{(\text{full})}(E; k, p) = -\frac{M_N}{2\pi^2} \times \frac{1}{2} \int_{-1}^1 d\cos\theta \mathcal{I}_{\text{bubble}}^{\text{full}}(E; \mathbf{k}, \mathbf{p}) \quad (6.93)$$

with

$$\begin{aligned} \mathcal{I}_{\text{bubble}}^{\text{full}}(E; \mathbf{k}, \mathbf{p}) &= \int_0^\infty dq q^2 T_{C,\lambda}\left(i\sqrt{3q^2/4 - M_N E}; \mathbf{k}, \mathbf{p}\right) \\ &\times \frac{1}{\sqrt{F}} \left[\log\left(\frac{A+B}{A-B}\right) - \log\left(\frac{B(2C+D) - A(D+2E) + 2\sqrt{F}\sqrt{C+E+D}}{B(2C-D) - A(D-2E) + 2\sqrt{F}\sqrt{C+E-D}}\right) \right], \end{aligned} \quad (6.94)$$

where in addition to Eqs. (6.92) we have defined

$$F = B^2C + A^2E - ABD. \quad (6.95)$$

The remaining momentum integral and the S-wave projection in Eq. (6.93) have to be carried out numerically. To evaluate the Coulomb T-matrix we use the expression in terms of hypergeometric functions derived in Section 4.4.2, which can be implemented efficiently with the fast routines for ${}_2F_1$ from Ref. [198].

Unfortunately, the above integrals cannot be used to simplify also the expression for the full box and triangle diagrams shown in Figs. 6.24b and c. In those cases, the Coulomb T-matrix also depends on the loop momentum, which means that the angular integrations can no longer be carried out analytically.

Finally, as shown in Fig. 6.25, the full Coulomb T-matrix directly between the dibaryons and the proton corresponds to an infinite series of subsequent Coulomb-photon exchanges. By including (at NLO and higher orders) the tree-level diagram in our integration kernel we already generate this term automatically. It is thus important not to include the diagram on the left-hand side in Fig. 6.25 explicitly, as otherwise we would be double-counting some contributions.

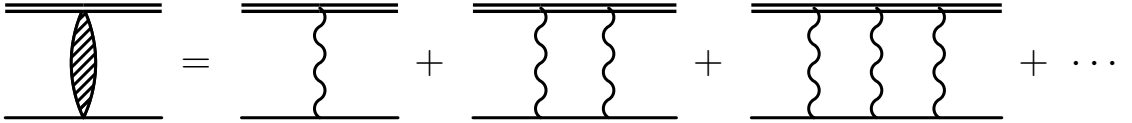


Figure 6.25: Full Coulomb T-matrix between deuteron and proton generated by subsequent Coulomb-photon exchanges.

6.7.3 Results

In the following, we give results for proton–deuteron scattering-lengths and study their dependence on the different variants in which the calculation can be carried out (expression for the bubble diagram and inclusion of other contributions).

¹⁷Note that the expression in Eq. (6.94) does not directly reduce to $\mathcal{I}_{\text{bubble}}$ as defined in Eq. (6.34) when the Coulomb T-matrix is replaced with a single photon exchange. Rather, in that limit, the kernel function $K_{\text{bub}}^{(\text{full})}(E; k, p)$ goes over into the LO-part of Eq. (6.39), including the overall prefactor $-\alpha M_N$.

With the expression for the full bubble diagram discussed in the previous section, the calculation already takes almost a day per data point,¹⁸ which is just about feasible when run in parallel on a couple of machines. If we also wanted to include the diagrams shown in Figs. 6.24b and c, which require at least one more numerical integration, the current approach would very inefficient. We will thus only include their one-photon exchange equivalents as shown Fig. 6.3 along with the full bubble diagram. Albeit somewhat inconsistent, this should still be a good approximation, the impact of which we will discuss further after showing the results. Due to the problematic situation with the doublet-channel calculation beyond leading order (see Section 6.6.5), we focus here on the quartet channel.

Quartet channel

We perform the numerical calculations for three different cutoffs $\Lambda = 120, 140, 160$ MeV and for photon masses λ between 0.2 MeV and 1.2 MeV. For each extraction of the scattering length we calculate the left-hand side of Eq. (6.86) for a center-of-mass momentum range $k \in [2, 4]$ MeV. Fig. 6.26 shows a representative plot. To the data points we fit a polynomial of the form

$$f(k) = x_0 + x_1 k^2 + x_2 k^4 \quad (6.96)$$

in order to extract the scattering length as $a_{p-d} = -1/x_0$. As noted in Section 6.7.1, we cannot also extract the effective range from x_1 because the modification of $h(\eta)$ due to the finite photons mass is not taken into account in our calculation. The k^4 term has been included to allow for some curvature.

In Fig. 6.27, we show the the photon-mass and cutoff dependence of the results at N²LO (using, as in the phase-shift calculation presented in Section 6.3.1, the fully resummed deuteron propagator since we keep the cutoff below its unphysical second pole). Since the λ -dependence is clearly linear, it is no problem to extrapolate the scattering lengths to the zero-screening limit ($\lambda \rightarrow 0$). The results, also for the LO- and NLO-calculations, are shown in Table 6.2.

Calculation	$a_{p-d}^4 / \text{fm (LO)}$	$a_{p-d}^4 / \text{fm (NLO)}$	$a_{p-d}^4 / \text{fm (N}^2\text{LO)}$
bubble approx.	9.31–9.48	10.51–10.67	12.39–12.58
no bubble approx.	8.93–9.01	9.82–9.85	11.52–11.56
bubble + box	8.40–8.48	9.29–9.31	10.89–10.92
full bubble + box	8.32–8.39	9.16–9.17	10.69–10.72

Table 6.2: Quartet-channel results for the p – d scattering length.

One can see that the bubble-diagram approximation has quite an impact on the result. Without the approximation, the scattering length is significantly shifted down towards smaller values and that its cutoff dependence becomes much weaker. Unlike the situation encountered for the scattering phase shifts above the deuteron breakup (see Section 6.6.5),

¹⁸This statement refers to performing the calculation for a given cutoff and photon mass on a reasonably modern (as of the writing of this thesis) desktop computer.

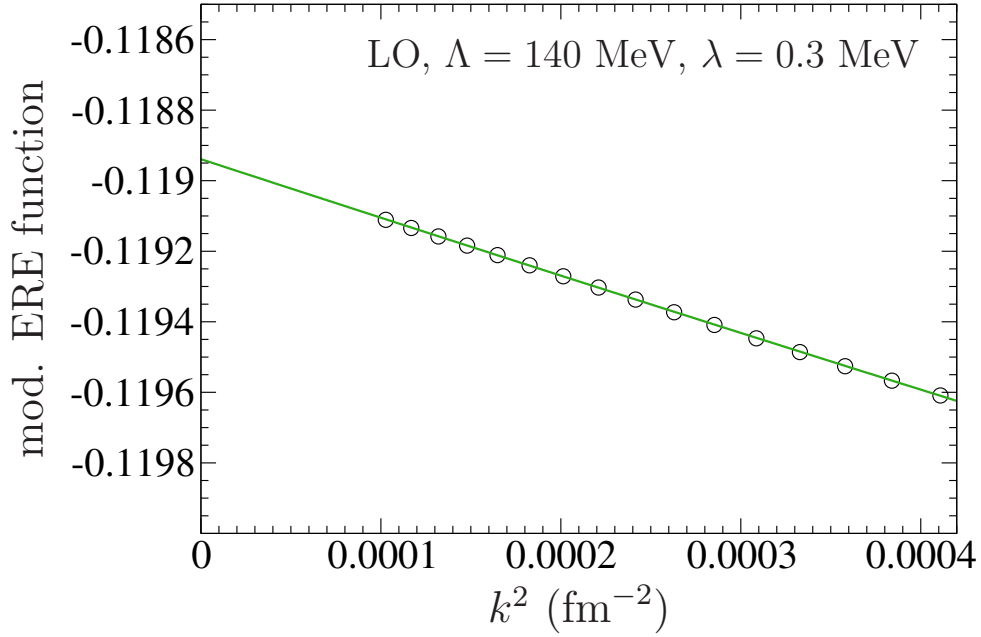


Figure 6.26: Coulomb-modified effective range plot for quartet-channel p - d scattering. The y -axis shows the left-hand side of Eq. (6.86); the line is the result of a fit to the formula given in Eq. (6.96).

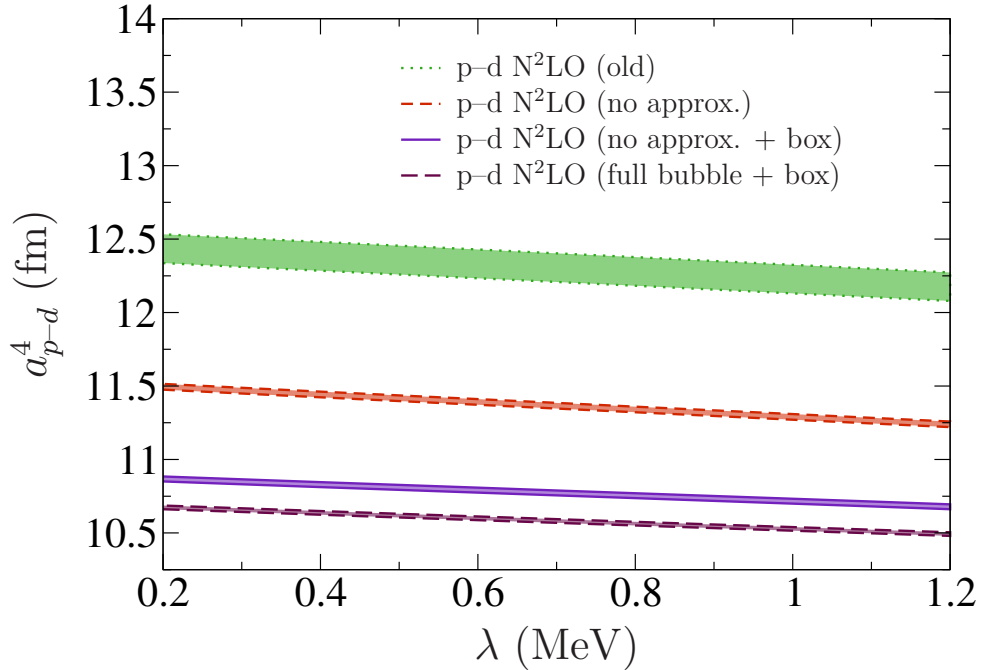


Figure 6.27: Photon-mass dependence of the quartet-channel p - d scattering length at N^2 LO. The bands were generated by varying the cutoff between 120 and 160 MeV. Dotted curve: result with the bubble diagram approximated. Dashed curve: result without approximating the bubble diagram. Solid curve: result with the additional Coulomb box diagram box included (and without approximating the bubble diagram). Long-dashed curve: same as solid curve, but using the full bubble diagram involving the off-shell Coulomb T-matrix.

the additional inclusion of the box diagram here does not compensate the unapproximated bubble diagram to give back the old result. Rather, it moves the scattering length further towards smaller values. Finally, the effect of using the full off-shell Coulomb T-matrix in the bubble diagram is surprisingly small and gives only a 2% change (at N²LO) in the result.

The reason for the latter observation might be that for consistency the full bubble diagram is also included in the pure Coulomb equation used to calculate the Coulomb-subtracted phase shifts and the Gamow factor. Since in principle this might give some cancellations, we cannot unambiguously conclude that using the full off-shell Coulomb T-matrix only has a small effect on the scattering length. To investigate this issue further, it might be interesting to also use the full T-matrix in box diagram. Although from the fact that this diagram is not enhanced by the Coulomb pole one should expect it to be only a small correction, it might still be interesting to include it because it only enters in the full (strong + Coulomb) calculation and not in the pure Coulomb equation. To proceed in this direction however, requires more sophisticated numerical methods to deal with the multi-dimensional integrals. Monte Carlo methods might be a useful tool to deal with the problem.

Another issue that has to be pointed out is that the changes from NLO to N²LO in Table 6.2 are somewhat larger than those from LO to NLO. This is not what one would expect from the EFT expansion parameter ~ 0.3 and certainly has to be investigated further. With that and the above discussion in mind, the results for the scattering lengths here should clearly be regarded as preliminary. For this reason, we have given the uncertainties only as far as they are created by the cutoff variation and not attempted to also propagate the errors from the fits used in the extraction. At least for a precision calculation at N²LO, where from the EFT expansion we would expect an accuracy of about 3%, a more sophisticated procedure might be advisable. Until the role of the full Coulomb T-matrix in the box diagram is settled, however, we make a conservative error estimate here and use the combination of the two dashed bands in Fig. 6.27 (extrapolated to $\lambda = 0$) to summarize our quartet-channel result as

$$a_{p-d}^4 = 11.1 \pm 0.4 \text{ fm}. \quad (6.97)$$

Incidentally, this is nicely compatible with the experimental determinations quoted in Table 5.2 in Chapter 5 that give a_{p-d}^4 between 11 and 12 fm. A more recent analysis and other theoretical calculations based on realistic nuclear potential models, however, have found somewhat larger values around 14 fm [199]. Furthermore, Fig. 6.27 suggests that with the inclusion of the box diagram, our results come out on the smaller side of the range given in Eq. (6.97). It will certainly be interesting to study this issue further.

Doublet channel

With the currently unclear situation in the doublet channel according to Sections 6.6 and 6.6.5, we only briefly discuss the extraction of scattering lengths for that case here. Since based on the phase-shift calculations we expect a rather strong cutoff dependence in this channel, and because to be consistent we can at best go up to NLO (due to second

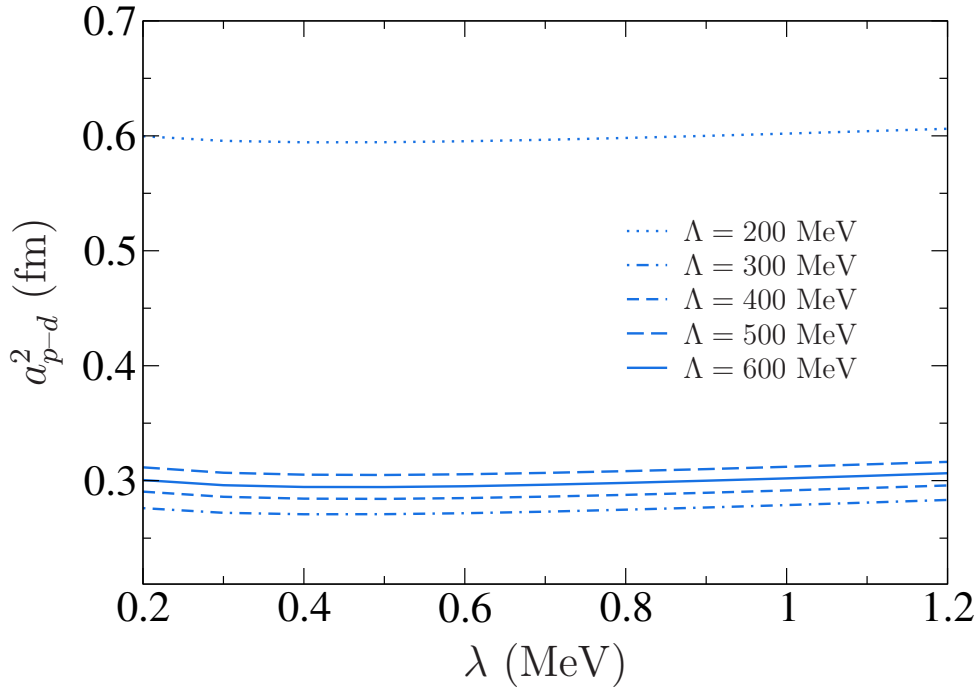


Figure 6.28: Photon-mass dependence of doublet-channel p - d scattering length at NLO.

three-nucleon force at N²LO that is not included in our calculation), it does not make sense at present to investigate here the effect of the full Coulomb T-matrix.

Instead, in order to perform a calculation that is at least internally consistent, we follow the approach that gave the lower panel of Fig. 6.21, *i.e.*, we use the same equation structure as for the bound-state calculation and fit the three-nucleon force to reproduce the experimental He-3 binding energy (instead of fitting the equation without Coulomb contributions to the triton system).

The NLO-result is shown in Fig. 6.28 for cutoffs between 200 and 600 MeV. Compared to the quartet-channel case, there is now some non-linearity in the photon-mass dependence, but still the curves are essentially flat. At the same time, the cutoff dependence is much stronger, but beyond 300 MeV the result is quite stable around $a^2_{p-d} \approx 0.3$ fm. At leading order, the situation is almost the same, but the cutoff dependence is somewhat larger (as expected from the EFT expansion). In that case, for larger cutoffs we find a scattering length that is approximately zero or slightly negative, but since the fit formula as in Eq. (6.96) becomes unstable in that regime, it is difficult to make a more quantitative statement here.

What we report here, of course, reflects the difficulty in determining the p - d doublet channel scattering lengths that we already mentioned in Section 5.5.2. Our results are at least qualitatively compatible with other determinations in finding mostly very small values for a^2_{p-d} . Improving upon this would first require solving the question of range corrections and correct renormalization beyond leading order in pionless EFT calculations with Coulomb effects included.

6.8 Summary and outlook

In this chapter, we have studied several aspects of the proton–deuteron system in pionless effective field theory. Using an optimized integration mesh we are able to calculate Coulomb-subtracted scattering phase shifts even at very low center-of-mass momenta, where the Coulomb interaction becomes highly non-perturbative.

In the bound-state regime, we have corrected our perturbative calculation of the ${}^3\text{He}$ – ${}^3\text{H}$ binding energy difference from Ref. [1] and additionally performed a nonperturbative calculation of the ${}^3\text{He}$ binding energy that agrees very well with the result with the result obtained by Ando and Birse [179] although we have only used Coulomb photons to include electromagnetic effects. Furthermore, at leading order both the perturbative and the nonperturbative calculation give results that are, within their respective uncertainties, in good agreement with the experimental value for the ${}^3\text{He}$ binding energy.

At next-to-leading order, the results of both calculations exhibit a strong cutoff dependence, indicating that the calculation is not renormalized properly. We have analyzed this situation by studying the ultraviolet behavior of the diagrams entering in the calculation and argued that a new three-body counterterm might be necessary to renormalize the charged doublet-channel system at NLO. To come to a more definite conclusion about this, one should carry out a fully perturbative calculation that does not resum any range corrections.

Our findings are supported by a closer examination of the doublet-channel scattering phase shifts, which also turn out not to converge when the cutoff in the calculation is chosen very large. This cutoff dependence however goes away when the three-nucleon force is fitted to reproduce the experimental ${}^3\text{He}$ binding energy, which we interpret as further evidence for a new charge-dependent counterterm. Since the modified fitting of the three-nucleon force requires using the same equation structure in the bound-state and scattering regime, we have critically reviewed the Coulomb power counting of Rupak and Kong [178] and come to the conclusion that it might be better to simply include all Coulomb diagrams of a given order in α . This approach is simpler and more consistent because it treats the scattering and the bound-state regime on an equal footing.

First results for proton–deuteron scattering lengths—obtained using a procedure that applies the new counting scheme and consistently extracts the Gamow factor for the Yukawa-screened Coulomb potential from the same calculation that gives the Coulomb-subtracted scattering phase shifts—look quite promising. It will certainly be interesting to follow this approach further and more closely investigate the role of nonperturbative Coulomb effects. To include the full off-shell Coulomb T-matrix in all relevant diagrams, however, requires more sophisticated numerical methods to deal with multi-dimensional integrals.

Chapter 7

Concluding remarks

In this thesis, we have covered a number of different topics, ranging from the study of finite-volume effects on bound states with angular momentum to formal investigations of causality and unitarity constraints on quantum systems with finite-range interactions and additional long-range tails, and finally to practical calculations of proton–deuteron scattering. All these loosely-connected things are tied together by the concepts of low-energy universality, effective field theory, and/or modifications thereof due to long-range forces.

In many parts of this work, the radial Schrödinger equation plays a prominent and essential role. Since physical processes at low energies do not probe the short-distance physics of the underlying interaction, it is often possible to reduce their theoretical description to an effective picture with finite-range interactions. This makes it possible to draw conclusions based only on the analytically-known tails of the wave functions and to encode the short-range details in a limited set of parameters given, for example, by the effective range expansion.

In Chapter 3 we have shown how this approach directly leads to a universal relation for the volume dependence of two-body binding energies. In this case, the details of the underlying short-range interaction only enter via the physical bound-state properties (the binding energy and the asymptotic normalization constant), allowing their extraction from numerical calculations in periodic boxes of different sizes. We have generalized this result to states with arbitrary orbital angular momentum, to two-dimensional systems, and also to the case of twisted boundary conditions that appear when one considers the scattering of composite particles in finite periodic boxes and then lead to correction factors that have to be taken into account in such calculations.

For the remaining part of this thesis the focus has been on systems of charged particles, where the Coulomb force plays a very important role at low energies. A vast number of analytic results have been obtained over the last century, a selection of which we have reviewed in Chapter 4. Despite this broad understanding, the Coulomb potential is notoriously difficult to handle due to its long-range nature.

It would certainly be interesting—in particular for applications in nuclear physics—to extend the finite-volume study of Chapter 3 to bound states of charged particles. Having

read Chapter 4 of this thesis one might think that this is just a matter of expressing the asymptotic wave functions in terms of appropriate Whittaker functions. Unfortunately, one runs into problems at a much earlier point of derivation because the very slow large-distance fall-off of the Coulomb potential forbids a straightforward implementation of periodic boundary conditions. To deal with this problem it might be interesting in the future to either adopt techniques from solid-state physics (*e.g.*, Ewald summation or a similar approach) or alternatively try to study screened Coulomb interactions in periodic boxes.

The derivation of causality bounds for charged particles given in Chapter 5 is conceptually straightforward and not fundamentally different from the pure finite-range case, but turns out to be quite involved when going into detail due to the complex analytic structure of the Coulomb wave functions with their “entanglement” of radial position and momentum variables. The final result for the case with Coulomb tails is ultimately very similar to what one finds for pure finite-range interactions. Interestingly, the situation is different for systems with van der Waals tails. Although these are still long-ranged, they fall off very fast and should thus be expected to give a result even closer to that for the system without long-range interactions. Yet, the result in this case is fundamentally different, an effect that can be traced back to the highly singular behavior of the van der Waals potential at *short* distances. It will certainly be interesting to study this behavior further also for other singular power-law potentials or perhaps directly from a more general point of view.

While causality bounds—with or without long-range forces—are primarily interesting from a formal point of view, they may also serve as a guide to improve the convergence of calculations in halo effective field theory or similar approaches. It has to be stressed here again, however, that the derivation of the causality bound is based on the assumption of an effective two-body system with energy-independent potentials. As such, its direct applicability is somewhat limited.

In Chapter 6 we have critically revised and extended earlier calculations of proton–deuteron and ^3He observables in pionless effective field theory and found that the question of how to include the effects of the Coulomb interaction does not seem to be as settled as previously believed. With our numerical methods we are able to study both p – d scattering at very low energies as well as the bound-state regime. In the latter case we find good agreement of our leading-order result for the ^3He binding energy from both perturbative and nonperturbative calculations, but encounter problems in calculations at next-to-leading order in the EFT power counting. Upon closer inspection the problem also shows up in the scattering regime and can be avoided by fitting the existing three-nucleon force to the ^3He system. We interpret these findings as evidence for a missing charge-dependent counterterm that is needed to correctly renormalize the p – d doublet-channel system at NLO. To come to a definite conclusion about this, however, it will be necessary to carry out a calculation that incorporates range corrections in a strictly perturbative manner.

Independent of that question we propose based on the new results that previously applied Coulomb power counting in pionless EFT should be given up in favor of a simpler scheme that includes all Coulomb contributions up to a given order at the same time and thus

treats the scattering and bound-state regimes on an equal footing.

Finally, we present a calculation of proton–deuteron scattering lengths in pionless EFT. These observables are interesting because the Coulomb interaction is particularly strong directly at the zero-momentum threshold. As a first step to study this, we have performed a calculation that involves—at least in the supposedly most important Coulomb diagram—a “partially screened” expression for the full off-shell T-matrix that we discussed previously in Chapter 4. While the results obtained so far look quite promising when compared with older experimental determinations of the scattering lengths, a more recent analysis and other theoretical calculations have found somewhat larger values. It will certainly be interesting to pursue this issue further.

Appendix A

The Coulomb wave functions of Bollé and Gesztesy

Generalizing results first obtained by Lambert [121], Bollé and Gesztesy [122] define the Coulomb wave functions

$$F_n^{(0)}(p, r) = r^{\frac{1}{2}+m} e^{-ipr} {}_1F_1\left(\frac{1}{2} + m - k, 1 + 2m; z\right) \quad (\text{A.1a})$$

and

$$G_n^{(0)}(p, r) = \frac{\Gamma\left(\frac{1}{2} + m - k\right)}{\Gamma(2m + 1)} (2ip)^{2m} r^{\frac{1}{2}+m} e^{-ipr} U\left(\frac{1}{2} + m - k, 1 + 2m; z\right), \quad (\text{A.1b})$$

where, in our case, $n = 2\ell + 3$ and m, k, z are as defined in Eqs. (4.5) and (4.6). Using Eq. (4.14) in the form¹

$$C_{\eta, \ell} = \frac{2^\ell e^{-\pi\eta/2} |\Gamma(\ell + 1 + i\eta)|}{(2\ell + 1)!}, \quad (\text{A.2})$$

one finds that

$$F_n^{(0)}(p, r) = \frac{1}{p^{\ell+1} C_{\eta, \ell}} F_\ell^{(p)}(r) \quad (\text{A.3a})$$

and

$$G_n^{(0)}(p, r) = p^\ell C_{\eta, \ell} \left[G_\ell^{(p)}(r) - i F_\ell^{(p)}(r) \right]. \quad (\text{A.3b})$$

It is shown in Ref. [122] that $F_n^{(0)}(p, r)$ is analytic in p^2 . Furthermore, from Eqs. (3.16), (3.17) and (4.1) in that paper it follows that

$$G_n^{(0)}(p, r) = \tilde{G}_n^{(0)}(p, r) + \left(\gamma \tilde{h}_\ell(p) - 2ip^{2\ell+1} C_{\eta, \ell}^2 \right) \cdot F_n^{(0)}(p, r), \quad (\text{A.4})$$

where $\tilde{h}_\ell(p)$ is the function defined in Eq. (4.29), and where $\tilde{G}_n^{(0)}(p, r)$ is analytic in p^2 .

¹This is Eq. (5.1) in Ref. [115]. From Eq. (3.1) in the same reference one directly sees that this is consistent with Eq. (4.30) in Section 4.2.

In Eq. (4.3) of Ref. [122], Bollé and Gesztesy give an explicit expression for $\tilde{G}_n^{(0)}(p, r)$. Since there are two typos in their original equation,² we quote the whole expression for completeness. Slightly altering the notation to match our conventions, we have

$$\begin{aligned}
\tilde{G}_n^{(0)}(p, r) &= [\Gamma(n-1)^{-2}] (2p)^{n-3} \left| \Gamma\left(\frac{n-1}{2} + \frac{i\gamma}{2p}\right) \right|^2 \left| \Gamma\left(1 + \frac{i\gamma}{2p}\right) \right|^{-2} \gamma \log(|\gamma|r) \cdot F_n^{(0)}(p, r) \\
&\quad - \gamma \operatorname{Re} \left\{ [\Gamma(n-1)^{-2}] (2p)^{n-3} \left| \Gamma\left(\frac{n-1}{2} + \frac{i\gamma}{2p}\right) \right|^2 \left| \Gamma\left(1 + \frac{i\gamma}{2p}\right) \right|^{-2} r^{(n-1)/2} e^{-ipr} \right. \\
&\quad \times \sum_{k=0}^{\infty} \frac{\Gamma\left(\frac{n-1}{2} + k - \frac{i\gamma}{2p}\right) \Gamma(n-1)(2ipr)^k}{\Gamma\left(\frac{n-1}{2} - \frac{i\gamma}{2p}\right) \Gamma(n-1+k)\Gamma(k+1)} [\psi(k+1) + \psi(k+n+1)] \left. \right\} \\
&\quad + \gamma \operatorname{Re} \left\{ [\Gamma(n-1)^{-2}] (2p)^{n-3} \left| \Gamma\left(\frac{n-1}{2} + \frac{i\gamma}{2p}\right) \right|^2 \left| \Gamma\left(1 + \frac{i\gamma}{2p}\right) \right|^{-2} r^{(n-1)/2} e^{-ipr} \right. \\
&\quad \times \sum_{k=0}^{\infty} \frac{\Gamma\left(\frac{n-1}{2} + k - \frac{i\gamma}{2p}\right) \Gamma(n-1)(2ipr)^k}{\Gamma\left(\frac{n-1}{2} - \frac{i\gamma}{2p}\right) \Gamma(n-1+k)\Gamma(k+1)} \sum_{s=1}^{\frac{n-1}{2}+k-1} \left(s - \frac{i\gamma}{2p}\right)^{-1} \left. \right\} \\
&\quad + \operatorname{Re} \left\{ (n-2)^{-1} (2ip)^{n-2} r^{(n-1)/2} e^{-ipr} \sum_{q=0}^{n-3} \frac{\Gamma\left(\frac{3-n}{2} + q - \frac{i\gamma}{2p}\right) \Gamma(3-n)(2ipr)^{q+2-n}}{\Gamma\left(\frac{3-n}{2} - \frac{i\gamma}{2p}\right) \Gamma(q+3-n)\Gamma(q+1)} \right\},
\end{aligned} \tag{A.5}$$

valid for any odd $n \geq 3$ and where the sum over s in the fourth line is defined to give zero for $n = 3$ and $k = 0$.

²The $i\gamma/k$ in the first line should be $i\gamma/(2k)$ and the $(q+1)$ in the last line should be $\Gamma(q+1)$.

Appendix B

Explicit expressions for the causality bound function

In this appendix, we give explicit expressions for the Coulomb causality bound functions $b_1^C(r)$ and $b_2^C(r)$. They were derived with the procedure outlined in Sections 5.3.4 and 5.3.5.

B.1 Repulsive case, $\gamma > 0$

The $\ell = 0$ result for a repulsive Coulomb potential is given by Eq. (5.45). For $\ell = 1$, we get

$$\begin{aligned}
 b_1^C(r) = \frac{6r^2}{5\gamma^3} (a_1^C)^{-2} & \left[3\gamma^2 r^2 {}_1F_2 \left(\frac{5}{2}; 3, 6; 4\gamma r \right) - 20\gamma r {}_1F_2 \left(\frac{3}{2}; 2, 5; 4\gamma r \right) \right. \\
 & \left. + 120 {}_1F_2 \left(\frac{1}{2}; 1, 4; 4\gamma r \right) - 120 {}_2F_3 \left(\frac{1}{2}, 2; 1, 3, 4; 4\gamma r \right) \right] \\
 & - \frac{4r^2}{\sqrt{\pi}} (a_1^C)^{-1} G_{2,4}^{2,2} \left(4\gamma r \left| \begin{array}{c} -1, \frac{1}{2} \\ 0, 3, -3, -2 \end{array} \right. \right) \\
 & - \frac{\sqrt{\pi}\gamma^3 r^2}{9} G_{2,4}^{4,0} \left(4\gamma r \left| \begin{array}{c} -1, \frac{1}{2} \\ -3, -2, 0, 3 \end{array} \right. \right) + \frac{\gamma}{54},
 \end{aligned} \tag{B.1}$$

and for $\ell = 2$ the result is

$$\begin{aligned}
 b_2^C(r) = \frac{50r^2}{63\gamma^5} (a_2^C)^{-2} & \left[7\gamma^4 r^4 {}_1F_2 \left(\frac{9}{2}; 5, 10; 4\gamma r \right) - 108\gamma^3 r^3 {}_1F_2 \left(\frac{7}{2}; 4, 9; 4\gamma r \right) \right. \\
 & \left. + 1296\gamma^2 r^2 {}_1F_2 \left(\frac{5}{2}; 3, 8; 4\gamma r \right) - 12096\gamma r {}_1F_2 \left(\frac{3}{2}; 2, 7; 4\gamma r \right) \right. \\
 & \left. + 108864 {}_1F_2 \left(\frac{1}{2}; 1, 6; 4\gamma r \right) - 108864 {}_2F_3 \left(\frac{1}{2}, 2; 1, 3, 6; 4\gamma r \right) \right] \\
 & - \frac{4r^2}{\sqrt{\pi}} (a_2^C)^{-1} G_{2,4}^{2,2} \left(4\gamma r \left| \begin{array}{c} -1, \frac{1}{2} \\ 0, 5, -5, -2 \end{array} \right. \right) \\
 & - \frac{\sqrt{\pi}\gamma^5 r^2}{3600} G_{2,4}^{4,0} \left(4\gamma r \left| \begin{array}{c} -1, \frac{1}{2} \\ -5, -2, 0, 5 \end{array} \right. \right) + \frac{\gamma^3}{21600}.
 \end{aligned} \tag{B.2}$$

B.2 Attractive case, $\gamma < 0$

For an attractive Coulomb potential, the $\ell = 0$ result is given by Eq. (5.46). The $\ell = 1$ result reads

$$\begin{aligned}
b_1^C(r) = & \frac{6r^2}{5\gamma^3} (a_1^C)^{-2} \left[3\gamma^2 r^2 {}_1F_2 \left(\frac{5}{2}; 3, 6; 4\gamma r \right) - 20\gamma r {}_1F_2 \left(\frac{3}{2}; 2, 5; 4\gamma r \right) \right. \\
& \left. + 120 {}_1F_2 \left(\frac{1}{2}; 1, 4; 4\gamma r \right) - 120 {}_2F_3 \left(\frac{1}{2}, 2; 1, 3, 4; 4\gamma r \right) \right] \\
& + 4\sqrt{\pi} r^2 (a_1^C)^{-1} G_{3,5}^{2,2} \left(-4\gamma r \left| \begin{array}{c} -1, \frac{1}{2}, -\frac{1}{2} \\ 0, 3, -3, -2, -\frac{1}{2} \end{array} \right. \right) \\
& + \frac{\pi^{3/2} \gamma^3 r^2}{18} \left[2 G_{3,5}^{4,0} \left(-4\gamma r \left| \begin{array}{c} -\frac{5}{2}, -1, \frac{1}{2} \\ -3, -2, 0, 3, -\frac{5}{2} \end{array} \right. \right) \right. \\
& \left. - G_{2,4}^{1,2} \left(-4\gamma r \left| \begin{array}{c} -1, \frac{1}{2} \\ 3, -3, -2, 0 \end{array} \right. \right) \right] + \frac{\gamma}{54},
\end{aligned} \tag{B.3}$$

and for $\ell = 2$ one finds

$$\begin{aligned}
b_2^C(r) = & \frac{50r^2}{63\gamma^5} (a_2^C)^{-2} \left[7\gamma^4 r^4 {}_1F_2 \left(\frac{9}{2}; 5, 10; 4\gamma r \right) - 108\gamma^3 r^3 {}_1F_2 \left(\frac{7}{2}; 4, 9; 4\gamma r \right) \right. \\
& + 1296\gamma^2 r^2 {}_1F_2 \left(\frac{5}{2}; 3, 8; 4\gamma r \right) - 12096\gamma r {}_1F_2 \left(\frac{3}{2}; 2, 7; 4\gamma r \right) \\
& \left. + 108864 {}_1F_2 \left(\frac{1}{2}; 1, 6; 4\gamma r \right) - 108864 {}_2F_3 \left(\frac{1}{2}, 2; 1, 3, 6; 4\gamma r \right) \right] \\
& + 4\sqrt{\pi} r^2 (a_2^C)^{-1} G_{3,5}^{2,2} \left(-4\gamma r \left| \begin{array}{c} -1, \frac{1}{2}, -\frac{1}{2} \\ 0, 5, -5, -2, -\frac{1}{2} \end{array} \right. \right) \\
& + \frac{\pi^{3/2} \gamma^5 r^2}{7200} \left[2 G_{3,5}^{4,0} \left(-4\gamma r \left| \begin{array}{c} -\frac{9}{2}, -1, \frac{1}{2} \\ -5, -2, 0, 5, -\frac{9}{2} \end{array} \right. \right) \right. \\
& \left. - G_{2,4}^{1,2} \left(-4\gamma r \left| \begin{array}{c} -1, \frac{1}{2} \\ 5, -5, -2, 0 \end{array} \right. \right) \right] + \frac{\gamma^3}{21600}.
\end{aligned} \tag{B.4}$$

Appendix C

Equivalence of ANC relations

In this appendix, we demonstrate the equivalence of our ANC relation derived in Chapter 5 to the one reported by Sparenberg *et al.* in Ref. [143].

Their ANC relation, translated to our notational convention, reads

$$|A| \frac{\ell!}{\Gamma(\ell + 1 + \hat{\eta})} \approx \kappa^{\ell+1} \sqrt{\tilde{a}_\ell^C}. \quad (\text{C.1})$$

The tilde on the \tilde{a}_ℓ^C is there to indicate that Sparenberg *et al.* use the convention for the Coulomb-modified effective range expansion of Refs. [124, 127, 128], which, as noted at the end of Section 4.2, differs from the one used in this work by an overall factor $[2^\ell \ell! / (2\ell + 1)!]^2$. Combining equations in Ref. [143] and again matching to our notation, one finds that

$$\frac{1}{\ell!^2} \prod_{s=1}^{\ell} (s^2 + \eta^2) \left[C_{\eta,0}^2 p^{2\ell+1} \cot \tilde{\delta}_\ell(p) + \gamma p^{2\ell} h(\eta) \right] = -\frac{1}{\tilde{a}_\ell^C} + \frac{1}{2} \tilde{r}_\ell^C p^2 + \dots \quad (\text{C.2})$$

Note that this is just Eq. (4.31) with the prefactors combined and the imaginary parts canceled. More explicitly, we have

$$\tilde{a}_\ell^C = \left(\frac{\ell! 2^\ell}{(2\ell + 1)!} \right)^2 a_\ell^C, \quad \tilde{r}_\ell^C = \left(\frac{(2\ell + 1)!}{\ell! 2^\ell} \right)^2 r_\ell^C, \quad \text{etc.} \quad (\text{C.3})$$

At the end of their derivation, Sparenberg *et al.* eliminate the effective range in favor of the scattering length. Without invoking this final step their relation reads

$$|A| \frac{2^\ell (2\ell + 1)!}{\Gamma(\ell + 1 + \hat{\eta})} \approx \kappa^\ell \left(-\frac{r_\ell^C}{2} + \frac{\gamma^{2\ell-1}}{3(2\ell + 1)!^2} \right)^{-1/2}, \quad (\text{C.4})$$

where we are now using our convention for the effective range expansion. With the definition of $\tilde{C}_{\eta,\ell}$ from Eq. (5.79) and the values for ΔZ_ℓ from Table 5.3 one sees that at least for $\ell = 0, 1, 2$ this is exactly equivalent to our Eq. (5.87) with the $\mathcal{O}(\kappa^2)$ set to zero. In order to prove the equivalence for arbitrary ℓ one would need a general expression for ΔZ_ℓ . This, in turn, requires knowledge of the constant terms in $W[g_2, g_0](r)$ for arbitrary

ℓ . It would thus probably be more interesting to turn the argument around, *i.e.*, take the equivalence of the relations for granted and derive from it a general expression for the constant terms in the Wronskians. The only additional ingredient one would need for this procedure is a general series expansion for the Meijer G -functions that arise from the integral of $g_0(r)^2$.

Appendix D

Bound states in nonrelativistic effective field theory

In this appendix we discuss the trinucleon wave functions used in Chapter 6 from a very general point of view on bound states in nonrelativistic field theory. In particular, we give a detailed derivation of the correct normalization condition for the effectively energy-dependent one-nucleon-exchange interaction.

The material presented here extends and—in some places—corrects that given in an analogous appendix in the author’s diploma thesis [169]. A considerable overlap with the previous work is accepted in order to make the discussion here self-contained.

D.1 Simplified nucleon–deuteron system

Although the results presented in the following are of a general nature and can easily also be applied to other nonrelativistic field theories (*e.g.*, the EFT for cold atomic systems with large scattering length [28]), we work here, for the sake of an explicit illustration, with a model set up to resemble the doublet-channel nucleon–deuteron system in pionless EFT.

Neglecting the isospin degree of freedom and thus also the virtual spin-singlet state, we write down a model Lagrangian of the form

$$\mathcal{L} = N^\dagger \left(i\partial_0 + \frac{\nabla^2}{2M_N} \right) N - \sigma_d d^{i\dagger} d^i + y_d \left[d^{i\dagger} (N^T P_d^i N) + \text{h.c.} \right] \quad (\text{D.1})$$

with

$$P_d^i = \frac{1}{\sqrt{8}} \sigma_2 \sigma^i \tau_2. \quad (\text{D.2})$$

The notation here is the same as in Chapter 6. From there we also quote the projection onto the doublet channel. If $(\mathcal{O}^i)_\alpha$ is a generic object with spin-1 index i and spin-1/2 index α , then

$$(\mathcal{O}^d)_\alpha = (\sigma^i)_\alpha^{\alpha'} (\mathcal{O}^i)_{\alpha'} \quad (\text{D.3})$$

gives the projection onto the spin-doublet channel. The (renormalized) nucleon and deuteron propagators are given by

$$\Delta_N^{\alpha\beta}(p) = \alpha \xrightarrow[p]{\hspace{1.5cm}} \beta = \frac{i\delta_{\beta}^{\alpha}}{p_0 - \frac{\mathbf{p}^2}{2M_N} + i\varepsilon} \quad (\text{D.4})$$

and

$$\Delta_d^{ij}(p) = i \xrightarrow[p]{\hspace{1.5cm}} j = -\frac{4\pi i}{M_N y_d^2} \cdot \frac{\delta^{ij}}{-\kappa_d + \sqrt{\frac{\mathbf{p}^2}{4} - M_N p_0} - i\varepsilon}, \quad (\text{D.5})$$

and the only interaction is given by the doublet-projected one-nucleon-exchange diagram

$$K(k_0, \mathbf{k}, p_0, \mathbf{p}; P) = \begin{array}{c} \rightarrow E = E_d + E_N \rightarrow \\ \text{k} \quad \begin{array}{c} \text{---} \\ \diagdown \\ \text{---} \\ \diagup \\ \text{---} \end{array} \quad \mathbf{p} \end{array} = \frac{-iy_d^2/2}{E_d - E_N + k_0 + p_0 - \frac{(\mathbf{k}+\mathbf{p})^2}{2M_N} + i\varepsilon} \quad (\text{D.6})$$

because for simplicity we also neglect the tree-nucleon force. Note that the expression above corresponds to kinematics where the center of mass of the two particles is at rest. In the following discussion we will work in a general frame, where $K = K(k, p; P)$ with $k = (k_0, \mathbf{k})$, $p = (p_0, \mathbf{p})$, and $P = (P_0, \mathbf{P}) = (E, \mathbf{P})$, but whenever we refer to the explicit form of the interaction we only need the kinematics as in Eq. (D.6).

D.2 Bethe–Salpeter equation

To start the discussion, we derive the Bethe–Salpeter equation for our model nucleon–deuteron system, being a little more careful than in [169] and, as already there, closely following the derivation in Lurie’s textbook [200]. The central object of interest is the full two-body nucleon–deuteron propagator (Green’s function)

$$(G^{ij})_{\alpha}^{\beta}(x_1, x_2; x_3, x_4) = \langle \Omega | T (d^j(x_1) N^{\beta}(x_2) d^{\dagger i}(x_3) N_{\alpha}^{\dagger}(x_4)) | \Omega \rangle, \quad (\text{D.7})$$

where $|\Omega\rangle$ and $T(\dots)$ denote the interacting vacuum of our effective field theory and the time-ordering operator, respectively. Diagrammatically, we have

$$(G^{ij})_{\alpha}^{\beta}(x_1, x_2; x_3, x_4) = \begin{array}{c} x_3 \quad x_1 \\ \bullet \quad \bullet \\ \diagdown \quad \diagup \\ \text{---} \\ \diagup \quad \diagdown \\ \bullet \quad \bullet \\ x_4 \quad x_2 \end{array} \cdot \quad (\text{D.8})$$

We furthermore define the Bethe–Salpeter wave functions

$$(\psi_{\mathbf{E}\mathbf{P}\mathbf{a}}^j)^{\beta}(x_1, x_2) = \langle \Omega | T (d^j(x_1) N^{\beta}(x_2)) | E, \mathbf{P}, \mathbf{a} \rangle, \quad (\text{D.9a})$$

$$(\psi_{\mathbf{E}\mathbf{P}\mathbf{a}}^{\dagger i})_{\alpha}(x_3, x_4) = \langle E, \mathbf{P}, \mathbf{a} | T (d^{\dagger i}(x_3) N_{\alpha}^{\dagger}(x_4)) | \Omega \rangle, \quad (\text{D.9b})$$

where $|E, \mathbf{P}, \mathbf{a}\rangle$ denotes a two-particle eigenstate with energy E and momentum \mathbf{P} of the Hamiltonian corresponding to our model Lagrangian. The index \mathbf{a} collectively denotes

the eigenvalues of any other operators (possibly) needed in order to form a complete set of states.

For notational, we always work with the doublet-projected quantities like

$$G(x_1, x_2; x_3, x_4) = (\sigma^i)_{\alpha}^{\alpha'} (G^{ij})_{\alpha'}^{\beta'}(x_1, x_2; x_3, x_4) (\sigma^j)_{\beta'}^{\beta} \Big|_{\alpha=\beta=1} \quad (\text{D.10})$$

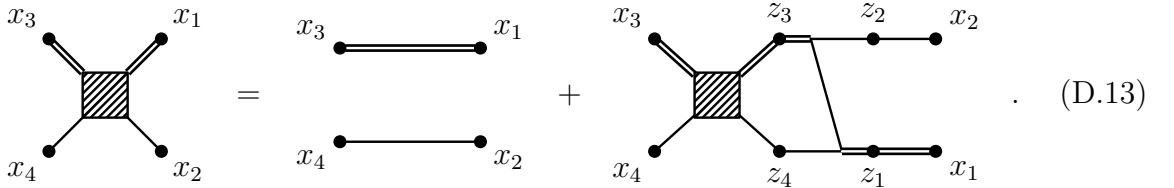
in the following, *i.e.*, all equations are to be understood with the doublet projection already applied. By using Wick's theorem and the general perturbation expansion we find the (inhomogeneous) Bethe–Salpeter equation

$$G(x_1, x_2; x_3, x_4) = G_0(x_1, x_2; x_3, x_4) + \int d^4 z_1 d^4 z_2 d^4 z_3 d^4 z_4 G_0(x_1, x_2; z_1, z_2) \times K(z_1, z_2; z_3, z_4) G(z_3, z_4; x_3, x_4), \quad (\text{D.11})$$

with

$$G_0(x_1, x_2; x_3, x_4) = \Delta_d(x_1, x_3) \Delta_N(x_2, x_4). \quad (\text{D.12})$$

Diagrammatically, Eq. (D.11) can be represented as



$$= \quad \text{Diagram 1} \quad + \quad \text{Diagram 2} \quad . \quad (\text{D.13})$$

D.2.1 Momentum space

By translation invariance, both $G(x_1, x_2; x_3, x_4)$ and $K(x_1, x_2; x_3, x_4)$ can only depend on the differences of coordinates, and the same of course holds for the propagators. We introduce center-of-mass and relative coordinates as

$$x = x_1 - x_2 \quad , \quad X = \eta_d x_1 + \eta_N x_2 \quad ; \quad x' = x_3 - x_4 \quad , \quad X' = \eta_d x_3 + \eta_N x_4 \quad (\text{D.14a})$$

and

$$X'' = X - X', \quad (\text{D.14b})$$

where

$$\eta_d = \frac{M_d}{M_d + M_N} \quad , \quad \eta_N = \frac{M_N}{M_d + M_N} \quad , \quad \text{i.e.} \quad \eta_d + \eta_N = 1. \quad (\text{D.14c})$$

Considering now

$$G_0(x_1, x_2; x_3, x_4) = \int \frac{d^4 q}{(2\pi)^4} \int \frac{d^4 q'}{(2\pi)^4} e^{-iq \cdot (x_1 - x_3)} e^{-iq' \cdot (x_2 - x_4)} \Delta_d(q) \Delta_N(q') \quad (\text{D.15})$$

and making the change of variables

$$q = \eta_d P + p \quad , \quad q' = \eta_N P - p, \quad (\text{D.16})$$

we get

$$G_0(x_1, x_2; x_3, x_4) = \int \frac{d^4 P}{(2\pi)^4} \int \frac{d^4 p}{(2\pi)^4} e^{-iP \cdot X''} e^{-ip \cdot (x-x')} \Delta_d(\eta_d P + p) \Delta_N(\eta_N P - p). \quad (\text{D.17})$$

Inserting an identity operator expressed in momentum space, we arrive at

$$G_0(x_1, x_2; x_3, x_4) = \int \frac{d^4 P}{(2\pi)^4} \int \frac{d^4 p}{(2\pi)^4} \int \frac{d^4 k}{(2\pi)^4} e^{-iP \cdot X''} e^{-ip \cdot x} e^{ik \cdot x'} (2\pi)^4 \delta^{(4)}(k - p) \\ \times \Delta_d(\eta_d P + p) \Delta_N(\eta_N P - p). \quad (\text{D.18})$$

Moreover, we have

$$G(x_1, x_2; x_3, x_4) \equiv G(X'', x, x') = \int \frac{d^4 P}{(2\pi)^4} \int \frac{d^4 p}{(2\pi)^4} \int \frac{d^4 k}{(2\pi)^4} e^{-iP \cdot X''} e^{-ip \cdot x} e^{ik \cdot x'} G(k, p; P), \quad (\text{D.19})$$

and an analogous expression for $K(x_1, x_2; x_3, x_4)$. Putting everything into Eq. (D.11) and making suitable changes of variables for the $d^4 z_i$ integrals yields the (inhomogeneous) Bethe-Salpeter equation in momentum space:

$$G(k, p; P) = G_0(k, p; P) + \int \frac{d^4 q}{(2\pi)^4} \int \frac{d^4 q'}{(2\pi)^4} G(k, q; P) K(q, q'; P) G_0(q', p; P) \quad (\text{D.20})$$

with

$$G_0(k, p; P) = (2\pi)^4 \delta^{(4)}(k - p) \cdot \Delta_d(\eta_d P + p) \Delta_N(\eta_N P - p). \quad (\text{D.21})$$

Diagrammatically, it can be written as

$$(\text{D.22})$$

One of the integrals in Eq. (D.20) can be cancelled with the delta function in G_0 , yielding

$$G(k, p; P) = \Delta_d(\eta_d P + p) \Delta_N(\eta_N P - p) \\ \times \left[(2\pi)^4 \delta^{(4)}(k - p) + \int \frac{d^4 q}{(2\pi)^4} G(k, q; P) \cdot K(q, p; P) \right], \quad (\text{D.23})$$

and finally

$$\int \frac{d^4 q}{(2\pi)^4} [G_0^{-1}(q, p; P) - K(q, p; P)] G(k, q; P) = (2\pi)^4 \delta^{(4)}(k - p) \quad (\text{D.24})$$

with

$$G_0^{-1}(k, p; P) = (2\pi)^4 \delta^{(4)}(k - p) \cdot [\Delta_d(\eta_d P + p)]^{-1} \cdot [\Delta_N(\eta_N P - p)]^{-1} \quad (\text{D.25})$$

as an alternative formulation of Eq. (D.20).

D.2.2 Bound state contribution

Going back to configuration space for the moment, we now assume the existence of a stable trinucleon bound state (which can be thought of as an unphysical triton if one identifies the uncharged single nucleon state in our model system with the neutron) with energy $E = -E_B < 0$. For simplicity, we also assume that it is non-degenerate, *i.e.*, that it is characterized by a unique set of quantum numbers \mathbf{a}_0 , which we omit in the following. Selecting the time-ordering $t_1, t_2 > t_3, t_4$ and inserting a complete set of states, we get

$$G(x_1, x_2; x_3, x_4) = \sum_{\mathbf{a}} \int \frac{d^3P}{(2\pi)^3} \int \frac{dE}{2\pi} \psi_{E\mathbf{P}\mathbf{a}}(x_1, x_2) \psi_{E\mathbf{P}\mathbf{a}}^\dagger(x_3, x_4) \quad , \quad (t_1, t_2 > t_3, t_4) \quad (\text{D.26})$$

with $dE = dP_0$. The bound-state contribution to this expression is

$$G_B(x_1, x_2; x_3, x_4) = \int \frac{d^3P}{(2\pi)^3} \psi_{B\mathbf{P}}(x_1, x_2) \psi_{B\mathbf{P}}^\dagger(x_3, x_4) \quad , \quad (t_1, t_2 > t_3, t_4) \quad , \quad (\text{D.27})$$

where we have introduced the short-hand notation $\psi_{B\mathbf{P}} \equiv \psi_{-E_B\mathbf{P}\mathbf{a}_0}$ for the bound-state wave function. By translation invariance, we can write

$$\psi_{B\mathbf{P}}(x_1, x_2) = \langle \Omega | T(d(x_1 + a)N(x_2 + a)) | -E_B, \mathbf{P}, \mathbf{a}_0 \rangle \cdot e^{iP \cdot a} \quad (\text{D.28})$$

with $P_0 = E = -E_B$ for any four-vector a . We use this with $a = -X$ and an analogous expression for $\psi_{B\mathbf{P}}^\dagger(x_3, x_4)$ to write

$$\psi_{B\mathbf{P}}(x_1, x_2) \psi_{B\mathbf{P}}^\dagger(x_3, x_4) = \psi_{B\mathbf{P}}(x) \psi_{B\mathbf{P}}^\dagger(x') \cdot e^{-iP \cdot X''} \quad , \quad (\text{D.29})$$

implicitly defining the Bethe–Salpeter wave functions $\psi_{B\mathbf{P}}(x)$ and $\psi_{B\mathbf{P}}^\dagger(x')$ for the relative motion. Using this, the bound-state contribution is

$$G_B(x_1, x_2; x_3, x_4) = \int \frac{d^3P}{(2\pi)^3} e^{-iP \cdot X''} \psi_{B\mathbf{P}}(x) \psi_{B\mathbf{P}}^\dagger(x') \cdot \theta \left(X_0'' - \frac{1}{2}|x_0| - \frac{1}{2}|x'_0| \right) \quad , \quad (\text{D.30})$$

where we have inserted the theta function in order to impose the time-ordering $t_1, t_2 > t_3, t_4$. Using the formula

$$\theta(y_0) = i \int \frac{dp_0}{2\pi} \frac{1}{p_0 + i\varepsilon} e^{-ip_0 y_0} \quad (\varepsilon \rightarrow 0 \text{ implied}) \quad (\text{D.31})$$

we get

$$G_B(x_1, x_2; x_3, x_4) = i \int \frac{d^3P}{(2\pi)^3} \int \frac{dE}{2\pi} e^{i\mathbf{P} \cdot \mathbf{X}''} e^{-iEX_0''} \frac{e^{\frac{i}{2}(E+E_B)|x_0|} \psi_{B\mathbf{P}}(x) e^{\frac{i}{2}(E+E_B)|x'_0|} \psi_{B\mathbf{P}}^\dagger(x')}{E + E_B + i\varepsilon} \quad , \quad (\text{D.32})$$

where we have changed the integration variable $p_0 \rightarrow E + E_B$. Defining new wave functions

$$\tilde{\psi}_{B\mathbf{P}}(x) = e^{\frac{i}{2}(E+E_B)|x_0|} \psi_{B\mathbf{P}}(x) \quad , \quad \tilde{\psi}_{B\mathbf{P}}^\dagger(x') = e^{\frac{i}{2}(E+E_B)|x'_0|} \psi_{B\mathbf{P}}^\dagger(x') \quad (\text{D.33})$$

and their Fourier transforms

$$\tilde{\psi}_{B\mathbf{P}}(x) = \int \frac{d^4p}{(2\pi)^4} e^{-ip \cdot x} \tilde{\psi}_{B\mathbf{P}}(p) \quad , \quad \tilde{\psi}_{B\mathbf{P}}^\dagger(x') = \int \frac{d^4k}{(2\pi)^4} e^{ik \cdot x'} \tilde{\psi}_{B\mathbf{P}}^\dagger(k) \quad , \quad (\text{D.34})$$

we finally arrive at

$$G_B(x_1, x_2; x_3, x_4) = i \int \frac{d^4 P}{(2\pi)^4} \int \frac{d^4 p}{(2\pi)^4} \int \frac{d^4 k}{(2\pi)^4} e^{-iP \cdot X''} e^{-ip \cdot x} e^{ik \cdot x'} \frac{\tilde{\psi}_{B\mathbf{P}}(p) \tilde{\psi}_{B\mathbf{P}}^\dagger(k)}{E + E_B + i\varepsilon} \quad (\text{D.35})$$

with $P_0 \equiv E$. Note that $\tilde{\psi}_{B\mathbf{P}} \rightarrow \psi_{B\mathbf{P}}$ for $E \rightarrow -E_B$, so we have

$$G(k, p; P) = i \frac{\psi_{B\mathbf{P}}(p) \psi_{B\mathbf{P}}^\dagger(k)}{E + E_B + i\varepsilon} + \text{terms regular at } E = -E_B \quad (\text{D.36})$$

in momentum space.

D.2.3 Homogeneous equation

Inserting the factorization (D.36) into Eq. (D.24) and multiplying by $(E + E_B)$ we find the homogeneous Bethe–Salpeter equation

$$\int \frac{d^4 q}{(2\pi)^4} [G_0^{-1}(q, p; P) - K(q, p; P)] \psi_{B\mathbf{P}}(q) = 0 \quad (\text{D.37})$$

after taking the limit $E \rightarrow -E_B$ and cancelling non-zero factors. Equivalently, we can also obtain this in the form

$$\psi_{B\mathbf{P}}(p) = \Delta_d(\eta_d P + p) \Delta_N(\eta_N P - p) \cdot \int \frac{d^4 q}{(2\pi)^4} K(q, p; P) \psi_{B\mathbf{P}}(q) \quad (\text{D.38})$$

from Eq. (D.20).

D.2.4 Three-dimensional reduction

We now consider a bound state at rest, $P = (-E_B, \mathbf{0})$, and define the *amputated wave function*

$$\mathcal{B}(p_0, \mathbf{p}) = \psi_{B\mathbf{0}}(p_0, \mathbf{p}) \cdot [\Delta_d(-\eta_d E_B + p_0, \mathbf{p})]^{-1} \cdot [\Delta_N(-\eta_N E_B - p_0, \mathbf{p})]^{-1}, \quad (\text{D.39})$$

which fulfills the equation

$$\mathcal{B}(p_0, \mathbf{p}) = \int \frac{d^4 q}{(2\pi)^4} K(q, p; -E_B) \Delta_d(-\eta_d E_B + q_0, \mathbf{q}) \Delta_N(-\eta_N E_B - q_0, \mathbf{q}) \mathcal{B}(q_0, \mathbf{q}). \quad (\text{D.40})$$

Carrying out the dq_0 integration picks up the residue from the nucleon propagator pole at $q_0 = -\eta_N E_B - \mathbf{q}^2/(2M_N) + i\varepsilon$. From the resulting right-hand side of Eq. (D.40) we then find that the function

$$\mathcal{B}(\mathbf{p}) \equiv \mathcal{B}\left(-\eta_N E_B - \frac{\mathbf{p}^2}{2M_N}, \mathbf{p}\right) \quad (\text{D.41})$$

fulfills the equation

$$\mathcal{B}(\mathbf{p}) = \int \frac{d^3q}{(2\pi)^3} K\left(\eta_N E - \frac{\mathbf{q}^2}{2M_N}, \mathbf{k}, \eta_N E - \frac{\mathbf{p}^2}{2M_N}, \mathbf{p}; E\right) \Delta_d\left(-E_B - \frac{\mathbf{q}^2}{2M_N}, \mathbf{q}\right) \mathcal{B}(\mathbf{q}). \quad (\text{D.42})$$

For future reference we also define the wave function

$$\phi(\mathbf{p}) = \int \frac{dp_0}{2\pi} \psi(p_0, \mathbf{p}), \quad (\text{D.43})$$

for which from Eq. (D.39) one immediately finds that

$$\phi(\mathbf{p}) = \Delta_d\left(-E_B - \frac{\mathbf{p}^2}{2M_N}, \mathbf{p}\right) \mathcal{B}(\mathbf{p}). \quad (\text{D.44})$$

D.3 Operator formalism

In order to focus on the essential, we now reformulate the results derived above in an abstract operator notation. The Bethe–Salpeter equation (D.20) can be written as

$$G = G_0 + GK G_0 = G_0 + G_0 K G, \quad (\text{D.45})$$

where the middle and the right-hand side are equivalent.¹ Assuming the existence of a bound state with energy $E = -E_B$, we have the factorization

$$G \sim i \frac{|\psi\rangle\langle\psi|}{E + E_B} \quad \text{for } E \rightarrow -E_B, \quad (\text{D.46})$$

as given explicitly in Eq. (D.36). Inserting this into Eq. (D.45), multiplying by $(E + E_B)$, and acting on $|\psi\rangle$, we obtain the homogeneous equation

$$|\psi\rangle = G_0 K |\psi\rangle \quad (\text{D.47})$$

after taking the limit $E \rightarrow -E_B$ and using that G_0 is regular for $E \rightarrow -E_B$. This is, of course, just Eq. (D.38). Note that all the operators here are in general functions of the total energy, $G = G(E)$, $K = K(E)$, etc., but that for the sake of notational simplicity we have not written out this dependence explicitly.

D.3.1 Lippmann–Schwinger equation

Defining the T-matrix operator T via the relation

$$K G = T G_0, \quad (\text{D.48})$$

we can rewrite Eq. (D.45) in the form

$$G = G_0 + G_0 T G_0. \quad (\text{D.49})$$

¹This can be seen, for example, by iterating both versions and noting that the results are the same.

Inserting this into both sides of the original Eq. (D.45), we get

$$G_0 + G_0 T G_0 = G_0 + G_0 K G_0 + G_0 K G_0 T G_0. \quad (\text{D.50})$$

After cancelling the common term G_0 and multiplying through by G_0^{-1} on both sides, we arrive at the familiar Lippmann–Schwinger equation

$$T = K + K G_0 T. \quad (\text{D.51})$$

The precise relation between this operator and the \mathcal{T} -matrix elements used in Chapter 6 will be discussed in Section D.4.3 below. As a remark we add here that G , with all momenta put on-shell and the propagator term G_0 removed (“amputated”), is just an S-matrix element. Going from Eq. (D.50) to (D.51) is essentially equivalent to using “ $S = \mathbf{1} + T$.”

D.4 Normalization condition

We are now finally equipped to derive the normalization for the Bethe-Salpeter wave functions and, subsequently, for the trinucleon wave functions used in Chapter 6. For the general derivation we stay in the abstract operator notation and only go back to the momentum-space formulation when we discuss the explicit form for our $N-d$ model system in Section D.4.2 below.

D.4.1 General derivation

Multiplying Eq. (D.45) by G^{-1} from the right and by G_0^{-1} from the left, we get

$$G_0^{-1} = G^{-1} + K, \quad (\text{D.52})$$

and hence

$$G(G_0^{-1} - K)G = G \quad (\text{D.53})$$

from the trivial identity $GG^{-1}G = G$. Inserting furthermore the factorization (D.46) at the bound-state pole, we find

$$\lim_{E \rightarrow -E_B} i^2 \frac{|\psi\rangle\langle\psi|G_0^{-1} - K|\psi\rangle\langle\psi|}{(E + E_B)^2} = \lim_{E \rightarrow -E_B} i \frac{|\psi\rangle\langle\psi|}{E + E_B}. \quad (\text{D.54})$$

Multiplying this by $(E + E_B)$ and furthermore with $|\psi\rangle$ from both sides, we find

$$\lim_{E \rightarrow -E_B} i \frac{\langle\psi|G_0^{-1} - K|\psi\rangle}{E + E_B} = 1 \quad (\text{D.55})$$

after cancelling the common factor $\langle\psi|\psi\rangle^2$. Using now l’Hôpital’s rule to evaluate the limit, we finally arrive at

$$i\langle\psi|\frac{d}{dE}(G_0^{-1} - K)|\psi\rangle\Big|_{E=-E_B} = 1. \quad (\text{D.56})$$

Note that for the standard case, where $G_0 \propto (E - H_0)^{-1}$ with the free Hamiltonian H_0 , and where the kernel (potential) does not depend on the energy, Eq. (D.56) reduces to the familiar condition $\langle \psi | \psi \rangle = 1$. As already remarked in Chapter 6, this kind of normalization condition for energy-dependent interactions is not at all a new result but has been known for a long time [192].

D.4.2 Explicit form in three dimensions

We now go back to the momentum-space basis and consider a bound state at rest, setting $P = (-E_B, \mathbf{0})$. We define a reduced two-body propagator \tilde{G} that only depends on the relative three-momenta \mathbf{k} and \mathbf{p} by integration over the energies:

$$\tilde{G}(\mathbf{k}, \mathbf{p}; -E_B) = \int \frac{dk_0}{2\pi} \int \frac{dp_0}{2\pi} G(k, p; P). \quad (\text{D.57})$$

By the definition (D.43), this implies

$$\tilde{G} \sim i \frac{|\phi\rangle\langle\phi|}{E + E_B} \quad \text{for } E \rightarrow -E_B. \quad (\text{D.58})$$

From Eq. (D.45) we get

$$\tilde{G} = \tilde{G}_0 + \widetilde{G_0 K G} = \tilde{G}_0 \left(\mathbf{1} + \tilde{G}_0^{-1} \widetilde{G_0 K G} \right) \quad (\text{D.59})$$

and hence

$$\tilde{G}^{-1} = \left(\mathbf{1} + \tilde{G}_0^{-1} \widetilde{G_0 K G} \right)^{-1} \tilde{G}_0^{-1}. \quad (\text{D.60})$$

We now define

$$\tilde{G}^{-1} - \tilde{G}_0^{-1} \equiv -\tilde{V} \quad (\text{D.61})$$

and find

$$\tilde{G} = \tilde{G} \left(\tilde{G}_0^{-1} - \tilde{V} \right) \tilde{G}. \quad (\text{D.62})$$

Repeating the procedure described in Section D.4.1 above then yields the normalization condition

$$i \langle \phi | \frac{d}{dE} \left(\tilde{G}_0^{-1} - \tilde{V} \right) | \phi \rangle \Big|_{E=-E_B} = 1. \quad (\text{D.63})$$

So far it seems that we have hardly done anything but complicate the notation, but the advantage will become apparent soon. For the first term in Eq. (D.63), we find

$$\begin{aligned} \tilde{G}_0(\mathbf{k}, \mathbf{p}; E) &= \int \frac{dk_0}{2\pi} \int \frac{dp_0}{2\pi} (2\pi)^4 \delta^{(4)}(k - p) \cdot \Delta_d(\eta_d E + p_0, \mathbf{p}) \Delta_N(\eta_N E - p_0, -\mathbf{p}) \\ &= (2\pi)^3 \delta^{(3)}(k - p) \cdot \int \frac{dp_0}{2\pi} \Delta_d(\eta_d E + p_0, \mathbf{p}) \cdot \frac{i}{\eta_N E - p_0 - \frac{\mathbf{p}^2}{2M_N} + i\epsilon} \\ &= (2\pi)^3 \delta^{(3)}(k - p) \cdot \Delta_d \left(E - \frac{\mathbf{p}^2}{2M_N}, \mathbf{p} \right), \end{aligned} \quad (\text{D.64})$$

and thus

$$\tilde{G}_0^{-1}(\mathbf{k}, \mathbf{p}; E) = (2\pi)^3 \delta^{(3)}(k - p) \cdot \left[\Delta_d \left(E - \frac{\mathbf{p}^2}{2M_N}, \mathbf{p} \right) \right]^{-1}. \quad (\text{D.65})$$

Now we consider \tilde{V} . From Eqs. (D.60) and (D.61) we get

$$\tilde{V} = \tilde{G}_0^{-1} - \left(\mathbf{1} + \tilde{G}_0^{-1} \widetilde{G_0 K G} \right)^{-1} \tilde{G}_0^{-1} = \tilde{G}_0^{-1} - \left[\sum_{n=0}^{\infty} \left(-\tilde{G}_0^{-1} \widetilde{G_0 K G} \right)^n \right] \tilde{G}_0^{-1}. \quad (\text{D.66})$$

Furthermore, iterated application of the Bethe–Salpeter equation (D.45) yields

$$\widetilde{G_0 K G} = \widetilde{G_0 K G_0} + G_0 \widetilde{K G_0 K G_0} + \dots, \quad (\text{D.67})$$

such that we have a double expansion in Eq. (D.66). We write

$$\tilde{V} \equiv \sum_{n=0}^{\infty} \tilde{V}_n = \underbrace{\tilde{G}_0^{-1} - \tilde{G}_0^{-1}}_{\tilde{V}_0} + \underbrace{\tilde{G}_0^{-1} \widetilde{G_0 K G_0} \tilde{G}_0^{-1}}_{\tilde{V}_1} + \dots, \quad (\text{D.68})$$

where the index indicates the number of insertions of K . In the following calculations we will frequently omit the arguments $(\mathbf{k}, \mathbf{p}; E)$ on the left-hand side of equations. It will, however, always be clear what they should be from the corresponding right-hand sides. With

$$\begin{aligned} \widetilde{G_0 K G_0} &= \int \frac{dk_0}{2\pi} \int \frac{dp_0}{2\pi} \left[\Delta_d(\eta_d E + k_0, \mathbf{k}) \Delta_N(\eta_N E - k_0, -\mathbf{k}) \cdot K(k_0, \mathbf{k}, p_0, \mathbf{p}; E) \right. \\ &\quad \left. \times \Delta_d(\eta_d E + p_0, \mathbf{p}) \Delta_N(\eta_N E - p_0, -\mathbf{p}) \right] \\ &= \Delta_d \left(E - \frac{\mathbf{k}^2}{2M_N}, \mathbf{k} \right) \cdot K \left(\eta_N E - \frac{\mathbf{k}^2}{2M_N}, \mathbf{k}, \eta_N E - \frac{\mathbf{p}^2}{2M_N}, \mathbf{p}; E \right) \cdot \Delta_d \left(E - \frac{\mathbf{p}^2}{2M_N}, \mathbf{p} \right) \end{aligned} \quad (\text{D.69})$$

and the \tilde{G}_0^{-1} from Eq. (D.65) amputating the deuteron propagators, we find that

$$\tilde{V}_1(\mathbf{k}, \mathbf{p}; E) = K \left(\eta_N E - \frac{\mathbf{k}^2}{2M_N}, \mathbf{k}, \eta_N E - \frac{\mathbf{p}^2}{2M_N}, \mathbf{p}; E \right). \quad (\text{D.70})$$

The important point is now that all higher contributions vanish. To see this, we first look at

$$\tilde{V}_2 = \tilde{G}_0^{-1} \left[G_0 \widetilde{K G_0 K G_0} - \widetilde{G_0 K G_0} \tilde{G}_0^{-1} \widetilde{G_0 K G_0} \right] \tilde{G}_0^{-1} \quad (\text{D.71})$$

and use the following

Lemma. *It holds that*

$$\dots \widetilde{G_0 \tilde{G}_0^{-1} G_0} \dots = \dots \widetilde{G_0} \dots \quad (\text{D.72})$$

Proof. We start by calculating the right hand side:

$$\begin{aligned}
\cdots \widetilde{G}_0 \cdots &= \int \frac{d^4 q_1}{(2\pi)^4} \int \frac{d^4 q_2}{(2\pi)^4} [\cdots] (2\pi)^4 \delta^{(4)}(q_1 - q_2) \\
&\quad \times \Delta_d(\eta_d E + q_1^0, \mathbf{q}_1) \cdot \frac{i}{\eta_N E - q_1^0 - \frac{\mathbf{q}_1^2}{2M_N} + i\epsilon} [\cdots] \\
&= \int \frac{d^3 q_1}{(2\pi)^3} [\cdots] \Delta_d\left(E - \frac{\mathbf{q}_1^2}{2M_N}, \mathbf{q}_1\right) [\cdots]. \quad (\text{D.73})
\end{aligned}$$

The left hand side is

$$\begin{aligned}
\cdots \widetilde{G}_0 \widetilde{G}_0^{-1} \widetilde{G}_0 \cdots &= \int \frac{d^4 p_1}{(2\pi)^4} \int \frac{d q_1^0}{2\pi} \int \frac{d^3 q_1}{(2\pi)^3} \int \frac{d^3 q_2}{(2\pi)^3} \int \frac{d q_2^0}{2\pi} \int \frac{d^4 p_2}{(2\pi)^4} [\cdots] \\
&\quad \times (2\pi)^4 \delta^{(4)}(p_1 - q_1) \cdot \Delta_d(\eta_d E + q_1^0, \mathbf{q}_1) \cdot \frac{i}{\eta_N E - q_1^0 - \frac{\mathbf{q}_1^2}{2M_N} + i\epsilon} \\
&\quad \times (2\pi)^3 \delta^{(3)}(\mathbf{q}_1 - \mathbf{q}_2) \cdot \left[\Delta_d\left(E - \frac{\mathbf{q}_1^2}{2M_N}, \mathbf{q}_1\right) \right]^{-1} \\
&\quad \times (2\pi)^4 \delta^{(4)}(q_2 - p_2) \cdot \Delta_d(\eta_d E + q_2^0, \mathbf{q}_2) \cdot \frac{i}{\eta_N E - q_2^0 - \frac{\mathbf{q}_2^2}{2M_N} + i\epsilon} [\cdots] \\
&= \int \frac{d^3 q_1}{(2\pi)^3} [\cdots] \Delta_d\left(E - \frac{\mathbf{q}_1^2}{2M_N}, \mathbf{p}\right) [\cdots] = \cdots \widetilde{G}_0 \cdots. \quad (\text{D.74})
\end{aligned}$$

The crucial point is that the residues of the nucleon propagators are always picked up in such a way that one deuteron propagator is cancelled by its inverse from the \widetilde{G}_0^{-1} , cf. Eq. (D.65). \square

This immediately shows that \widetilde{V}_2 vanishes, and for the higher terms it is just a matter of checking the relative signs that they also do. For example, we have

$$\begin{aligned}
\widetilde{V}_3 &= \widetilde{G}_0^{-1} \left[G_0 K \widetilde{G}_0 K \widetilde{G}_0 K G_0 - \widetilde{G}_0 K \widetilde{G}_0 \widetilde{G}_0^{-1} G_0 K \widetilde{G}_0 K G_0 \right. \\
&\quad \left. - G_0 K \widetilde{G}_0 K \widetilde{G}_0 \widetilde{G}_0^{-1} \widetilde{G}_0 K \widetilde{G}_0 + \widetilde{G}_0 K \widetilde{G}_0 \widetilde{G}_0^{-1} G_0 K \widetilde{G}_0 \widetilde{G}_0^{-1} \widetilde{G}_0 K \widetilde{G}_0 \right] \widetilde{G}_0^{-1} = 0. \quad (\text{D.75})
\end{aligned}$$

Altogether, we have found that

$$\begin{aligned}
\widetilde{V}(\mathbf{k}, \mathbf{p}; E) &= K \left(\eta_N E - \frac{\mathbf{k}^2}{2M_N}, \mathbf{k}, \eta_N E - \frac{\mathbf{p}^2}{2M_N}, \mathbf{p}; E \right) \\
&= \frac{iM_N y_d^2}{2} \cdot \frac{1}{\mathbf{k}^2 + \mathbf{k} \cdot \mathbf{p} + \mathbf{p}^2 - M_N E - i\epsilon}. \quad (\text{D.76})
\end{aligned}$$

D.4.3 Factorization of the T-matrix

What remains is to establish the connection between the quantities defined here and the \mathcal{T} -matrix elements and wave functions used in Chapter 6. Comparing Eqs. (D.42)

and (D.76) with the interaction as given in Section 6.2.4 already suggests that there is a direct correspondence between the states $\mathcal{B}(\mathbf{p})$ introduced here and the trinucleon wave functions of Chapter 6.

For the T operator introduced in Eq. (D.48) we find from Eq. (D.50) that

$$\widetilde{G_0 T G_0} = \widetilde{G_0 K G_0} + G_0 \widetilde{K G_0 T G_0}. \quad (\text{D.77})$$

Applying the Lemma (D.72) to the second term on the right-hand side gives

$$G_0 \widetilde{K G_0 T G_0} = \widetilde{G_0 K G_0} \widetilde{G_0^{-1} G_0 T G_0}. \quad (\text{D.78})$$

Inserting into this the identity in the form

$$\mathbf{1} = \widetilde{G_0} \widetilde{G_0^{-1}} \quad (\text{D.79})$$

and multiplying Eq. (D.77) with $\widetilde{G_0^{-1}}$ from both sides we find that

$$\widetilde{G_0^{-1} G_0 T G_0 G_0^{-1}} = \left[\widetilde{G_0^{-1} G_0 K G_0 G_0^{-1}} \right] \widetilde{G_0} \left[\widetilde{G_0^{-1} G_0 T G_0 G_0^{-1}} \right], \quad (\text{D.80})$$

where from the discussion in Section D.4.2 we see that the interaction is the same as in the normalization condition:

$$\widetilde{G_0^{-1} G_0 K G_0 G_0^{-1}} = \widetilde{V}. \quad (\text{D.81})$$

Comparing this now with the integral equations in Chapter 6, we can conclude that the \mathcal{T} -matrix there is

$$i\mathcal{T}(E; \mathbf{k}, \mathbf{p}) = \langle \mathbf{k} | \widetilde{G_0^{-1} G_0 T G_0 G_0^{-1}} | \mathbf{p} \rangle, \quad (\text{D.82})$$

where all operators are of course functions of the energy E .

As $E \rightarrow -E_B$ we now have, using Eq. (D.49) and noting that the bound state cannot be in G_0 since it has to arise from the interaction,

$$\begin{aligned} \widetilde{G_0^{-1} G_0 T G_0 G_0^{-1}} &= \widetilde{G_0^{-1} G_0 G_0^{-1}} + \text{regular terms} \\ &= i \frac{\widetilde{G_0^{-1}} |\phi\rangle \langle \phi| \widetilde{G_0^{-1}}}{E + E_B} + \text{regular terms}, \end{aligned} \quad (\text{D.83})$$

where the second identity follows from Eq. (D.58). Now, according to Eqs. (D.44) and (D.64) we have

$$|\phi\rangle = \widetilde{G_0} |\mathcal{B}\rangle \iff |\mathcal{B}\rangle = \widetilde{G_0^{-1}} |\phi\rangle, \quad (\text{D.84})$$

which implies

$$\langle \mathcal{B} | = \langle \phi | (\widetilde{G_0^{-1}})^\dagger. \quad (\text{D.85})$$

But, up to a delta function, $\widetilde{G_0^{-1}}$ is just the deuteron propagator Δ_d which, from Eq. (D.5) we find to be a purely imaginary quantity.² Hence,

$$(\widetilde{G_0^{-1}})^\dagger = -\widetilde{G_0^{-1}}, \quad \text{for } E < 0 \quad (\text{D.86})$$

²Note the overall i in the prefactor in Eq. (D.5) and that the rest is real for $p_0 < 0$ and $\varepsilon \rightarrow 0$.

and

$$\tilde{G}_0^{-1} \widetilde{G_0 T G_0} \tilde{G}_0^{-1} = -i \frac{|\mathcal{B}\rangle\langle\mathcal{B}|}{E + E_B} + \text{regular terms as } E \rightarrow -E_B. \quad (\text{D.87})$$

For the \mathcal{T} -matrix of Chapter 6 we then find from Eq. (D.82) that

$$\mathcal{T}(E; \mathbf{k}, \mathbf{p}) = -\frac{\mathcal{B}^\dagger(\mathbf{k}) \mathcal{B}(\mathbf{p})}{E + E_B} + \text{regular terms as } E \rightarrow -E_B. \quad (\text{D.88})$$

Finally, for the normalization condition (D.63) written in terms of the $|\mathcal{B}\rangle$ we analogously find

$$-i \langle \mathcal{B} | \tilde{G}_0 \left[\frac{d}{dE} (\tilde{G}_0^{-1} - \tilde{V}) \right] \tilde{G}_0 | \mathcal{B} \rangle \Big|_{E=-E_B} = 1. \quad (\text{D.89})$$

D.5 Some remarks

In order to fully establish the connection of the results derived here with the formalism of Chapter 6, a few remarks are in order.

Starting from a formulation in terms of four-dimensional energy-momentum vectors we have, in the preceding sections, obtained functions that only depend on three-momenta by explicitly integrating over the zero components. Essentially, this corresponds to imposing an equal-time condition on the Bethe–Salpeter amplitudes in order to get back ordinary Schrödinger wave functions (*cf.* Section 9.1 in Ref. [200]). To see this, consider an arbitrary amplitude $\psi_{E\mathbf{P}}(x) = \psi_{E\mathbf{P}}(x_0, \mathbf{x})$ defined analogously to what was done for the bound-state contribution in Eqs. (D.28) and (D.29). Since its Fourier transform is

$$\psi_{E\mathbf{P}}(q) = \psi_{E\mathbf{P}}(q_0, \mathbf{q}) = \int dx_0 e^{iq_0 \cdot x_0} e^{-i\mathbf{q} \cdot \mathbf{x}} \psi_{E\mathbf{P}}(x_0, \mathbf{x}), \quad (\text{D.90})$$

integrating over q_0 gives a delta function $\delta(x_0) = \delta(t_1 - t_2)$. As used in Sections D.2.4 and D.4.2, in loops the integration over the zero components of the four-momenta always picks up the on-shell pole of a nucleon propagator.

In the equations reduced in this manner we have kept the full dependence on the three-momenta, whereas in Chapter 6 we work with S-wave projected quantities that only depend on the moduli of the momenta. There is, however, a simple and direct correspondence. Since the interaction K (and thus also the T-matrix) only depends on one angle, and the propagators in G_0 , on the other hand, have no angular dependence, the projection can be (almost) trivially applied to all equations by replacing functions with their S-wave projected analogs and changing, at the same time, the operator products in the momentum-space representation according to

$$AB = \int \frac{d^3q}{(2\pi)^3} A(\dots, \mathbf{q}) B(\mathbf{q}, \dots) \longrightarrow \frac{1}{2\pi^2} \int dq q^2 A(\dots, q) B(q, \dots), \quad (\text{D.91})$$

cf. Eq. (6.29).

Finally, due to the isospin symmetry that was neglected here for simplicity, in the real N - d spin-doublet system of Chapter 6 one has a coupled-channel problem. The results derived

here can be directly generalized to an arbitrary number of channels n by promoting all operators to be $n \times n$ -matrices in channel space. In Chapter 6, the channels are determined by the combination of in- and outgoing dibaryon legs (giving $n = 2$ or $n = 3$), and \tilde{G}_0 is just a diagonal matrix containing the individual dibaryon propagators. Due to the coupling, the bound-state pole appears simultaneously in all components of the \mathcal{T} -matrix and the corresponding wave functions are vectors with n components. This is exactly the scenario discussed in Sections 6.4.1 and 6.4.2.

Bibliography

- [1] S. KÖNIG and H.-W. HAMMER, Low-energy p-d scattering and He-3 in pionless EFT, *Phys. Rev. C* **83**, 064001 (2011).
- [2] S. KÖNIG, D. LEE, and H.-W. HAMMER, Volume Dependence of Bound States with Angular Momentum, *Phys. Rev. Lett.* **107**, 112001 (2011).
- [3] S. BOUR, S. KÖNIG, D. LEE, H.-W. HAMMER, and U.-G. MEISSNER, Topological phases for bound states moving in a finite volume, *Phys. Rev. D* **84**, 091503(R) (2011).
- [4] S. KÖNIG, D. LEE, and H.-W. HAMMER, Non-relativistic bound states in a finite volume, *Annals Phys.* **327**, 1450–1471 (2012).
- [5] S. KÖNIG, D. LEE, and H.-W. HAMMER, Causality constraints for charged particles, *J. Phys. G: Nucl. Part. Phys.* **40**, 045106 (2013).
- [6] S. KÖNIG and H.-W. HAMMER, The Low-Energy p–d System in Pionless EFT, *Few-Body Syst.* **54**, 231–234 (2013).
- [7] S. ELHATISARI, S. KÖNIG, D. LEE, and H.-W. HAMMER, Causality, universality, and effective field theory for van der Waals interactions, *Phys. Rev. A* **87**, 052705 (2013).
- [8] M. LÜSCHER, Volume Dependence of the Energy Spectrum in Massive Quantum Field Theories. 1. Stable Particle States, *Commun. Math. Phys.* **104**, 177 (1986).
- [9] J. R. TAYLOR, *Scattering Theory: The Quantum Theory of Nonrelativistic Collisions* (Dover Publications, Inc., Mineola; New York, 2006).
- [10] H.-W. HAMMER and D. LEE, Causality and the effective range expansion, *Annals Phys.* **325**, 2212–2233 (2010).
- [11] J. D. JACKSON and J. M. BLATT, The Interpretation of Low Energy Proton–Proton Scattering, *Rev. Mod. Phys.* **22**, 77–118 (1950).
- [12] J. M. BLATT and J. D. JACKSON, On the Interpretation of Neutron-Proton Scattering Data by the Schwinger Variational Method, *Phys. Rev.* **76**, 18–37 (1949).
- [13] H. A. BETHE, Theory of the Effective Range in Nuclear Scattering, *Phys. Rev.* **76**, 38–50 (1949).
- [14] M. L. GOLDBERGER and K. M. WATSON, *Collision Theory* (John Wiley & Sons, Inc., 1967).
- [15] A. R. CHOUDHARY, Improved effective range formula, *Phys. Rev. C* **27**, 398–404 (1983).

- [16] J. J. de SWART, C. P. F. TERHEGGEN, and V. G. J. STOKS, The Low-energy n p scattering parameters and the deuteron, (1995), arXiv:nucl-th/9509032 [nucl-th].
- [17] H. van HAERINGEN and L. P. KOK, Modified effective-range function for two-range potentials, Czech. J. Phys. B **32**, 307–310 (1982).
- [18] M. J. SEATON, Quantum defect theory, Rep. Prog. Phys. **46**, 167–257 (1983).
- [19] C. GREENE, U. FANO, and G. STRINATI, General form of the quantum-defect theory, Phys. Rev. A **19**, 1485–1509 (1979).
- [20] C. H. GREENE, A. R. P. RAU, and U. FANO, General form of the quantum-defect theory. II, Phys. Rev. A **26**, 2441–2459 (1982).
- [21] B. GAO, General form of the quantum-defect theory for $1/r^\alpha$ type of potentials with $\alpha > 2$, Phys. Rev. A **78**, 012702 (2008).
- [22] H. M. XU, C. A. GAGLIARDI, R. E. TRIBBLE, A. M. MUKHAMEDZHANOV, and N. K. TIMOFEYUK, Overall Normalization of the Astrophysical S Factor and the Nuclear Vertex Constant for Be-7 (p , γ) B-8 Reactions, Phys. Rev. Lett. **73**, 2027–2030 (1994).
- [23] J. J. SAKURAI, *Modern Quantum Mechanics*, Revised Edition (Addison Wesley, Reading; Menlo Park; New York, 1993).
- [24] R. G. NEWTON, *Scattering Theory of Waves and Particles*, Second Edition (Springer-Verlag, New York; Heidelberg; Berlin, 1982).
- [25] V. EFIMOV, Energy Levels Arising from Resonant Two-Body Forces in a Three-Body System, Phys. Lett. B **33**, 563–564 (1970).
- [26] R. D. AMADO and J. V. NOBLE, On Efimov’s effect: A New Pathology of Three-Particle Systems, Phys. Lett. B **35**, 25–27 (1971).
- [27] R. D. AMADO and J. V. NOBLE, Efimov’s Effect: A New Pathology of Three-Particle Systems. II, Phys. Rev. D **5**, 1992–2002 (1972).
- [28] E. BRAATEN and H.-W. HAMMER, Universality in Few-Body Systems with Large Scattering Length, Phys. Rept. **428**, 259–390 (2006).
- [29] V. G. J. STOKS, R. A. M. KLOMP, C. P. F. TERHEGGEN, and J. J. de SWART, Construction of High Quality N N Potential Models, Phys. Rev. C **49**, 2950–2962 (1994).
- [30] R. B. WIRINGA, V. G. J. STOKS, and R. SCHIAVILLA, An Accurate Nucleon–Nucleon Potential with Charge Independence Breaking, Phys. Rev. C **51**, 38–51 (1995).
- [31] R. MACHLEIDT, The High-Precision, Charge-Dependent Bonn Nucleon–Nucleon Potential (CD-Bonn), Phys. Rev. C **63**, 024001 (2001).
- [32] R. MACHLEIDT and I. SLAUS, The Nucleon-nucleon interaction: Topical review, J. Phys. G: Nucl. Part. Phys. **27**, R69–R108 (2001).
- [33] N. KALANTAR-NAYESTANAKI, E. EPELBAUM, J. G. MESSCHENDORP, and A. NOGGA, Signatures of three-nucleon interactions in few-nucleon systems, Rept. Prog. Phys. **75**, 016301 (2012).

- [34] S. WEINBERG, Phenomenological Lagrangians, *Physica A* **96**, 327–340 (1979).
- [35] S. WEINBERG, Nonlinear Realizations of Chiral Symmetry, *Phys. Rev.* **166**, 1568–1577 (1968).
- [36] J. GASSER and H. LEUTWYLER, Chiral Perturbation Theory To One Loop, *Annals Phys.* **158**, 142–210 (1984).
- [37] J. GASSER and H. LEUTWYLER, Chiral Perturbation Theory: Expansions in the Mass of the Strange Quark, *Nucl. Phys. B* **250**, 465–516 (1985).
- [38] E. JENKINS and A. V. MANOHAR, Baryon Chiral Perturbation Theory Using a Heavy Fermion Lagrangian, *Phys. Lett. B* **255**, 558–562 (1991).
- [39] V. BERNARD, N. KAISER, J. KAMBOR, and U.-G. MEISSNER, Chiral Structure of the Nucleon, *Nucl. Phys. B* **388**, 315–345 (1992).
- [40] V. BERNARD, N. KAISER, and U.-G. MEISSNER, Chiral dynamics in nucleons and nuclei, *Int. J. Mod. Phys. E* **4**, 193–346 (1995).
- [41] S. WEINBERG, Nuclear forces from chiral Lagrangians, *Phys. Lett. B* **251**, 288–292 (1990).
- [42] S. WEINBERG, Effective chiral Lagrangians for nucleon-pion interactions and nuclear forces, *Nucl. Phys. B* **363**, 3–18 (1991).
- [43] E. EPELBAUM, H.-W. HAMMER, and U.-G. MEISSNER, Modern Theory of Nuclear Forces, *Rev. Mod. Phys.* **81**, 1773–1825 (2009).
- [44] R. MACHLEIDT and D. R. ENTEM, Chiral effective field theory and nuclear forces, *Phys. Rept.* **503**, 1–75 (2011).
- [45] C. W. BAUER, S. FLEMING, D. PIRJOL, and I. W. STEWART, An Effective field theory for collinear and soft gluons: Heavy to light decays, *Phys. Rev. D* **63**, 114020 (2001).
- [46] C. W. BAUER, D. PIRJOL, and I. W. STEWART, Soft collinear factorization in effective field theory, *Phys. Rev. D* **65**, 054022 (2002).
- [47] S. R. BEANE, P. F. BEDAQUE, W. C. HAXTON, D. R. PHILLIPS, and M. J. SAVAGE, From hadrons to nuclei: Crossing the border, (2000), arXiv:nucl-th/0008064 [nucl-th].
- [48] C. van der LEUN and C. ANDERLIESTEN, The Deuteron Binding Energy, *Nucl. Phys. A* **380**, 261–269 (1982).
- [49] D. B. KAPLAN, M. J. SAVAGE, and M. B. WISE, Two-Nucleon Systems from Effective Field Theory, *Nucl. Phys. B* **534**, 329–355 (1998).
- [50] D. B. KAPLAN, M. J. SAVAGE, and M. B. WISE, A New Expansion for Nucleon–Nucleon Interactions, *Phys. Lett. B* **424**, 390–396 (1998).
- [51] J. GEGELIA, EFT and NN -Scattering, *Phys. Lett. B* **429**, 227–231 (1998).
- [52] U. van KOLCK, Effective Field Theory of Short-Range Forces, *Nucl. Phys. A* **645**, 273–302 (1999).
- [53] P. F. BEDAQUE, H.-W. HAMMER, and U. van KOLCK, The Three-Boson System with Short-Range Interactions, *Nucl. Phys. A* **646**, 444–466 (1999).

- [54] P. F. BEDAQUE, H.-W. HAMMER, and U. van KOLCK, Effective Theory of the Triton, *Nucl. Phys. A* **676**, 357–370 (2000).
- [55] F. GABBIANI, P. F. BEDAQUE, and H. W. GRIESSHAMMER, Higher Partial Waves in an Effective Field Theory Approach to nd Scattering, *Nucl. Phys. A* **675**, 601–620 (2000).
- [56] K. HELFRICH, “Few-body physics in quantum gases”, Doctoral thesis (Dissertation) (Universität Bonn, 2011).
- [57] M. V. ZHUKOV, B. V. DANILIN, D. V. FEDOROV, J. M. BANG, I. J. THOMPSON, et al., Bound state properties of Borromean Halo nuclei: He-6 and Li-11, *Phys. Rept.* **231**, 151–199 (1993).
- [58] K. RIISAGER, Nuclear halo states, *Rev. Mod. Phys.* **66**, 1105–1116 (1994).
- [59] H.-W. HAMMER and D. R. PHILLIPS, Electric properties of the Beryllium-11 system in Halo EFT, *Nucl. Phys. A* **865**, 17–42 (2011).
- [60] C. A. BERTULANI, H.-W. HAMMER, and U. van KOLCK, Effective field theory for halo nuclei, *Nucl. Phys. A* **712**, 37–58 (2002).
- [61] P. F. BEDAQUE, H.-W. HAMMER, and U. van KOLCK, Narrow resonances in effective field theory, *Phys. Lett. B* **569**, 159–167 (2003).
- [62] R. HIGA, H.-W. HAMMER, and U. van KOLCK, alpha alpha Scattering in Halo Effective Field Theory, *Nucl. Phys. A* **809**, 171–188 (2008).
- [63] G. RUPAK and R. HIGA, Model-Independent Calculation of Radiative Neutron Capture on Lithium-7, *Phys. Rev. Lett.* **106**, 222501 (2011).
- [64] L. FERNANDO, R. HIGA, and G. RUPAK, Resonance Contribution to Radiative Neutron Capture on Lithium-7, *Eur. Phys. J. A* **48**, 24 (2012).
- [65] D. L. CANHAM and H.-W. HAMMER, Universal properties and structure of halo nuclei, *Eur. Phys. J. A* **37**, 367–380 (2008).
- [66] D. L. CANHAM and H.-W. HAMMER, Range corrections for two-neutron halo nuclei in effective theory, *Nucl. Phys. A* **836**, 275–292 (2010).
- [67] J. ROTUREAU and U. van KOLCK, Effective Field Theory and the Gamow Shell Model: The ${}^6\text{He}$ Halo Nucleus, (2012), arXiv:1201.3351 [nucl-th].
- [68] P. HAGEN, H.-W. HAMMER, and L. PLATTER, Charge form factors of two-neutron halo nuclei in halo EFT, (2013), arXiv:1304.6516 [nucl-th].
- [69] K. G. WILSON, Confinement of Quarks, *Phys. Rev. D* **10**, 2445–2459 (1974).
- [70] C. DAVIES, Lattice QCD, 105–146 (2002), arXiv:hep-ph/0205181 [hep-ph].
- [71] R. GUPTA, Introduction to lattice QCD: Course, 83–219 (1997), arXiv:hep-lat/9807028 [hep-lat].
- [72] C. HOELBLING, Light hadron spectroscopy and pseudoscalar decay constants, *PoS LATTICE2010*, 011 (2010).
- [73] H.-W. LIN, Review of Baryon Spectroscopy in Lattice QCD, *Chin. J. Phys.* **49**, 827–870 (2011).

- [74] M. GÖCKELER et al., Extracting the rho resonance from lattice QCD simulations at small quark masses, PoS **LATTICE2008**, 136 (2008).
- [75] X. LI et al., Anisotropic lattice calculation of pion scattering using an asymmetric box, JHEP **0706**, 053 (2007).
- [76] X. FENG, K. JANSEN, and D. B. RENNER, The pi+ pi+ scattering length from maximally twisted mass lattice QCD, Phys. Lett. B **684**, 268–274 (2010).
- [77] J. J. DUDEK, R. G. EDWARDS, M. J. PEARDON, D. G. RICHARDS, and C. E. THOMAS, The phase-shift of isospin-2 pi-pi scattering from lattice QCD, Phys. Rev. D **83**, 071504 (2011).
- [78] S. R. BEANE, W. DETMOLD, K. ORGINOS, and M. J. SAVAGE, Nuclear Physics from Lattice QCD, Prog. Part. Nucl. Phys. **66**, 1–40 (2011).
- [79] G. COLANGELO, S. DURR, A. JUTTNER, L. LELLOUCH, H. LEUTWYLER, et al., Review of lattice results concerning low energy particle physics, Eur. Phys. J. C **71**, 1695 (2011).
- [80] D. LEE, Lattice simulations for few- and many-body systems, Prog.Part.Nucl.Phys. **63**, 117–154 (2009).
- [81] J. E. DRUT and A. N. NICHOLSON, Lattice methods for strongly interacting many-body systems, J. Phys. G: Nucl. Part. Phys. **40**, 043101 (2013).
- [82] E. EPELBAUM, H. KREBS, D. LEE, and U.-G. MEISSNER, Lattice effective field theory calculations for A = 3,4,6,12 nuclei, Phys. Rev. Lett. **104**, 142501 (2010).
- [83] E. EPELBAUM, H. KREBS, D. LEE, and U.-G. MEISSNER, Lattice Calculations for A=3,4,6,12 Nuclei Using Chiral Effective Field Theory, Eur. Phys. J. A **45**, 335–352 (2010).
- [84] S. C. PIEPER, Quantum Monte Carlo calculations of light nuclei, Riv. Nuovo Cim. **31**, 709–740 (2008).
- [85] P. NAVRATIL, S. QUAGLIONI, I. STETCU, and B. R. BARRETT, Recent developments in no-core shell-model calculations, J. Phys. G: Nucl. Part. Phys. **36**, 083101 (2009).
- [86] E. EPELBAUM, H. KREBS, D. LEE, and U.-G. MEISSNER, Ab initio calculation of the Hoyle state, Phys. Rev. Lett. **106**, 192501 (2011).
- [87] E. EPELBAUM, H. KREBS, T. A. LÄHDE, D. LEE, and U.-G. MEISSNER, Structure and rotations of the Hoyle state, Phys. Rev. Lett. **109**, 252501 (2012).
- [88] M. LÜSCHER, Volume Dependence of the Energy Spectrum in Massive Quantum Field Theories. 2. Scattering States, Commun. Math. Phys. **105**, 153–188 (1986).
- [89] A. BAZAVOV, D. TOUSSAINT, C. BERNARD, J. LAIHO, C. DETAR, et al., Non-perturbative QCD simulations with 2+1 flavors of improved staggered quarks, Rev. Mod. Phys. **82**, 1349–1417 (2010).
- [90] Z. DAVOUDI and M. J. SAVAGE, Improving the Volume Dependence of Two-Body Binding Energies Calculated with Lattice QCD, Phys. Rev. D **84**, 114502 (2011).
- [91] T. LUU and M. J. SAVAGE, Extracting Scattering Phase-Shifts in Higher Partial-Waves from Lattice QCD Calculations, Phys. Rev. D **83**, 114508 (2011).

- [92] V. A. NOVIKOV, L. B. OKUN, M. A. SHIFMAN, A. I. VAINSHTEIN, M. B. VOLOSHIN, et al., Charmonium and Gluons: Basic Experimental Facts and Theoretical Introduction, *Phys. Rept.* **41**, 1–133 (1978).
- [93] J. M. BULAVA, R. G. EDWARDS, E. ENGELSON, J. FOLEY, B. JOO, et al., Excited State Nucleon Spectrum with Two Flavors of Dynamical Fermions, *Phys. Rev. D* **79**, 034505 (2009).
- [94] A. MATSUYAMA, T. SATO, and T.-S. H. LEE, Dynamical coupled-channel model of meson production reactions in the nucleon resonance region, *Phys. Rept.* **439**, 193–253 (2007).
- [95] S. R. BEANE et al., The Deuteron and Exotic Two-Body Bound States from Lattice QCD, *Phys. Rev. D* **85**, 054511 (2012).
- [96] C. A. REGAL, C. TICKNOR, J. L. BOHN, and D. S. JIN, Tuning p-wave interactions in an ultracold Fermi gas of atoms, *Phys. Rev. Lett.* **90**, 053201 (2003).
- [97] C. H. SCHUNCK et al., Feshbach resonances in fermionic ${}^6\text{Li}$, *Phys. Rev. A* **71**, 045601 (2005).
- [98] J. P. GAEBLER, J. T. STEWART, J. L. BOHN, and D. S. JIN, p -Wave Feshbach Molecules, *Phys. Rev. Lett.* **98**, 200403 (2007).
- [99] S. TYPEL and G. BAUR, Effective-range approach and scaling laws for electromagnetic strength in neutron-halo nuclei, *Phys. Rev. Lett.* **93**, 142502 (2004).
- [100] A. TOHSAKI, H. HORIUCHI, P. SCHUCK, and G. ROPKE, Alpha cluster condensation in C-12 and O-16, *Phys. Rev. Lett.* **87**, 192501 (2001).
- [101] M. CHERNYKH, H. FELDMEIERS, T. NEFF, P. von NEUMANN-COSEL, and A. RICHTER, Structure of the Hoyle State in C-12, *Phys. Rev. Lett.* **98**, 032501 (2007).
- [102] M. LÜSCHER, Two particle states on a torus and their relation to the scattering matrix, *Nucl. Phys. B* **354**, 531–578 (1991).
- [103] M. ABRAMOWITZ and I. A. STEGUN, *Pocketbook of Mathematical Functions* (Verlag Harri Deutsch, Thun; Frankfurt am Main, 1984).
- [104] V. BERNARD, M. LAGE, U.-G. MEISSNER, and A. RUSSETSKY, Resonance properties from the finite-volume energy spectrum, *JHEP* **0808**, 024 (2008).
- [105] P. DYKE et al., Crossover from 2D to 3D in a Weakly Interacting Fermi Gas, *Phys. Rev. Lett.* **106**, 105304 (2011).
- [106] B. FRÖHLICH et al., Radio-Frequency Spectroscopy of a Strongly Interacting Two-Dimensional Fermi Gas, *Phys. Rev. Lett.* **106**, 105301 (2011).
- [107] S. R. BEANE, Ground state energy of the interacting Bose gas in two dimensions: An Explicit construction, *Phys. Rev. A* **82**, 063610 (2010).
- [108] D. LEE, *Notes on topological volume corrections for bound states*, Private communication, 2011.
- [109] S. BOUR, X. LI, D. LEE, U.-G. MEISSNER, and L. MITAS, Precision benchmark calculations for four particles at unitarity, *Phys. Rev. A* **83**, 063619 (2011).

- [110] M. LÜSCHER, Signatures of unstable particles in finite volume, *Nucl. Phys. B* **364**, 237–254 (1991).
- [111] V. G. GORSHKOV, On the Coulomb Green's function, *Sov. Phys. JETP* **20**, 234–238 (1965).
- [112] F. L. YOST, J. A. WHEELER, and G. BREIT, Coulomb Wave Functions in Repulsive Fields, *Phys. Rev.* **49**, 174–189 (1936).
- [113] M. H. HULL and G. BREIT, “Encyclopedia of Physics / Handbuch der Physik”, in, Vol. XLI/1, edited by S. FLÜGGE (Springer Verlag, Berlin Heidelberg, 1959) Chap. “Coulomb Wave Functions”, pp. 408–465.
- [114] L. J. SLATER, *Confluent Hypergeometric Functions* (Cambridge University Press, 1960).
- [115] J. BOERSMA, Expansions for Coulomb Wave Functions, *Math. Comp.* **23**, 51–59 (1969).
- [116] F. S. LEVIN and D. A. MICHA, eds., *Coulomb Interactions in Nuclear and Atomic Few-Body Collisions* (Plenum Press, New York; London, 1996).
- [117] X. KONG and F. RAVNDAL, Coulomb effects in low-energy proton proton scattering, *Nucl. Phys. A* **665**, 137–163 (2000).
- [118] N. F. MOTT and H. S. W. MASSEY, *The Theory of Atomic Collisions*, Third Edition (Clarendon Press, Oxford, 1965).
- [119] W. GORDON, Ueber den Stoß zweier Punktladungen nach der Wellenmechanik, *Zeitschr. f. Phys.* **48**, 180–191 (1928).
- [120] W. F. FORD, Anomalous Behavior of the Coulomb T Matrix, *Phys. Rev.* **133**, B1616–B1621 (1964).
- [121] E. LAMBERT, Fonction de portée effective et déplacement en énergie des états liés en présence d'un potentiel coulombien modifié, *Helv. Phys. Acta* **42**, 667–677 (1968).
- [122] D. BOLLÉ and F. GESZTESY, Scattering observables in arbitrary dimension $n \geq 2$, *Phys. Rev. A* **30**, 1279–1293 (1984).
- [123] M. J. SEATON, Coulomb functions for attractive and repulsive potentials and for positive and negative energies, *Comp. Phys. Comm.* **146**, 225–249 (2002).
- [124] J. W. de MAAG, L. P. KOK, and H. van HAERINGEN, Coulomb-modified scattering parameters for Coulomb-plus-separable potentials for all l , *J. Math. Phys.* **25**, 684–692 (1984).
- [125] D. R. HARRINGTON, Separable Potentials and Coulomb Interactions, *Phys. Rev.* **139**, B691–B695 (1965).
- [126] H. van HAERINGEN and L. P. KOK, Modified Effective Range Function, *Phys. Rev. A* **26**, 1218–1225 (1982).
- [127] J. HAMILTON, I. ØVERBÖ, and B. TROMBORG, Coulomb corrections in non-relativistic scattering, *Nucl. Phys. B* **60**, 443–477 (1973).
- [128] H. van HAERINGEN, T matrix and effective range function for Coulomb plus rational separable potentials especially for $l=1$, *J. Math. Phys.* **18**, 927–940 (1977).

- [129] J. HUMBLET, Analytical structure and properties of Coulomb wave functions for real and complex energies, *Annals Phys.* **155**, 461–493 (1984).
- [130] A. DZIECIOL, S. YNGVE, and P. O. FRÖMAN, Coulomb wave functions with complex values of the variable and the parameters, *J. Math. Phys.* **40**, 6145–6166 (1999).
- [131] J. C. Y. CHEN and A. C. CHEN, Nonrelativistic off-shell two-body Coulomb amplitude, *Adv. Atom. Mol. Phys.* **8**, 72–129 (1972).
- [132] L. HOSTLER, Coulomb Green’s Functions and the Furry Approximation, *J. Math. Phys.* **5**, 591–611 (1964).
- [133] L. HOSTLER, Nonrelativistic Coulomb Green’s Function in Momentum Space, *J. Math. Phys.* **5**, 1235–1240 (1964).
- [134] E. P. WIGNER, Lower Limit for the Energy Derivative of the Scattering Phase Shift, *Phys. Rev.* **98**, 145–147 (1955).
- [135] D. R. PHILLIPS and T. D. COHEN, How short is too short? Constraining contact interactions in nucleon-nucleon scattering, *Phys. Lett. B* **390**, 7–12 (1997).
- [136] M. PAVON VALDERRAMA and E. RUIZ ARRIOLA, Renormalization of NN interaction with chiral two pion exchange potential. central phases and the deuteron, *Phys.Rev. C* **74**, 054001 (2006).
- [137] A. CALLE CORDON and E. RUIZ ARRIOLA, Renormalization vs Strong Form Factors for One Boson Exchange Potentials, *Phys. Rev. C* **81**, 044002 (2010).
- [138] A. C. CORDON and E. RUIZ ARRIOLA, Low energy universality and scaling of Van der Waals forces, *Phys. Rev. A* **81**, 044701 (2010).
- [139] H.-W. HAMMER and D. LEE, Causality and universality in low-energy quantum scattering, *Phys. Lett. B* **681**, 500–503 (2009).
- [140] S. ELHATISARI and D. LEE, Causality bounds for neutron-proton scattering, *Eur. Phys. J. A* **48**, 110 (2012).
- [141] G. P. LEPAGE, What is renormalization?, (2005), arXiv:hep-ph/0506330.
- [142] G. P. LEPAGE, How to renormalize the Schrodinger equation, (1997), arXiv:nuc1-th/9706029.
- [143] J.-M. SPARENBERG, P. CAPEL, and D. BAYE, Influence of low energy scattering on loosely bound states, *Phys. Rev. C* **81**, 011601 (2010).
- [144] J. P. NAISSE, On Precision Analyses of the Low-Energy pp Data, *Nucl. Phys. A.* **278**, 506–524 (1977).
- [145] J. R. BERGERVOET, P. C. van CAMPEN, W. A. van der SANDEN, and J. J. de SWART, Phase shift analysis of 0-30 MeV pp scattering data, *Phys. Rev. C* **38**, 15–50 (1988).
- [146] J. ARVIEUX, Phase Shift Analysis of Elastic Proton-Deuteron Scattering Cross Sections and ^3He Excited States, *Nucl. Phys. A* **221**, 253–268 (1973).
- [147] P. HUTTEL et al., Phase-Shift Analysis of pd Elastic Scattering Below Break-Up Threshold, *Nucl. Phys. A.* **406**, 443–455 (1983).

- [148] T. V. DANIELS, C. W. ARNOLD, J. M. CESARATTO, T. B. CLEGG, A. H. COUTURE, et al., Spin-Correlation Coefficients and Phase-Shift Analysis for $p+^3\text{He}$ Elastic Scattering, *Phys. Rev. C* **82**, 034002 (2010).
- [149] R. A. ARNDT, D. D. LONG, and L. D. ROPER, Nucleon-alpha elastic scattering analyses: (I). Low-energy n -alpha and p -alpha analyses, *Nucl. Phys. A.* **209**, 429–446 (1973).
- [150] S. A. AFZAL, A. A. Z. AHMAD, and S. ALI, Systematic Survey of the alpha-alpha Interaction, *Rev. Mod. Phys.* **41**, 247–273 (1969).
- [151] K. A. SCALDEFERRI, D. R. PHILLIPS, C. W. KAO, and T. D. COHEN, Short range interactions in an effective field theory approach for nucleon-nucleon scattering, *Phys. Rev. C* **56**, 679–688 (1997).
- [152] Y. V. ORLOV and Y. P. OREVKOV, Doublet coulomb-nuclear scattering length and other parameters of the effective-range function for proton-deuteron scattering from an analysis of present-day data, *Phys. Atom. Nucl.* **69**, 828–840 (2006).
- [153] D. LEE, Private communication, 2010.
- [154] C. R. BRUNE, W. H. GEIST, R. W. KAVANAGH, and K. D. VEAL, Sub-Coulomb alpha Transfers on C-12 and the C-12 (alpha,gamma) O-16 S Factor, *Phys. Rev. Lett.* **83**, 4025–4028 (1999).
- [155] G. WALLERSTEIN et al., Synthesis of the elements in stars: forty years of progress, *Rev. Mod. Phys.* **69**, 995–1084 (1997).
- [156] L. BUCHMANN, R. E. AZUMA, C. A. BARNES, J. HUMBLET, and K. LANGANKE, Analysis of the total C-12 (alpha, gamma) O-16 cross section based on available angular distributions and other primary data, *Phys. Rev. C* **54**, 393–410 (1996).
- [157] P. TISCHHAUSER, A. COUTURE, R. DETWILER, J. GORRES, C. UGALDE, et al., Measurement of elastic C-12 + alpha scattering: Details of the experiment, analysis, and discussion of phase shifts, *Phys. Rev. C* **79**, 055803 (2009).
- [158] S. ADHIKARI and C. BASU, The ANC of O-16 subthreshold states from C-12(Li-6, d) reaction at energies near the barrier, *Phys. Lett. B* **704**, 308–311 (2011).
- [159] A. BELHOUT et al., Measurement and DWBA analysis of the $^{12}\text{C}(^6\text{Li},d)^{16}\text{O}$ α -transfer reaction cross sections at 48.2 MeV. R-matrix analysis of $^{12}\text{C}(\alpha,\gamma)^{16}\text{O}$ direct capture reaction data, *Nucl. Phys. A.* **793**, 178–211 (2007).
- [160] J.-M. SPARENBERG, P. CAPEL, and D. BAYE, Deducing physical properties of weakly bound states from low-energy scattering data. Application to O-16 and C-12 + alpha, *J. Phys. Conf. Ser.* **312**, 082040 (2011).
- [161] W. M. FRANK, D. J. LAND, and R. M. SPECTOR, Singular Potentials, *Rev. Mod. Phys.* **43**, 36–98 (1971).
- [162] T. F. O'MALLEY, L. SPRUCH, and L. ROSENBERG, Modification of Effective-Range Theory in the Presence of a Long-Range (r^4) Potential, *J. Math. Phys.* **2**, 491–498 (1961).
- [163] B. GAO, Solutions of the Schrödinger equation for an attractive $1/r^6$ potential, *Phys. Rev. A* **58**, 1728–1734 (1998).

- [164] B. GAO, Analytic description of atomic interaction at ultracold temperatures: The case of a single channel, *Phys. Rev. A* **80**, 012702 (2009).
- [165] B. GAO, Quantum-defect theory of atomic collisions and molecular vibration spectra, *Phys. Rev. A* **58**, 4222–4225 (1998).
- [166] S. INOUE, J. STENGER, H.-J. MIESNER, D. M. STAMPER-KURN, and W. KETTERLE, Observation of Feshbach resonances in a Bose-Einstein condensate, *Nature* **392**, 151–154 (1998).
- [167] T. KÖHLER, K. GÓRAL, and P. S. JULIENNE, Production of cold molecules via magnetically tunable Feshbach resonances, *Rev. Mod. Phys.* **78**, 1311–1361 (2006).
- [168] B. GAO, Analytic description of atomic interaction at ultracold temperatures. II. Scattering around a magnetic Feshbach resonance, *Phys. Rev. A* **84**, 022706 (2011).
- [169] S. KÖNIG, “Coulomb effects in pionless effective field theory”, Diploma thesis (Diplomarbeit) (Universität Bonn, 2010).
- [170] V. EFIMOV, Qualitative treatment of three-nucleon properties, *Nucl. Phys. A* **362**, 45–70 (1981).
- [171] H.-W. HAMMER and L. PLATTER, Efimov States in Nuclear and Particle Physics, *Ann. Rev. Nucl. Part. Sci.* **60**, 207–236 (2010).
- [172] X. KONG and F. RAVNDAL, Proton proton scattering lengths from effective field theory, *Phys. Lett. B* **450**, 320–324 (1999).
- [173] S.-I. ANDO, J. W. SHIN, C. H. HYUN, and S. W. HONG, Low energy proton-proton scattering in effective field theory, *Phys. Rev. C* **76**, 064001 (2007).
- [174] T. BARFORD and M. C. BIRSE, A Renormalization group approach to two-body scattering in the presence of long range forces, *Phys. Rev. C* **67**, 064006 (2003).
- [175] S.-I. ANDO and M. C. BIRSE, Renormalization-group analysis for low-energy scattering of charged particles, *Phys. Rev. C* **78**, 024004 (2008).
- [176] X. KONG and F. RAVNDAL, Proton proton fusion in effective field theory, *Phys. Rev. C* **64**, 044002 (2001).
- [177] S.-I. ANDO, J. W. SHIN, C. H. HYUN, S. W. HONG, and K. KUBODERA, Proton-proton fusion in pionless effective theory, *Phys. Lett. B* **668**, 187–192 (2008).
- [178] G. RUPAK and X.-W. KONG, Quartet S-wave pd Scattering in EFT, *Nucl. Phys. A* **717**, 73–90 (2003).
- [179] S. ANDO and M. C. BIRSE, Effective Field Theory of ^3He , *J. Phys. G: Nucl. Part. Phys.* **37**, 105108 (2010).
- [180] J. KIRSCHER, H. W. GRIESSHAMMER, D. SHUKLA, and H. M. HOFMANN, Universal Correlations in Pion-less EFT with the Resonating Group Model: Three and Four Nucleons, *Eur. Phys. J. A* **44**, 239–256 (2010).
- [181] P. F. BEDAQUE and H. W. GRIESSHAMMER, Quartet S Wave Neutron Deuteron Scattering in Effective Field Theory, *Nucl. Phys. A* **671**, 357–379 (2000).
- [182] H. W. GRIESSHAMMER, M. R. SCHINDLER, and R. P. SPRINGER, Parity-violating neutron spin rotation in hydrogen and deuterium, *Eur. Phys. J. A* **48**, 7 (2012).

- [183] D. R. PHILLIPS, G. RUPAK, and M. J. SAVAGE, Improving the convergence of N N effective field theory, *Phys. Lett. B* **473**, 209–218 (2000).
- [184] H. W. GRIESSHAMMER, Improved convergence in the three-nucleon system at very low energies, *Nucl. Phys. A* **744**, 192–226 (2004).
- [185] P. F. BEDAQUE and U. van KOLCK, Effective field theory for few nucleon systems, *Ann. Rev. Nucl. Part. Sci.* **52**, 339–396 (2002).
- [186] M. WALZL, U.-G. MEISSNER, and E. EPELBAUM, Charge dependent nucleon-nucleon potential from chiral effective field theory, *Nucl. Phys. A* **693**, 663–692 (2001).
- [187] P. F. BEDAQUE, G. RUPAK, H. W. GRIESSHAMMER, and H.-W. HAMMER, Low Energy Expansion in the Three Body System to All Orders and the Triton Channel, *Nucl. Phys. A* **714**, 589–610 (2003).
- [188] C. JI and D. R. PHILLIPS, Effective Field Theory Analysis of Three-Boson Systems at Next-To-Next-To-Leading Order, (2012) 10.1007/s00601-013-0710-5, arXiv:1212.1845 [nucl-th].
- [189] H. W. GRIESSHAMMER, Naive dimensional analysis for three-body forces without pions, *Nucl. Phys. A* **760**, 110–138 (2005).
- [190] R. S. CHRISTIAN and J. L. GAMMEL, Elastic Scattering of Protons and Neutrons by Deuterons, *Phys. Rev.* **91**, 100–121 (1953).
- [191] L. PLATTER, The Three-nucleon system at next-to-next-to-leading order, *Phys. Rev. C* **74**, 037001 (2006).
- [192] V. K. AGRAWALA, J. G. BELINFANTE, and G. H. RENNINGER, On the cutkosky-leon normalization conditions, *Nuov. Cim. A* **44**, 740–744 (1966).
- [193] L. P. KOK, D. J. STRUIK, and H. van HAERINGEN, *On the exact solution of three-particle equations with Coulomb interaction. The driving terms*, Internal Report 151 (University of Groningen, 1979).
- [194] L. P. KOK, D. J. STRUIK, J. E. HOLWERDA, and H. van HAERINGEN, *On the exact solution of three-particle equations with Coulomb interaction. II. Bound states*, Internal Report 170 (University of Groningen, 1981).
- [195] M. HOFERICHTER, Private communication, 2010.
- [196] L. PLATTER and D. R. PHILLIPS, The Three-Boson System at Next-To-Next-To-Leading Order, *Few Body Syst.* **40**, 35–55 (2006).
- [197] J. VANASSE, Fully Perturbative Calculation of *nd* Scattering to Next-to-next-to-leading-order, (2013), arXiv:1305.0283 [nucl-th].
- [198] N. MICHEL and M. STOITSOV, Fast computation of the Gauss hypergeometric function with all its parameters complex with application to the Pöschl–Teller–Ginocchio potential wave functions, *Comput. Phys. Comm.* **178**, 535–551 (2008).
- [199] T. C. BLACK et al., Determination of proton-deuteron scattering lengths, *Phys. Lett. B* **471**, 103–107 (1999).
- [200] D. LURIÉ, *Particles and Fields* (Interscience Publishers, New York; London; Sydney, 1968).

Acknowledgments

I would like to express my sincere gratitude to a number of people who supported me in this work—both directly and indirectly and in various ways—over the course of the last three years.

First of all I would like to thank Prof. Hans-Werner Hammer, my thesis advisor in Bonn, and Prof. Dean Lee at the North Carolina State University for suggesting many interesting topics, keeping me on the right track, and in general for providing advice, support, and encouragement, regarding both this thesis and my career in general. I consider myself very lucky to have been their student. To Dean Lee I am furthermore grateful for inviting me to stay at NC State for two months and for taking such good care of me there.

My thanks also go to Prof. Ulf-G. Meißner for carefully reading the manuscript of this thesis, for providing many valuable comments and corrections, and beyond that for further support and encouragement.

I would like to thank the “Studientiftung des deutschen Volkes” for providing me with a doctoral scholarship to cover my living expenses, and furthermore for offering summer schools and student meetings that I had a lot of fun at. I am also grateful to the Bonn–Cologne Graduate School of Physics and Astronomy (BCGS) for additional support.

For the many opportunities to travel that I had over the course of this work, I would in particular like to thank the organizers of the APFB2011 conference for the chance to visit Seoul (and letting me stay at the university guest house for the weekend after the conference), the Institute of Nuclear Theory at the University of Washington for its hospitality for three weeks during the program “Light nuclei from first principles,” the organizers of which I would furthermore like to thank for inviting me. Thanks also to Profs. Roxanne Springer and Thomas Mehen for hosting me at Duke University for two weeks, and to Profs. Daniel Phillips and Richard Furnstahl for inviting me to give seminar talks at Ohio University and Ohio State University (a trip that I enjoyed very much) while I was at NC State, and for interesting discussions.

Moreover, I would like to thank Prof. Harald Griesshammer for many useful discussions about pionless effective field theory (in particular, about the ${}^3\text{He}$ problem at NLO), and for providing valuable comments on the corresponding part of this thesis. My thanks also go to all other people I had the chance to collaborate with, in particular to Serdar Elhatisari for putting so much work into the van der Waals causality project, and to Shahin Bour and Jared Vanasse.

I would like to thank the group of Prof. Hammer and all my colleagues at the HISKP,

both present and former, for providing a great working atmosphere. In particular, my thanks go to my office mate Philipp Hagen, and moreover to Sebastian Schneider, Martin Hoferichter, Bastian Kubis, and Simon Tölle, for numerous interesting and enjoyable discussions—not at all limited to physics topics—throughout the years.

Finally, I would like to thank my parents and grandparents for their continued support during the years, for steady encouragement, and most of all for providing a home that I could always come back to when I needed it.

Last, but most certainly not least, thank you, Jan, for being there and everything.